December 2016

Biodegradable Thermoplastic Elastomers and Smart Composites

Erin McMullin
Syracuse University

Abstract

There is a need for biodegradable thermoplastic elastomers for a variety of medical applications. This dissertation aims at (i) developing and characterizing biodegradable elastomers and (ii) developing and characterizing biodegradable smart composites, both to be used as biomaterials. First, in **Chapter 1**, an overview was given of the literature of relevant background information on polymers, biomaterials, and previous biodegradable elastomers and responsive elastomeric systems.

The first biodegradable elastomer developed and investigated, as presented in **Chapter 2**, is a novel thermoplastic polyurethane that has a biodegradable soft segment and a crystalline hard segment (POSS). By varying the composition of the poly(caprolactone)-based soft segment as well as the soft segment to hard segment ratio, the thermal and mechanical properties could be controlled. Increasing the comonomer (glycolide or d,l-lactide) content caused a decrease in the thermal and mechanical properties, while increasing POSS caused an increase in these properties. Overall, the synthesized polyurethanes had low moduli, high strain-to-failure, and high elasticity.

In **Chapter 3**, these polymers were degraded *in vitro* in phosphate-buffered saline (PBS) solution to investigate their properties throughout degradation. It was found that increasing the amount of comonomer (glycolide or d,l-lactide) in the soft segment increased the rate of degradation at 37 °C. The mechanical properties of all materials with comonomer decreased before 12 w, even if > 95% of the initial mass remained. Interestingly, different trends were seen in the 60 °C degradation study. All materials tested lost their mechanical properties by 4 w. While materials with d,l-lactide decreased over time, the material without comonomer saw a sharp decrease in mass after almost no mass loss during the first weeks of degradation.

The POSS-based polyurethane elastomers were then tested for cytocompatibility using a non-contact cell viability assay in **Chapter 4**. It was found that all of the materials developed in Chapter 2 had low cell viability. Therefore, it was hypothesized that residual tin catalyst (tin-POMS) from synthesis was causing this cytotoxicity. A study was performed systematically varying the tin catalyst used to synthesize PCL_{1k}:POSS. Polymers were synthesized with 1 – 0.01 wt.% tin-POMs, 0.1 – 0.01 wt. % dibutyltin dilaurate, or processed with repeated dissolutions and precipitations to try to wash away the tin. It was found that the polyurethane synthesized from lowest concentration of tin-POMS catalyst (0.01 wt. %) had the best cell viability without compromising the mechanical properties.

The biodegradable, elastomeric polyurethanes and a thermoplastic semi-crystalline polymer, poly(caprolactone), were combined by dual-electrospinning and compaction to fabricate a smart composite. **Chapter 5** presents the processing and characterization of these shape memory elastomeric composites, or SMECs. The composites had high elasticity and extensibility while having shape memory capabilities, or the ability to fix into a temporary shape and return to its original shape upon heating. These materials were tested extensively for thermal, mechanical and shape memory properties for different compositions. Increasing poly(caprolactone) generally increased thermal properties, mechanical properties, and fixing. Next, a single composition was degraded at different fixed strains. It was determined that up to 100% fixed strain had no effect on the SMEC degradation profile.

In order to produce lower-cost biomaterials, a second type of polyurethane was developed that utilized different length poly(caprolactone) diols as both the hard and soft segments and is presented in **Chapter 6**. These materials had a higher modulus than the POSS-based materials but

had high elasticity. One composition, because of its high molecular weight and therefore high entanglements, had shape memory properties.

Finally, in **Chapter 7**, conclusions and future directions for this work was presented.

BIODEGRADABLE THERMOPLASTIC ELASTOMERS AND SMART COMPOSITES

By

ERIN MCMULLIN

B.S. Engineering Science (Biomedical), The College of New Jersey, 2011

DISSERTATION

Submitted in partial fulfillment of the requirements for the
degree of Doctor of Philosophy in Bioengineering

Syracuse University
December 2016

To Mom, Dad, Grandma, and Papa.

Thank you for always believing in me.

Acknowledgements

I would like to thank the people whose support and guidance made this dissertation possible.

First and foremost, I'd like to thank Prof. Mather for his teachings, support, and guidance throughout my graduate school experience. I am grateful for all of the inspiration, insight and opportunities he has provided me. With his guidance, I have grown to become a more confident and independent researcher. Thank you for teaching me to persevere through challenges and for pushing me to succeed.

I would like to thank my dissertation committee, Dr. Michelle Blum, Dr. Jeremy Gilbert, Dr. Julie Hasenwinkel, Dr. Jay Henderson, and Dr. Zhen Ma, for their time and for their insightful feedback and suggestions for my dissertation.

I am grateful to the companies that funded my research and to the talented researchers who I was fortunate to work with. Thank you to Procter & Gamble, and especially Ward Ostendorf, for funding the work that built my basis of knowledge for my dissertation. Thank you to Gerry Fredrickson and Laura Christakis of Boston Scientific Corporation for funding and influencing the work presented in this dissertation. I am grateful for your extensive knowledge and feedback.

I would like to thank the present and past members of the Mather Research Group, the Syracuse Biomaterials Institute, and the BMCE Department who I have had the pleasure of working with. Thank you to Dr. Kazuki Ishida for mentoring me. I wish everyone had his dedication to science. Thank you to Dr. Eric Finkelstein for not only maintaining the SBI facility but also for performing all of the cell work in this dissertation. To Dr. Debbie Kerwood, thank you for all your help with NMR. My research would not have been possible without the help of several high school and undergraduate students, including Alex Judge, Ryan Mather, Emily Messing, and Margaret Geary but especially to Hannah Rebar, Phillip Falcone, and Euphemia Frie, whose tremendous work made this dissertation possible. Thank you to the many graduate students I collaborated with, but especially Melodie Lawton whose collaboration made the drug delivery study possible and to Jaimee Robertson for the help with the SMEC work. To Lynore, Karen, Dawn, and Jason, thank you for taking care of the day-to day and allowing the lab to function. I'd also like to thank all of people who I've met here and am lucky enough to call my friends. They know who they are.

Finally, I'd like to thank my family who provided constant love and support during this process. To my parents, grandparents, and to Danielle, Shannon and Ryan, thank you for always being there for me. I am forever grateful. Lastly, I would like to thank my fiancé, Chris, for his endless love and support. I cannot express how grateful I am to have you in my life, and I am so excited to start the next chapter in our lives.

Table of Contents

List of Tables ..... **xx**

List of Schemes ..... **xxii**

List of Figures ..... **xxiii**

Chapter 1: Introduction and Scope of Dissertation **1**

1.1 Biomaterials and Polymers 1

1.2 Polyurethanes 2

1.3 Biodegradable Polymers 3

1.4 Biodegradable Elastomers 5

1.5 Polyhedral Oligomeric Silsesquioxane (POSS) 6

1.6 Shape Memory Materials 7

1.7 Shape Memory Elastomeric Materials 8

1.8 Scope of Dissertation 9

1.9 References 10

Chapter 2: Biodegradable Thermoplastic Elastomers Incorporating POSS: Synthesis, Microstructure, and Mechanical Properties* **20**

2.1 Synopsis 20

2.2 Introduction 20

2.3 Methods 24

2.3.1 Materials 24

2.3.2 Diol Synthesis 24

2.3.3 Polyurethane Synthesis 25

2.3.4 Proton Nuclear Magnetic Resonance (^{1}H-NMR) 26

2.3.5 Gel Permeation Chromatography (GPC) 26

2.3.6 Differential Scanning Calorimetry (DSC) 27

2.3.7 Compression Molding 27

2.3.8 Wide-Angle X-Ray Scattering (WAXS) 28

2.3.9 Tensile Testing 28

2.3.10 Elasticity Testing 28

2.3.11 Dynamic Mechanical Analysis (DMA) 29

2.3.12 Impact of Pre-strain on Elasticity 29

2.3.13 Statistical Analysis 29

2.4 Results 29

2.4.1 Diol Synthesis and Characterization 29

2.4.2 Polyurethane Synthesis and Molecular Characterization 30

2.4.3 Differential Scanning Calorimetry 31

2.4.4 Wide-Angle X-ray Scattering 32

2.4.5 Tensile Testing 32

2.4.6 Elasticity Testing 33

2.4.7 Dynamic Mechanical Analysis 34

2.4.8 Impact of Pre-strain on Elasticity 35

2.5 Discussion 35

2.6 Conclusions 39

2.7 References 39

Chapter 3: Degradation Behavior of Novel Biodegradable Thermoplastic Elastomers Incorporating POSS 62

3.1 Synopsis 62

3.2 Introduction 62

3.3 Methods 65

3.3.1 Materials 65

3.3.2 Diol and Polyurethane Synthesis 65

3.3.3 Proton Nuclear Magnetic Resonance (^{1}H-NMR) 65

3.3.4 Gel Permeation Chromatography (GPC) 66

3.3.5 Differential Scanning Calorimetry 66

3.3.6 Compression Molding 66

3.3.7 X-Ray Diffraction 67

3.3.8 Tensile Testing 67

3.3.9 Scanning Electron Microscopy 67

3.3.10 Degradation Study 68

3.3.11 Degradation Study Modeling 69

3.3.12 Statistical Analysis 70

3.4 Results 70

3.4.1 Polyurethanes in Degradation Study 70

3.4.2 Mass Loss and Water Uptake (37 °C Degradation Study) 70

3.4.3 Film Surface (37 °C Degradation Study) 71

3.4.4 Molecular Weight (37 °C Degradation Study) 71

3.4.5 Molecular Composition (37 °C Degradation Study) 72

3.4.6 Thermal Properties (37 °C Degradation Study) 74

3.4.7 Mechanical Properties (37 °C Degradation Study) 74

3.4.8 Accelerated Degradation Study (60 °C Degradation Study) 76

3.4.9 Degradation Study Modeling 77

3.5 Discussion 78

3.6 Conclusions 82

3.7 References 83

Chapter 4: Effect of Catalyst Concentration on PCL_{1k}:POSS Polyurethanes' Physical Properties and Cell Viability.....105

4.1 Synopsis.....105

4.2 Introduction.....105

4.3 Methods.....107

4.3.1 Materials.....107

4.3.2 Cell Viability Testing of PCL:POSS, PGCL:POSS, and PLCL:POSS Polyurethanes.....107

4.3.3 Polymer Synthesis.....108

4.3.4 Proton Nuclear Magnetic Resonance (^{1}H-NMR).....109

4.3.5 Gel Permeation Chromatography (GPC).....109

4.3.6 Differential Scanning Calorimetry (DSC).....109

4.3.7 Compression Molding.....109

4.3.8 Tensile Testing.....110

4.3.9 Cell Viability Testing of the PCL_{1k}:POSS Polyurethanes.....110

4.3.10 Statistical Analysis.....110

4.4 Results.....111

4.4.1 Cell Viability Testing of PCL:POSS, PGCL:POSS, and PLCL:POSS Polyurethanes.....111

4.4.2 Polymer Synthesis and Molecular Properties.....111

4.4.3 Differential Scanning Calorimetry.....112

4.4.4 Tensile Testing.....112

4.4.5 Cell Viability Testing of the PCL_{1k}:POSS Polyurethanes.....113

4.5 Discussion.....114

4.6 Conclusions.....117

4.7 References.....117

Chapter 5: Biodegradable Thermoplastic Shape Memory Elastomeric Composites (SMECs) Via Dual-Electrospinning.....129

5.1 Synopsis.....129

5.2 Introduction.....129

5.3 Methods.....131

5.3.1 Materials.....131

5.3.2 Polyurethane Synthesis.....132

5.3.3 Dual-Electrospinning.....133

5.3.4 Compression Molding.....133

5.3.5 Scanning Electron Microscopy.....133

5.3.6 Differential Scanning Calorimetry (DSC).....134

5.3.7 Dynamic Mechanical Analysis.....134

5.3.8 Tensile Testing.....134

5.3.9 Elasticity Testing 135

5.3.10 Shape Memory Testing 135

5.3.11 X-Ray Diffraction (XRD) 136

5.3.12 Degradation Study I 136

5.3.13 Degradation Study II 136

5.3.14 Statistical Analysis 137

5.4 Results 137

5.4.1 Polyurethane Synthesis I 137

5.4.2 Dual-Electrospinning, Compression Molding, and Scanning Electron Microscopy 138

5.4.3 Differential Scanning Calorimetry (DSC) 139

5.4.4 Dynamic Mechanical Analysis 139

5.4.5 Tensile Testing 140

5.4.6 Elasticity Testing 141

5.4.7 Shape Memory Testing 141

5.4.8 Degradation Study I 141

5.4.9 Polyurethane Synthesis II and Degradation Study II 142

5.4.9.1 Polyurethane Synthesis 142

5.4.9.2 SMEC Processing, Fixing, and Thicknesses 143

5.4.9.3 Mass Remaining, Water Uptake, and Fixed Strain Throughout Degradation....143

5.4.9.4 Surface Morphology Throughout Degradation....144

5.4.9.5 Crystallinity and Alignment Throughout Degradation....144

5.4.9.6 Recovery After Degradation....145

5.5 Discussion....145

5.6 Conclusion....150

5.7 References....150

Chapter 6: Biodegradable Polyurethanes with Alternative Hard Blocks to POSS-PCL$_{1k}$:PCL Polyurethanes....180

6.1 Synopsis....180

6.2 Introduction....180

6.3 Methods....182

6.3.1 Materials....182

6.3.2 Diol Synthesis....183

6.3.3 Polyurethane Synthesis....183

6.3.4 Gel Permeation Chromatography (GPC)....184

6.3.5 Differential Scanning Calorimetry (DSC)....184

6.3.6 Compression Molding....184

6.3.7 Wide-Angle X-Ray Scattering (WAXS)....185

6.3.8 Dynamic Mechanical Analysis 185

6.3.9 Elasticity Testing 185

6.3.10 Shape Memory Testing 186

6.3.11 Statistical Analysis 186

6.4 Results 187

6.4.1 Diol and Polymer Synthesis and Molecular Properties 187

6.4.2 Differential Scanning Calorimetry 187

6.4.3 Wide-Angle X-Ray Scattering 188

6.4.4 Dynamic Mechanical Analysis 188

6.4.5 Elasticity Testing 189

6.4.6 Shape Memory Testing 190

6.5 Discussion 190

6.6 Conclusions 192

6.7 References 193

Chapter 7: Conclusions and Future Work 210

7.1 Overall Conclusions 210

7.2 Biodegradable Thermoplastic Elastomers Incorporating POSS: Synthesis, Microstructure and Mechanical Properties 211

7.2.1 Conclusions 211

7.2.2 Future Directions 211

7.3 Degradation Behavior of Novel Biodegradable, Thermoplastic Elastomers Incorporating POSS 212

7.3.1 Conclusions.....212

7.3.2 Future Directions 212

7.4 Effect of Catalyst Concentration on PCL_{1k}:POSS Polyurethanes' Physical Properties and Cell Viability.....212

7.4.1 Conclusions.....212

7.4.2 Future Directions 213

7.5 Biodegradable Thermoplastic Shape Memory Elastomeric Composites (SMECs) Via Dual-Electrospinning 213

7.5.1 Conclusions.....213

7.5.2 Future Directions 214

7.6 Biodegradable Polyurethanes with Alternative Hard Blocks to POSS: PCL:PCL Polyurethanes.....214

7.6.1 Conclusions.....214

7.6.2 Future Directions 214

7.7 Other Future Directions 215

7.8 References.....216

Appendix: Development of a Biodegradable, Shape Memory Polymer with Controlled Physical Properties.....219

A.1 Introduction.....219

A.2 Methods.....220

A.3 Results.....221

A.4 Conclusions and Future Work.....223

A.5 References.....223

VITA.....233

List of Tables

Table 2-1: Diols used as the soft segment in polyurethane synthesis. 45

Table 2-2: Molecular characterization of synthesized polyurethanes. 50

Table 2-3: Thermal transitions and crystallinity of each polymer from the DSC thermograms. 52

Table 2-4: Summary of mechanical properties from tensile tests. 56

Table 2-5: Summary of the storage moduli (E') and Tanδ values at 25 and 37 °C.60

Table 3-1: Summary of polyurethane syntheses and their molecular properties. .87

Table 3-2: Summary of thermal and mechanical properties of the elastomers. 88

Table 3-3: Summary of initial (t=0) film molecular weights. 91

Table 3-4: Summary of initial film molecular weights (t=0) for the 60 °C degradation study. 99

Table 4-1: Summary of polyurethanes synthesized with varying catalyst type, concentration and precipitation numbers with their molecular properties. 122

Table 4-2: Summary of the thermal properties of the PCL_{1k}:POSS polyurethanes.124

Table 4-3: Summary of the mechanical properties from tensile testing. 126

Table 5-1: Molecular and thermal properties of PCL_{1k}:$(PG_5CL_{95})_{1k}$:POSS. 155

Table 5-2: Summary of the thermal transitions of each compacted material from the DSC thermograms. 159

Table 5-3: Summary of the storage moduli and tanδ values at 25 °C and 37 ° C of the four materials. 161

Table 5-4: Summary of the mechanical properties from tensile tests (n=5). 163

Table 5-5: Summary of the fixing and recovery ratios for 15% PCL SMEC and 25% PCL SMEC. 166

Table 5-6: Summary of the mechanical properties during degradation. 168

Table 5-7: Molecular and thermal properties of $(PG_5CL_{95})_{1k}$:POSS. 170

Table 6-1: Summary of the properties of the hard block alternatives (not including the isocyanate). 196
Table 6-2: Characteristics of the diol synthesized. 198
Table 6-3: Synthesized polyurethanes and their molecular weights. 200
Table 6-4: Summary of the thermal properties from DSC. 202
Table 6-5: Summary of the storage moduli and tanδ values from DMA. 206
Table 6-6: Fixing and recovery values of PCL_{1k}:PCL_{12k} 90:10 for three cycles.209
Table A-1: Summary of (PEG:PCL):POSS syntheses and their molecular properties. 225
Table A-2: Summary of the thermal properties. 227
Table A-3: Summary of the thermal characteristics of the soft segment upon cooling. 232

List of Schemes

Scheme 1-1: A schematic of a urethane bond formation from a hydroxyl and an isocyanate. 16

Scheme 1-2: a) Schematics of the caprolactone, lactide, and glycolide monomers and their respective polymers. b) The monomers of the different chiral forms of lactide: l-lactide, d-lactide, and meso-lactide. 17

Scheme 1-3: A POSS molecule, with some examples of R and R_1 groups. 18

Scheme 2-1: a) Schematic of diol synthesis and b) structures of the resulting poly(glycolide-co-caprolactone and poly(d,l-lactide-co-caprolactone). 43

Scheme 2-2: Example schematic of polyurethane synthesis. 46

Scheme 4-1: PCL_{1k}:POSS polyurethane synthesis. 121

Scheme 5-1: Polyurethane synthesis of PCL_{1k}:$(PG_5CL_{95})_{1k}$:POSS polyurethane.154

Scheme 5-2: Schematic of SMEC processing. a) Dual-electrospinning set-up. b) Compaction of dual-electrospun films. 156

Scheme 5-3: Diol and polyurethane synthesis of $(PG_5CL_{95})_{1k}$:POSS. 169

Scheme 5-4: Schematic of fixing samples for a degradation study: a) removal of thermal history and b) fixing samples to 0%, 50% and 100% strain. 171

Scheme 6-1: Schematic of poly(caprolactone) diol synthesis. 197

Scheme 6-2: Schematic of polyurethane synthesis with poly(caprolactone) as the soft block and hard block. 199

Scheme 7-1: Process of imbibing the biodegradable elastomers and PCL with Rhodamine B (RhB): a) "The Sponge Method" is when a material is soaked in a solution of RhB. b) Electrospinning a polymer/RhB solution. Both result in RhB-infused elastomers. 217

Scheme A-1: Schematics of a) diol synthesis and b) polyurethane synthesis. 224

List of Figures

Figure 1-1: a) A schematic of a one-way shape memory cycle. b) A three-dimensional plot of stress, temperature, and strain of a one-way shape memory cycle. 19

Figure 2-1: ^{1}H-NMR spectra of a) $(PGCL)_{1k}$ and b) $(PLCL)_{1k}$ diol. 44

Figure 2-2: H-NMR spectra for a) PCL_{1k}:POSS, b) $(PGCL)_{1k}$:POSS and c) $(PLCL)_{1k}$:POSS polyurethanes. 49

Figure 2-3: Differential scanning calorimetry (DSC) curves for: (i) PCL_{1k}:POSS 100:0, (ii) PCL_{1k}:POSS 90:10, (iii) PCL_{1k}:POSS 80:20, (iv) PCL_{1k}:POSS 70:30, (v) $(PG_5CL_{95})_{1k}$:POSS 70:30, (vi) $(PG_{25}CL_{75})_{1k}$:POSS 70:30, (vii) $(PL_5CL_{95})_{1k}$:POSS 70:30, and (viii) $(PL_{25}CL_{75})_{1k}$:POSS 70:30, with the second heat shown (exotherm up) of the full temperature range (left) and for higher temperature range for POSS (right). 51

Figure 2-4: Wide-angle x-ray scattering (WAXS) pictograms of (i) PCL_{1k}:POSS 100:0, (ii) PCL_{1k}:POSS 90:10, (iii) PCL_{1k}:POSS 80:20, (iv) PCL_{1k}:POSS 70:30, (v) $(PG_5CL_{95})_{1k}$:POSS 70:30, (vi) $(PG_{25}CL_{75})_{1k}$:POSS 70:30, (vii) $(PL_5CL_{95})_{1k}$:POSS 70:30, and (viii) $(PL_{25}CL_{75})_{1k}$:POSS 70:30..53

Figure 2-5: Plot of intensity vs. diffraction angle for materials (i) PCL_{1k}:POSS 100:0, (ii) PCL_{1k}:POSS 90:10, (iii) PCL_{1k}:POSS 80:20, (iv) PCL_{1k}:POSS 70:30, (v) $(PG_5CL_{95})_{1k}$:POSS 70:30, (vi) $(PG_{25}CL_{75})_{1k}$:POSS 70:30, (vii) $(PL_5CL_{95})_{1k}$:POSS 70:30, and (viii) $(PL_{25}CL_{75})_{1k}$:POSS 70:30..54

Figure 2-6: Engineering stress-strain curves for (i) PCL_{1k}:POSS 100:0, (ii) PCL_{1k}:POSS 90:10, (iii) PCL_{1k}:POSS 80:20, (iv) PCL_{1k}:POSS 70:30, (v) $(PG_5CL_{95})_{1k}$:POSS 70:30, (vi) $(PG_{25}CL_{75})_{1k}$:POSS 70:30, (vii) $(PL_5CL_{95})_{1k}$:POSS 70:30, and (viii) $(PL_{25}CL_{75})_{1k}$:POSS 70:30 (n=5). 55

Figure 2-7: Elasticity testing of all materials: a) An example of a material stretched to 50% strain for 3 cycles, b) a picture of an elastomer being stretched, c) strain recovery for each of the three cycles of PCL:POSS elastomers with changing PCL and POSS content, and d) strain recovery for each of the three cycles for all 70:30 materials with different soft segments (n=3). 57

Figure 2-8: Energy stored in the elastomers: a) An example of loading curve looking at the energy stored (area under the curve) b) an example of an unloading curve looking at the energy released (area under the curve), c) the energy dissipated (difference between two energies), d) energy calculations for elastomers with changing PCL and POSS content, and e) energy calculations for all 70:30 materials with changing soft segments (n=3). 58

Figure 2-9: Dynamic mechanical analysis of (i) PCL_{1k}:POSS 100:0, (ii) PCL_{1k}:POSS 90:10, (iii) PCL_{1k}:POSS 80:20, and (iv) PCL_{1k}:POSS 70:30. 59

Figure 2-10: Pre-stretching of elastomers: a) Pre-stretching of $(PG_5CL_{95})_{1k}$:POSS samples to 25, 50, 100 and 250% strain. b) An example of stretching this material to 50% strain. c) The recovery of the 50% strain after each pre-stretch, d) enthalpy of melting of the PGCL and POSS as an effect of increasing pre-strain e) Wide-angle x-ray (WAXS) 2D scattering of 0%, 50%, and 250% strain with strain direction indicated by the arrows. Red arrows indicate POSS alignment and yellow arrows indicate PGCL alignment..61

Figure 3-1: a) Mass remaining and b) water uptake for PCL_{1k}:POSS 70:30 (○), $(PG_5CL_{95})_{1k}$:POSS 70:30 (□), $(PG_{25}CL_{75})_{1k}$:POSS 70:30 (■), $(PL_5CL_{95})_{1k}$:POSS 70:30 (◊), and $(PL_{25}CL_{75})_{1k}$:POSS 70:30 (♦).89

Figure 3-2: Scanning electron micrographs of the surfaces of film over time for: PCL_{1k}:POSS at (i) 0 w, (ii) 4 w, (iii) 8 w, and (iv)12 w; $(PG_5CL_{95})_{1k}$:POSS at (v) 0 w, (vi) 4 w, (vii) 8 w, and (viii) 12 w; $(PG_{25}CL_{75})_{1k}$:POSS at (ix) 0 w, (x) 4 w, (xi) 8 w, and (xii) 12; $(PL_5CL_{95})_{1k}$:POSS at (xiii) 0 w, (xiv) 4 w, (xv) 8 w, (xvi) 12 w; and $(PL_{25}CL_{75})_{1k}$:POSS at (xvii) 0 w, (xviii) 4 w, (xix) 8 w and (xx)12 w. The scale bar equals 50 μm. 90

Figure 3-3: Molecular weight (M_w) as a percentage of the original, for PCL_{1k}:POSS 70:30 (○), $(PG_5CL_{95})_{1k}$:POSS 70:30 (□), $(PG_{25}CL_{75})_{1k}$:POSS 70:30 (■), $(PL_5CL_{95})_{1k}$:POSS 70:30 (◊), and $(PL_{25}CL_{75})_{1k}$:POSS 70:30 (♦).92

Figure 3-4: Weight percentage ratios for a) the soft segment and b) POSS for PCL_{1k}:POSS 70:30 (○), $(PG_5CL_{95})_{1k}$:POSS 70:30 (□), $(PG_{25}CL_{75})_{1k}$:POSS 70:30 (■), $(PL_5CL_{95})_{1k}$:POSS 70:30 (◊), and $(PL_{25}CL_{75})_{1k}$:POSS 70:30 (♦) as determined by ^{1}H-NMR. 93

Figure 3-5: Melting enthalpies for a) the soft segment and b) POSS for 1st heat (●) and 2nd heat (○) of PCL_{1k}:POSS and 1st heat (■) and 2nd heat (□) of $(PL_5CL_{95})_{1k}$:POSS.....94

Figure 3-6: a) Modulus, b) strain-to-failure, and c) elasticity, as a percentage of the original, for PCL_{1k}:POSS 70:30 (○), $(PG_5CL_{95})_{1k}$:POSS 70:30 (□), $(PG_{25}CL_{75})_{1k}$:POSS 70:30 (■), $(PL_5CL_{95})_{1k}$:POSS 70:30 (◊), and $(PL_{25}CL_{75})_{1k}$:POSS 70:30 (♦). d) Strain-to-failure for $(PG_5CL_{95})_{1k}$:POSS 70:30 over time for materials tested at dry at room temperature (gray bars) and materials tested in saline at 37 °C (white bars). 96

Figure 3-7: a) Mass loss, b) water uptake, c) molecular weight, and d) soft segment weight % for PCL_{1k}:POSS 70:30 (●), $(PL_5CL_{95})_{1k}$:POSS 70:30 (□), and $(PL_{25}CL_{75})_{1k}$:POSS 70:30 (■) for materials degraded at 60 °C. .98

Figure 3-8: a) Molecular weight (M_n) plotted on a linear scale and b) semi-log scale as a ratio with linear fits for PCL_{1k}:POSS 70:30 degraded at 23 ° C (●), 37 °C (■), and 60 °C (♦). c) Linear fit of the rate constants and temperature to determine the activation energy from the Arrhenius equation..101

Figure 3-9: Wide-angle x-ray scattering analysis of $(PL_5CL_{95})_{1k}$:POSS. 2-D scattering plots of films degraded for a) 0 w, b) 6 w) and c) 12 w. 1-D plots of intensity at each angle is shown for the d) full range of 2θ and e) a close-up of POSS's crystalline peak. 102

Figure 3-10: Small-angle x-ray scattering analysis of $(PL_5CL_{95})_{1k}$:POSS. 2-D scattering plots of films degraded for a) 0 w, b) 6 w) and c) 12 w. 1-D plots of the d) full range of q. 103

Figure 3-11: Water uptake for PCL_{1k}:POSS 100:0 (●) and PCL_{1k}:POSS 70:30 (■). 104

Figure 4-1: Cell viability (%), compared to a positive control (100%), for a) PCL_{1k}:POSS 100:0, b) PCL_{1k}:POSS 90:10, c) PCL_{1k}:POSS 80:20, d) PCL_{1k}:POSS 70:30, e) $(PG_5CL_{95})_{1k}$:POSS 70:30, f) $(PG_{25}CL_{75})_{1k}$:POSS 70:30, g) $(PL_5CL_{95})_{1k}$:POSS 70:30, and h) $(PL_{25}CL_{75})_{1k}$:POSS 70:30. These materials were incubated in media for 24, 48, and 72 h. The reference line is 70% cell viability. 120

Figure 4-2: Differential scanning calorimetry of PCL_{1k}:POSS 70:30, with second heat shown, synthesized with i) 1 wt. % tin-POMS, ii) 0.5 wt. % tin-POMS, iii) 0.1 wt. % tin-POMS, iv) 0.05 wt. % tin-POMS, v) 0.01 wt. % tin-POMS, vi) 1 wt. % tin-POMS-2P, vii) 1 wt. % tin-POMS-3P, vii) 0.1 wt. % DBTDL, and ix) 0.01 wt. % DBTDL.....123

Figure 4-3: Tensile properties of the PCL_{1k}:POSS polyurethanes a) synthesized with different catalysts and b) processed with repeated precipitations.125

Figure 4-4: Cell viability from the CCK-8 assay of materials from all synthesis and processing conditions after incubation in media for 24 h. All experimental conditions are normalized to the control of 100% cell viability. The reference line is 70% cell viability.....127

Figure 4-5: Cell viability from the CCK-8 assay of materials from all synthesis and processing conditions after incubation in media for 72 h. All experimental conditions are normalized to the control of 100% cell viability. The reference line is set at 70% cell viability. 128

Figure 5-1: Scanning electron micrographs and photographs of the different electrospun materials and dual-electrospun composites. Scanning electron micrographs of the electrospun or dual-electrospun webs for (i) TPE, (ii) 15% PCL SMEC, (iii) 25% PCL SMEC, and (iv) PCL. In the second row, images of the compacted films are shown for (v) TPE, (vi) 15% PCL SMEC, (vii) 25% PCL SMEC, and (viii) PCL. The third row of images shows the surfaces of the compacted films: (ix) TPE, (x) 15% PCL SMEC, (xi) 25% PCL SMEC, and (xii) PCL. The bottom row shows the cross section of these materials: (xiii) TPE, (xiv) 15% PCL SMEC, (xv) 25% PCL SMEC, and (xvi) PCL. 157

Figure 5-2: Differential scanning calorimetry, with the second heat shown (exotherm up) of (i) TPE, (ii) 15% PCL SMEC, (iii) 25% PCL SMEC, and (iv) PCL. 158

Figure 5-3: Dynamic mechanical analysis of (i) TPE, (ii) 15% PCL SMEC, (iii) 25% PCL SMEC, and (iv) PCL.....160

Figure 5-4: a) Tensile testing of TPE: (i) dry at room temperature and (ii) hydrated at 37 °C. b) Tensile testing hydrated (in saline solution) at 37 °C of (i) TPE, (ii) 15% PCL SMEC, (iii) 25% PCL SMEC, and (iv) PCL. Representative stress-strain curves are shown. 162

Figure 5-5: Elasticity testing of all materials. a) An example curve of a material (here TPE) stretched to 50% strain and recovered for 3 cycles. b) Strain recovery (R_E) for each material. 164

Figure 5-6: Shape memory testing for 3 cycles of the composite materials: a) 15% PCL SMEC and b) 25% PCL SMEC. 165

Figure 5-7: Mechanical properties of materials throughout degradation: a) Young's modulus (MPa) and b) strain-to-failure (%) (n=5). 167

Figure 5-8: Samples before degradation: a) actual fixed strain with reference lines indicating the target fixed strain and (b) thickness (n=3). 172

Figure 5-9: Properties of fixed SMECs throughout degradation: a) mass loss and b) water uptake (n=3). 173

Figure 5-10: Fixed strain before and after degradation (n=3). 174

Figure 5-11: Scanning electron micrographs for the SMECs degraded at different fixed strains. Surface images of a SMEC with 0% strain at (i) 0 w, (ii) 4 w, (iii) and 8 w; 50% strain at (iv) 0 w, (v) 4 w, and (vi) 8 w; and 100% strain at (vii) 0 w, (viii) 4 w, and (ix) 8 w. Scale bar represents 50 μm. 175

Figure 5-12: Scanning electron micrographs for the SMECs degraded at different fixed strains. Cross sectional images of a SMEC with 0% strain at (i) 0 w, (ii) 4 w, and (iii) 8 w; 50% strain at (iv) 0 w, (v) 4 w, and (vi) 8 w; and 100% strain at (vii) 0 w, (viii) 4 w, and (ix) 8 w. Scale bar represents 50 μm.176

Figure 5-13: The enthalpy of melting of the PCL (ΔH_{PCL}) portion of the SMECS fixed at 0% strain, 50% strain, and 100% strain (n = 3), determined from differential scanning calorimetry throughout degradation. 177

Figure 5-14: X-ray diffraction of the SMEC with different fixed strains through degradation with WAXS 2-D images on the left and SAXS 2-D images on the right. The direction of stretch is ↔.....178

Figure 5-15: Recovery profile of the SMECs with fixed strain by heating at 70 °C for several hours after they were degraded for 8 w. WAXS and SAXS profiles of before and after recovery for each. Stretch direction is ↔. Alignment of PCL in WAXS is indicated by the red arrows, alignment of POSS in WAXS is indicated by the yellow arrows, and alignment of PCL in SAXS is indicated by the white arrows. 179

Figure 6-1: Molecules that could be used with hexamethylene diisocyanate as the hard block in our polyurethanes. 195

Figure 6-2: Differential scanning calorimetry of (i) PCL_{1k}:PCL_{3k} 90:10, (ii) PCL_{1k}:PCL_{3k} 70:30, (iii) PCL_{1k}:PCL_{12k} 90:10, (iv) PCL_{80k}, (v) PCL_{1k} diol, (vi) PCL_{3k} diol, and (vii) PCL_{12k} diol. 201

Figure 6-3: Wide-angle x-ray 1-D plots of (i) PCL_{80k}, (ii) PCL_{1k}:PCL_{3k} 70:30, (iii) PCL_{1k}:PCL_{3k} 90:10, and (iv) PCL_{1k}:PCL_{12k} 90:10. 203

Figure 6-4: Wide-angle x-ray 2-D pictograms of (i) PCL_{1k}:PCL_{3k} 90:10, (ii) PCL_{1k}:PCL_{3k} 70:30, (iii) PCL_{1k}:PCL_{12k} 90:10, and (iv) PCL_{80k}. 204

Figure 6-5: Dynamic mechanical analysis of (i) PCL_{1k}:PCL_{3k} 90:10, (ii) PCL_{1k}:PCL_{3k} 70:30, (iii) PCL_{1k}:PCL_{12k} 90:10 and (iv) PCL_{80k}. 205

Figure 6-6: Elasticity testing of a) PCL_{1k}:PCL_{3k} 90:10, b) PCL_{1k}:PCL_{3k} 70:30, and c) PCL_{1k}:PCL_{12k} 90:10 at room temperature; and d) PCL_{1k}:PCL_{12k} 90:10 at 37 °C. e) Quantification of elastic recovery. 207

Figure 6-7: Shape memory test of PCL_{1k}:PCL_{12k} 90:10 polyurethane with three cycles. 208

Figure 7-1: Cumulative drug release of the four tested materials over a) 100 h and b) 6 h. 218

Figure A-1: Differential scanning calorimetry of a) soft segments with a molecular weight of 12 kDa and b) soft segment with a molecular weight of 6 kDa.226

Figure A-2: Contact angle measurements of polyurethanes with a) soft segments with a molecular weight of 12 kDa and b) soft segment with a molecular weight of 6 kDa. 228

Figure A-3: Dynamic mechanical analysis of the polyurethanes with a) soft segments with a molecular weight of 12 kDa and b) soft segment with a molecular weight of 6 kDa. 229

Figure A-4: Shape memory testing of each polyurethane with images of the dogbone initially, after fixing, and after recovery. 230

Figure A-5: Differential scanning calorimetry of two polyurethanes, with first cooling shown (exotherm up). 231

Chapter 1: Introduction and Scope of Dissertation

1.1 Biomaterials and Polymers

Biomaterials are synthetic or natural materials that are not food or drugs and interact with biological systems for treatment, augmentation or replacement of tissues.[1, 2] Biomaterials could be comprised of metals (metallic), ceramics, or polymers (polymeric). Polymers are long chain molecules that are made of repeating units.[3] Many polymers exist in nature, including wood, starch, and biological molecules such as proteins and deoxyribonucleic acids (DNA). An early example of a natural polymeric biomaterial was utilizing wood for the replacement of teeth. Alternatively, an early example synthetic of a biomaterial was poly(methyl methacrylate) (PMMA) for dentistry in the 1930s. Synthetic polymers, or polymers not found in nature, were first introduced in the 1800s and could allow for a large distribution of material.

Polymers have a variety of architectures with one or several repeating units, or monomers. Polymers with a single monomer (A) are considered homopolymers (-A-A-A-A-A-) while polymers with two or more repeating units (A) and (B) are copolymers and could be sub-classified as alternating (-A-B-A-B-A-B-), block (-A-A-A-A-B-B-B-B-) or random (-A-B-A-A-B-B-A-B-B-B-B-A-). Also, a polymer's architecture could be linear or branched. Linear polymers, or thermoplastic polymers, could be heated and flow at high temperatures, while highly branched and cross-linked, or thermoset, polymers cannot flow when heated. Polymers are synthesized by two main routes: step-growth or chain-growth polymerization. The former synthesis route is the random union of molecules while the latter is the controlled addition of monomers.

Many properties of polymers are important for its function. One important property of thermoplastic polymers is molecular weight, as the polymer's molecular weight will determine its

physical properties. Increasing a polymer's molecular weight will increase its mechanical properties to an upper limit, although a very high molecular weight could make processing difficult. Processing of polymers could be done by a variety of methods including compression molding, casting, or electrospinning (applying a high voltage to a polymer solution to produce nano- to micron-scale fibers). Other material properties include molecular, thermal, mechanical, and structural properties. Molecular properties consist of molecular weight as well as molecular composition. Thermal properties include a material's degradation profile due to temperature as well as any thermal transitions in the material, such as a glass transition (T_g), melting transition (T_m), or crystallization transition (T_c). Commonly determined mechanical properties include storage modulus, loss modulus, Young's modulus, strain-to-failure, and elastic recovery. Structural properties include nano-, micro- and macrostructure.

For biomaterials, one important property is a material's biocompatibility. Biocompatibility is defined as "the ability of a material to perform with an appropriate host response in a specific situation."[4] For some materials, this means being inert within the body and not causing toxicity. For other materials, this means interacting with tissues to elicit a specific response, such as tissue growth, wound healing, or even cell death.

1.2 Polyurethanes

Polyurethanes are a class of polymers that have urethane linkages formed by a reaction of a hydroxyl and isocyanate group, as shown in **Scheme 1-1**.[5, 6] Polyurethanes are commonly multi-block copolymers with a soft block, consisting of a polyol with flexible components and a hard block, consisting of a diisocyanate and chain extender. Generally, the hard block has a higher melting transition than the soft block. The soft block provides elasticity and extensibility while the hard block provides rigidity and strength. Many chemistries could be used in the soft segments

and chain extenders. Several isocyanate chemistries are also available, although aliphatic isocyanates are preferred over aromatic isocyanates due to the debatable toxicity of aromatic isocyanates. Finally, catalysts are generally required to synthesize polyurethanes. While many catalysts are used in research and industry, organometallic catalysts, such as organotin catalysts, are the most common.

The first commercially available polyurethane was introduced in the 1930s, although it took about 30 years before polyurethanes were used as biomaterials. Several early medical polyurethanes included a polyurethane coating for vascular grafts, as well as implantable bone fixation devices. Although there were early problems with premature degradation of polyurethanes designed for long-term implants, polyurethanes remained a prevalent biomaterial for both long-term and temporary uses. The development of biodegradable polyurethanes is the focus of this dissertation.

1.3 Biodegradable Polymers

Biodegradable polymers are materials that break down into smaller constituents within the body's environment. These constituents could be incorporated into the body's metabolic processes or removed safely (by excretion, for example).[7, 8] Biomaterials would benefit from being biodegradable, as implantable materials could to leave the body without the patient needing a second surgery or procedure to remove it. The process of degradation could occur by one of two principle modes: bulk or surface degradation. Bulk degradation occurs by random chain scission throughout the material and is characterized by a decrease in the materials molecular weight. Alternatively, surface degradation occurs only at the interface where the material interacts with the environment. The remaining material usually has a constant molecular weight. These processes could be further characterized by mechanism, which include hydrolytic or enzymatic degradation.

Hydrolytic degradation occurs when the addition of water cleaves a covalent bond. Polymers containing amide, urethane, ester, carbonate, or other bonds are susceptible to hydrolysis. Alternatively, enzymatic degradation occurs when the polymer is broken down by enzymes. Natural polymers are broken down by enzymatic degradation, as well as some synthetic polymers (such as poly(caprolactone)). Importantly, these two mechanisms are not mutually exclusive.

Several biodegradable polymers of interest, and are studied extensively in this dissertation, include poly(caprolactone), poly(lactide) and poly(glycolide), as shown in **Scheme 1-2a**. These materials are thermoplastic poly(α-esters) with hydrolytically labile ester bonds in their backbone. Poly(caprolactone) (PCL) is synthesized by ring-opening polymerization of caprolactone. PCL is a semi-crystalline polymer having a sub-ambient glass transition temperature (-60 °C) and a melting transition around 55-60 °C, which could be lowered by copolymerization with a comonomer, such as glycolide.[9-11] Its semi-crystalline nature yields desirable ductility, with a modulus around 200 MPa at room temperature. Hydrolytic degradation of this material occurs over 2-3 years due to its hydrophobicity although this degradation rate can be increased with copolymerization.[11] Also, PCL has been found to degrade faster in the presence of lipase, a digestive enzyme found in the pancreas. Poly(caprolactone) does not have a toxic effect in the body and is commercially available as a long-term contraceptive device (Capronor™).

Poly(lactide) is another commercially available polymer, which is synthesized by the ring-opening polymerization of lactide. Because the lactide monomer is chiral, it exists as three distinct forms: l-lactide, d-lactide, and meso-lactide, as shown in **Scheme 1-2b**. Homopolymers of d- or l-lactide are highly crystalline. They have a glass transition around 60-65 °C and a melting transition around 175 °C, resulting in a high modulus (~5 GPa) and slow degradation (6 months – 5 years). Copolymers of equal (or near-equal) amounts of d-lactide and l-lactide are amorphous and have a

lower glass transition around 55-60 °C. This material has a lower modulus than the lactide homopolymers around 1.9 GPa. Both poly(lactide) homopolymers and copolymers are approved for use in implantable biomedical products such as the Phantom Suture Anchor® or Resomer®, respectively.

Poly(glycolide) is synthesized by the ring-opening polymerization of glycolide. Poly(glycolide) is another semi-crystalline polymer with a glass transition temperature about 35-40 °C and a melting transition over 200 °C. Due to its super-ambient glass transition temperature and high crystallinity, this polymer has a high modulus (12.5 GPa at room temperature). Poly(glycolide) is more hydrophilic than PCL and degrades more rapidly with loss of mechanical properties occurring within the first month and mass loss after two months. Poly(glycolide) is currently FDA-approved for the use in orthopedic implant Biofix® and for the vascular closure EXOSEAL™.

1.4 Biodegradable Elastomers

Elastomers are rubber-like materials that have a recoverable strain upon stretching and are generally characterized by a low modulus and a high strain-to-failure.[12] Commonly, elastomers are polymers that are cross-linked above their glass transition temperatures. However, elastomers could be thermoplastic or thermoset with either physical or chemical cross-links, respectively. There are many elastomers used by a variety of research groups and many for biomedical applications.[12, 13] Some of the common biologically-stable thermoset elastomers include silicones, thermoset polyurethanes, and vulcanized rubber, while stable thermoplastic elastomers include polyurethanes or styrene-based polymers.

As mentioned above, biodegradable elastomers would benefit medical technology, as they would allow short-term implants or medical devices. Several thermoset biodegradable elastomers

have been studied including poly(caprolactone-co-glycolide),[14] poly(diol citrate),[15] poly(ethylene glycol-co-citric acid),[16] poly(glycerol-sebacic acid),[17] and poly(anhydride).[18] These polymers are limited in the way they can be processed, as they are cured into their final geometric shape.

Several thermoplastic biodegradable elastomers have been developed to be processable. One such system is a blend of two polymers, poly(d,l-lactide-co-glycolide) and poly(d,l-lactide-co-caprolactone).[19] This system had a variable modulus range (0.9 – 670 MPa) and strain-to-failure range up to 700%. Another thermoplastic system includes poly(ethylene oxide)/poly(caprolactone) copolymers with varying block sizes.[20] The same group also developed poly(caprolactone)/poly(lactide) polyurethanes with short-chain PCL components and various lengths of the PLA components.[21] These materials had a modulus as low as 30 MPa. Another polyurethane elastomer includes a polyurethane synthesized with poly(d,l-lactide-co-caprolactone), butane diol and hexamethylene diisocyante.[22] This material had controllable modulus, strain-to-failure (600-1300%), and high elasticity. A recent polyurethane incorporated supramolecular ionic interactions by incorporating PCL, alginate (anionic functionality) and n-methyldiethanolamine (cationic functionality) with a diisocyanate.[23] This material had a high modulus (30-100 MPa) and high elastic recovery.

1.5 Polyhedral Oligomeric Silsesquioxane (POSS)

One moiety that has been incorporated into many polymers is polyhedral oligomeric silsesquioxane, or POSS. POSS is a hybrid silicon-oxygen caged structure with a chemical structure of ($R_nSi_nO_{1.5n}$). An example of a POSS molecule is shown in **Scheme 1-3**. The organic side groups (R and R_1) at the vertex of the cage can be varied to control solubility and reactivity. POSS is generally 1-3 nm in size and has a melting point of 120 °C as a pendant group when

incorporated into polymers. Several reviews on POSS and POSS-containing materials are available in the literature.[24-27]

When incorporated into polymers, POSS has been found to provide physical cross-links,[28] oxidative stability[29] and thermal stability.[30, 31] When incorporated into biomaterials, POSS has been found to be non-toxic both *in vitro*[32] and *in vivo*[33] as part of the polymer structure and as a degradation product. POSS has also been shown to delay hydrolytic degradation[34] and suppress the enzymatic degradation.[35] POSS has been incorporated in many biodegradable materials[28, 36-38] and recently thermoset biodegradable elastomers.[39, 40]

1.6 Shape Memory Materials

Medical devices could benefit from smart technology, such as shape memory. Shape memory polymers (SMPs) are smart materials that can be fixed into a temporary shape and recovered to the original permanent shape by a stimulus such as heat,[41-43] solvent,[44, 45] light,[46, 47] pH,[48, 49] magnetism[50, 51] or electrical current.[52, 53] Many SMPs are recovered by heat, which will be the focus in this dissertation. In order for a polymer to have shape memory it must meet two requirements: 1) cross-links and 2) a switching segment.[54, 55] Cross-links allow the permanent shape to be remembered, allowing the material to recover upon the stimulus. Cross-links could be either chemical (via covalent bonds) or physical (via entanglements or crystallization). The switching segment provides mobility via a transition temperature (melting transition for semi-crystalline polymers or glass transition for amorphous polymers) that allows the material to fix in its temporary shape upon crystallization or vitrification. Upon reheating, the polymer chains are remobilized to drive the polymer back to its permanent, lower-energy shape.

One-way shape memory testing is performed in several steps, showed schematically in **Figure 1-1.**[56] First, the material is heated above its transition temperature and deformed. Under

stress, the material is cooled below its transition temperature and the material is fixed. The stress is removed, and fixing can be quantified by the fixing ratio (R_f), or how much of the strain remains after the material is unloaded. Finally, the material is reheated above its transition temperature, and the material returns to its original shape in a process called recovery. This can be quantified by the recovery ratio (R_r), or the amount of the strain that returns from the fixed state, compared to the initial strain.

1.7 Shape Memory Elastomeric Materials

Biodegradable elastomers with shape memory capabilities would be beneficial in implantable medical devices as the materials could degrade, have smart technology and would mimic the mechanical properties of many soft tissues. Several elastomeric, non-biodegradable SMPs have been developed previously.[43, 57-60] In Prof. Mather's research group, shape memory elastomeric composites (SMECs) were developed that utilized different materials for fixing and recovery. These composites were fabricated by electrospinning poly(caprolactone) and curing a poly(dimethyl siloxane) matrix around it.[61] These materials had low moduli and good shape memory properties, but the processing time with curing took several days. In order to reduce processing time and have better control of the fixing and recovery components, SMECs were fabricated by dual-electrospinning two thermoplastic polymers, Pellethane® and poly(caprolactone).[62] Thermal, mechanical and shape memory properties could be controlled by varying the composition by easily adjusting the flow rates during electrospinning. However, these SMECs were not fully biodegradable.

Recently, biodegradable shape memory elastomers have been developed with a wide array of chemistries and architectures including polycitrates,[15, 63] polyurethanes with poly(caprolactone) and poly(hydroxybutyrate),[64] of poly(lactic acid)-co-poly(amide)[65] and interpenetrating networks

of poly(ethylene glycol) dimethacrylate and poly(esterurethane).[66] From the Mather research group, shape memory elastomeric composites were developed with electrospun poly(caprolactone) and a cured poly(anhydride) to form a fully biodegradable shape memory elastomeric composite.[67] Although poly(anhydride) is considered a thermoset, it is capable of reconfiguring its permanent shape, allowing the composite to be reprocessed into a new permanent shape. This composite's matrix degrades quickly, within several days.

1.8 Scope of Dissertation

This dissertation focuses on the development of novel thermoplastic biodegradable elastomers and smart composites to be used as biomaterials, specifically focusing on low modulus materials that have high elasticity and degradation capabilities. In **Chapter 2** (adapted from McMullin et al. *Macromolecules*, 2016, [49]) a series of biodegradable elastomeric polyurethanes utilizing biodegradable soft segments and POSS as a hard segment are introduced.[68] The composition of the material was systematically varied to determine the effect of soft segment composition as well as the amount of POSS on the polyurethanes' properties. **Chapter 3** contains the report of a study of the materials of Chapter 2, which were degraded in saline solution at 37 °C and 60 °C to determine how the soft segment composition affected hydrolytic degradation. **Chapter 4** contains a report of a study wherein the same polymers were tested *in vitro* with fibroblast cells to determine cell viability. When the resultant cell viability was determined to be poor, it was hypothesized that the tin catalyst utilized in polyurethane synthesis was causing cytotoxicity. Then, study went on to vary tin catalyst concentration and type, allowing determination of the optimal amount of catalyst for synthesis.

In **Chapter 5**, the POSS-based polyurethanes introduced previously were combined with linear poly(caprolactone) via dual-electrospinning to create shape memory elastomeric composites

(SMECs). Several compositions were fabricated and tested. A single composition was also degraded at different fixed strains to determine how a fixed strain affected hydrolytic degradation. In **Chapter 6**, several replacements for POSS as the hard segment were considered to create a lower-cost elastomer, as POSS's cost is relatively high. Polyurethanes with two distinct poly(caprolactone) lengths for use as the hard segment and soft segment were synthesized. The thermal and mechanical properties of these materials were studied for several different polyurethanes with different hard block sizes and soft segment to hard segment ratios.

In **Chapter 7**, conclusions and future directions for this work are presented.

Finally, the **Appendix** highlights initial molecular, thermal and mechanical characterization of poly(ethylene glycol)-poly(caprolactone):POSS polyurethanes for soft, biodegradable semi-crystalline shape memory polymers.

1.9 References

1. Langer, R.; Tirrell, D. A., Designing materials for biology and medicine. *Nature* **2004,** *428,* 487-492.

2. Williams, D. F., On the nature of biomaterials. *Biomaterials* **2009,** *30* (30), 5897-5909. DOI: http://dx.doi.org/10.1016/j.biomaterials.2009.07.027.

3. Stevens, M. P., *Polymer Chemistry: An Introduction*. Oxford University Press: 1999.

4. Williams, D. F., On the mechanisms of biocompatibility. *Biomaterials* **2008,** *29* (20), 2941-2953. DOI: http://dx.doi.org/10.1016/j.biomaterials.2008.04.023.

5. Guelcher, S. A., Biodegradable Polyurethanes: Synthesis and Applications in Regenerative Medicine. *Tissue Engineering Part B: Reviews* **2008,** *14* (1), 3-17. DOI: http://dx.doi.org/10.1089/teb.2007.0133.

6. Gogolewski, S., Selected topics in biomedical polyurethanes. A review. *Colloid and polymer science* **1989,** *267* (9), 757-785. DOI: 10.1007/BF01410115.

7. Nair, L. S.; Laurencin, C. T., Biodegradable polymers as biomaterials. *Progress in Polymer Science* **2007,** *32* (8-9), 762-798. DOI: 10.1016/j.progpolymsci.2007.05.017.

8. Hutmacher, D. W., Scaffolds in tissue engineering bone and cartilage. *Biomaterials* **2000,** *21* (24), 2529-2543. DOI: http://dx.doi.org/10.1016/S0142-9612(00)00121-6.

9. Pack, J. W.; Kim, S. H.; Cho, I. W.; Park, S. Y.; Kim, Y. H., Microstructure analysis and thermal property of copolymers made of glycolide and epsilon-caprolactone by stannous octoate. *Journal of Polymer Science Part a-Polymer Chemistry* **2002,** *40* (4), 544-554. DOI: 10.1002/pola.10123.

10. Cai, Q.; Bei, J. Z.; Wang, S. G., Synthesis and properties of ABA-type triblock copolymers of poly(glycolide-co-caprolactone) (A) and poly(ethylene glycol) (B). *Polymer* **2002,** *43* (13), 3585-3591. DOI: 10.1016/s0032-3861(02)00197-0.

11. Kelch, S.; Steuer, S.; Schmidt, A. M.; Lendlein, A., Shape-memory polymer networks from oligo[(epsilon-hydroxycaproate)-co-glycolate]dimethacrylates and butyl acrylate with adjustable hydrolytic degradation rate. *Biomacromolecules* **2007,** *8* (3), 1018-1027.

12. Chen, Q.; Liang, S.; Thouas, G. A., Elastomeric biomaterials for tissue engineering. *Progress in Polymer Science* **2013,** *38* (3–4), 584-671. DOI: http://dx.doi.org/10.1016/j.progpolymsci.2012.05.003.

13. Yoda, R., Elastomers for biomedical applications. *Journal of Biomaterials Science, Polymer Edition* **1998,** *9* (6), 561-626. DOI: 10.1163/156856298X00046.

14. Amsden, B.; Wang, S.; Wyss, U., Synthesis and Characterization of Thermoset Biodegradable Elastomers Based on Star-Poly(ε-caprolactone-co-d,l-lactide). *Biomacromolecules* **2004,** *5* (4), 1399-1404. DOI: 10.1021/bm034538j.

15. Serrano, M. C., Novel Biodegradable Shape-Memory Elastomers with Drug-Releasing Capabilities. *Advanced materials (Weinheim) 23* (19), 2211-2215. DOI: 10.1002/adma.201004566.

16. Ding, T.; Liu, Q.; Shi, R.; Tian, M.; Yang, J.; Zhang, L., Synthesis, characterization and in vitro degradation study of a novel and rapidly degradable elastomer. *Polymer Degradation and Stability* **2006,** *91* (4), 733-739. DOI: http://dx.doi.org/10.1016/j.polymdegradstab.2005.06.007.

17. Wang, Y.; Ameer, G. A.; Sheppard, B. J.; Langer, R., A tough biodegradable elastomer. *Nat Biotech* **2002,** *20* (6), 602-606. DOI: http://www.nature.com/nbt/journal/v20/n6/suppinfo/nbt0602-602_S1.html.

18. Poetz, K. L.; Mohammed, H. S.; Snyder, B. L.; Liddil, G.; Samways, D. S. K.; Shipp, D. A., Photopolymerized Cross-Linked Thiol–Ene Polyanhydrides: Erosion, Release, and Toxicity Studies. *Biomacromolecules* **2014,** *15* (7), 2573-2582. DOI: 10.1021/bm500420q.

19. Wang, L.; Zhang, Z.; Chen, H.; Zhang, S.; Xiong, C., Preparation and characterization of biodegradable thermoplastic Elastomers (PLCA/PLGA blends). *Journal of Polymer Research* **2010,** *17* (1), 77-82. DOI: 10.1007/s10965-009-9292-9.

20. Cohn, D.; Stern, T.; González, M. F.; Epstein, J., Biodegradable poly(ethylene oxide)/poly(ϵ-caprolactone) multiblock copolymers. *Journal of Biomedical Materials Research* **2002,** *59* (2), 273-281. DOI: 10.1002/jbm.1242.

21. Cohn, D.; Hotovely Salomon, A., Designing biodegradable multiblock PCL/PLA thermoplastic elastomers. *Biomaterials* **2005,** *26* (15), 2297-2305. DOI: http://dx.doi.org/10.1016/j.biomaterials.2004.07.052.

22. Wang, W.; Ping, P.; Yu, H.; Chen, X.; Jing, X., Synthesis and characterization of a novel biodegradable, thermoplastic polyurethane elastomer. *Journal of Polymer Science, Part A: Polymer Chemistry* **2006,** *44* (19), 5505-5512. DOI: 10.1002/pola.21643.

23. Daemi, H.; Rajabi-Zeleti, S.; Sardon, H.; Barikani, M.; Khademhosseini, A.; Baharvand, H., A robust super-tough biodegradable elastomer engineered by supramolecular ionic interactions. *Biomaterials* **2016,** *84*, 54-63. DOI: http://dx.doi.org/10.1016/j.biomaterials.2016.01.025.

24. Li, G.; Wang, L.; Ni, H.; Pittman, C. U., Polyhedral Oligomeric Silsesquioxane (POSS) Polymers and Copolymers: A Review. *Journal of Inorganic and Organometallic Polymers 11* (3), 123-154. DOI: 10.1023/A:1015287910502.

25. Wu, J.; Mather, P. T., POSS Polymers: Physical Properties and Biomaterials Applications. *Polymer Reviews* **2009,** *49* (1), 25-63. DOI: 10.1080/15583720802656237.

26. Joshi, M.; Butola, B. S., Polymeric Nanocomposites—Polyhedral Oligomeric Silsesquioxanes (POSS) as Hybrid Nanofiller. *Journal of Macromolecular Science, Part C* **2004,** *44* (4), 389-410. DOI: 10.1081/MC-200033687.

27. Tanaka, K., Advanced functional materials based on polyhedral oligomeric silsesquioxane (POSS). *Journal of materials chemistry* **2012,** *22* (5), 1733-1746. DOI: 10.1039/C1JM14231C.

28. Knight, P. T.; Lee, K. M.; Qin, H.; Mather, P. T., Biodegradable Thermoplastic Polyurethanes Incorporating Polyhedral Oligosilsesquioxane. *Biomacromolecules* **2008,** *9* (9), 2458-2467. DOI: 10.1021/bm8004935.

29. Janowski, B.; Pielichowski, K., Thermo(oxidative) stability of novel polyurethane/POSS nanohybrid elastomers. *Thermochimica Acta* **2008,** *478* (1-2), 51-53. DOI: 10.1016/j.tca.2008.08.015.

30. Lewicki, J. P.; Pielichowski, K.; De la Croix, P. T.; Janowski, B.; Todd, D.; Liggat, J. J., Thermal degradation studies of polyurethane/POSS nanohybrid elastomers. *Polymer Degradation and Stability* **2010,** *95* (6), 1099-1105. DOI: 10.1016/j.polymdegradstab.2010.02.021.

31. Chattopadhyay, D. K., Thermal stability and flame retardancy of polyurethanes. *Progress in polymer science 34* (10), 1068-1133. DOI: 10.1016/j.progpolymsci.2009.06.002.

32. Gupta, A.; Vara, D. S.; Punshon, G.; Sales, K. M.; Winslet, M. C.; Seifalian, A. M., In vitro small intestinal epithelial cell growth on a nanocomposite polycaprolactone scaffold. *Biotechnology and Applied Biochemistry* **2009,** *54*, 221-229. DOI: 10.1042/ba20090214.

33. Knight, P. T.; Kirk, J. T.; Anderson, J. M.; Mather, P. T., In vivo kinetic degradation analysis and biocompatibility of aliphatic polyester polyurethanes. *Journal of Biomedical Materials Research Part A* **2010,** *94A* (2), 333-343. DOI: 10.1002/jbm.a.32806.

34. Kannan, R. Y.; Salacinski, H. J.; Odlyha, M.; Butler, P. E.; Seifalian, A. M., The degradative resistance of polyhedral oligomeric silsesquioxane nanocore integrated polyurethanes: An in vitro study. *Biomaterials* **2006,** *27* (9), 1971-1979. DOI: http://dx.doi.org/10.1016/j.biomaterials.2005.10.006.

35. Gu, X.; Wu, J.; Mather, P. T., Polyhedral Oligomeric Silsesquioxane (POSS) Suppresses Enzymatic Degradation of PCL-Based Polyurethanes. *Biomacromolecules* **2011,** *12* (8), 3066-3077. DOI: 10.1021/bm2006938.

36. Knight, P. T., PLGA−POSS End-Linked Networks with Tailored Degradation and Shape Memory Behavior. *Macromolecules 42* (17), 6596-6604. DOI: 10.1021/ma901237h.

37. Liu, Y., Star-shaped poly(ε-caprolactone) with polyhedral oligomeric silsesquioxane core. *Polymer (Guilford)* **2006,** *47* (19), 6814-6825. DOI: 10.1016/j.polymer.2006.07.050.

38. Pan, H.; Qiu, Z., Biodegradable Poly(l-lactide)/Polyhedral Oligomeric Silsesquioxanes Nanocomposites: Enhanced Crystallization, Mechanical Properties, and Hydrolytic Degradation. *Macromolecules* **2010,** *43* (3), 1499-1506. DOI: 10.1021/ma9023685.

39. Du, Y.; Yu, M.; Chen, X.; Ma, P. X.; Lei, B., Development of Biodegradable Poly(citrate)-Polyhedral Oligomeric Silsesquioxanes Hybrid Elastomers with High Mechanical Properties and Osteogenic Differentiation Activity. *ACS Applied Materials & Interfaces* **2016,** *8* (5), 3079-3091. DOI: 10.1021/acsami.5b10378.

40. Xie, M.; Ge, J.; Lei, B.; Zhang, Q.; Chen, X.; Ma, P. X., Star-Shaped, Biodegradable, and Elastomeric PLLA-PEG-POSS Hybrid Membrane With Biomineralization Activity for Guiding Bone Tissue Regeneration. *Macromolecular Bioscience* **2015,** *15* (12), 1656-1662. DOI: 10.1002/mabi.201500237.

41. Lendlein, A.; Langer, R., Biodegradable, Elastic Shape-Memory Polymers for Potential Biomedical Applications. *Science* **2002,** *296* (5573), 1673.

42. Tobushi, H., Thermomechanical properties in a thin film of shape memory polymer of polyurethane series. *Smart materials and structures 5* (4), 483-491. DOI: 10.1088/0964-1726/5/4/012.

43. Liu, C., Chemically Cross-Linked Polycyclooctene: Synthesis, Characterization, and Shape Memory Behavior. *Macromolecules 35* (27), 9868-9874. DOI: 10.1021/ma021141j.

44. Huang, W. M., Water-driven programmable polyurethane shape memory polymer: Demonstration and mechanism. *Applied physics letters* **2005,** *86* (11), 114105. DOI: 10.1063/1.1880448.

45. Hu, Z., Synthesis and application of modulated polymer gels. *Science (New York, N.Y.)* **1995,** *269* (5223), 525-527.

46. Lendlein, A.; Jiang, H.; Jünger, O.; Langer, R., Light-induced shape-memory polymers. *Nature* **2005,** *434* (7035), 879-882. DOI: 10.1038/nature03496.

47. Lee, K. M., Light-activated shape memory of glassy, azobenzene liquid crystalline polymer networks. *Soft matter* **2011,** *7* (9), 4318. DOI: 10.1039/c1sm00004g.

48. Hu, Y., A Shape-Memory DNA-Based Hydrogel Exhibiting Two Internal Memories. *Angewandte Chemie (International ed.) 55* (13), 4210-4214. DOI: 10.1002/anie.201511201.

49. Han, X.-J., pH-Induced Shape-Memory Polymers. *Macromolecular rapid communications. 33* (12), 1055-1060. DOI: 10.1002/marc.201200153.

50. Mohr, R.; Kratz, K.; Weigel, T.; Lucka-Gabor, M.; Moneke, M.; Lendlein, A., Initiation of shape-memory effect by inductive heating of magnetic nanoparticles in thermoplastic polymers. *Proceedings of the National Academy of Sciences of the United States of America* **2006,** *103* (10), 3540-3545.

51. Schmidt, A. M., Electromagnetic Activation of Shape Memory Polymer Networks Containing Magnetic Nanoparticles. *Macromolecular Rapid Communications* **2006,** *27* (14), 1168-1172. DOI: 10.1002/marc.200600225.

52. Luo, X., Conductive shape memory nanocomposites for high speed electrical actuation. *Soft matter* **2010,** *6* (10), 2146-2149. DOI: 10.1039/c001295e.

53. Cho, J. W., Electroactive Shape-Memory Polyurethane Composites Incorporating Carbon Nanotubes. *Macromolecular rapid communications. 26* (5), 412-416. DOI: 10.1002/marc.200400492.

54. Lendlein, A.; Kelch, S., Shape-Memory Polymers. *Angewandte Chemie International Edition* **2002,** *41* (12), 2034-2057. DOI: 10.1002/1521-3773(20020617)41:12<2034::AID-ANIE2034>3.0.CO;2-M.

55. Liu, C.; Qin, H.; Mather, P. T., Review of progress in shape-memory polymers. *Journal of Materials Chemistry* **2007,** *17* (16), 1543-1558. DOI: 10.1039/B615954K.

56. Mather, P. T.; Luo, X.; Rousseau, I. A., Shape Memory Polymer Research. *Annual Review of Materials Research* **2009,** *39* (1), 445-471. DOI: 10.1146/annurev-matsci-082908-145419.

57. Rousseau, I. A., Shape Memory Effect Exhibited by Smectic-C Liquid Crystalline Elastomers. *Journal of the American Chemical Society 125* (50), 15300-15301. DOI: 10.1021/ja039001s.

58. Heuwers, B., Shape-Memory Natural Rubber: An Exceptional Material for Strain and Energy Storage. *Macromolecular chemistry and physics 214* (8), 912-923. DOI: 10.1002/macp.201200649.

59. Li, J., Semi-crystalline two-way shape memory elastomer. *Polymer (Guilford) 52* (23), 5320-5325. DOI: 10.1016/j.polymer.2011.09.030.

60. Wilson, T. S., Shape memory polymers based on uniform aliphatic urethane networks. *Journal of applied polymer science 106* (1), 540-551. DOI: 10.1002/app.26593.

61. Luo, X., Preparation and Characterization of Shape Memory Elastomeric Composites. *Macromolecules 42* (19), 7251-7253. DOI: 10.1021/ma9015888.

62. Robertson, J. M.; Birjandi Nejad, H.; Mather, P. T., Dual-Spun Shape Memory Elastomeric Composites. *ACS Macro Letters* **2015,** *4* (4), 436-440. DOI: 10.1021/acsmacrolett.5b00106.

63. Espinha, A.; Concepción Serrano, M.; Blanco, Á.; López, C. In *Shape-memory effect for self-healing and biodegradable photonic systems*, 2014; pp 91270B-91270B-13.

64. Hsu, S.-h., Synthesis and characterization of waterborne polyurethane containing poly(3-hydroxybutyrate) as new biodegradable elastomers. *Journal of materials chemistry. B, Materials for biology and medicine* **2015,** *3* (47), 9089-9097. DOI: 10.1039/C5TB01773D.

65. Zhang, W., Surprising shape-memory effect of polylactide resulted from toughening by polyamide elastomer. *Polymer (Guilford) 50* (5), 1311-1315. DOI: 10.1016/j.polymer.2009.01.032.

66. Zhang, S.; Feng, Y.; Zhang, L.; Sun, J.; Xu, X.; Xu, Y., Novel interpenetrating networks with shape-memory properties. *Journal of Polymer Science Part A: Polymer Chemistry* **2007,** *45* (5), 768-775. DOI: 10.1002/pola.21832.

67. Lawton, M. I.; Tillman, K. R.; Mohammed, H. S.; Kuang, W.; Shipp, D. A.; Mather, P. T., Anhydride-Based Reconfigurable Shape Memory Elastomers. *ACS Macro Letters* **2016,** *5* (2), 203-207. DOI: 10.1021/acsmacrolett.5b00854.

68. McMullin, E.; Rebar, H. T.; Mather, P. T., Biodegradable Thermoplastic Elastomers Incorporating POSS: Synthesis, Microstructure, and Mechanical Properties. *Macromolecules* **2016,** *49* (10), 3769-3779. DOI: 10.1021/acs.macromol.6b00470.

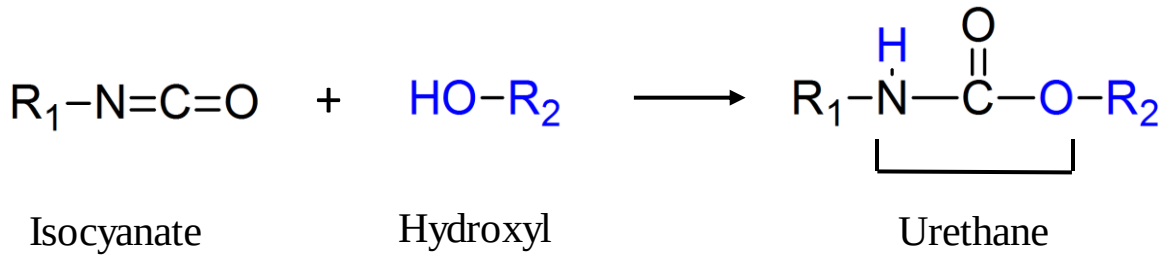

Scheme 1-1: A schematic of a urethane bond formation from a hydroxyl and an isocyanate.

a)

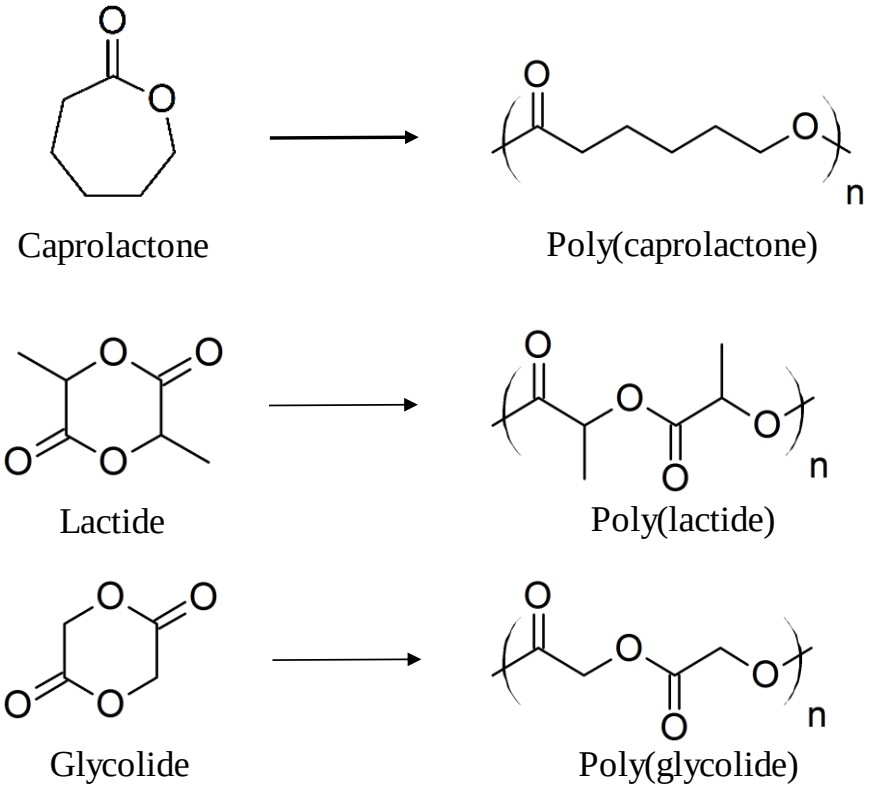

b)

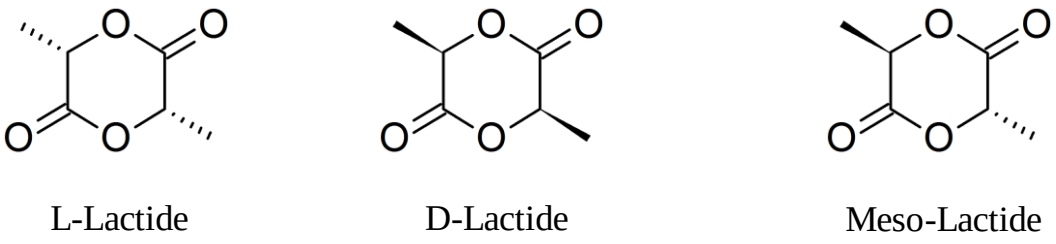

Scheme 1-2: a) Schematics of the caprolactone, lactide, and glycolide monomers and their respective polymers. b) The monomers of the different chiral forms of lactide: l-lactide, d-lactide, and meso-lactide.

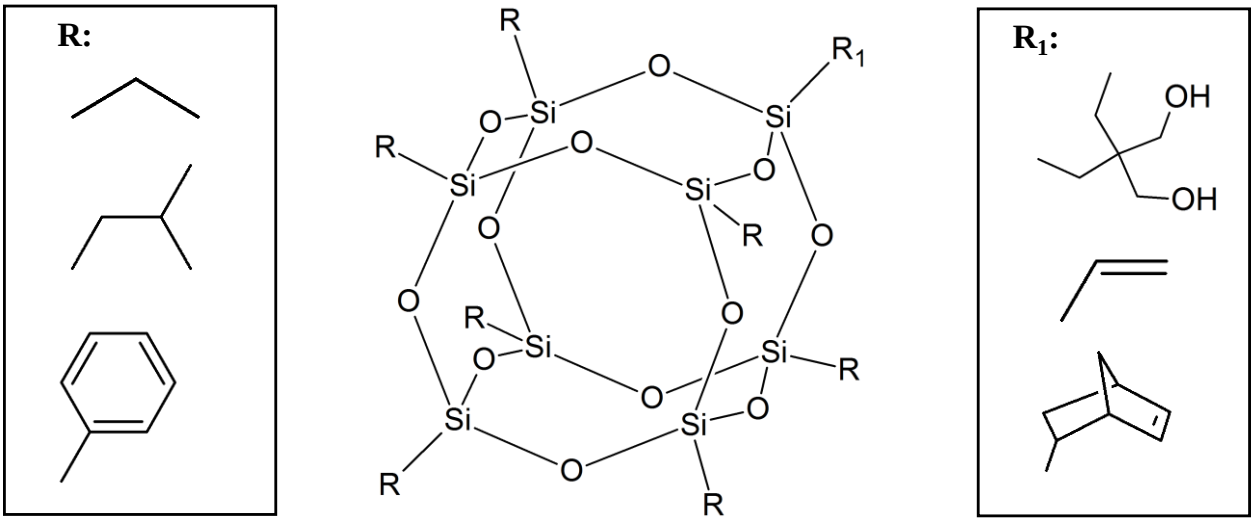

Scheme 1-3: A POSS molecule, with some examples of R and R_1 groups.

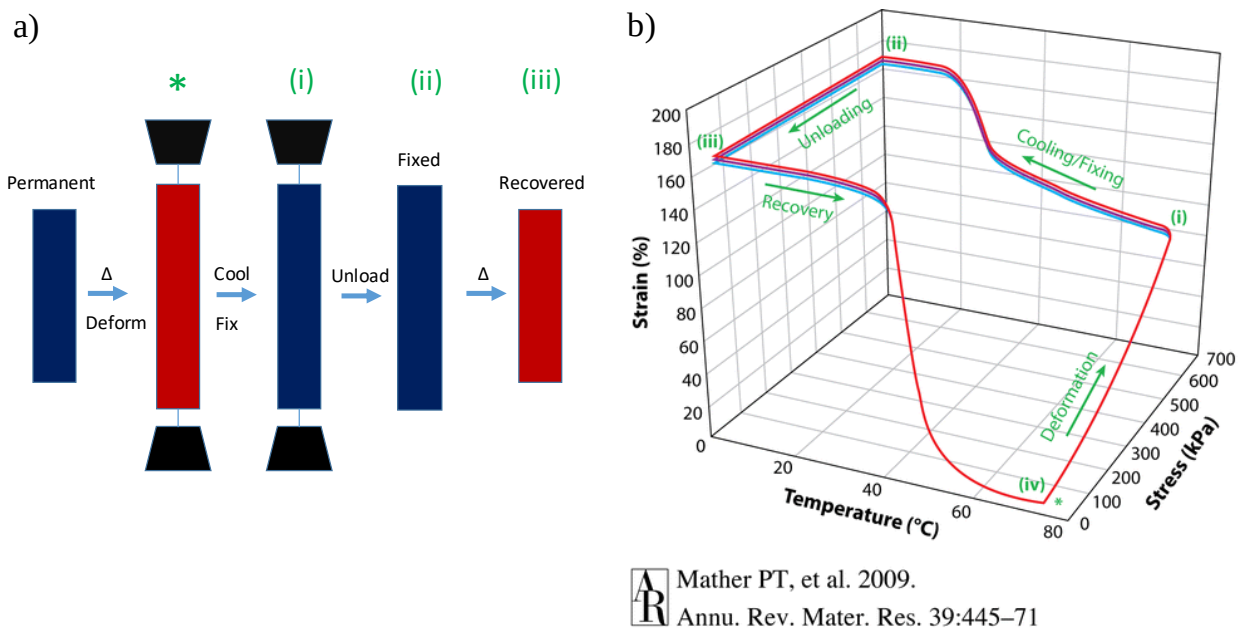

Figure 1-1: a) A schematic of a one-way shape memory cycle. b) A three-dimensional plot of stress, temperature, and strain of a one-way shape memory cycle.

*Chapter 2: Biodegradable Thermoplastic Elastomers Incorporating POSS: Synthesis, Microstructure, and Mechanical Properties**

2.1 Synopsis

A need exists for biodegradable thermoplastic elastomers with tailorable mechanical and degradation properties. Toward meeting this need, we introduce a family of biodegradable thermoplastic elastomers that feature soft segments based on caprolactone, caprolactone-d,l-lactide or caprolactone-glycolide copolymers of low crystallinity, combined with a POSS-based hard segment with relatively low melting transition. Molecular characterization of the polyols and polyurethanes indicate good control over the composition and molecular weights, with high molecular weights for the polyurethanes, as desired. Thermal, mechanical, and microstructural characterization enabled establishment of structure-property relationships. Incorporation of two different comonomers was effective in diminishing soft segment crystallinity, positively impacting elasticity, while increasing POSS content proved effective in establishing thermally robust elastic behavior as well as mechanically reinforcing the polyurethanes. Pre-straining the new thermoplastic elastomers was found to positively impact elasticity, which we attribute to enhancement of phase separation of the two blocks with support from thermal and x-ray diffraction studies.

2.2 Introduction

There is a need for biodegradable thermoplastic elastomers that meet requirements of softness and elasticity in a variety of applications, while being amenable to conventional plastics processing technology. Applications range from medical device coatings to drug delivery and even tissue engineering. For example, biodegradable elastomeric scaffolds could enable the construction or modeling of several soft tissues that include blood vessels, cartilage, smooth

*Reprinted with permission from Biodegradable Thermoplastic Elastomers Incorporating POSS: Synthesis, Microstructure, and Mechanical Properties. Erin McMullin, Hannah T. Rebar, and Patrick T. Mather. *Macromolecules* **2016** *49* (10), 3769-3779. DOI: 10.1021/acs.macromol.6b00470.

muscle cells and cardiovascular tissue.[1, 2] Further, a multitude of implantable devices, such as stents,[3] sutures,[4] and biosensors[5] could benefit from the integration of a biodegradable elastomer within their design. In light of this strong need, an increasing level of attention has been given to the development biodegradable elastomers with tailored properties.

A number of implantable devices that have been approved by the FDA contain biodegradable (but not elastomeric) polymers, including: poly(caprolactone), poly(glycolide), and poly(d,l-lactide).[6] These materials have distinct properties controlled by their compositions. Poly(caprolactone) (PCL) is semi-crystalline, has a low glass transition temperature (-60 °C) and a melting transition temperature around 55-60 °C.[6] Its semi-crystalline morphology yields desirable ductility at room temperature. Hydrolytic degradation of this polymer occurs over 2-3 years due to its hydrophobicity. PCL is non-toxic, and is approved for commercial use in biomedical devices, including a long-term contraceptive device (Capronor™)[7] and in a surgical suture (Artelon™). Poly(glycolide) is another semi-crystalline polymer with a higher glass transition temperature between 35 and 40 °C and a melting transition over 200 °C.[6] Owing to its super-ambient T_g and high crystallinity, this polymer has a high modulus -- around 12.5 GPa at room temperature. Unlike PCL, the hydrophilicity of poly(glycolide) results in degradation (mass loss) after 2 months with loss of mechanical properties during the first month.[7] Poly(glycolide) is currently FDA-approved for use in the orthopedic implant Biofix®[7] and for the vascular closure device EXOSEAL™. Poly(lactide) is still another biodegradable, commercially available polymer, which is synthesized by ring-opening polymerization of lactide. Because the lactide monomer is chiral it exists in three forms, l-lactide, d-lactide, and meso-lactide. Homopolymers of l-lactide or d-lactide are highly crystalline with a glass transition between 60-65 °C and a melting transition around 175 °C, while co-polymers of equal (and near-equal) amounts of l-lactide and d-

lactide are amorphous, with a glass transition temperature between 55-60 °C. Poly(l-lactide) has a relatively high modulus (4.8 GPa) and degrades more slowly (6 months – 5 years) than poly(d,l-lactide), which has a lower modulus (1.9 GPa) and degrades more quickly.[6]

There are two main types of biodegradable elastomers: thermosets and thermoplastics. Biodegradable thermosets are covalently cross-linked materials generally synthesized by melt polycondensation or UV curing. This type of synthesis has been used to develop a variety of polymer and copolymer systems: poly(caprolactone-co-lactide),[8] poly(diol citrate),[9] poly(ethylene glycol-co-citric acid),[10] poly(anhydride),[11] and poly(glycerol-sebacic acid).[12] While these polymers have tunable mechanical and degradation properties, they are limited to processes that simultaneously cross-link and geometrically form the final articles.

Alternatively, thermoplastic elastomers (TPEs) can be processed by a variety of methods and several thermoplastic, biodegradable elastomers have been reported. One such thermoplastic system featured a blend of two polymers, poly(d,l-lactide-co-caprolactone) and poly(d,l-lactide-co-glycolide).[13] This system allowed a wide range of moduli (0.9 – 670 MPa) and a range of strains-to-failure up to 700%. In addition, a number of TPEs reported have been copolymer polyurethanes that feature facile composition variation. One such copolymer is a polyurethane with poly(d,l-lactide-co-caprolactone), butane diol and hexamethylene diisocyanate.[14] This material has a controllable modulus (10-47 MPa), strain-to-failure (600-1300%), and high elasticity. However, the melt temperature of this material is > 170 °C which introduces the potential for premature degradation during melt processing. Another TPE utilizing urethane chemistry is a polymer that incorporates supramolecular ionic interactions to achieve high elasticity.[15] This material incorporates PCL, alginate (anionic functionality) and n-methyldiethanolamine (cationic functionality) with a diisocyanate to form a polyurethane. This

material has high elasticity that can withstand many cycles without hysteresis, but the modulus of these materials (30-100 MPa) may be too high for some applications.

The approach we have adopted for the present work involves the use of polyhedral oligomeric silsesquioxane (subsequently referred to as POSS), a silicon-oxygen caged structure ($R_nSi_nO_{1.5n}$) that is about 3 nm in size and has a melting point around 120 °C as a pendant group within polymers. Several reviews on POSS and POSS-containing materials are reported in the literature.[16-19] POSS has been incorporated into many polymers to provide thermal stability,[20, 21] oxidative stability,[22] and physical cross-links.[23] Incorporated into biomaterials, POSS is biocompatible *in vitro*[24] and *in* vivo[25] as part of a polymer structure and as a product of polymer degradation. Interestingly, particular compositions involving both POSS and PEO have been shown to suppress enzymatic degradation of PCL *in vitro.*[26] POSS has been incorporated into many biodegradable materials[23, 27-29] and recently, thermoset biodegradable elastomers.[30, 31]

Our goal with the present study was to develop biodegradable thermoplastic elastomers that have a low modulus (<15 MPa), high strain-to-failure, low melt processing temperatures and the potential for controllable degradation. Our approach to designing these elastomers was to synthesize linear polyurethanes with a short, biodegradable soft segment and POSS in the hard segment. The soft segment could be designed to control the thermal and degradation properties of the material and POSS would serve as a physical cross-linker that holds adjacent chains together. In this way, the properties of the elastomers could be engineered by controlling both the soft segment:POSS ratio and the chemical composition of the soft segment.

2.3 Methods

2.3.1 Materials

1,4-butanediol (≥ 99%), 1,4-dioxane-2,5-dione (glycolide, ≥ 99%), 3,6-dimethyl-1,4-dioxane-2,5-dione (d,l-lactide), ε-caprolactone (≥ 97%), and tin(II) 2-ethylhexanoate (stannous octoate, 95%) were all purchased from Sigma-Aldrich. Glycolide and d,l-lactide were purified by recrystallization by dissolving in ethyl acetate (Fisher Scientific, Inc.) under reflux at a concentration of 0.2 g/mL, placed in a -4 °C freezer overnight, and vacuum dried extensively prior to use. ε-Caprolactone was purified by vacuum distillation prior to use. Poly(ε-caprolactone) diol (M_w ~ 1,250 g/mol) was purchased from Polysciences, Inc. 1,2-PropanediolIsobutyl POSS (AL0130), subsequently referred to as POSS diol, and Tin-POMS catalyst were purchased from Hybrid Plastics. Hexamethylene diisocyanate (HDI) was purchased from Sigma-Aldrich and used as received. Toluene, tetrahydrofuran (THF), and *n*-hexanes were purchased from Fisher Scientific. Toluene was dried by refluxing over calcium hydride (Sigma-Aldrich) several times until collection prior to use, and stored over 3 Å molecular sieves (Sigma-Aldrich). Deuterated chloroform (chloroform-d, 99.8% atom D) and HPLC-grade THF were purchased from Sigma-Aldrich.

2.3.2 Diol Synthesis

Poly(glycolide-co-caprolactone)$_{1k}$ diols $(PGCL)_{1k}$ and Poly(d,l-lactide-co-caprolactone)$_{1k}$ $(PLCL)_{1k}$ diols were synthesized by ring-opening polymerization of glycolide or d,l-lactide and caprolactone in the presence of butane diol with a target molecular weight (M_n) of 1,000 g/mol (1 kDa), as shown in **Scheme 2-1**. As a representative example, the detailed procedure to synthesize $(PG_{25}CL_{75})_{1k}$ (with 25 mol % of glycolide, and 75 mol % of caprolactone) is described. Here, one mole of glycolide indicates one mole of monomer rings (with two repeating units each when ring-

opened). In a 250 mL Schlenk flask, 5.11 g (0.044 moles) of glycolide were added with a magnetic stir bar. The flask was vacuumed extensively and purged with nitrogen gas several times. Next, 15.08 g (0.132 moles, 14.64 mL) of ε-caprolactone, 2.0 g (0.22 moles, 1.96 mL) of butane diol, and 5 drops of tin 2-ethylhexanoate were added via syringe to the air-free flask. The flask was then heated to 140 °C (over the course of a half hour) and reacted for 10 h under nitrogen. Once the reaction was complete, the flask was cooled to room temperature. The resulting polymer was a tacky white solid (or a clear liquid for higher amounts of comonomer). The polymer was dissolved in 40 mL of THF and precipitated in excess cold n-hexanes (~400 mL). The diol was collected, dried and characterized for molecular and thermal composition and properties prior to polyurethane synthesis.

2.3.3 Polyurethane Synthesis

Either a purchased poly(caprolactone)$_{1k}$ (PCL_{1k}) diol or a synthesized diol ($(PGCL)_{1k}$ or $(PLCL)_{1k}$) was used as the soft block for the polyurethane reactions, POSS diol was used in the hard block, and hexamethylene diisocyanate (HDI) was the diisocyanate used to link the diols, resulting in a random, multi-block polyurethane, shown in **Scheme 2-2**. Nomenclature of the polymers includes the soft block (either PCL_{1k}, $(PGCL)_{1k}$, or $(PLCL)_{1k}$) and POSS with the weight percent ratios (PCL_{1k}:POSS 70:30 for 70 wt. % of PCL_{1k} and 30 wt. % of POSS). As a representative example, a detailed explanation of PCL_{1k}:POSS 70:30 will be given. Prior to synthesis, all solid reactants were dried under vacuum overnight. First 7 g (5.60 mmol) of PCL_{1k} and 3 g (3.16 mmol) of POSS were added to a 250 mL air-free Schlenk flask with a magnetic stir bar. The flask was then vacuumed extensively and purged with nitrogen gas several times. 100 mL of toluene (10% weight/volume) was added to the reaction flask, and heated to 65 °C for the reactants to dissolve. Once dissolved, 1.48 g HDI (8.80 mmol or 1.41 mL) was added to the flask,

which was heated to 100 °C. Tin-POMS (1 wt. %) was added to the flask, which was reacted at 100 °C under nitrogen for 20 hours. For $(PGCL)_{1k}$:POSS and $(PLCL)_{1k}$:POSS syntheses, small amounts of HDI were added over time to compensate for the broad distribution of the soft segment molecular weights and slightly high estimation of the molecular weight as determined by GPC. For example, if the polymer was determined to have an M_w of 2 kDa, HDI was added for diol M_w corresponding to 2 kDa, and then the difference in HDI was added for diol M_w equal to 1.95 kDa, 1.9 kDa, 1.85 kDa, etc. until a slight increase in viscosity of the reaction flask was observed, indicating an increase in molecular weight. The polyurethane product was precipitated in an excess of cold n-hexanes (600 mL n-hexanes/ 100 mL toluene) leading to a white, stretchy precipitate. This polymer was collected and dried for 3 d in a vacuum oven at room temperature.

2.3.4 Proton Nuclear Magnetic Resonance (^{1}H-NMR)

Diols and polyurethanes were dissolved in deuterated chloroform ($CDCl_3$) at a concentration of 10-20 mg/mL. The samples were analyzed in a Bruker Avance III HD 400 MHz spectrometer equipped with a 5 mm outer diameter Prodigy probe. A standard 1D pulse sequence was used with a 30° pulse, relaxation delay time of 1 s at a temperature of 25 °C.

2.3.5 Gel Permeation Chromatography (GPC)

Molecular weight (M_n and M_w) and polydispersity index (M_w/M_n) were determined from gel permeation chromatography (GPC). Samples were dissolved in tetrahydrofuran (THF) at a concentration of 2-5 mg/mL and were passed through a 0.2 μm PTFE filter before injection. A Waters Isocratic HPLC System equipped with a temperature controlled differential refractometer (Waters 2414) was used along with a multi-angle laser light scattering system (Wyatt miniDAWN) using three angles (45°, 90°, 135°) for in-line absolute molecular weight determination.

2.3.6 Differential Scanning Calorimetry (DSC)

Thermal properties of the materials were studied by differential scanning calorimetry (DSC) using the TA Q200 instrument. Heat flow was collected while the sample was heated to 200 °C (to remove thermal history), cooled to -70 °C, and heated a second time to 200 °C. The heating rate was 10 °C/min and the cooling rate was 5 °C/min. The second heat was used to determine glass transition temperature (T_g, a step in the curve) and the change in heat capacity or melting transitions (T_m, the peak of the endotherm) and the enthalpy of melting (ΔH, area under the curve). Crystallinity of the soft segment (χ_{Diol}) was calculated from the following equation:

$$\chi_{Diol}\,(\%) = \frac{\Delta H_{PCL}}{\Delta H_{o,PCL}} * \frac{1}{W_{PCL}} * 100 \qquad \textbf{(2-1)}$$

Where $\Delta H_{o,PCL}$ is 126 J/g[32] and W_{PCL} is the weight fraction of PCL in the polymer.

2.3.7 Compression Molding

The PCL_{1k}:POSS, $(PGCL)_{1k}$:POSS, and $(PLCL)_{1k}$:POSS polyurethanes were compression molded into films using a Carver 3851-0 press with heating platens. The platens were heated to 130 ºC, slightly above the T_m of POSS, or 70 °C for PCL_{1k}:POSS 100:0 (as the melting point of this material was only 31 °C). After the platens equilibrated, the polymer was placed between two Teflon sheets with a 0.45 mm thick Teflon spacer. A compressive force of 1 metric ton was applied at elevated temperature and held for 2 minutes. Then the film was cooled to 70 °C, where the polymer was annealed for 30 minutes to promote hard block crystallization, and was then cooled to room temperature. PCL_{1k}:POSS 100:0 was not annealed (as there was no POSS to crystallize during annealing). The resulting films were flexible and between 0.4 and 0.5 mm in thickness, determined by a digital caliper. All films except PCL_{1k}:POSS 100:0 were transparent, while 100:0 was white.

2.3.8 Wide-Angle X-Ray Scattering (WAXS)

Wide-angle x-ray scattering (WAXS) experiments were conducted to ascertain the molecular and nano-scale ordering and orientation of the various polymeric samples. For this purpose, a Rigaku S-MAX3000 pinhole camera system was utilized, with a MicroMax-002 generator operating with Cu Kα emission (λ = 1.5406), voltage of 45 kV and current of 0.88 mA. Wide-angle scattering patterns were collected at a sample-detector distance of 122.7 mm (resulting in scattering angles $3° < 2\theta < 40°$) using Fujifilm image plates (CR HR-V) with a FujiFilm FLA7000 reader. Samples were exposed to radiation to achieve adequate x-ray counts for analysis, which was performed using SAXSgui software v2.03.04.

2.3.9 Tensile Testing

A Linkam TST 350 apparatus and TestResources Model 100P Universal Testing Machine were both utilized to determine the tensile properties of the materials. Samples were cut in a dogbone geometry (ASTM Standard D638-03 Type IV, scaled down by a factor of 4) and stretched at a rate of 50 µm/s at room temperature (about 23 °C). Young's modulus and strain-to-failure were determined from engineering stress vs. engineering strain plots.

2.3.10 Elasticity Testing

Elasticity, here termed R_E, was determined using the "squeeze/pull off" test of a TA AR-G2 Rheometer with custom tensile clamps (**Figure 2-7b**). Dogbone samples were stretched 50 µm/s to a 50% strain and then returned to the starting position at the same rate. Elasticity was determined from the following equation:

$$R_E\,(\%) = \frac{\varepsilon_f - \varepsilon_r}{\varepsilon_f - \varepsilon_i} * 100 \qquad \textbf{(2-2)}$$

Where ε_i is a small initial strain (where stress equals zero), ε_f is the strain that the polymer is stretched to, and ε_r is the strain recovered (where stress equals zero upon unloading).

2.3.11 Dynamic Mechanical Analysis (DMA)

A TA Instruments Q800 dynamic mechanical analyzer (DMA) was utilized to determine the temperature-dependent viscoelastic properties of the polyurethanes. Samples in a dogbone geometry were loaded at room temperature, cooled to -20 °C and heated to 140 °C at a rate of 3 °C/minute. In order to maintain tension, applied load was kept at 108% of dynamic load. All experiments were performed with a frequency of 1 Hz and 15 μm (<0.1%) amplitude.

2.3.12 Impact of Pre-strain on Elasticity

Samples in a dogbone geometry were stretched to a variety of strains (25%, 50%, 100% and 250%) and then allowed to recover to their maximum extent upon unloading. The effect of such pre-stretching was studied with first-heat DSC and WAXS. Pre-stretched samples were also tested for elasticity using a common strain percentage (50%) and observing recovery, as described above.

2.3.13 Statistical Analysis

T-tests were performed on two means with unequal variances to determine the statistical significance of different sets of data. Two-tailed t-tests with a confidence value of $\alpha = 0.05$ was used for all tests.

2.4 Results

2.4.1 Diol Synthesis and Characterization

Diols with a targeted molecular weight of 1 kDa were synthesized by ring-opening polymerization of caprolactone and a comonomer (glycolide or d,l-lactide) in the presence of butane diol (the initiator), as shown in **Scheme 2-1**. Polyols were synthesized with a 5 or 25 mol % (feed ratio) of either d,l-lactide or glycolide. The results of the syntheses and PCL_{1k} diol are summarized in **Table 2-1**. ^{1}H-NMR, with example spectra displayed in **Figure 2-1,** revealed

product comonomer ratios close to the targeted values. The molecular weights were higher than expected (with M_w about 2.5 kDa for all synthesized diols) and low polydispersity (PDI < 1.3), typical for chain growth polymers. Incorporation of small amounts of comonomer in the diols resulted in a lower melting point than that of PCL_{1k} diol, which had a melting point of 32.3 °C. Increasing the amount of comonomer lowered the melting point, enthalpy of melting, and glass transition temperature of poly(ε-caprolactone) for both glycolide and d,l-lactide. The glass transition temperature was affected by incorporation amount, with T_g being ~ -5 °C for 5 mol % of either comonomer or ~ -60 °C for 25 mol % of either comonomer.

2.4.2 Polyurethane Synthesis and Molecular Characterization

Polyurethanes were synthesized from the five different soft segments, POSS and HDI. A schematic of the polyurethane synthesis is shown in **Scheme 2-2**. A summary of the polymers synthesized and their molecular characteristics is shown in **Table 2-2**. The first four syntheses systematically varied the input ratio of PCL_{1k}:POSS, from 100:0 PCL_{1k}:POSS to 70:30 PCL_{1k}:POSS. The actual ratio, as determined by ^{1}H-NMR, was close to the targeted value. An ^{1}H-NMR spectrum for an example PCL_{1k}:POSS polyurethane is shown in **Figure 2-2.** There was less incorporation of POSS than the input ratio, which is typical of POSS polymers.[23] The molecular weights (M_w) for these polymers range from 76 – 138 kDa.

Additionally, four polymers were synthesized to have a uniform input ratio of diol:POSS, but had a varying soft segment using the four synthesized diols. The measured weight percents of the diol:POSS were close to the target ratio of 70:30 for these syntheses, with slightly less incorporation of POSS for three of the polymers. Example ^{1}H-NMR spectra of the polyurethanes with comonomer are shown in **Figure 2-2**. Uniquely, incorporation of POSS in

$(PG_{25}CL_{75})_{1k}$:POSS 70:30 was above the target at 32.3 wt. % POSS. These polymers had admirably high molecular weights with M_w > 200 kDa.

2.4.3 Differential Scanning Calorimetry

Differential scanning calorimetry (DSC) was performed for all polymers to study the thermal properties of these materials. The second heat of each thermogram is shown in **Figure 2-3**, with analysis quantities summarized in **Table 2-3**. It was found that increasing POSS diol from 0 to 30 wt. % caused an increase in the T_m and ΔH of POSS. The melting transition appeared for POSS in the PCL_{1k}:POSS 80:20 polymer with as little as 15 wt. % POSS. The T_m of PCL_{1k} decreased with increasing POSS content, from 31.4 °C to 20.4 °C for PCL_{1k}:POSS 100:0 and PCL_{1k}:POSS 70:30, respectively. The breadth of the melting transition also decreased, as the melting point (from onset to completion) spanned 55 °C for PCL_{1k}:POSS 100:0 and 39 °C for PCL_{1k}:POSS 70:30, respectively. Interestingly, the enthalpy of melting also decreased, with the maximum enthalpy of melting for PCL_{1k}:POSS 90:10. Subsequently, the crystallinity of the soft segment as determined from **Equation 2-1** was also the lowest for PCL_{1k}:POSS 70:30 at 5.4%.

Evidently, incorporation of the comonomers in the soft segment caused a decrease of the soft segment T_m and width of the melting transition. Glycolide reduced the T_m of the soft segment to 14.0 °C for 4 mol % glycolide and to -5.5 °C for 21 mol % glycolide and the width to 39 and 23 °C, respectively. The soft segment crystallinity and enthalpy of melting also decreased systematically, as desired for elastomeric behavior. While T_g increased with incorporating glycolide, it remained below 0 °C. The trend for incorporating d,l-lactide was similar to that of glycolide: T_g increased with increasing d,l-lactide content. However, the T_m of $(PL_5CL_{95})_{1k}$ segment with 2% d,l-lactide was the lowest at -9.9 °C (breadth: 29 °C). The melting transition increased with additional d,l-lactide to -3.6 °C with 19 mol % d,l-lactide although the width of

melting transition decreased to 24 °C. Finally, all of the polymers featuring comonomers in the soft segment had clear melting transitions of POSS with $\Delta H \geq 1.5$ J/g.

2.4.4 Wide-Angle X-ray Scattering

Wide-angle x-ray scattering (WAXS) was performed to examine molecular-level organization of the polymers. It was found that there was an increase in POSS crystallinity with increasing amounts of POSS, shown by the increasing intensity of the inner ring in the 2-D WAXS shown in **Figure 2-4**. This is clearly evident in the 1D scans in **Figure 2-5**, which showed increased peak sizes and sharpness at $2\theta = 8.23°$ and 11.17° which correspond to *d*-spacings associated with the rhombohedral unit cell[33] of 10.7 Å and 7.9 Å, respectively. The soft segment produces an amorphous halo, shown by the broad outer ring in **Figure 2-4** and broad peak spanning $2\theta = 14.60°$ to 27.55° in **Figure 2-5**. This corresponds to *d*-spacing range spanning 6.0 Å to 3.2 Å.

2.4.5 Tensile Testing

Tensile testing was performed to determine the Young's modulus and strain-to-failure for each material. A representative example of each curve is shown in **Figure 2-6**, and the averages of five tests per sample are summarized in **Table 2-4**. Young's moduli for the PCL_{1k} and POSS materials increase with increasing amount of POSS. The 100:0 and 90:10 materials featured moduli of about 2.2 MPa (2.1 ± 0.8 and 2.2 ± 1.4, respectively). Further increasing the amount of POSS increases the modulus to 6.6 ± 1.1 and 13.2 ± 3.7 MPa for 20% and 30% POSS ($p < 0.05$). Incorporating comonomer into the soft segment also affected the modulus. Increasing glycolide from 5 to 25 mol % resulted in a decreased modulus from 10.95 ± 0.7 and 9.92 MPa. Incorporation of d,l-lactide also reduced the modulus to 7.36 ± 0.7 ($p < 0.05$) and 6.16 ± 0.6 MPa ($p < 0.05$) for 5% and 25% incorporations, respectively. When comparing comonomers of equal amounts, d,l-lactide causes a greater reduction of modulus compared to the glycolide containing materials ($p <$

0.05). All materials (except $(PG_{25}CL_{75})_{1k}$:POSS 70:30) had a strain-to-failure greater than 1200% strain (the instrument limit). The 25% glycolide containing material had a lower strain-to-failure at 493 ± 144 % strain.

2.4.6 Elasticity Testing

All materials were tested for elasticity by stretching to 50% strain and observing the strain recovered upon unloading, as shown in **Figure 2-7b**. An example curve of $(PL_5CL_{95})_{1k}$:POSS 70:30 is shown in **Figure 2-7a**. PCL_{1k}:POSS 100:0 was found to have the highest elastic recovery of 85% ± 5% during the first cycle, as shown in **Figure 2-7c**. There's a minimum for recovery at 90:10 PCL_{1k}:POSS with 65 ± 4%, which increased to 70% ± 3% for 80:20 and 73% ± 2% for 70:30 ($p < 0.05$). Incorporation of comonomer (**Figure 2-7d**) only affected elasticity for the 25% d,l-lactide sample, resulting in increased elasticity during the first cycle ($p < 0.05$); all other comonomers did not affect elasticity when compared to PCL_{1k}:POSS 70:30 ($p > 0.05$).

Elastic recovery increased with each consecutive cycle for most of the synthesized polymers. PCL_{1k}:POSS 80:20 recovered more for cycles 2 and 3 than cycle 1 ($p < 0.05$). PCL_{1k}:POSS 70:30 had the recovery increase between cycles 1 and 2 ($p < 0.05$) and cycles 2 and 3 ($p < 0.05$). This phenomenon was also observed in the materials incorporating comonomers. For all commoner compositions, the elasticity increases from cycles 1 to 2 and from 1 to 3 ($p < 0.01$).

The area under the curve of elasticity testing was examined to determine the elastic work done during loading, the elastic work recovered during unloading, and the energy dissipated in the process (the difference between the two),[34] shown in **Figure 2-8a-c**. For loading, the trends followed that of the mechanical testing: the larger the modulus, the larger the area under the curve for loading. For the PCL_{1k}:POSS polymers, the energy of loading increased with increasing POSS content. This is shown by the black bars in **Figure 2-8d**. The energy for loading was 17.7 ± 3.0,

14.2 ± 2.7, 42.2 ± 6.4 ($p < 0.05$), and 76.8 ± 1.3 ($p < 0.05$) MJ/m^3 for PCL_{1k}:POSS 100:0, 90:10, 80:20 70:30, respectively. When looking at the materials with comonomers in the soft segment (**Figure 2-8e**), the loading curves decreased compared to PCL_{1k}:POSS 70:30, resulting in 69.5 ± 9.0 MJ/m^3 for 5 mol % glycolide and 67.6 ± 6.1 for MJ/m^3 for 25% glycolide. For the d,l-lactide containing polymers, this was reduced further to 59.3 ± 2.8 MJ/m^3 ($p < 0.05$) and 50.2 ± 1.9 MJ/m^3 ($p < 0.01$).

Materials dissipate energy during strain cycling. The dissipation of energy (indicated by the dark gray bars in **Figure 2-8**) of PCL_{1k}:POSS 70:30 is highest at 39.4 ± 1.5 MJ/m^3. Decreasing the POSS content decreased the energy dissipated to 22.7 ± 5.6 MJ/m^3 for 80:20 ($p < 0.05$), to 8.7 ± 2.3 MJ/m^3 for 90:10 ($p < 0.01$) and to 7.2 ± 1.4 MJ/m^3 for 100:0 ($p < 0.01$). When comonomers were incorporated into the soft segment, the energy dissipated is lowered from the PCL_{1k}:POSS 70:30 value to 37.6 ± 6.6 MJ/m^3 for 5% glycolide ($p < 0.05$), 32.1 ± 4.4 for 25% glycolide, 31.4 ± 2.5 for 5% d,l-lactide ($p < 0.01$), and 23.5 ± 0.5 MJ/m^3 for 25 mol % d,l-lactide ($p < 0.01$). The values for dissipation are expected to be rate dependent, although examination of this was beyond the scope of the present study.

2.4.7 Dynamic Mechanical Analysis

Dynamic mechanical analysis was performed on the PCL_{1k}:POSS materials to observe the effect of temperature on modulus. The modulus at body temperature (37 °C) (as indicated by the dashed line in **Figure 2-9**) increased with increasing POSS incorporation. The storage modulus (**Table 2-5**) for the PCL_{1k}:POSS 100:0 is the lowest at 0.30 MPa, and increases to 2.30, 7.27, and 11.83 MPa for PCL_{1k}:POSS 90:10, 80:20, and 70:30 respectively. Also, the temperature range of the rubbery plateau broadened with increasing amounts of POSS, as was intended.

2.4.8 Impact of Pre-strain on Elasticity

Based on the results of the elasticity testing, pre-stretching of $(PG_5CL_{95})_{1k}$:POSS 70:30 was performed to determine how this would affect the resulting elasticity. Materials were pre-stretched to 25, 50, 100, and 250% strain and allowed to recover in strain upon complete unloading, as shown in **Figure 2-10a**. Materials were then stretched to 50% strain from their new neutral point (not stretched and not compressed), and the strain recovery was observed. An example 50% strain recovery (after 50% pre-strain) is shown in **Figure 2-10b**. The resulting elastic recovery of the 50% strain for all pre-strains is shown in **Figure 2-10c**, which reveals increasing recovery with increasing amounts of pre-strain. A pre-strain of 250% led to the highest elastic recovery of 90% for 50% strain testing. To better understand this phenomenon, DSC and WAXS were performed after the pre-stretching stage. In **Figure 2-10d**, the enthalpy of melting of the first heat is plotted for both the soft segment, $(PG_5CL_{95})_{1k}$, and POSS. Both melting enthalpies increased with increasing strain, indicating strain-induced crystallization. The 2-D WAXS profiles for 0%, 50% and 250% strain are shown in **Figure 2-10e**, revealing modest POSS and PGCL alignment, indicated by the intensification of the rings along the equator of the PGCL ring and meridian of the POSS ring, relative to the strain direction.

2.5 Discussion

Polyurethane synthesis was performed in two steps to easily control the composition of the soft segment and resulting polyurethane. In this manner, the soft segment could be tailored to a specific chemical composition for thermal or degradation properties. The soft segments utilized were designed to have a melting point below ambient temperature, increasing chain mobility and maximizing the elasticity of the resulting polyurethane. Glycolide or d,l-lactide, when incorporated in the soft segment, disrupted caprolactone crystallization and lowered the melting point and

melting enthalpy of the material. The higher melting point and melting enthalpy for the d,l-lactide polymers compared to the glycolide-containing polymers could be attributed to the decreased incorporation of d,l-lactide into the synthesized material compared to glycolide. These inconsistencies in incorporation were also seen in copolymers of glycolide and lactide.[35] The sub-ambient T_g was also lowered by the incorporation of the comonomers which is indicative of the increased amount of material in the amorphous phase.

Polyurethane syntheses were performed to determine the effect of changing the PCL_{1k} and POSS ratios as well as the composition of the soft segment while keeping the POSS content uniform. Increasing POSS content caused an increase in POSS crystallization and disruption of caprolactone crystallization, which has been shown previously in PCL-POSS diols[33] and polyurethanes.[36] While changing the composition of the soft segment did not affect the crystallinity of the POSS phase, POSS incorporation did interfere with the soft segment crystallization as it did with PCL_{1k}. While diols containing d,l-lactide had a greater enthalpy of melting and melting point than glycolide containing diols, when incorporated into the polyurethane the combination of d,l-lactide in POSS had a greater affect in disrupting PCL's crystallinity than POSS and glycolide. We attribute this to the amorphous nature of d,l-lactide. Also, the glass transition temperature (T_g) of the polyurethanes increased with increasing amount of comonomer, which we attribute to mixing of the caprolactone and comonomer in the soft, amorphous phase.

Wide-angle x-ray scattering (WAXS) was performed to probe the crystalline phases that form on a sub-micron scale in the polymer. As anticipated, POSS forms crystallites with *d*-spacing of planes around 10.7 and 7.9 Å, corresponding to Miller indices of 101 and 110 for a rhombohedral unit cell, which has seen previously in PCL-POSS polyurethanes.[33] The amorphous nature of the

PCL phase (indicated by the broad halo), correlates to the amount crystallinity of the soft segments, manifested as a decrease in relative height with increasing POSS content in the 1D WAXS patterns.

The modulus of these elastomers was affected by both the soft segment:POSS ratio and the composition of the soft segment. Increasing POSS content increased the modulus, as seen in other studies where POSS incorporation reinforces the materials.[37, 38] Introducing glycolide into the soft segment decreased the modulus of the elastomer, due to the decreased crystallinity in the soft segment. However, due to the high POSS content of the 25% glycolide sample (32.3%), the modulus of that composition was only slightly lower than the 5% glycolide material, despite the large change in crystallinity of the soft segment. Incorporation of d,l-lactide, a non-crystallizing comonomer, caused a greater decrease in the modulus than glycolide, a crystallizable comonomer, due to the decreased crystallinity of the soft segment of the polyurethane. The strain-to-failure of all materials except $(PG_{25}CL_{75})_{1k}$:POSS was higher than 1200%. The lower strain-to-failure of the 25% glycolide polymer could be due to chain scission during the compression molding process, due to the susceptibility of glycolide to thermal degradation, especially when hydrated due to trace moisture.

The first cycle elasticities of our materials at room temperature were more affected by the POSS content than by the chemical composition of the soft segment. The highest elasticity was found for the PCL_{1k}:POSS 100:0 elastomer, which has high elasticity due to the high crystallinity of PCL above room temperature. When incorporated in small amounts (such as in the 90:10 polymer), POSS disrupted the PCL crystallinity without providing cross-links, resulting in the lowest elasticity. Increasing POSS content causes an increase in elasticity due to the physical cross-links formed. Only 25% d,l-lactide caused an increase in elasticity when compared with PCL_{1k}:POSS 70:30, which could be due to the amorphous nature of the soft segment and its low

modulus. All materials containing 30% POSS featured elasticity >70% for the first cycle. While this is lower than another thermoplastic polyurethane,[14] our material has lower modulus and lower processing temperature, which is desired. Also, our material can have increased recovery with pre-straining, discussed further below.

The material's Young's modulus was positively correlated with the energy that was stored during stretching, while a combination of the elasticity and modulus correlated with the energy that was released during recovery. For example, $(PL_{25}CL_{75})_{1k}$:POSS has a lower modulus and higher elasticity than $(PL_5CL_{95})_{1k}$:POSS, and had dissipated less energy upon unloading. Ideally, an elastomer follows the same stress-strain curve upon loading and unloading. However, due to the thermoplastic nature of these materials, this is not the case in practice for TPEs. Nevertheless, more energy can be returned if the materials contain a higher amount of comonomer.

Dynamic mechanical analysis was performed to determine the effect of POSS content on thermo-mechanical properties, in which it was found that more POSS resulted in a higher modulus at body temperature as well as an increased rubbery plateau above the PCL melting transition. POSS, when incorporated into a polymer, has a melting transition at about 120 °C, and with 23% POSS in the material, the polymer is stable (does not melt) above 100 °C. Alternatively, the narrow rubbery plateau after the melting transition in the POSS in PCL_{1k}:POSS 100:0 material could be due to entanglements of the polymer chains. The results indicate that although PCL_{1k}:POSS 100:0 had high elasticity at room temperature, it would lose its structural integrity at body temperature. Also, it is evident that at least 15% POSS (in PCL_{1k}:POSS 80:20) is needed for an elastomer be stable above 60 °C.

Pre-straining $(PG_5CL_{95})_{1k}$:POSS caused an increase in the material's recovery of strain when stretched by 50%. First-heat DSC and WAXS were performed for each strain to understand

this effect. When examining the enthalpies of melting of each pre-strain of first heat DSC, it is evident that increasing the amount of pre-strain caused increases in the ΔH for both the soft segment and hard segment. The WAXS patterns also show alignment of both the PGCL segment and POSS crystals, with the crystals aligning in opposite orientations, which is typical of POSS. From these results, it is hypothesized that the pre-stretch causes the two phases (PGCL and POSS) that are partially mixed to separate from each other more completely and subsequently form larger crystals of the different components which would cause denser cross-linking and result in higher elasticity.

2.6 Conclusions

Novel, thermoplastic biodegradable elastomers were developed utilizing a biodegradable soft segment and POSS as the hard segment. These materials had controllable thermal and mechanical properties based on the POSS content and composition of the soft segment. These materials had high elasticity (>70% recovery) which could be increased with pre-straining the material. These materials offer the potential for use as soft and elastic implantable biodegradable materials. Current efforts are focused on examination of the degradation and cytocompatibility of these materials.

2.7 References

1. Amsden, B., Curable, biodegradable elastomers: emerging biomaterials for drug delivery and tissue engineering. *Soft Matter* **2007,** *3* (11), 1335-1348. DOI: 10.1039/B707472G.

2. Bettinger, C. J., Biodegradable Elastomers for Tissue Engineering and Cell-Biomaterial Interactions. *Macromolecular bioscience 11* (4), 467-482. DOI: 10.1002/mabi.201000397.

3. Lee, S. H., In-vivo biocompatibility evaluation of stents coated with a new biodegradable elastomeric and functional polymer. *Coronary artery disease* **2002,** *13* (4), 237-241. DOI: 10.1097/00019501-200206000-00006.

4. Lendlein, A.; Langer, R., Biodegradable, Elastic Shape-Memory Polymers for Potential Biomedical Applications. *Science* **2002,** *296* (5573), 1673.

5. Hwang, S.-W.; Lee, C. H.; Cheng, H.; Jeong, J.-W.; Kang, S.-K.; Kim, J.-H.; Shin, J.; Yang, J.; Liu, Z.; Ameer, G. A.; Huang, Y.; Rogers, J. A., Biodegradable Elastomers and Silicon Nanomembranes/Nanoribbons for Stretchable, Transient Electronics, and Biosensors. *Nano Letters* **2015,** *15* (5), 2801-2808. DOI: 10.1021/nl503997m.

6. Nair, L. S.; Laurencin, C. T., Biodegradable polymers as biomaterials. *Progress in Polymer Science* **2007,** *32* (8-9), 762-798. DOI: 10.1016/j.progpolymsci.2007.05.017.

7. Hutmacher, D. W., Scaffolds in tissue engineering bone and cartilage. *Biomaterials* **2000,** *21* (24), 2529-2543. DOI: http://dx.doi.org/10.1016/S0142-9612(00)00121-6.

8. Amsden, B.; Wang, S.; Wyss, U., Synthesis and Characterization of Thermoset Biodegradable Elastomers Based on Star-Poly(ε-caprolactone-co-d,l-lactide). *Biomacromolecules* **2004,** *5* (4), 1399-1404. DOI: 10.1021/bm034538j.

9. Serrano, M. C., Novel Biodegradable Shape-Memory Elastomers with Drug-Releasing Capabilities. *Advanced materials (Weinheim) 23* (19), 2211-2215. DOI: 10.1002/adma.201004566.

10. Ding, T.; Liu, Q.; Shi, R.; Tian, M.; Yang, J.; Zhang, L., Synthesis, characterization and in vitro degradation study of a novel and rapidly degradable elastomer. *Polymer Degradation and Stability* **2006,** *91* (4), 733-739. DOI: http://dx.doi.org/10.1016/j.polymdegradstab.2005.06.007.

11. Poetz, K. L.; Mohammed, H. S.; Snyder, B. L.; Liddil, G.; Samways, D. S. K.; Shipp, D. A., Photopolymerized Cross-Linked Thiol–Ene Polyanhydrides: Erosion, Release, and Toxicity Studies. *Biomacromolecules* **2014,** *15* (7), 2573-2582. DOI: 10.1021/bm500420q.

12. Wang, Y.; Ameer, G. A.; Sheppard, B. J.; Langer, R., A tough biodegradable elastomer. *Nat Biotech* **2002,** *20* (6), 602-606. DOI: http://www.nature.com/nbt/journal/v20/n6/suppinfo/nbt0602-602_S1.html.

13. Wang, L.; Zhang, Z.; Chen, H.; Zhang, S.; Xiong, C., Preparation and characterization of biodegradable thermoplastic Elastomers (PLCA/PLGA blends). *Journal of Polymer Research* **2010,** *17* (1), 77-82. DOI: 10.1007/s10965-009-9292-9.

14. Wang, W.; Ping, P.; Yu, H.; Chen, X.; Jing, X., Synthesis and characterization of a novel biodegradable, thermoplastic polyurethane elastomer. *Journal of Polymer Science, Part A: Polymer Chemistry* **2006,** *44* (19), 5505-5512. DOI: 10.1002/pola.21643.

15. Daemi, H.; Rajabi-Zeleti, S.; Sardon, H.; Barikani, M.; Khademhosseini, A.; Baharvand, H., A robust super-tough biodegradable elastomer engineered by supramolecular ionic interactions. *Biomaterials* **2016,** *84*, 54-63. DOI: http://dx.doi.org/10.1016/j.biomaterials.2016.01.025.

16. Wu, J.; Mather, P. T., POSS Polymers: Physical Properties and Biomaterials Applications. *Polymer Reviews* **2009,** *49* (1), 25-63. DOI: 10.1080/15583720802656237.

17. Li, G.; Wang, L.; Ni, H.; Pittman, C. U., Polyhedral Oligomeric Silsesquioxane (POSS) Polymers and Copolymers: A Review. *Journal of Inorganic and Organometallic Polymers 11* (3), 123-154. DOI: 10.1023/A:1015287910502.

18. Tanaka, K., Advanced functional materials based on polyhedral oligomeric silsesquioxane (POSS). *Journal of materials chemistry* **2012,** *22* (5), 1733-1746. DOI: 10.1039/C1JM14231C.

19. Joshi, M.; Butola, B. S., Polymeric Nanocomposites—Polyhedral Oligomeric Silsesquioxanes (POSS) as Hybrid Nanofiller. *Journal of Macromolecular Science, Part C* **2004,** *44* (4), 389-410. DOI: 10.1081/MC-200033687.

20. Lewicki, J. P.; Pielichowski, K.; De la Croix, P. T.; Janowski, B.; Todd, D.; Liggat, J. J., Thermal degradation studies of polyurethane/POSS nanohybrid elastomers. *Polymer Degradation and Stability* **2010,** *95* (6), 1099-1105. DOI: 10.1016/j.polymdegradstab.2010.02.021.

21. Chattopadhyay, D. K., Thermal stability and flame retardancy of polyurethanes. *Progress in polymer science 34* (10), 1068-1133. DOI: 10.1016/j.progpolymsci.2009.06.002.

22. Janowski, B.; Pielichowski, K., Thermo(oxidative) stability of novel polyurethane/POSS nanohybrid elastomers. *Thermochimica Acta* **2008,** *478* (1-2), 51-53. DOI: 10.1016/j.tca.2008.08.015.

23. Knight, P. T.; Lee, K. M.; Qin, H.; Mather, P. T., Biodegradable Thermoplastic Polyurethanes Incorporating Polyhedral Oligosilsesquioxane. *Biomacromolecules* **2008,** *9* (9), 2458-2467. DOI: 10.1021/bm8004935.

24. Gupta, A.; Vara, D. S.; Punshon, G.; Sales, K. M.; Winslet, M. C.; Seifalian, A. M., In vitro small intestinal epithelial cell growth on a nanocomposite polycaprolactone scaffold. *Biotechnology and Applied Biochemistry* **2009,** *54*, 221-229. DOI: 10.1042/ba20090214.

25. Knight, P. T.; Kirk, J. T.; Anderson, J. M.; Mather, P. T., In vivo kinetic degradation analysis and biocompatibility of aliphatic polyester polyurethanes. *Journal of Biomedical Materials Research Part A* **2010,** *94A* (2), 333-343. DOI: 10.1002/jbm.a.32806.

26. Gu, X.; Wu, J.; Mather, P. T., Polyhedral Oligomeric Silsesquioxane (POSS) Suppresses Enzymatic Degradation of PCL-Based Polyurethanes. *Biomacromolecules* **2011,** *12* (8), 3066-3077. DOI: 10.1021/bm2006938.

27. Knight, P. T., PLGA−POSS End-Linked Networks with Tailored Degradation and Shape Memory Behavior. *Macromolecules 42* (17), 6596-6604. DOI: 10.1021/ma901237h.

28. Pan, H.; Qiu, Z., Biodegradable Poly(l-lactide)/Polyhedral Oligomeric Silsesquioxanes Nanocomposites: Enhanced Crystallization, Mechanical Properties, and Hydrolytic Degradation. *Macromolecules* **2010,** *43* (3), 1499-1506. DOI: 10.1021/ma9023685.

29. Liu, Y., Star-shaped poly(ε-caprolactone) with polyhedral oligomeric silsesquioxane core. *Polymer (Guilford)* **2006,** *47* (19), 6814-6825. DOI: 10.1016/j.polymer.2006.07.050.

30. Du, Y.; Yu, M.; Chen, X.; Ma, P. X.; Lei, B., Development of Biodegradable Poly(citrate)-Polyhedral Oligomeric Silsesquioxanes Hybrid Elastomers with High Mechanical Properties and Osteogenic Differentiation Activity. *ACS Applied Materials & Interfaces* **2016,** *8* (5), 3079-3091. DOI: 10.1021/acsami.5b10378.

31. Xie, M.; Ge, J.; Lei, B.; Zhang, Q.; Chen, X.; Ma, P. X., Star-Shaped, Biodegradable, and Elastomeric PLLA-PEG-POSS Hybrid Membrane With Biomineralization Activity for Guiding Bone Tissue Regeneration. *Macromolecular Bioscience* **2015,** *15* (12), 1656-1662. DOI: 10.1002/mabi.201500237.

32. Mark, J. E., *Polymer Data Handbook*. Oxford University Press: 1999.

33. Alvarado-Tenorio, B.; Romo-Uribe, A.; Mather, P. T., Microstructure and Phase Behavior of POSS/PCL Shape Memory Nanocomposites. *Macromolecules* **2011,** *44* (14), 5682-5692. DOI: 10.1021/ma2005662.

34. Hayden, H. W.; Moffatt, W. G.; Wulff, J., *The Structure and Properties of Materials*. John Wiley & Sons: 1967.

35. Gilding, D. K.; Reed, A. M., Biodegradable polymers for use in surgery—polyglycolic/poly(actic acid) homo- and copolymers: 1. *Polymer* **1979,** *20* (12), 1459-1464. DOI: http://dx.doi.org/10.1016/0032-3861(79)90009-0.

36. Huitron-Rattinger, E.; Ishida, K.; Romo-Uribe, A.; Mather, P. T., Thermally modulated nanostructure of poly(ε-caprolactone)–POSS multiblock thermoplastic polyurethanes. *Polymer* **2013,** *54* (13), 3350-3362. DOI: http://dx.doi.org/10.1016/j.polymer.2013.04.015.

37. Huang, J.-c., Polyimide/POSS nanocomposites: interfacial interaction, thermal properties and mechanical properties. *Polymer (Guilford) 44* (16), 4491-4499. DOI: 10.1016/S0032-3861(03)00434-8.

38. Mather, P. T., Mechanical Relaxation and Microstructure of Poly(norbornyl-POSS) Copolymers. *Macromolecules* **1999,** *32* (4), 1194-1203.

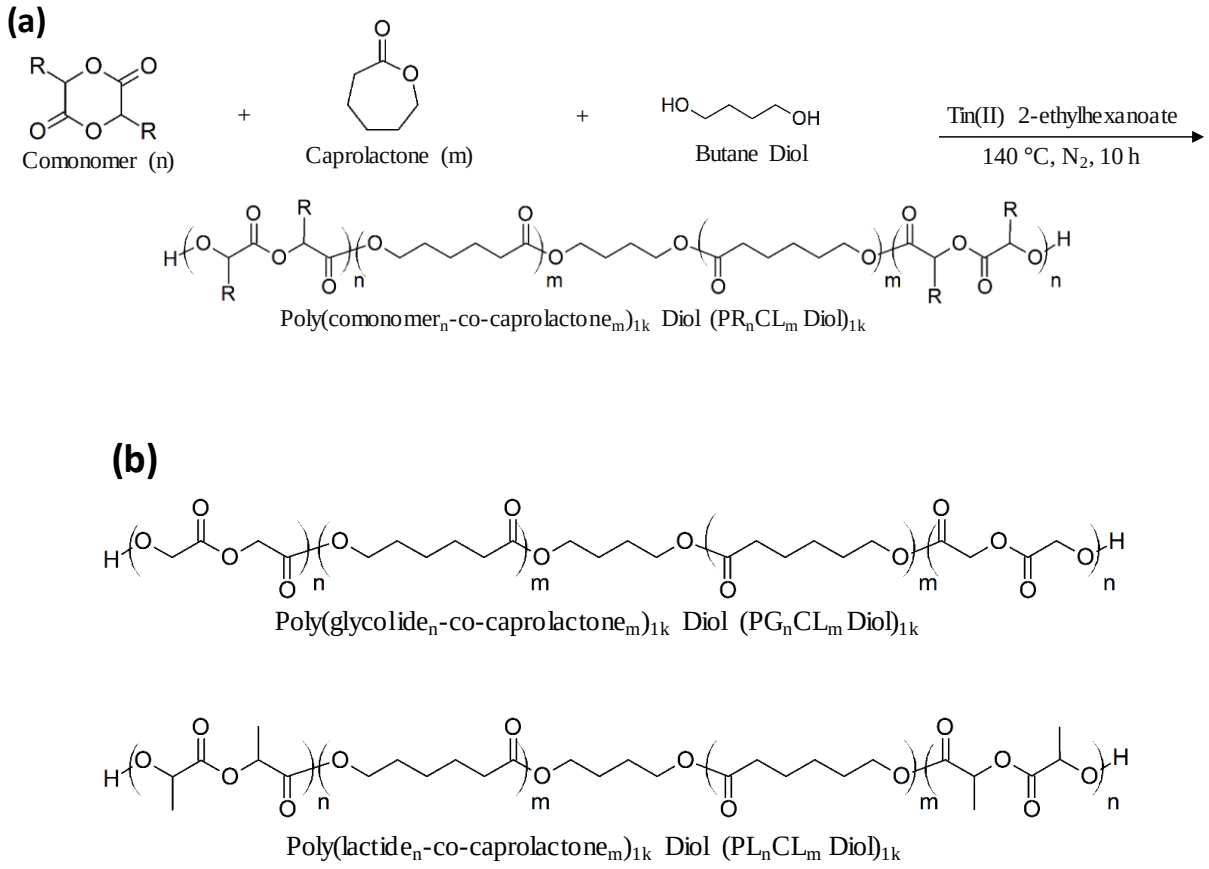

Scheme 2-1: a) Schematic of diol synthesis and b) structures of the resulting poly(glycolide-co-caprolactone and poly(d,l-lactide-co-caprolactone).

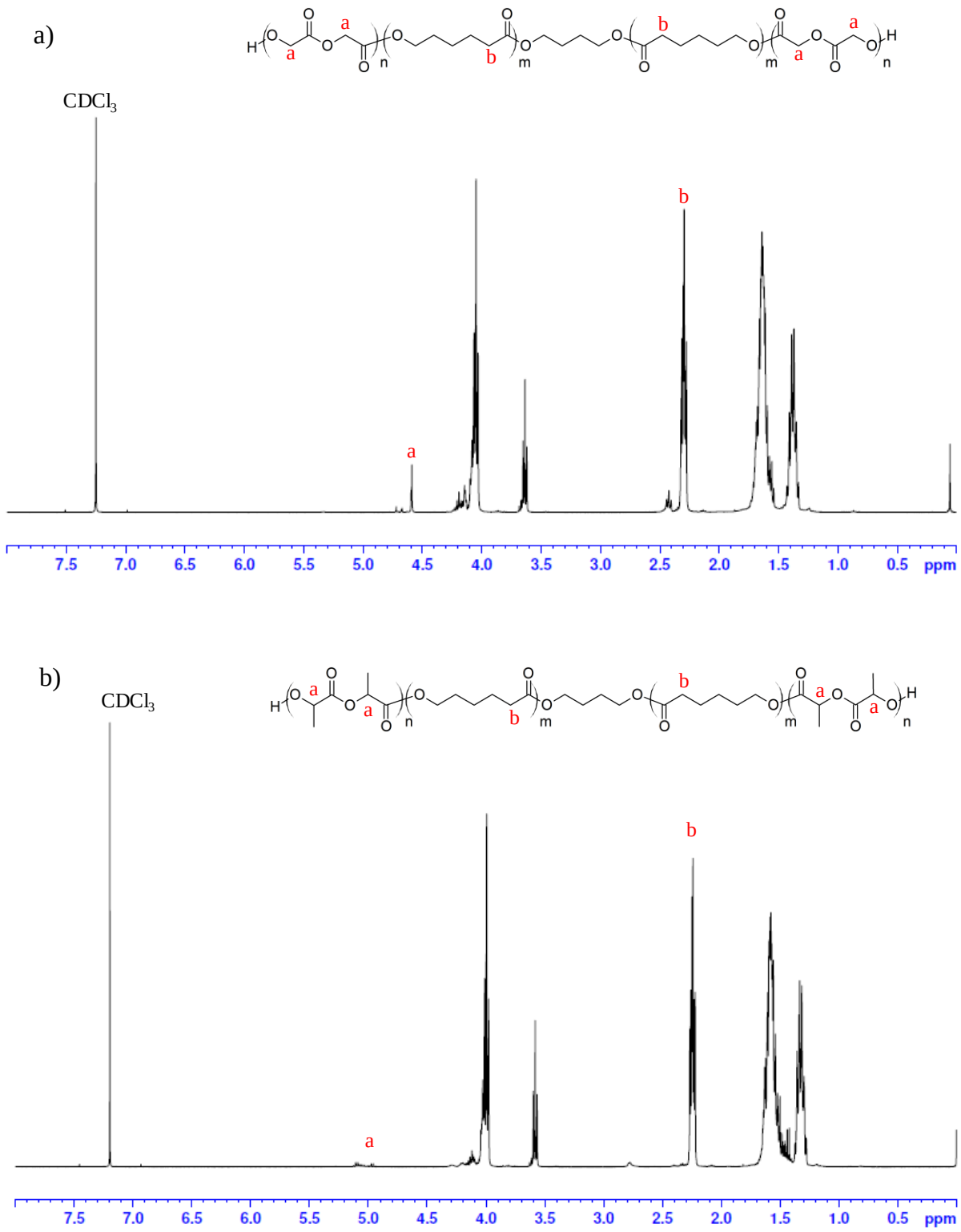

Figure 2-1: ^{1}H-NMR spectra of a) $(PGCL)_{1k}$ and b) $(PLCL)_{1k}$ diol.

Table 2-1: Diols used as the soft segment in polyurethane synthesis.

Synthesis	Input Comonomer: Caprolactone Ratio (Molar)	Actual[a] Comonomer: Caprolactone Ratio (Molar)	M_n[b] (kDa)	M_w[b] (kDa)	PDI[b]	T_g[c] (°C)	$T_{m,\ PRCL}$[c] (°C)	$\Delta H_{,\ PRCL}$[c] (J/g)
*PCL_{1k}	-	-	-	1.25	-	-1.4	32.3/39.3	50.1
$(PG_5CL_{95})_{1k}$	5 : 95	4 : 96	1.67	1.84	1.10	-5.2	19.4/25.1	48.8
$(PG_{25}CL_{75})_{1k}$	25 : 75	21:79	1.91	2.45	1.28	-61.4	4.8	0.1
$(PL_5CL_{95})_{1k}$	5 : 95	2 : 98	2.19	2.46	1.12	-5.0	28.2	59.1
$(PL_{25}CL_{75})_{1k}$	25 : 75	19 : 81	2.29	2.47	1.09	-57.5	12.3	0.9

*PCL_{1k} diol was purchased.
[a]Determined from proton nuclear magnetic resonance.
[b]Determined from gel permeation chromatography.
[c]Determined from second heat differential scanning calorimetry.

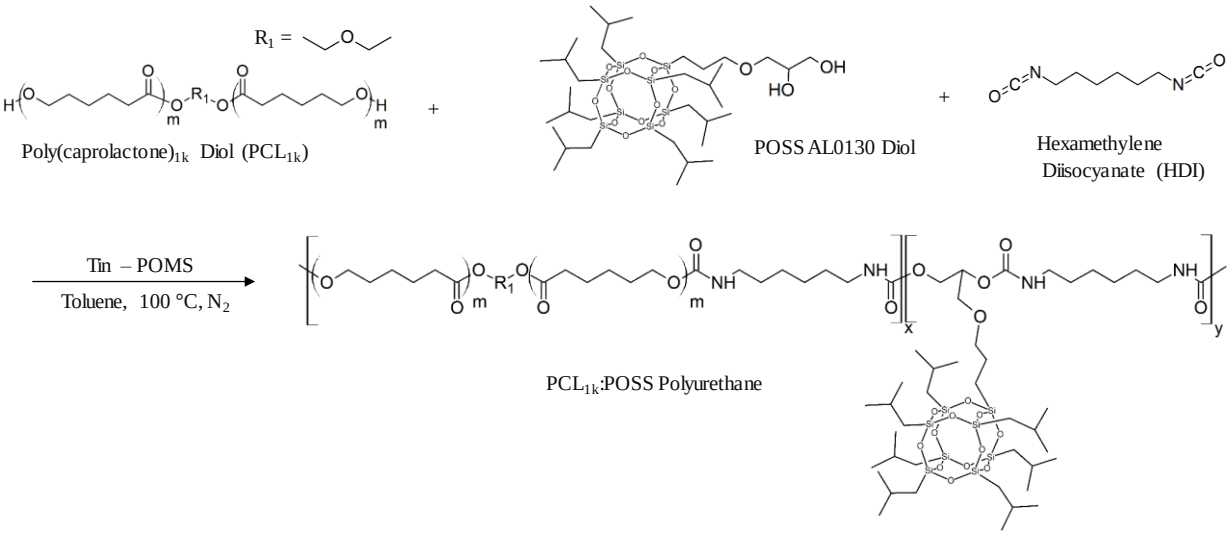

Scheme 2-2: Example schematic of polyurethane synthesis.

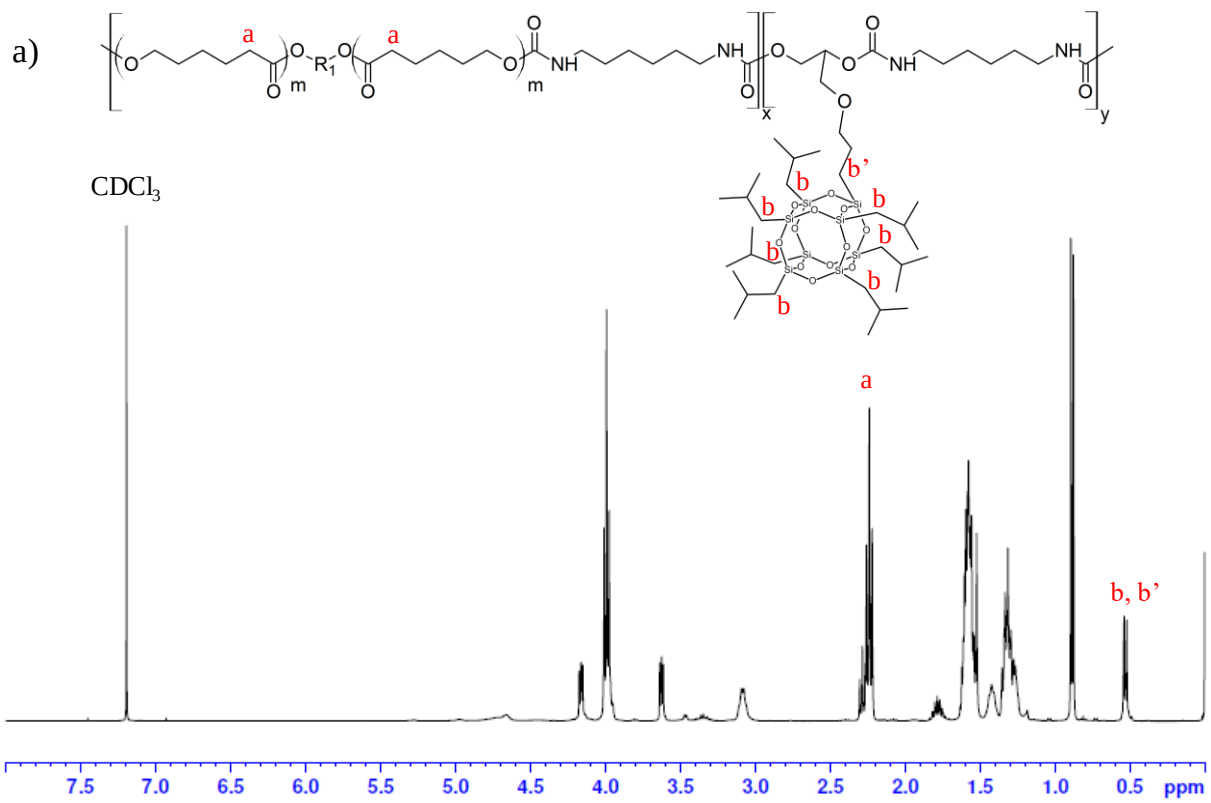
a)
a
a
O
NH
NH
NH
O
m
m
x
y
R1
b'
b
b
b
b
b
b
b
CDCl3
a
b, b'
7.5
7.0
6.5
6.0
5.5
5.0
4.5
4.0
3.5
3.0
2.5
2.0
1.5
1.0
0.5
ppm

b)

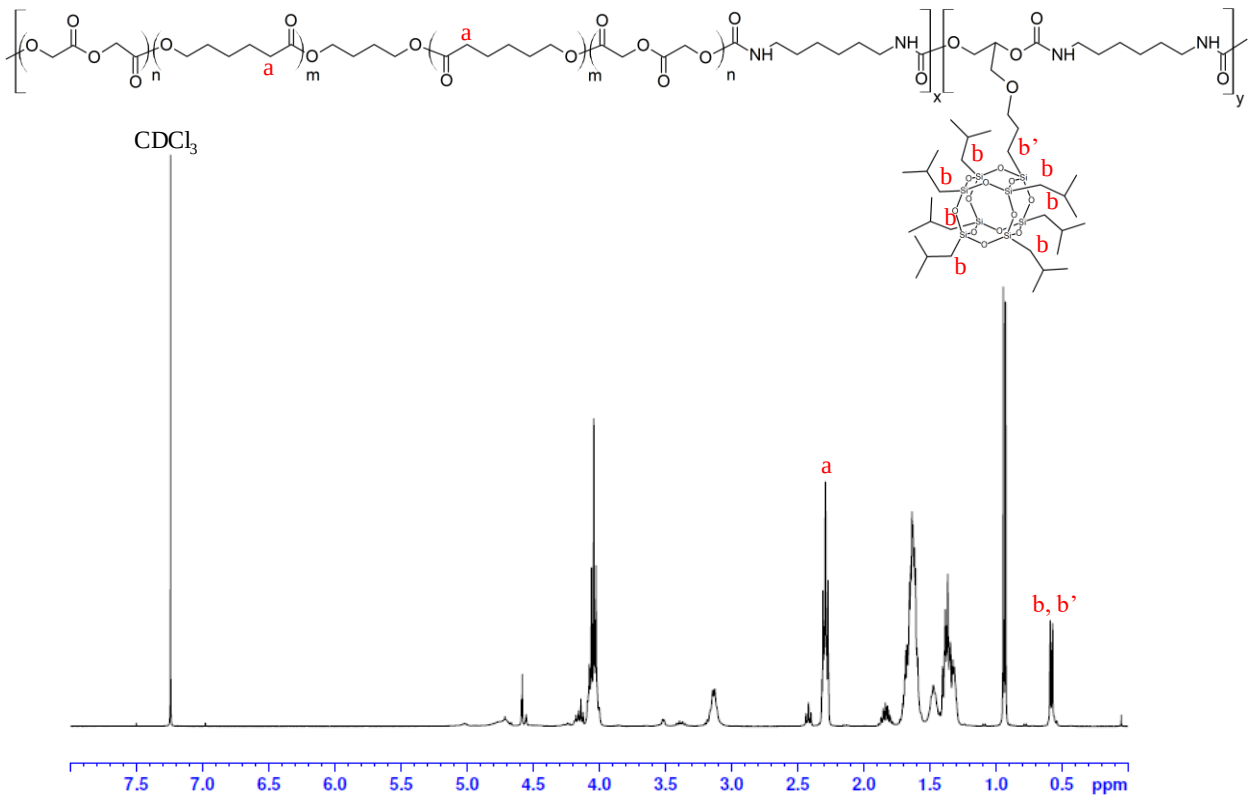

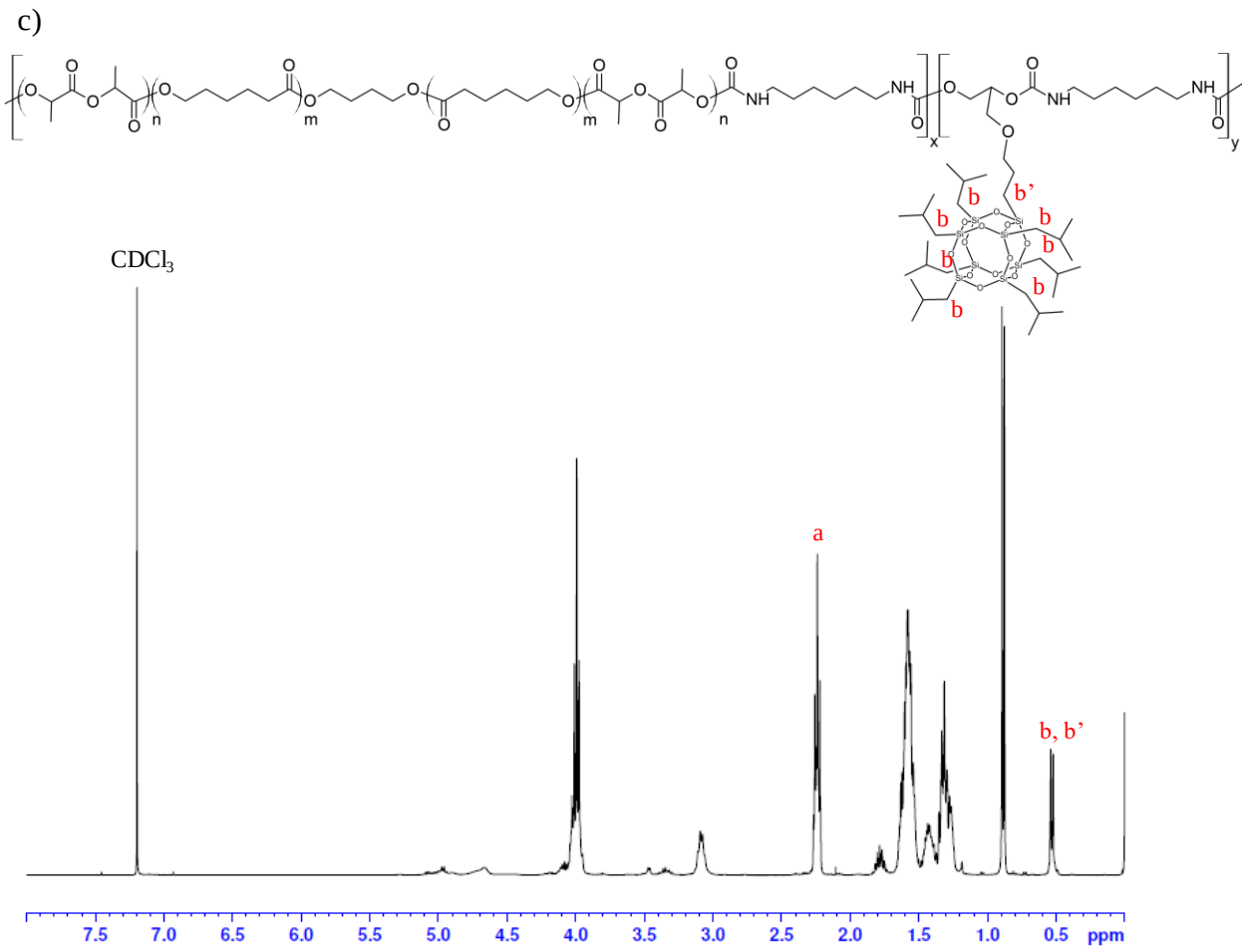

Figure 2-2: H-NMR spectra for a) PCL_{1k}:POSS, b) $(PGCL)_{1k}$:POSS and c) $(PLCL)_{1k}$:POSS polyurethanes.

Table 2-2: Molecular characterization of synthesized polyurethanes.

Synthesis	Input Diol:POSS Ratio (Wt. %)	Actual[a] Diol:POSS Ratio (Wt. %)	Mn[b] (kDa)	Mw[b] (kDa)	PDI[b]
PCL_{1k} : POSS 100 : 0	100 : 0	100 : 0	86	138	1.60
PCL_{1k} : POSS 90 : 10	90 : 10	92.2 : 7.8	34	111	3.26
PCL_{1k} : POSS 80 : 20	80 : 20	84.3 : 15.7	54	77	1.43
PCL_{1k} : POSS 70 : 30	70 : 30	77.2 : 22.8	49	76	1.55
$(PG_5CL_{95})_{1k}$: POSS 70 : 30	70 : 30	73.5 : 26.5	94	204	2.17
$(PG_{25}CL_{75})_{1k}$: POSS 70 : 30	70 : 30	67.7 : 32.3	445	607	1.36
$(PL_5CL_{95})_{1k}$: POSS 70 : 30	70 : 30	73.8 : 26.2	162	338	2.09
$(PL_{25}CL_{75})_{1k}$: POSS 70 : 30	70 : 30	71.5 : 28.5	202	320	1.58

[a]Determined from proton nuclear magnetic resonance.
[b]Determined from gel permeation chromatography.

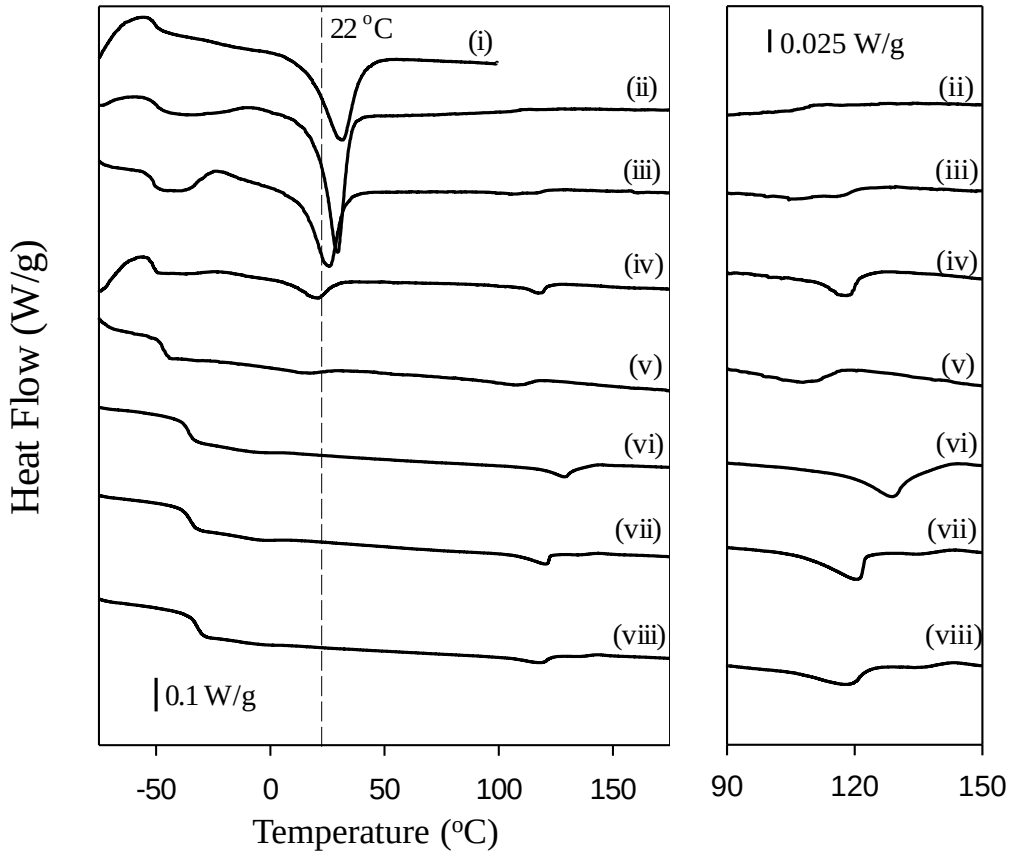

Figure 2-3: Differential scanning calorimetry (DSC) curves for: (i) PCL_{1k}:POSS 100:0, (ii) PCL_{1k}:POSS 90:10, (iii) PCL_{1k}:POSS 80:20, (iv) PCL_{1k}:POSS 70:30, (v) $(PG_5CL_{95})_{1k}$:POSS 70:30, (vi) $(PG_{25}CL_{75})_{1k}$:POSS 70:30, (vii) $(PL_5CL_{95})_{1k}$:POSS 70:30, and (viii) $(PL_{25}CL_{75})_{1k}$:POSS 70:30, with the second heat shown (exotherm up) of the full temperature range (left) and for higher temperature range for POSS (right).

Table 2-3: Thermal transitions and crystallinity of each polymer from the DSC thermograms.

Synthesis	T_g (°C)	$T_{m,Diol}$ (°C)	ΔH_{Diol} (J/g)	χ_{Diol} [a] (%)	$T_{m,POSS}$ (°C)	ΔH_{POSS} (J/g)
PCL_{1k} : POSS 100 : 0	-50.0	31.4	22.5	17.9	-	-
PCL_{1k} : POSS 90 : 10	-49.6	29.4	28.7	24.7	-	-
PCL_{1k} : POSS 80 : 20	-52.5	25.8	21.1	19.9	104.5	1.0
PCL_{1k} : POSS 70 : 30	-51.5	20.4	5.3	5.4	118.1	2.0
$(PG_5CL_{95})_{1k}$: POSS 70 : 30	-47.4	14.0	1.1	1.1	107.9	1.5
$(PG_{25}CL_{75})_{1k}$: POSS 70 : 30	-35.9	-5.5	0.4	0.5	128.7	2.7
$(PL_5CL_{95})_{1k}$: POSS 70 : 30	-48.5	-9.9	0.4	0.4	113.3	1.9
$(PL_{25}CL_{75})_{1k}$: POSS 70 : 30	-35.1	-3.6	0.5	0.6	120.4	1.8

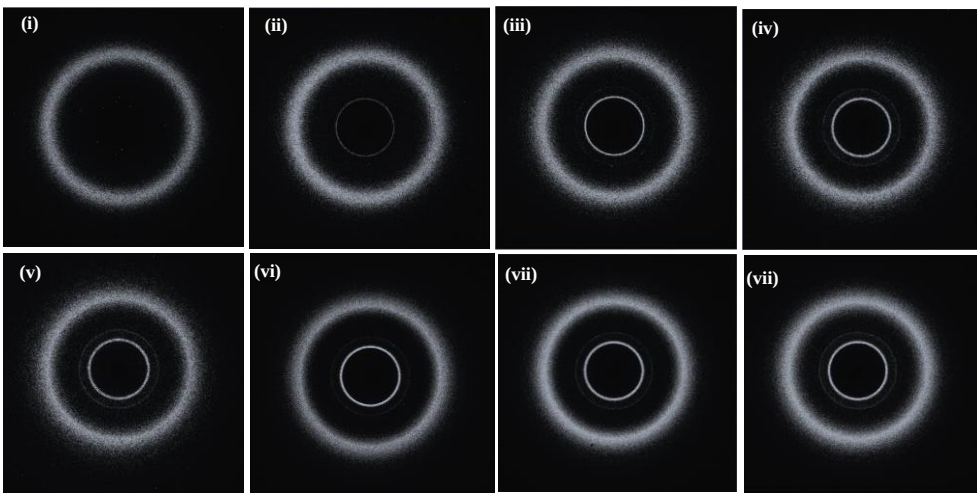

Figure 2-4: Wide-angle x-ray scattering (WAXS) pictograms of (i) PCL_{1k}:POSS 100:0, (ii) PCL_{1k}:POSS 90:10, (iii) PCL_{1k}:POSS 80:20, (iv) PCL_{1k}:POSS 70:30, (v) $(PG_5CL_{95})_{1k}$:POSS 70:30, (vi) $(PG_{25}CL_{75})_{1k}$:POSS 70:30, (vii) $(PL_5CL_{95})_{1k}$:POSS 70:30, and (viii) $(PL_{25}CL_{75})_{1k}$:POSS 70:30.

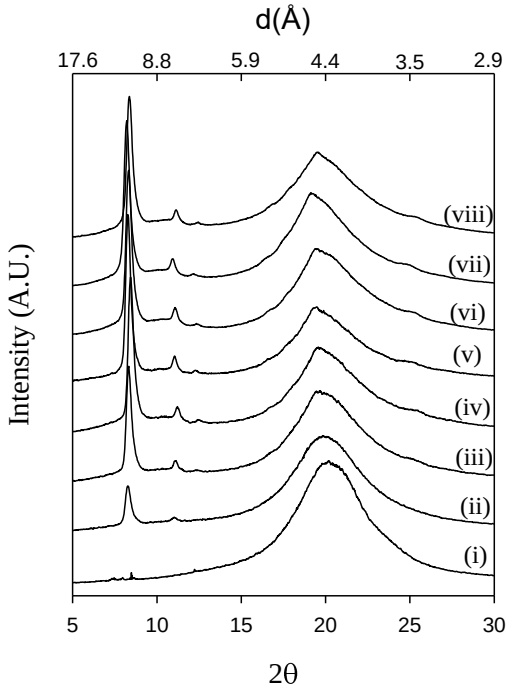

Figure 2-5: Plot of intensity vs. diffraction angle for materials (i) PCL_{1k}:POSS 100:0, (ii) PCL_{1k}:POSS 90:10, (iii) PCL_{1k}:POSS 80:20, (iv) PCL_{1k}:POSS 70:30, (v) $(PG_5CL_{95})_{1k}$:POSS 70:30, (vi) $(PG_{25}CL_{75})_{1k}$:POSS 70:30, (vii) $(PL_5CL_{95})_{1k}$:POSS 70:30, and (viii) $(PL_{25}CL_{75})_{1k}$:POSS 70:30.

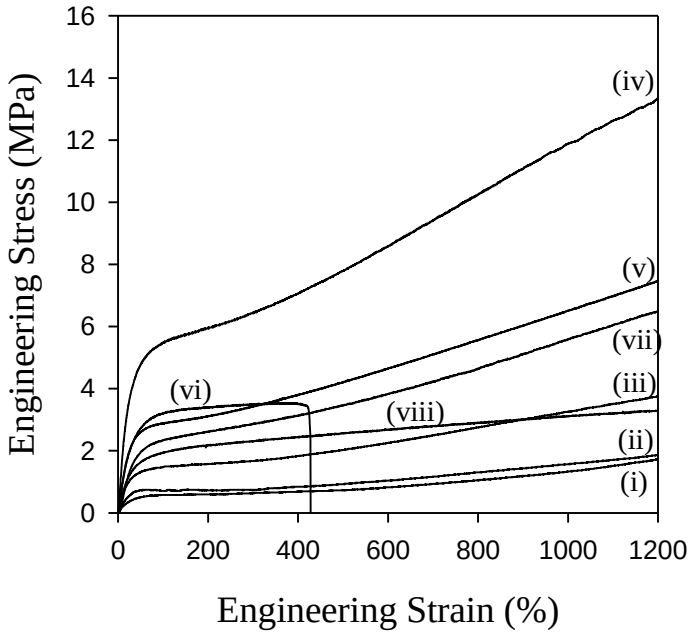

Figure 2-6: Engineering stress-strain curves for (i) PCL_{1k}:POSS 100:0, (ii) PCL_{1k}:POSS 90:10, (iii) PCL_{1k}:POSS 80:20, (iv) PCL_{1k}:POSS 70:30, (v) $(PG_5CL_{95})_{1k}$:POSS 70:30, (vi) $(PG_{25}CL_{75})_{1k}$:POSS 70:30, (vii) $(PL_5CL_{95})_{1k}$:POSS 70:30, and (viii) $(PL_{25}CL_{75})_{1k}$:POSS 70:30 (n=5).

Table 2-4: Summary of mechanical properties from tensile tests.

Synthesis	Modulus (MPa)	Strain to Failure (%)
PCL_{1k} : POSS 100 : 0	2.11 ± 0.8	> 1200
PCL_{1k} : POSS 90 : 10	2.28 ± 1.4	> 1200
PCL_{1k} : POSS 80 : 20	6.64 ± 1.1	> 1200
PCL_{1k} : POSS 70 : 30	13.15 ± 3.7	> 1200
$(PG_5CL_{95})_{1k}$: POSS 70 : 30	10.95 ± 0.7	> 1200
$(PG_{25}CL_{75})_{1k}$: POSS 70 : 30	9.92 ± 0.7	493 ± 144
$(PL_5CL_{95})_{1k}$: POSS 70 : 30	7.36 ± 0.7	> 1200
$(PL_{25}CL_{75})_{1k}$: POSS 70 : 30	6.16 ± 0.6	> 1200

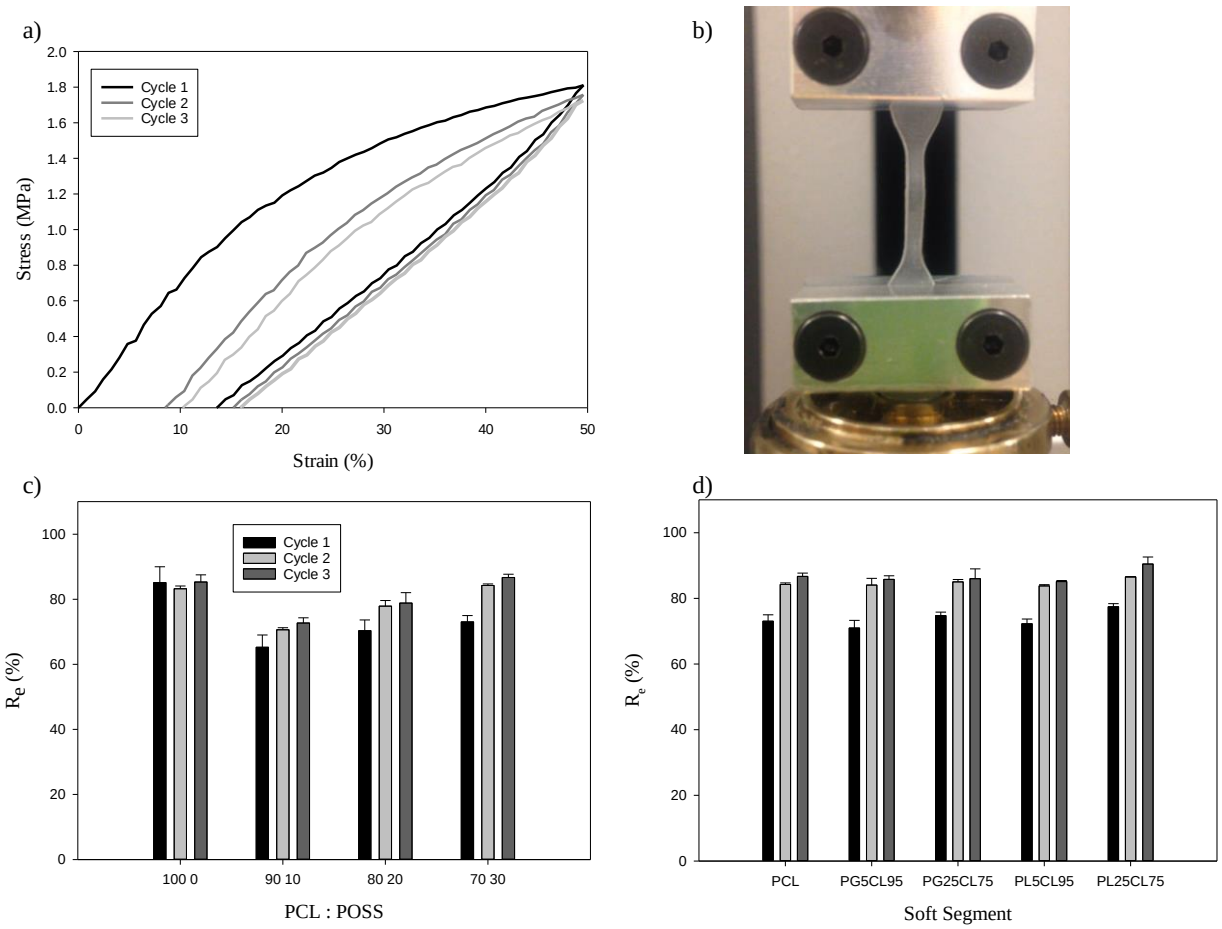

Figure 2-7: Elasticity testing of all materials: a) An example of a material stretched to 50% strain for 3 cycles, b) a picture of an elastomer being stretched, c) strain recovery for each of the three cycles of PCL:POSS elastomers with changing PCL and POSS content, and d) strain recovery for each of the three cycles for all 70:30 materials with different soft segments (n=3).

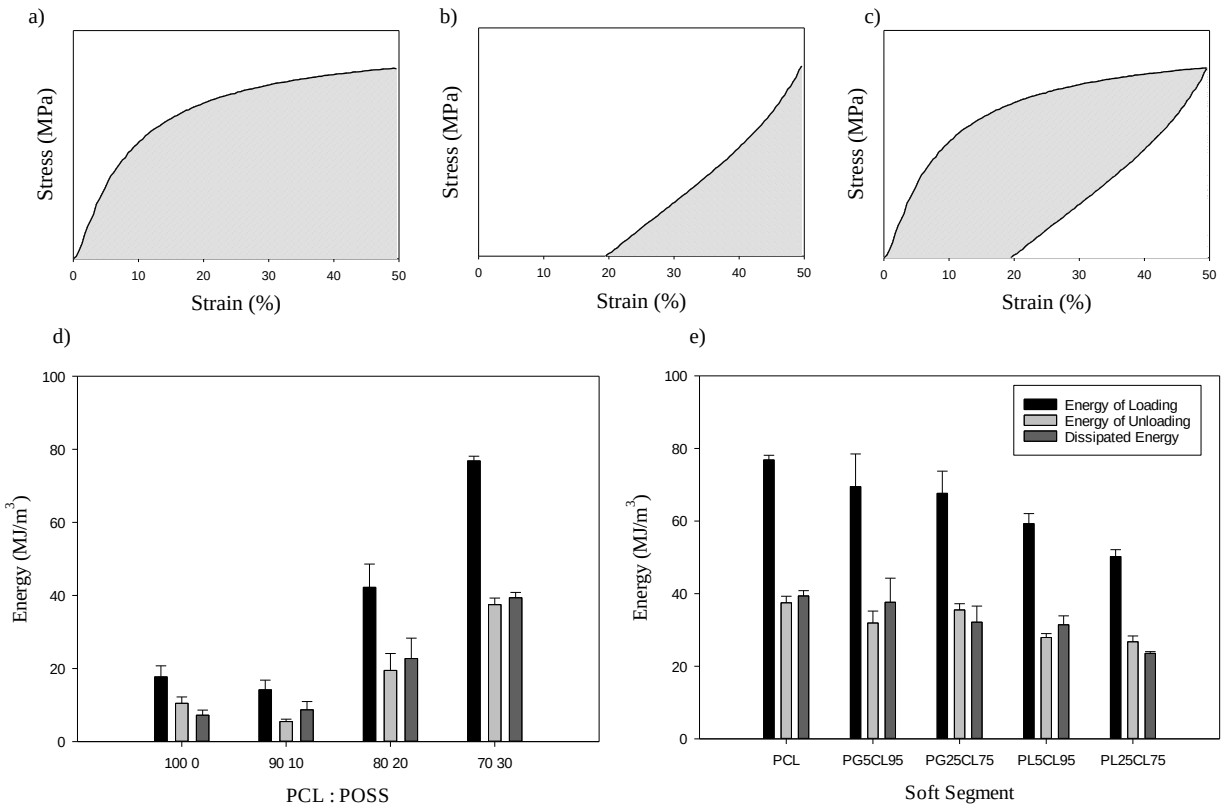

Figure 2-8: Energy stored in the elastomers: a) An example of loading curve looking at the energy stored (area under the curve) b) an example of an unloading curve looking at the energy released (area under the curve), c) the energy dissipated (difference between two energies), d) energy calculations for elastomers with changing PCL and POSS content, and e) energy calculations for all 70:30 materials with changing soft segments (n=3).

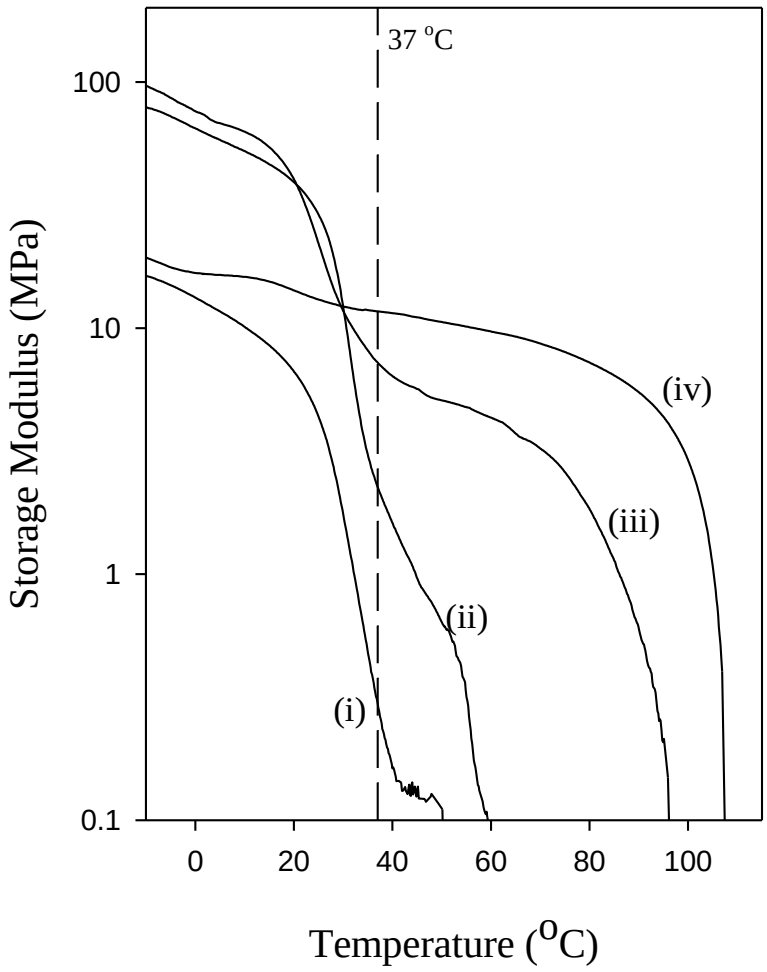

Figure 2-9: Dynamic mechanical analysis of (i) PCL_{1k}:POSS 100:0, (ii) PCL_{1k}:POSS 90:10, (iii) PCL_{1k}:POSS 80:20, and (iv) PCL_{1k}:POSS 70:30.

Table 2-5: Summary of the storage moduli (E') and Tanδ values at 25 and 37 °C.

Polymer	E'_{25} (MPa)	E'_{37} (MPa)	Tanδ at 25 °C	Tanδ at 37 °C
PCL_{1k} : POSS 100 : 0	6.71	0.30	0.089	0.532
PCL_{1k} : POSS 90 : 10	38.98	2.30	0.078	0.360
PCL_{1k} : POSS 80 : 20	39.56	7.27	0.083	0.151
PCL_{1k} : POSS 70 : 30	14.24	11.83	0.070	0.081

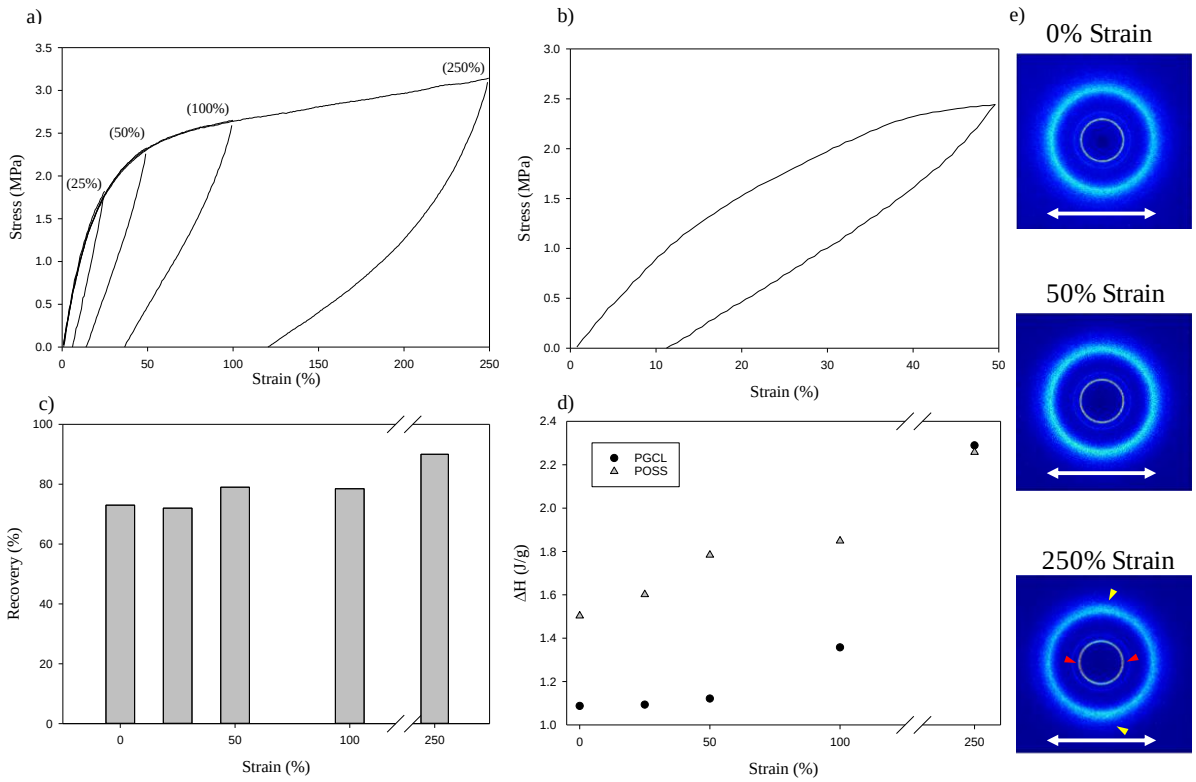

Figure 2-10: Pre-stretching of elastomers: a) Pre-stretching of $(PG_5CL_{95})_{1k}$:POSS samples to 25, 50, 100 and 250% strain. b) An example of stretching this material to 50% strain. c) The recovery of the 50% strain after each pre-stretch, d) enthalpy of melting of the PGCL and POSS as an effect of increasing pre-strain e) Wide-angle x-ray (WAXS) 2D scattering of 0%, 50%, and 250% strain with strain direction indicated by the arrows. Red arrows indicate POSS alignment and yellow arrows indicate PGCL alignment.

Chapter 3: Degradation Behavior of Novel Biodegradable Thermoplastic Elastomers Incorporating POSS

3.1 Synopsis

In vitro degradation studies were performed to determine the effect of soft segment composition on the degradation behavior of the PCL:POSS, PGCL:POSS, and PLCL:POSS elastomers from Chapter 2. At body temperature, an increased amount of comonomer, either glycolide or d,l-lactide, in the soft segment of the polyurethane caused an increase in degradation by hydrolysis. This was evident in molecular, morphological and mechanical properties and showed that the amount of comonomer had more effect on degradation rate than the chemistry of the comonomer. Another degradation study was performed at 60 °C. At an elevated temperature, PCL_{1k}:POSS had a sharp decrease in mass remaining after 2 w while the materials with d,l-lactide in the soft segment degraded more regularly over time. Finally, PCL_{1k}:POSS was degraded for several days at different temperatures. The rates of molecular weight loss were fit to the Arrhenius equation with high correlation, suggesting that the 60 °C degradation study could be indicative of a long-term degradation study at body temperature.

3.2 Introduction

Biodegradable elastomers are being developed for a wide variety of biomedical applications including medical devices,[1-3] drug delivery[4] and tissue engineering scaffolds[5] for soft tissues. In light of this need, there has been an increase in published manuscripts on biodegradable elastomers with tailored properties. One property of importance is the degradation rate after it is implanted in the body. The mode and speed of degradation affects the time the elastomer is usable within the body. Many factors have been shown to affect degradation: porosity,[6-8] hydrophobicity/hydrophilicity,[9] chain mobility[10] and crystallinity.[11]

Chemical degradation of polymers proceeds by one of two principle modes: bulk or surface degradation.[12] Bulk degradation occurs throughout the material and is characterized by a decrease in molecular weight over time, while surface degradation occurs where the surface of the material interfaces with its environment. In such cases, there is no loss in molecular weight over time in the vast majority of cases. Degradation can be characterized further by underlying mechanism-hydrolytic, oxidative, or enzymatic. Hydrolytic degradation occurs when there is a chemical cleavage of a bond due to a reaction with water. Polymers containing amides, urethanes, esters, anhydrides, carbonates, etc. are susceptible to hydrolysis and will be the focus of the present study. Alternatively, oxidative degradation occurs when a bond is cleaved by oxygen and usually occurs in materials at elevated temperatures; enzymatic degradation occurs when the material is broken down by enzymes. Importantly, these modes are not mutually exclusive.

Several FDA-approved ester-containing synthetic polymers are commonly used as biodegradable polymers including poly(caprolactone), poly(glycolide) and poly(d,l-lactide).[13-15] For more background information about these materials, please refer to Section 2.2. There are many other biodegradable polymers; however, here we focused on the polymers relevant to the present study.

Hydrolytic degradation of poly(caprolactone), poly(glycolide) and poly(d,l-lactide) occurs similarly in several steps.[16-19] Water diffuses into the material, causing random chain scission of ester bonds (forming carboxyl and hydroxyl end groups) and the molecular weight drops. When a critical molecular weight is met (M_n = 5 kDa for PCL and M_n = 15 kDa for poly(d,l-lactide)),[17] the chain can diffuse out of the material, causing mass loss. The voids allow for more water to infiltrate, and the process propagates as carboxyl groups produced by hydrolysis auto-catalyze this reaction. The degradation products of these materials can be safely eliminated from the body.[19, 20]

For example, the degradation products glycolic acid from poly(glycolide) and lactic acid from poly(d,l-lactide) can be incorporated into the body's citric acid cycle that produces adenosine triphosphate (ATP), the body's energy source. Alternatively, studies have shown that degradation products of poly(caprolactone) can be eliminated from the body through excretion in urine.[21]

As mentioned earlier, urethane linkages are also susceptible to hydrolytic degradation, resulting in an amine end group, alcohol end group, and carbon dioxide. There are several review articles on polyurethanes as biomaterials and polyurethane degradation.[22-24] These reviews focus on the chemistry of the soft blocks, hard blocks, and chain extenders, the ratio of the components, and filler effects on degradation rates. The different mechanisms of urethane degradation are also discussed. Hydrolytic degradation of the urethane group itself is slow. It was found that when deoxygenated phosphate buffered saline solution was used as the solvent for degradation of polyether polyurethanes, where only the urethane linkage was susceptible to hydrolysis, degradation was essentially eliminated, with the half-life of mass loss increasing to 80 years.[25]

POSS, a robust molecule that was utilized in our biodegradable elastomers, has interesting properties regarding degradation. POSS is a silicon-oxygen caged structure ($R_nSi_nO_{1.5n}$) that is incorporated into polymers as a pendant group with a melting transition around 120 °C. Several review articles have been written on POSS molecules and POSS polymers.[26-29] POSS has been shown to improve thermal[30, 31] and oxidative stability,[32] and when incorporated into biodegradable polymers, has been shown to suppress hydrolytic[33] and enzymatic degradation.[34] It has also been shown to be biocompatible both *in vitro*[35] and *in vivo*[36] as part of the polymer and as a degradation product.

As mentioned above, we have previously developed thermoplastic biodegradable polyurethane elastomers that utilize poly(caprolactone), poly(glycolide-co-caprolactone), or

poly(d,l-lactide-co-caprolactone) as a soft segment, POSS as a hard segment, and hexamethylene diisocyanate (Chapter 2).[37] We determined that the concentration and type of comonomer (5% or 25% glycolide or d,l-lactide) affects the thermal and mechanical properties. However, we did not examine the degradation profiles of these materials nor the effect the comonomer has on the degradation profile. This study aims to understand the degradation profile of these biodegradable elastomers with regard to: mass loss, water uptake, molecular properties, thermal properties, mechanical properties and morphology. We anticipated that increasing the comonomer concentration would increase degradation rate, and materials with glycolide would degrade faster than materials with d,l-lactide, based on their homopolymer degradation rates. We examined materials at both 37 °C and 60 °C to determine how temperature affected degradation.

3.3 Methods

3.3.1 Materials

For synthesis materials, see Section 2.3.1. Phosphate-buffered saline (pH of 7.4), deuterated chloroform (chloroform D, 99.8% atom D) and HPLC-grade THF were purchased from Sigma-Aldrich.

3.3.2 Diol and Polyurethane Synthesis

Please refer to Sections 2.3.2 and 2.3.3 for diol and polyurethane synthesis.

3.3.3 Proton Nuclear Magnetic Resonance (^{1}H-NMR)

Diols and polyurethanes were dissolved in deuterated chloroform ($CDCl_3$) at a concentration of 10-20 mg/mL. The samples were analyzed in a Bruker Avance III HD 400 MHz spectrometer equipped with a 5 mm outer diameter Prodigy probe. A standard 1D pulse sequence was used with a 30° pulse, relaxation delay time of one second and a temperature of 25 °C.

3.3.4 Gel Permeation Chromatography (GPC)

Molecular weight (M_n and M_w) and polydispersity were determined from gel permeation chromatography (GPC). Samples were dissolved in tetrahydrofuran (THF) at a concentration of 2-5 mg/mL and were passed through a 0.2 µm PTFE filter before injection. Waters Isocratic HPLC System equipped with a temperature controlled differential refractometer (Waters 2414) was used for analysis. Multi-angle laser light scattering was employed (Wyatt miniDAWN) using three angles (45°, 90°, 135°) for in-line absolute molecular weight determination.

3.3.5 Differential Scanning Calorimetry

Thermal properties of the materials were studied by differential scanning calorimetry (DSC) using the TA Q200 instrument. Heat flow was collected while each sample was heated to 200 °C (to remove thermal history), cooled to -70 °C, and heated a second time to 200 °C. The heating rates were 10 °C/min and cooling rates were 5 °C/min. The second heat was used to determine glass transition temperature (T_g, a step in the curve) and the change in heat capacity or melting transitions (T_m, the peak of the endotherm) and the enthalpy of melting (ΔH_m, area under the curve).

3.3.6 Compression Molding

The PCL_{1k}:POSS, $(PGCL)_{1k}$:POSS, and $(PLCL)_{1k}$:POSS polyurethanes were compression molded into films using a Carver 3851-0 press with heated platens. The platens were heated to 130 ºC, slightly above the T_m of POSS. After the platens were thermally equilibrated, the polymer was placed between two Teflon sheets with a 0.45 mm thick Teflon spacer. A compressive stress of 1 metric ton was applied at elevated temperatures and held for 2 min. Then the film was cooled to 70 °C, where the polymer was annealed for 30 min to allow for crystallization of the POSS hard

block before it was cooled to room temperature. The resulting films were flexible and between 0.4 and 0.5 mm in thickness, determined by a digital caliper.

3.3.7 X-Ray Diffraction

Wide-angle x-ray scattering (WAXS) and small-angle x-ray scattering (SAXS) experiments were conducted to ascertain the molecular and nano-scale ordering and orientation of the various polymeric samples. For this purpose, a Rigaku S-MAX3000 pinhole camera system was utilized, with a MicroMax-002 generator operating with Cu Kα emission ($\lambda = 1.5406$), voltage of 45 kV and current of 0.88 mA. Wide-angle scattering patterns were collected at a sample-detector distance of 122.7 mm (resulting in scattering angles $3° < 2\theta < 40°$) using Fujifilm image plates (CR HR-V) with a FujiFilm FLA7000 reader. Small-angle scattering patterns were collected using an area detector at a sample-detector distance of 1550 mm. Data were recorded in the range of $0.0054 < q < 0.16$ Å^{-1}, where $q=(4\pi/\lambda)\sin\theta$, where 2θ is the scattering angle. Samples were exposed to radiation for 30 minutes to achieve adequate x-ray counts for analysis, which was performed using SAXSgui software v2.03.04.

3.3.8 Tensile Testing

A Linkam TST 350 apparatus and TestResources Model 100P Universal Testing Machine were both utilized to determine the tensile properties of the materials. Samples were cut in a dogbone geometry (ASTM Standard D638-03 Type IV, scaled down by a factor of 4) and stretched at a rate of 50 μm/s at room temperature (about 23 °C). Young's modulus and strain-to-failure were determined from engineering stress vs. engineering strain plots.

3.3.9 Scanning Electron Microscopy

A JEOL JSM-5600 scanning electron microscope (SEM) was utilized to visualize the surface of the compacted films. Films were visualized in secondary electron mode with an

accelerating voltage of 7 kV. Samples were sputter-coated with gold for 40 seconds prior to imaging.

3.3.10 Degradation Study

In order to determine the degradation profile of the biomaterials, compression molded films of each material in a dogbone shapes (0.4 – 0.5 mm in thickness) were immersed in phosphate-buffered saline (PBS) at 37 °C or 60 °C using an incubator shaker table (New Brunswick Scientific) agitated at 60 RPM. Samples were initially weighed and immersed for up to 12 w, with buffer replaced with new buffer every week. The samples were removed from PBS (3 dogbones per composition every 2 w), rinsed with DI water, removed of excess water, and weighed to determine their wet mass. After extensive drying, samples were weighed again for their dried mass. The following equations were used to determine mass remaining and water uptake:

$$\text{mass remaining } (\%) = \left(\frac{m_d}{m_i}\right) * 100 \qquad \textbf{(3-1)}$$

$$\text{water uptake } (\%) = \left(\frac{m_{wet} - m_d}{m_d}\right) * 100 \qquad \textbf{(3-2)}$$

with m_i being the initial mass of the sample, m_{wet} being the mass of the wet sample, and m_d the mass of the dry sample. Each sample's molecular weight and molecular composition were determined from GPC and ^{1}H-NMR, as described above. Molecular weight was analyzed as a function of the original molecular weight of each film and plotted using the equation below:

$$\mathrm{M}_w\ (\%) = \left(\frac{M_{w,d}}{M_{w,o}}\right) * 100 \qquad \textbf{(3-3)}$$

Where $M_{w,d}$ is the molecular weight (M_w) of the dry material and $M_{w,o}$ is the initial molecular weight (M_w) of each film. PCL_{1k}:POSS and $(PL_5CL_{95})_{1k}$:POSS were tested for thermal properties throughout degradation with DSC, as described above. The mechanical properties- elasticity, modulus and strain-to-failure- of the degraded, dry materials were determined from

elasticity tests: the materials were stretched to 50% strain and the strain recovered was determined using an AR-G2 rheometer with a rate of 50 μ/s for loading and unloading. Elasticity was determined from the following equation:

$$R_E\ (\%) = \frac{\varepsilon_f - \varepsilon_r}{\varepsilon_f - \varepsilon_i} * 100 \qquad \textbf{(3-4)}$$

Where ε_i is a small initial strain (where stress equals zero), ε_f is the strain that the polymer is stretched to, and ε_r is the strain recovered (where stress equals zero upon unloading).

A more detailed investigation of mechanical property degradation was pursued for a particularly promising composition. Mechanical properties, specifically modulus and strain-to-failure, were compared for a batch of $(PG_5CL_{95})_{1k}$:POSS degraded at 37 °C for materials tested dry at room temperature or hydrated at body temperature (37 °C). At given time points, wet mechanical testing was performed using a TestResources Model 100P Universal Testing Machine with an environmental bath containing saline solution (9 g NaCl/1 L DI water), heated to 37 °C. Other samples were dried extensively and tested at room temperature (~23 °C) to compare hydrated and dry mechanical properties.

3.3.11 Degradation Study Modeling

In order to further examine the effect of temperature on degradation, samples of PCL_{1k}:POSS 70:30 were degraded at various temperatures (23, 37, and 60 °C) over the course of 15 days. At each time point (every 3 d) samples were removed and dried extensively in a room-temperature vacuum oven. The molecular weight of the dried samples was determined by GPC. The drop in the molecular weight (M_n) was plotted semi-logarithmically on a $\ln(M_t/M_o)$ vs time plot. The data was fit with a linear curve, the slope of which is the rate constant k (d^{-1}). The rate constants were then fit to the Arrhenius equation to solve for activation energy:

$$k = Ae^{-E_A/RT} \qquad \textbf{(3-5)}$$

Where k is the rate constant, A is the pre-exponential factor (s^{-1}) E_A is the activation energy (kJ/mol), R is the universal gas constant (8.3145 kJ/mol*K), and T is temperature (in Kelvin).

3.3.12 Statistical Analysis

T-tests were performed on two means with unequal variances to determine the statistical significance of different sets of data. Two-tailed t-tests with a confidence value of $\alpha = 0.05$ was used for all tests in making comparisons.

3.4 Results

3.4.1 Polyurethanes in Degradation Study

Polyurethanes were synthesized in Chapter 2 with varying soft segment chemistries and a soft segment:POSS ratio of 70:30. The materials utilized in this degradation study were PCL_{1k}:POSS 70:30, $(PG_5CL_{95})_{1k}$:POSS 70:30, $(PG_{25}CL_{75})_{1k}$:POSS 70:30, $(PL_5CL_{95})_{1k}$:POSS and $(PL_{25}CL_{75})_{1k}$:POSS 70:30. A summary of the molecular properties of the polyurethanes tested for degradation are presented in **Table 3-1**. Thermal and mechanical properties of the polyurethanes were determined previously and are summarized in **Table 3-2**.

3.4.2 Mass Loss and Water Uptake (37 °C Degradation Study)

The five compositions were tested for degradation at body temperature by submerging films (of dogbone geometry) in PBS at 37 °C for 12 weeks. Mass remaining and water uptake were determined every two weeks and the results are shown in **Figure 3-1**. PCL_{1k}:POSS had the lowest amount of water uptake (10.4 ± 2.2 % at 12 w) and had 98.9 ± 0.1 % mass remaining at 12 w. $(PG_5CL_{95})_{1k}$:POSS had slightly more mass loss than PCL_{1k}:POSS during weeks 4 to 10 ($p < 0.01$), and after 12 w had 97.5 ± 1.1 % ($p > 0.05$ compared to PCL_{1k}:POSS) mass remaining. This material had 17.0 ± 1.1 % ($p < 0.05$ compared to PCL_{1k}:POSS) water uptake after 12 w. Similarly to $(PG_5CL_{95})_{1k}$:POSS, $(PL_5C_{95})_{1k}$:POSS had less mass remaining than PCL_{1k}:POSS with 97.5 ± 0.3

% ($p < 0.05$) mass remaining after 8 w. During weeks 10 and 12, this polymer slightly increased in mass to be over 100% mass remaining ($p < 0.01$). $(PL_5CL_{95})_{1k}$:POSS had a higher water uptake than PCL_{1k}:POSS ($p < 0.05$) and $(PG_5CL_{95})_{1k}$:POSS until 10 w ($p < 0.05$), where the water uptake profile was the same as the 5% glycolide material.

The 25% comonomer polyurethanes showed greater mass loss and water uptake than the other materials. $(PG_{25}CL_{75})_{1k}$:POSS had greater mass loss and water uptake than PCL_{1k}:POSS ($p < 0.05$) and $(PG_5CL_{95})_{1k}$:POSS ($p < 0.05$). After 12 w, $(PG_{25}CL_{75})_{1k}$:POSS had 75.4 ± 1.1% mass remaining and 72.4 ± 8.7 % water uptake. $(PL_{25}CL_{75})_{1k}$:POSS had 79.4 ± 5.4% mass remaining and 98.8 ± 15.3 % water uptake at 12 w, which was higher than the water uptake of PCL_{1k}:POSS ($p < 0.05$) and $(PL_5CL_{95})_{1k}$:POSS ($p < 0.05$). Unlike the 5% comonomer materials, the 25% comonomer materials' water uptake was statistically not different ($p > 0.05$).

3.4.3 Film Surface (37 °C Degradation Study)

The surfaces of the films were examined with scanning electron microscopy every 4 w, as shown in **Figure 3-2**. PCL_{1k}:POSS 70:30's surface had no visible changes throughout 12 w. $(PG_5CL_{95})_{1k}$:POSS had a smooth surface until 12 w, at which point surface buckling became evident. Texture was present on $(PG_{25}CL_{75})_{1k}$:POSS's surface after 4 w, and surface buckling was seen at 8 w. By 12 w, the film surface cracked. For $(PL_5CL_{75})_{1k}$:POSS the surface of the film was unchanged through 8 w, although there was surface roughness present after 12 w of degradation. Finally, $(PL_{25}CL_{75})_{1k}$:POSS had surface buckling at 8 w and 12 w, with higher amplitude buckling at the later time.

3.4.4 Molecular Weight (37 °C Degradation Study)

Molecular weight evolution during degradation was analyzed by gel permeation chromatography to determine how molecular weight, specifically weight-averaged molecular

weight (M_w), changed over time. The molecular weight at each time was compared to the polymer film's initial molecular weight and the results are presented in **Figure 3-3**. The molecular weights of the films before degradation (at t=0) are listed in **Table 3-3**. PCL_{1k}:POSS, despite having the lowest initial M_w, had the highest relative molecular weight through 12 w. Uniquely, the molecular weight increased from 6 w to 12 w. The molecular weights of materials with comonomers decreased at a faster rate with time. The polymer with 5% glycolide had a lower percentage of the original molecular weight for every time point after week 2 than PCL_{1k}:POSS ($p < 0.05$). Despite having the highest initial molecular weight, $(PG_{25}CL_{75})_{1k}$:POSS had the largest decline of molecular weight, and by 12 w featured only 6.7 ± 1.6% ($p < 0.05$ compared to all polymers) of the original M_w. It had a lower molecular weight at each time point than PCL_{1k}POSS and $(PG_5CL_{95})_{1k}$:POSS ($p < 0.05$). The d,l-lactide materials showed similar trends to the glycolide materials. $(PL_5CL_{95})_{1k}$:POSS's molecular weight decreased more over time than PCL_{1k}:POSS ($p < 0.01$ w 8 – 12). $(PL_{25}CL_{75})_{1k}$:POSS's molecular weight decreased over time at a faster rate than $(PL_5CL_{95})_{1k}$:POSS through week 8 ($p < 0.01$) and PCL_{1k}:POSS ($p < 0.01$) for all weeks. For the same mol % of comonomer, the molecular weight decreased more quickly for the glycolide-containing materials than the d,l-lactide containing materials, although this is only statistically significant for weeks 4, 8 and 12 for 5% comonomer ($p < 0.05$) and week 12 for 25% comonomer ($p < 0.05$).

3.4.5 Molecular Composition (37 °C Degradation Study)

To determine the evolution of molecular composition for each material over time, ^{1}H-NMR was performed every 2 w throughout degradation (**Figure 3-4**). From this data, the weight ratios of the soft segments and hard segments were determined. See **Figure 2-2** for example ^{1}H-NMR structures. PCL_{1k}:POSS initially featured 76.5 ± 0.1% PCL_{1k} and 23.5 ± 0.1% POSS. These ratios

were maintained throughout degradation, and after 12 w the ratios were 76.5 ± 0.1 wt.% PCL_{1k} and 23.5 ± 0.1 wt. % POSS. Incorporation of a comonomer yielded a trend of decreasing soft segment content (PGCL or PLCL) and increasing POSS content throughout degradation. $(PG_5CL_{95})_{1k}$:POSS decreased from 71.0 ± 0.1% $(PG_5CL_{95})_{1k}$ to 70.2 ± 0.1% $(PG_5CL_{95})_{1k}$ and had the corresponding increase in POSS during the 12 w degradation study. Incorporation of more glycolide caused a more significant compositional change, with $(PG_{25}CL_{75})_{1k}$ dropping from 65.4 ± 0.4% to 56.3 ± 1.2% by week 12. Similar trends for d,l-lactide incorporation were evident. The elastomer with 5% d,l-lactide had a similar decrease in soft segment as 5% glycolide from 73.9 ± 0.1% to 72.9 ± 0.2%. $(PL_{25}CL_{75})_{1k}$:POSS had a larger decrease in soft segment and corresponding increase in POSS: 71.9 ± 0.3% to 67.4 ± 0.2% $(PL_{25}CL_{75})_{1k}$ and 28.1 ± 0.3% to 32.6 ± 0.2% POSS during 2 w and 12 w, respectively.

Statistical significance of these molecular compositional changes was determined by comparing the slopes of the linear fit curves (data not shown). The soft segment compositional changes had slopes of -.015 ± 0.004 %/w for PCL_{1k}, -0.065 ± 0.02 %/w for $(PG_5CL_{95})_{1k}$, -0.804 ± 0.1 %/w for $(PG_{25}CL_{75})_{1k}$, -0.094 ± 0.03 %/w for $(PL_5CL_{95})_{1k}$, and -0.424 ± 0.04 %/w for $(PL_{25}CL_{75})_{1k}$ ($R^2 > 0.75$ for all). When performing t-tests on these slopes, PCL_{1k}:POSS had a smaller change in molecular composition than the 5% comonomer polymers ($p < 0.05$) and the 25% comonomers ($p < 0.01$). The 5% comonomers had a slower change in composition than their respective 25% comonomers ($p < 0.01$). When comparing the same percentage of comonomers, $(PL_5CL_{95})_{1k}$:POSS had similar rate of compositional change as $(PG_5CL_{95})_{1k}$:POSS. However, $(PG_{25}CL_{75})_{1k}$:POSS had a faster rate of change than $(PL_{25}CL_{75})_{1k}$:POSS ($p < 0.05$).

3.4.6 Thermal Properties (37 °C Degradation Study)

Differential scanning calorimetry was performed for PCL_{1k}:POSS and $(PL_5CL_{95})_{1k}$:POSS throughout degradation to determine the change in enthalpy over time. First and second heat melting enthalpies are depicted for the soft segment and POSS in **Figures 3-5a** and **3-5b**, respectively. For PCL_{1k}, the first and second heat melting enthalpies did not follow any consistent trends and oscillated around 3 J/g and 10 J/g, respectively. For $(PL_5CL_{95})_{1k,}$ the melting enthalpy increased from 1.0 ± 0.4 to 4.7 ± 0.1 J/g ($p < 0.01$) during the first heat, and increased from 2.5 ± 0.4 to 13.7 ± 0.4 J/g ($p < 0.01$) for second heat. As for POSS, the enthalpies did not show much change, although the first heat for $(PL_5CL_{95})_{1k}$:POSS increased from 1.7 ± 0.3 to 2.8 ± 0.8 J/g ($p > 0.05$) during the 12 w degradation study.

3.4.7 Mechanical Properties (37 °C Degradation Study)

Mechanical properties were studied over the course of degradation, and the results are depicted in **Figure 3-6**. Dry mechanical properties were studied by straining samples to 50% strain and determining modulus (**Figure 3-6a**), strain-to-failure (**Figure 3-6b**), and elasticity (**Figure 3-6c**). Generally, the modulus of all materials decreased with degradation. Materials that could not be tested due to lack of mechanical integrity are depicted as having a modulus of 0 MPa for convenience. PCL_{1k}:POSS had the highest starting modulus of 10.2 ± 0.3 MPa, which decreased over time to 7.6 ± 0.5 MPa at 12 w. While $(PG_5CL_{95})_{1k}$:POSS had a lower starting modulus than PCL_{1k}:POSS at 9.2 ± 0.02 MPa, it increased to 11.3 ± 0.5 MPa during 6 w, which was greater than any other material ($p < 0.01$). $(PG_5CL_{95})_{1k}$:POSS's modulus then dropped to 7.8 ± 0.8 MPa at 10 w and was similar to PCL_{1k}:POSS at 12 w ($p > 0.05$). While $(PG_{25}CL_{75})_{1k}$:POSS's modulus was not different from PCL_{1k}:POSS and $(PG_5CL_{95})_{1k}$:POSS at 0 and 2 w ($p > 0.05$), it lost mechanical integrity during 4 w of degradation and could not be tested ($p < 0.01$ compared to PCL_{1k}:POSS and $(PG_5CL_{95})_{1k}$:POSS). $(PL_5CL_{95})_{1k}$:POSS and $(PL_{25}CL_{75})_{1k}$:POSS had lower starting moduli

than the other compositions at 8.3 ± 0.9 MPa and 7.1 ± 0.1 MPa, respectively. After 12 w of degradation, the modulus of $(PL_5CL_{95})_{1k}$:POSS had decreased to 4.0 ± 0.2 MPa ($p < 0.01$). $(PL_{25}CL_{75})_{1k}$:POSS like $(PG_{25}CL_{75})_{1k}$:POSS lost its structural integrity, although it maintained its mechanical integrity longer and failed after 6 w.

Strain-to-failure evolution was also examined as part of the elasticity test. If the sample did not break during the test, its strain-to-failure was designated > 50%. PCL_{1k}:POSS has greater than 50% strain-to-failure for all time points during the three month study. However, materials with comonomer had strain-to-failure values decrease over time to below 50% strain. $(PG_{25}CL_{75})_{1k}$:POSS and $(PL_{25}CL_{75})_{1k}$:POSS both had strains-to-failure less than 50% at 2 w. The strain-to-failure decreased over time until the materials were not testable at 4 and 6 w, respectively. The strain-to-failure for these materials were only statistically significantly different during week 6 ($p < 0.05$). $(PG_5CL_{95})_{1k}$:POSS and $(PL_5CL_{95})_{1k}$:POSS had strain-to-failure > 50% strain through 6 weeks. Afterward, the strains-to-failure decreased until 12 w, where the 5% glycolide and d,l-lactide-containing materials had 25.2 ± 5.3 % and 21.9 ± 12.4 % strain-to-failure, respectively. While different from PCL_{1k}:POSS and the 25% comonomer materials ($p < 0.05$), the strains-to-failure of the 5% comonomer materials were not different ($p > 0.05$).

Finally, elasticity was measured by stretching to 50% strain and determining the strain recovered (when stress returned to zero upon unloading). The elastic recovery (R_E) was determined and was compared to its original elastic recovery (R_E,o) in **Figure 3-6c**. Because the 25% comonomer materials' strains-to-failure were < 50% after 2 w, their elasticity was 0% throughout the degradation study. Conversely, PCL_{1k}:POSS had greater than 100% its original elastic recovery throughout degradation. $(PG_5CL_{95})_{1k}$:POSS and $(PL_5CL_{95})_{1k}$:POSS had greater than 100% elasticity through 6 w, where they lost their elasticity.

Tensile testing was also performed on a batch of $(PG_5CL_{95})_{1k}$:POSS every 4 w for 8 w to determine if there was a difference in the mechanical properties when tested dry at room temperature or in saline solution at 37 °C (**Figure 3-6d**) after degradation in PBS at 37 °C. Before degradation (t=0), the material had a higher strain-to-failure when tested wet ($p > 0.05$), where it reached the limits of the instrument (> 3000 % strain). When dry tested at room temperature, $(PG_5CL_{95})_{1k}$:POSS had a strain-to-failure of 2800 ± 150 %. The strains-to-failure decreased over time and by 4 w, $(PG_5CL_{95})_{1k}$:POSS has a dry strain-to-failure of 280 ± 70 %, which was higher than the heated, hydrated strain-to-failure of 70 ± 3 % ($p < 0.01$). At 8 w, the dry strain-to-failure was again higher than the hydrated, heated strain-to-failure, as their strains-to-failure were 40 ± 6 % and 20 ± 7 % ($p < 0.01$), respectively.

3.4.8 Accelerated Degradation Study (60 °C Degradation Study)

An accelerated degradation study was performed at 60 °C for PCL_{1k}:POSS, $(PL_5CL_{95})_{1k}$:POSS and $(PL_{25}CL_{75})_{1k}$:POSS to determine how these materials would behave after 12 w at 37 °C. Mass remaining, water uptake, molecular weight characterization and molecular composition over time are illustrated in **Figure 3-7**. After 2 w, the materials showed similar mass loss trends as the study at 37 °C, as displayed in **Figure 3-7a**. PCL_{1k}:POSS had 98.9 ± 0.5% mass remaining, while $(PL_5CL_{95})_{1k}$:POSS and $(PL_{25}CL_{75})_{1k}$:POSS had 94.7 ± 0.3% and 42.2 ± 5.3% mass remaining. However, after 2 w, PCL_{1k}:POSS lost its mass much more quickly than the d,l-lactide-containing materials and by 12 w has the lowest remaining mass ($p < 0.05$). At 12 w, PCL_{1k}:POSS had only 7.0 ± 4.1% mass remaining, while $(PL_5CL_{95})_{1k}$:POSS had 67.4 ± 1.1% mass remaining and $(PL_{25}CL_{75})_{1k}$:POSS had 18.4 ± 1.2% mass remaining.

Water uptake was the least for the 5% d,l-lactide polyurethane after 12 w, as shown in **Figure 3-7b**. At 2 w, PCL_{1k}:POSS had less water uptake than $(PL_5CL_{95})_{1k}$:POSS and

$(PL_{25}CL_{75})_{1k}$:POSS ($p < 0.05$), but after 2 w it had more water uptake than the others. By 12 w, PCL_{1k}:POSS had a water uptake of 1850 ± 1200%, while $(PL_5CL_{95})_{1k}$:POSS had 122 ± 3.8%. $(PL_{25}CL_{75})_{1k}$:POSS had the most water uptake initially with 544 ± 91% at 2 w. Although the water uptake increased to 950 ± 330% by week 8, it decreased to 650 ± 60% by 12 w.

The molecular characteristics of the materials degrading at 60 °C were also characterized. All molecular weights (**Figure 3-7c**) had dropped to about 15% of their original M_w (**Table 3-4**) by 2 w, with $(PL_{25}CL_{75})_{1k}$:POSS having the lowest molecular weight at 12 ± 1% of its original ($p < 0.05$). PCL_{1k}:POSS had a lower percentage of M_w at 6 w and 8 w. By 10 w, it had become insoluble in THF and was unable to be characterized. At 12 w, $(PL_5CL_{95})_{1k}$:POSS and $(PL_{25}CL_{75})_{1k}$:POSS had 8.2 ± 2 and 9.6 ± 4% of their initial molecular weights, respectively, which were statistically not different ($p > 0.05$). When examining molecular composition (**Figure 3-7d**), the d,l-lactide polymers showed similar compositional changes as in the 37 °C study, but with a larger magnitude. The soft segment in $(PL_5CL_{95})_{1k}$:POSS decreased in percentage present from 72.4 ± 0.4% to 66.4 ± 0.5% during the 12 w study, while the soft segment decreased in percentage present from 73.8 ± 0.1% to 23.9 ± 3.8% in $(PL_{25}CL_{75})_{1k}$:POSS. Uniquely, PCL_{1k}:POSS did not decrease in PCL_{1k} content over time, but instead increased in PCL_{1k} content from 77.3 ± 0.2% to 82.4 ± 0.1% at 8 w. After that, the material was insoluble in $CDCl_3$. The slopes of the linear fit curves for the soft segments, 0.903 ± 0.1 %/w for PCL_{1k}, -0.593 ± 0.1 %/w for $(PL_5CL_{95})_{1k}$, and -4.80 0.6 %/w for $(PL_{25}CL_{75})_{1k}$ ($R^2 > 0.8$ for all) are all distinct from each other ($p < 0.01$).

3.4.9 Degradation Study Modeling

PCL_{1k}:POSS was degraded at multiple temperatures to model the degradation behavior and determine the activation energy (ΔE_A) of the system from the Arrhenius equation. The resulting molecular weights (M_n) and modeling are shown in **Figure 3-8**. **Figure 3-8a** shows the changes

in molecular weight for each degradation temperature over 15 days. The higher the temperature of degradation, the lower the molecular weight was over time. This data was plotted as $\ln(M_t/M_o)$ in **Figure 3-8b**, where M_t was the molecular weight at time t and M_o was the initial molecular weight. The curves were fit to linear trends with the slopes equal to rate constants k (d^{-1}). These rate constants were 0.041, 0.069, and 0.149 for 23, 37, and 60 °C with R^2 values of 0.96, 0.91, and 0.92, respectively. The rate constants were plotted as a function of temperature (in K), then fitted to a line, where the slope is $-E_A/R$ and R is the universal gas constant. From the plot in **Figure 3-8c,** the linear fit curve has an R^2 value of 0.999 and a slope of 4295.4 K. This resulted in an activation energy for the system of 35.7 kJ/mol.

3.5 Discussion

A degradation study was conducted to examine mass loss, water uptake, morphological changes, molecular changes, and crystallinity changes throughout *in vitro* degradation in PBS at 37 °C and at 60 °C. This study revealed how soft segment chemistry affected degradation.

Based on mass loss and water uptake at 37 °C, the level of comonomer incorporation had a larger effect on degradation than the chemistry of the comonomer, with increasing comonomer content accelerating hydrolytic degradation. Hydrolysis occurs when water diffuses into a material, causing chain scission (usually of ester bonds) into carboxyl and hydroxyl groups. Although glycolide is more hydrophilic than d,l-lactide and has been shown to degrade faster,[16, 38] the same amount of comonomer led to the same mass loss profile. The 5% comonomer materials had statistically similar degradation profiles for mass remaining until the $(PL_5CL_{95})_{1k}$:POSS increased in mass. The increase in mass seen at 10 and 12 w can be attributed to salt retention, although more testing needs to be done to confirm. The 25% comonomer materials also had similar mass loss profiles after 6 w. Therefore, when small amounts of comonomer (≤ 25 mol %) were present in

our elastomers, the degradation profile was characteristic of the amorphous nature of the soft segment, not the polymer's precise composition (glycolide vs d,l-lactide). The comonomers disrupted the crystallinity of poly(caprolactone) and made the soft segment more susceptible to hydration and therefore hydrolysis, as amorphous regions have more mobile chains than crystalline regions and the increased mobility allows for more rapid water infiltration. It is interesting that, although the soft segments were all melted at 37 °C, the increased mobility of the chains affected their degradation rates.

Surface structure, as shown with SEM, did not show any major surface changes throughout degradation. The surface roughness that appeared occurred simultaneously with macroscopic changes in the films during degradation (data not shown). This could be because degradation was occurring predominantly molecularly by chain scission, which is shown in the molecular weight data.

The change in molecular weight over time was indicative of bulk-degrading polymers, as surface-degrading polymers would have a constant molecular weight over time. As a polymer's molecular weight falls below its entanglement length, chains are capable of diffusing out of the bulk causing a decrease in mass. The molecular weight decreased more quickly for the higher comonomer materials as these materials were more susceptible to hydrolysis. This was consistent with molecular weight loss. As for molecular composition, the soft segments were more susceptible to degradation than the hard segment, as hard segments are generally less susceptible to degradation due to increased hardness or crystallinity.[39] Specifically, when POSS is utilized as a hard segment, it has been shown to prevent degradation of materials by hydrolysis,[33] oxidation,[32] and enyzmes.[34]

As for mechanical properties of the degrading materials, the strain-to-failure decreased over time as the chains decreased in molecular weight. Molecularly, chains entangle or slide past each other and as chains decrease in length, they become less entangled and cause macroscopic mechanical failure at a lower strain. The materials with 5% comonomer had similar strain-to-failure profiles, with strain-to-failure falling below 50% after 6 weeks. Of the 25% comonomer materials, $(PL_{25}CL_{75})_{1k}$:POSS had a higher strain-to-failure than $(PG_{25}CL_{75})_{1k}$:POSS through 6 w. This could be due to the fact that glycolide is more hydrophilic and thus more susceptible to degradation by hydrolysis, resulting in lower mechanical properties from shorter chains. Alternatively, because the initial strain-to-failure was much lower for $(PG_{25}CL_{75})_{1k}$:POSS (493 ± 144 %) than the other materials (> 1200%), the strain-to-failure values were lower throughout degradation. The PCL_{1k}:POSS material maintained its high strain-to-failure throughout degradation, despite its low starting molecular weight. Elasticity was maintained while the strains-to-failure of the materials were greater than 50% strain, which would be beneficial for many elastomeric applications.

The moduli of all of the materials decreased over time, despite the lack of change (PCL_{1k}) or increase in melting enthalpy (PL_5CL_{95}) of the soft and hard segments of the polyurethane as shown in differential scanning calorimetry. Wide-angle x-ray and small-angle x-ray scattering analysis was also performed on $(PL_5CL_{95})_{1k}$:POSS to determine if crystallinity changes over time could explain the change in modulus. From the WAXS and SAXS patterns (**Figure 3-9** and **Figure 3-10**, respectively), there was no change in crystallinity, indicating that crystallinity changes were not the cause of the modulus change. The modulus decrease over time could be due to the creation of voids within the polymer as the material is hydrolyzing (as the materials become opaque in buffer, pictures not shown). These voids collapsed upon drying, returning the materials to a clear

appearance. These voids are not load-bearing, and therefore the modulus decreased over time. The reduction in modulus could also be caused by a decrease in cross-links between chains as hydrolysis occurs and the molecular weight falls.

When comparing wet and dry mechanical properties, the strain-to-failure was lower for the wet materials than the dry materials. As with the decreasing moduli over time, this could be due to voids in the material that are evident when immersed in PBS and the films turn white (photo not shown). When tested in the hydrated state, the saline solution in the voids could disrupt the film, and because they are not load bearing, cause the film to have lower mechanical properties than when dry and the voids are collapse. Crystallinity could also have been lower wet than dry resulting in lower mechanical properties for the hydrated materials, as amorphous polymers have lower moduli than semi-crystalline polymers of the same chemistry.

Under accelerated degradation conditions, the d,l-lactide-containing polymers followed the trends that were evident in the 37 °C study. However, after two weeks of degradation, PCL_{1k}:POSS degraded more quickly than the other materials and by the end of the 12 w study had the lowest mass loss and highest water uptake. Mechanical properties could not be performed on any material after week 2 due to their degraded nature. Also of interest, unlike the other materials, PCL_{1k}:POSS increased in soft segment content, indicating that POSS was leaving the polymer more quickly than the PCL_{1k}. This could be due to the packing of PCL being more compact than POSS, as PCL_{1k}:POSS 70:30 was found to uptake more water than PCL_{1k}:POSS 100:0 (**Figure 3-11**). However, the POSS could have also disrupted the crystallinity of PCL in the 70:30 polyurethane, creating more voids and allowing more water to infiltrate. Alternatively, it has been hypothesized that POSS acts as a passivating layer during enzymatic degradation as POSS accumulates at the surface during degradation.[34] It also has been shown that in accelerated degradation of PCL, the

mode of degradation switches from bulk to surface.[40] It is hypothesized that POSS was concentrated at the surface during degradation, and a combination of surface and bulk degradation occurred, causing POSS to leave the material before PCL, leaving PCL. More testing would need to be done to verify this postulation.

Finally, PCL_{1k}:POSS was degraded at several temperatures to find its activation energy of degradation. The rate constants found by the molecular weight loss at degradation temperatures between the soft segment melting point and POSS's melting point showed a linear trend line with high correlation. The activation energy of degradation was found to be about 36 kJ/mol, which is lower than the activation energy for hydrolysis of PCL (M_w ~ 80 kDa) and poly(l-lactide) (PLLA) in melted form at about 72 kJ/mol and 51 kJ/mol, respectively.[41] Our ability to linearly fit the curve to the Arrhenius equation suggests that the increased temperature degradation could shed light on later time points of degradation at 37 °C. This would indicate that although PCL_{1k}:POSS would maintain its properties longer, once it started to degrade it would degrade more quickly than the lactide-containing materials.

3.6 Conclusions

In conclusion, the biodegradable elastomers previously developed degrade hydrolytically, the rate of which depends on the amount of comonomer in the soft segment. Increasing comonomer content caused an in increase in mass loss, water uptake, and a decrease in molecular weight and mechanical properties. The soft segments' ester bonds are cleaved, indicated by the decrease in soft segment concentration. Hydrated, heated mechanical properties were found to be inferior to dry, room temperature mechanical properties. At higher temperatures, materials with no comonomer degraded more quickly (after a lag time) than the comonomer materials. The activation energy of degradation was found using the Arrhenius equation with high correlation,

indicating the higher temperature degradation study could be indicative of a long-term study at body temperature.

3.7 References

1. Lee, S. H., In-vivo biocompatibility evaluation of stents coated with a new biodegradable elastomeric and functional polymer. *Coronary artery disease* **2002,** *13* (4), 237-241. DOI: 10.1097/00019501-200206000-00006.

2. Lendlein, A.; Langer, R., Biodegradable, Elastic Shape-Memory Polymers for Potential Biomedical Applications. *Science* **2002,** *296* (5573), 1673.

3. Hwang, S.-W.; Lee, C. H.; Cheng, H.; Jeong, J.-W.; Kang, S.-K.; Kim, J.-H.; Shin, J.; Yang, J.; Liu, Z.; Ameer, G. A.; Huang, Y.; Rogers, J. A., Biodegradable Elastomers and Silicon Nanomembranes/Nanoribbons for Stretchable, Transient Electronics, and Biosensors. *Nano Letters* **2015,** *15* (5), 2801-2808. DOI: 10.1021/nl503997m.

4. Amsden, B., Curable, biodegradable elastomers: emerging biomaterials for drug delivery and tissue engineering. *Soft Matter* **2007,** *3* (11), 1335-1348. DOI: 10.1039/B707472G.

5. Bettinger, C. J., Biodegradable Elastomers for Tissue Engineering and Cell-Biomaterial Interactions. *Macromolecular bioscience 11* (4), 467-482. DOI: 10.1002/mabi.201000397.

6. Wu, L.; Ding, J., Effects of porosity and pore size on in vitro degradation of three-dimensional porous poly(D,L-lactide-co-glycolide) scaffolds for tissue engineering. *Journal of Biomedical Materials Research Part A* **2005,** *75A* (4), 767-777. DOI: 10.1002/jbm.a.30487.

7. van Tienen, T. G.; Heijkants, R. G. J. C.; Buma, P.; de Groot, J. H.; Pennings, A. J.; Veth, R. P. H., Tissue ingrowth and degradation of two biodegradable porous polymers with different porosities and pore sizes. *Biomaterials* **2002,** *23* (8), 1731-1738. DOI: http://dx.doi.org/10.1016/S0142-9612(01)00280-0.

8. Cunha-reis, C.; Tuzlakoglu, K.; Baas, E.; Yang, Y.; Haj, A. E.; Reis, R. L., Influence of porosity and fibre diameter on the degradation of chitosan fibre-mesh scaffolds and cell adhesion. *Journal of Materials Science : Materials in Medicine* **2007,** *18* (2), 195-200. DOI: http://dx.doi.org/10.1007/s10856-006-0681-x.

9. Reed, A. M.; Gilding, D. K., Biodegradable polymers for use in surgery — poly(glycolic)/poly(Iactic acid) homo and copolymers: 2. In vitro degradation. *Polymer* **1981,** *22* (4), 494-498. DOI: http://dx.doi.org/10.1016/0032-3861(81)90168-3.

10. Alteheld, A.; Feng, Y.; Kelch, S.; Lendlein, A., Biodegradable, Amorphous Copolyester-Urethane Networks Having Shape-Memory Properties. *Angewandte Chemie International Edition* **2005,** *44* (8), 1188-1192. DOI: 10.1002/anie.200461360.

11. Kweon, H.; Yoo, M. K.; Park, I. K.; Kim, T. H.; Lee, H. C.; Lee, H.-S.; Oh, J.-S.; Akaike, T.; Cho, C.-S., A novel degradable polycaprolactone networks for tissue engineering. *Biomaterials* **2003,** *24* (5), 801-808. DOI: http://dx.doi.org/10.1016/S0142-9612(02)00370-8.

12. Göpferich, A., Polymer Scaffolding and Hard Tissue EngineeringMechanisms of polymer degradation and erosion. *Biomaterials* **1996,** *17* (2), 103-114. DOI: http://dx.doi.org/10.1016/0142-9612(96)85755-3.

13. Nair, L. S.; Laurencin, C. T., Biodegradable polymers as biomaterials. *Progress in Polymer Science* **2007,** *32* (8-9), 762-798. DOI: 10.1016/j.progpolymsci.2007.05.017.

14. Hutmacher, D. W., Scaffolds in tissue engineering bone and cartilage. *Biomaterials* **2000,** *21* (24), 2529-2543. DOI: http://dx.doi.org/10.1016/S0142-9612(00)00121-6.

15. Gunatillake, P. A., Biodegradable synthetic polymers for tissue engineering. *European cells & materials* **2003,** *5*, 1-16.

16. Li, S., Hydrolytic degradation characteristics of aliphatic polyesters derived from lactic and glycolic acids. *Journal of biomedical materials research* **1999,** *48* (3), 342-353. DOI: 10.1002/(SICI)1097-4636(1999)48:3<342::AID-JBM20>3.0.CO;2-7.

17. Pitt, G. G.; Gratzl, M. M.; Kimmel, G. L.; Surles, J.; Sohindler, A., Aliphatic polyesters II. The degradation of poly (DL-lactide), poly (ε-caprolactone), and their copolymers in vivo. *Biomaterials* **1981,** *2* (4), 215-220. DOI: http://dx.doi.org/10.1016/0142-9612(81)90060-0.

18. Hurrell, S.; Cameron, R. E., Polyglycolide: degradation and drug release. Part I: Changes in morphology during degradation. *Journal of Materials Science : Materials in Medicine* **2001,** *12* (9), 811-6. DOI: http://dx.doi.org/10.1023/A:1017925019985.

19. Pitt, C. G., Aliphatic polyesters. I. The degradation of poly(ϵ-caprolactone). *Journal of applied polymer science* **1981,** *26* (11), 3779-3787. DOI: 10.1002/app.1981.070261124.

20. Maurus, P. B.; Kaeding, C. C., Bioabsorbable implant material review. *Operative Techniques in Sports Medicine* **2004,** *12* (3), 158-160. DOI: http://dx.doi.org/10.1053/j.otsm.2004.07.015.

21. Sun, H.; Mei, L.; Song, C.; Cui, X.; Wang, P., The in vivo degradation, absorption and excretion of PCL-based implant. *Biomaterials* **2006,** *27* (9), 1735-1740. DOI: http://dx.doi.org/10.1016/j.biomaterials.2005.09.019.

22. Howard, G. T., Biodegradation of polyurethane: a review. *International Biodeterioration & Biodegradation* **2002,** *49* (4), 245-252. DOI: http://dx.doi.org/10.1016/S0964-8305(02)00051-3.

23. Santerre, J. P.; Woodhouse, K.; Laroche, G.; Labow, R. S., Understanding the biodegradation of polyurethanes: From classical implants to tissue engineering materials. *Biomaterials* **2005,** *26* (35), 7457-7470. DOI: http://dx.doi.org/10.1016/j.biomaterials.2005.05.079.

24. Guelcher, S. A., Biodegradable Polyurethanes: Synthesis and Applications in Regenerative Medicine. *Tissue Engineering Part B: Reviews* **2008,** *14* (1), 3-17. DOI: http://dx.doi.org/10.1089/teb.2007.0133.

25. Chaffin, K. A.; Chen, X.; McNamara, L.; Bates, F. S.; Hillmyer, M. A., Polyether Urethane Hydrolytic Stability after Exposure to Deoxygenated Water. *Macromolecules* **2014,** *47* (15), 5220-5226. DOI: 10.1021/ma500904d.

26. Wu, J.; Mather, P. T., POSS Polymers: Physical Properties and Biomaterials Applications. *Polymer Reviews* **2009,** *49* (1), 25-63. DOI: 10.1080/15583720802656237.

27. Tanaka, K., Advanced functional materials based on polyhedral oligomeric silsesquioxane (POSS). *Journal of materials chemistry* **2012,** *22* (5), 1733-1746. DOI: 10.1039/C1JM14231C.

28. Joshi, M.; Butola, B. S., Polymeric Nanocomposites—Polyhedral Oligomeric Silsesquioxanes (POSS) as Hybrid Nanofiller. *Journal of Macromolecular Science, Part C* **2004,** *44* (4), 389-410. DOI: 10.1081/MC-200033687.

29. Li, G.; Wang, L.; Ni, H.; Pittman, C. U., Polyhedral Oligomeric Silsesquioxane (POSS) Polymers and Copolymers: A Review. *Journal of Inorganic and Organometallic Polymers 11* (3), 123-154. DOI: 10.1023/A:1015287910502.

30. Chattopadhyay, D. K., Thermal stability and flame retardancy of polyurethanes. *Progress in polymer science 34* (10), 1068-1133. DOI: 10.1016/j.progpolymsci.2009.06.002.

31. Lewicki, J. P.; Pielichowski, K.; De la Croix, P. T.; Janowski, B.; Todd, D.; Liggat, J. J., Thermal degradation studies of polyurethane/POSS nanohybrid elastomers. *Polymer Degradation and Stability* **2010,** *95* (6), 1099-1105. DOI: 10.1016/j.polymdegradstab.2010.02.021.

32. Janowski, B.; Pielichowski, K., Thermo(oxidative) stability of novel polyurethane/POSS nanohybrid elastomers. *Thermochimica Acta* **2008,** *478* (1-2), 51-53. DOI: 10.1016/j.tca.2008.08.015.

33. Kannan, R. Y.; Salacinski, H. J.; Odlyha, M.; Butler, P. E.; Seifalian, A. M., The degradative resistance of polyhedral oligomeric silsesquioxane nanocore integrated polyurethanes: An in vitro study. *Biomaterials* **2006,** *27* (9), 1971-1979. DOI: http://dx.doi.org/10.1016/j.biomaterials.2005.10.006.

34. Gu, X.; Wu, J.; Mather, P. T., Polyhedral Oligomeric Silsesquioxane (POSS) Suppresses Enzymatic Degradation of PCL-Based Polyurethanes. *Biomacromolecules* **2011,** *12* (8), 3066-3077. DOI: 10.1021/bm2006938.

35. Gupta, A.; Vara, D. S.; Punshon, G.; Sales, K. M.; Winslet, M. C.; Seifalian, A. M., In vitro small intestinal epithelial cell growth on a nanocomposite polycaprolactone scaffold. *Biotechnology and Applied Biochemistry* **2009,** *54*, 221-229. DOI: 10.1042/ba20090214.

36. Knight, P. T.; Kirk, J. T.; Anderson, J. M.; Mather, P. T., In vivo kinetic degradation analysis and biocompatibility of aliphatic polyester polyurethanes. *Journal of Biomedical Materials Research Part A* **2010,** *94A* (2), 333-343. DOI: 10.1002/jbm.a.32806.

37. McMullin, E.; Rebar, H. T.; Mather, P. T., Biodegradable Thermoplastic Elastomers Incorporating POSS: Synthesis, Microstructure, and Mechanical Properties. *Macromolecules* **2016,** *49* (10), 3769-3779. DOI: 10.1021/acs.macromol.6b00470.

38. Wu, L., In vitro degradation of three-dimensional porous poly(d,l-lactide-co-glycolide) scaffolds for tissue engineering. *Biomaterials* *25* (27), 5821-5830. DOI: 10.1016/j.biomaterials.2004.01.038.

39. da Silva, G. R.; da Silva-Cunha Jr, A.; Behar-Cohen, F.; Ayres, E.; Oréfice, R. L., Biodegradation of polyurethanes and nanocomposites to non-cytotoxic degradation products. *Polymer Degradation and Stability* **2010,** *95* (4), 491-499. DOI: http://dx.doi.org/10.1016/j.polymdegradstab.2010.01.001.

40. Christopher, X. F. L. a. M. M. S. a. S.-H. T. a. D. W. H., Dynamics of in vitro polymer degradation of polycaprolactone-based scaffolds: accelerated versus simulated physiological conditions. *Biomedical Materials* **2008,** *3* (3), 034108.

41. Tsuji, H.; Ono, T.; Saeki, T.; Daimon, H.; Fujie, K., Hydrolytic degradation of poly(ε-caprolactone) in the melt. *Polymer Degradation and Stability* **2005,** *89* (2), 336-343. DOI: http://dx.doi.org/10.1016/j.polymdegradstab.2005.01.018.

Table 3-1: Summary of polyurethane syntheses and their molecular properties.

Synthesis	Input Comonomer: Caprolactone Ratio (Molar)	Actual[a] Comonomer: Caprolactone Ratio (Molar)	Input Diol:POSS Ratio (Wt. %)	Actual[a] Diol:POSS Ratio (Wt. %)	Mn[b] (kDa)	Mw[b] (kDa)	PDI[b]
PCL_{1k} : POSS 70 : 30	-	-	70 : 30	77.2 : 22.8	49	76	1.55
$(PG_5CL_{95})_{1k}$: POSS 70 : 30	5 : 95	4 : 96	70 : 30	73.5 : 26.5	94	204	2.17
$(PG_{25}CL_{75})_{1k}$: POSS 70 : 30	25 : 75	21:79	70 : 30	67.7 : 32.3	445	607	1.36
$(PL_5CL_{95})_{1k}$: POSS 70 : 30	5 : 95	2 : 98	70 : 30	74.5 : 25.5	162	338	2.09
$(PL_{25}CL_{75})_{1k}$: POSS 70 : 30	25 : 75	19 : 81	70 : 30	71.5 : 28.5	202	320	1.58

[a]Determined from proton nuclear magnetic resonance.
[b]Determined from gel permeation chromatography.

Table 3-2: Summary of thermal and mechanical properties of the elastomers.

Synthesis	T_g[a] (°C)	$T_{m,Diol}$[a] (°C)	ΔH_{Diol}[a] (J/g)	$T_{m,POSS}$[a] (°C)	ΔH_{POSS}[a] (J/g)	Modulus[b] (MPa)	Strain to Failure[b] (%)
PCL_{1k} : POSS 70 : 30	-51.5	20.4	5.3	118.1	2.0	13.15 ± 3.7	> 1200
$(PG_5CL_{95})_{1k}$: POSS 70 : 30	-47.4	14.0	1.1	107.9	1.5	10.95 ± 0.7	> 1200
$(PG_{25}CL_{75})_{1k}$: POSS 70 : 30	-35.9	-5.5	0.4	128.7	2.7	9.92 ± 0.7	493 ± 144
$(PL_5CL_{95})_{1k}$: POSS 70 : 30	-48.5	-9.9	0.4	113.3	1.9	7.36 ± 0.7	> 1200
$(PL_{25}CL_{75})_{1k}$: POSS 70 : 30	-35.1	-3.6	0.5	120.4	1.8	6.16 ± 0.6	> 1200

[a]Determined from differential scanning calorimetry
[b]Determined from tensile testing at room temperature at a rate of 50 μ/s.

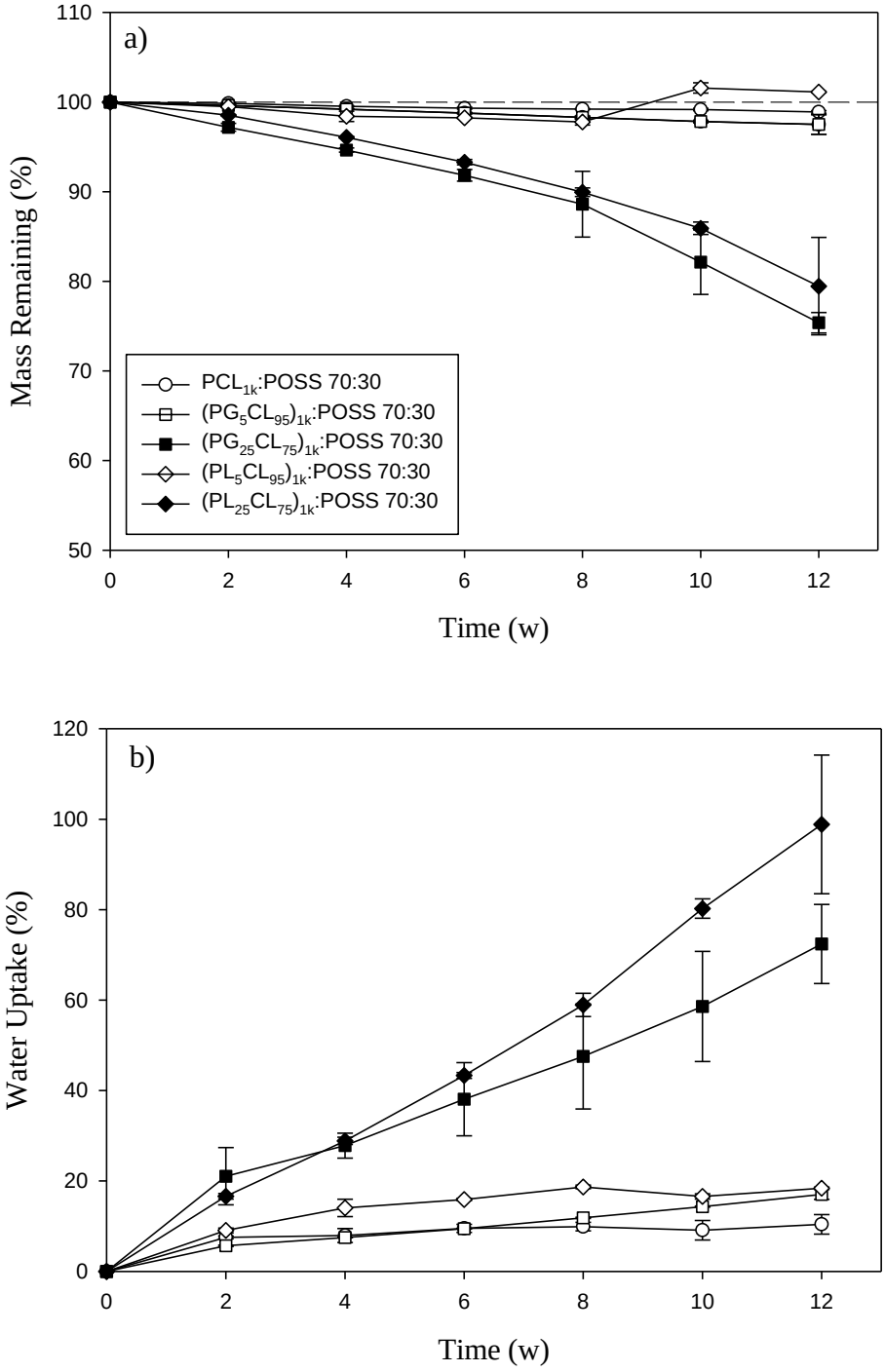

Figure 3-1: a) Mass remaining and b) water uptake for PCL_{1k}:POSS 70:30 (○), $(PG_5CL_{95})_{1k}$:POSS 70:30 (□), $(PG_{25}CL_{75})_{1k}$:POSS 70:30 (■), $(PL_5CL_{95})_{1k}$:POSS 70:30 (◊), and $(PL_{25}CL_{75})_{1k}$:POSS 70:30 (♦).

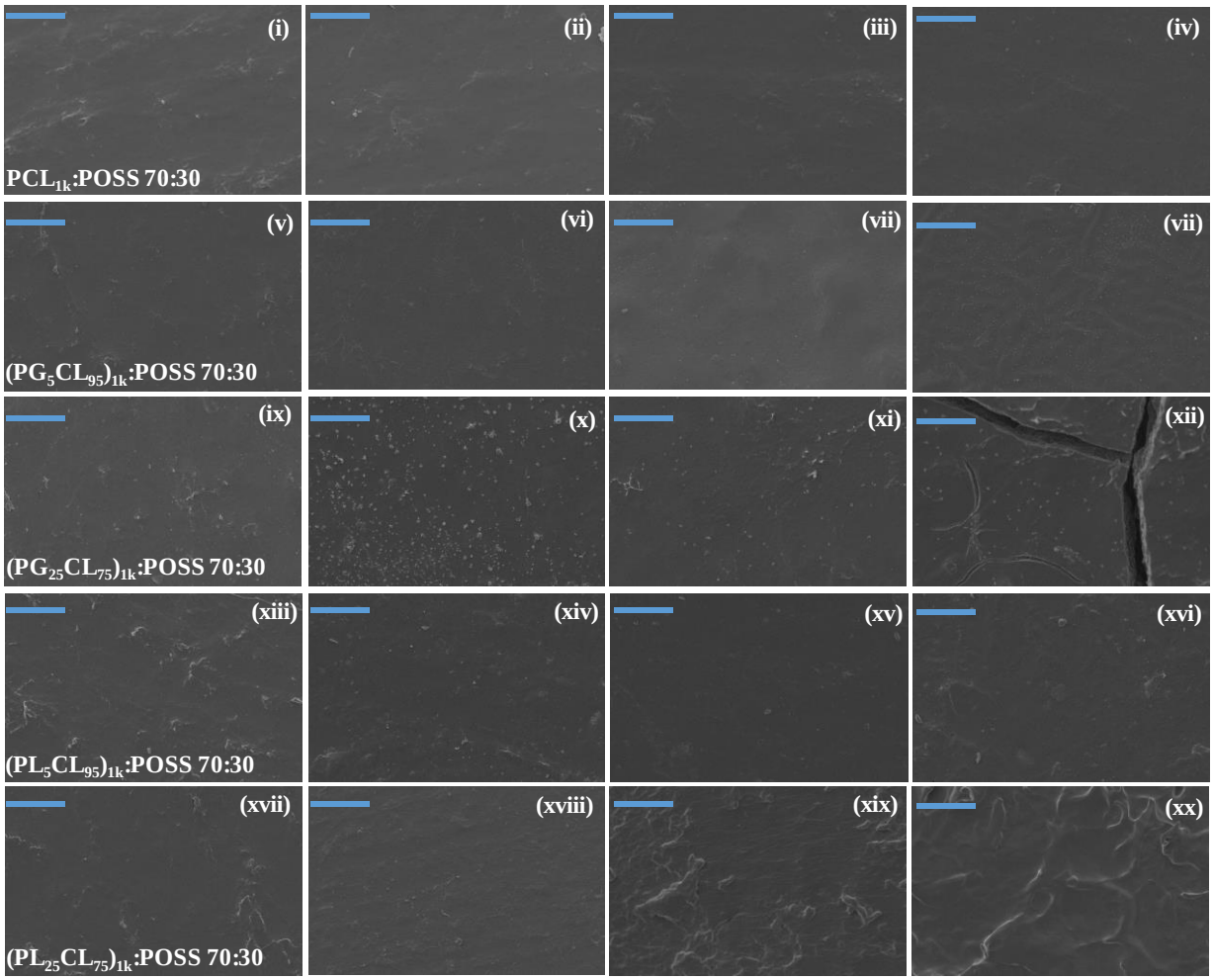

Figure 3-2: Scanning electron micrographs of the surfaces of film over time for: PCL_{1k}:POSS at (i) 0 w, (ii) 4 w, (iii) 8 w, and (iv)12 w; $(PG_5CL_{95})_{1k}$:POSS at (v) 0 w, (vi) 4 w, (vii) 8 w, and (viii) 12 w; $(PG_{25}CL_{75})_{1k}$:POSS at (ix) 0 w, (x) 4 w, (xi) 8 w, and (xii) 12; $(PL_5CL_{95})_{1k}$:POSS at (xiii) 0 w, (xiv) 4 w, (xv) 8 w, (xvi) 12 w; and $(PL_{25}CL_{75})_{1k}$:POSS at (xvii) 0 w, (xviii) 4 w, (xix) 8 w and (xx)12 w. The scale bar equals 50 μm.

Table 3-3: Summary of initial (t=0) film molecular weights.

Synthesis	M_w[a] (kDa)
PCL_{1k} : POSS 70 : 30	48.7
$(PG_5CL_{95})_{1k}$: POSS 70 : 30	114.4
$(PG_{25}CL_{75})_{1k}$: POSS 70 : 30	224.0
$(PL_5CL_{95})_{1k}$: POSS 70 : 30	66.1
$(PL_{25}CL_{75})_{1k}$: POSS 70 : 30	77.1

[a]Determined from gel permeation chromatography.

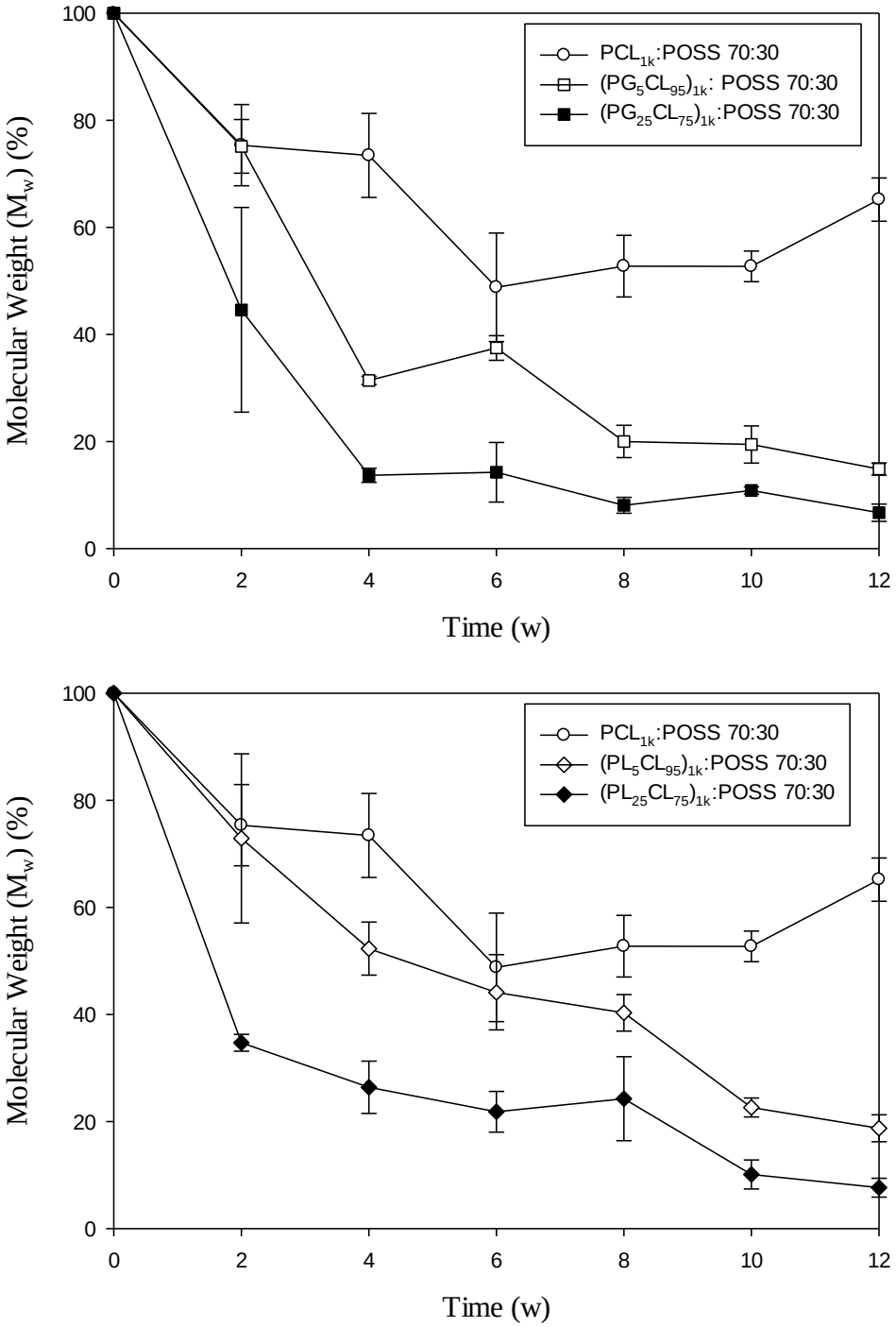

Figure 3-3: Molecular weight (M_w) as a percentage of the original, for PCL_{1k}:POSS 70:30 (○), $(PG_5CL_{95})_{1k}$:POSS 70:30 (□), $(PG_{25}CL_{75})_{1k}$:POSS 70:30 (■), $(PL_5CL_{95})_{1k}$:POSS 70:30 (◊), and $(PL_{25}CL_{75})_{1k}$:POSS 70:30 (♦).

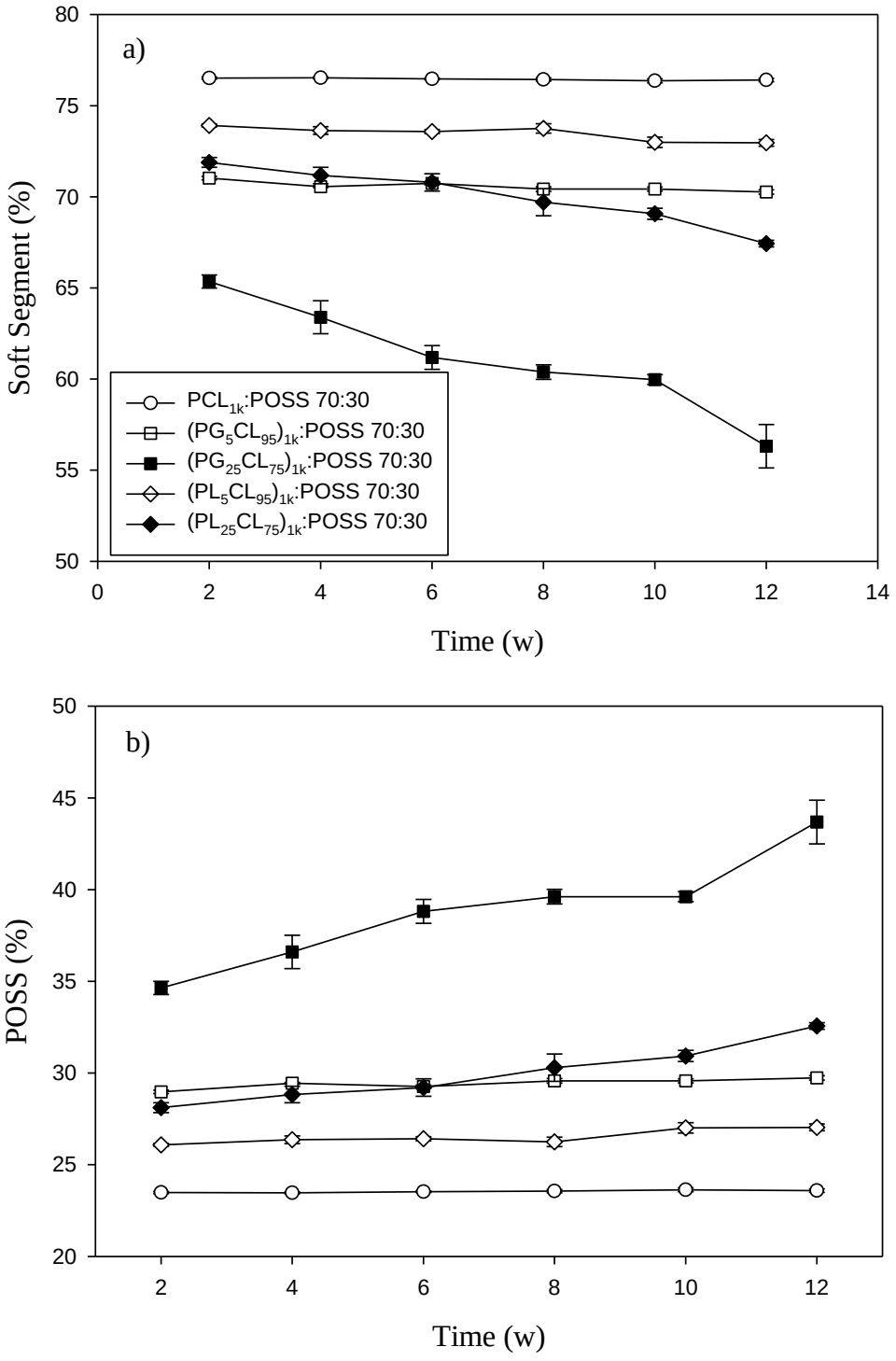

Figure 3-4: Weight percentage ratios for a) the soft segment and b) POSS for PCL_{1k}:POSS 70:30 (○), $(PG_5CL_{95})_{1k}$:POSS 70:30 (□), $(PG_{25}CL_{75})_{1k}$:POSS 70:30 (■), $(PL_5CL_{95})_{1k}$:POSS 70:30 (◊), and $(PL_{25}CL_{75})_{1k}$:POSS 70:30 (♦) as determined by ^{1}H-NMR.

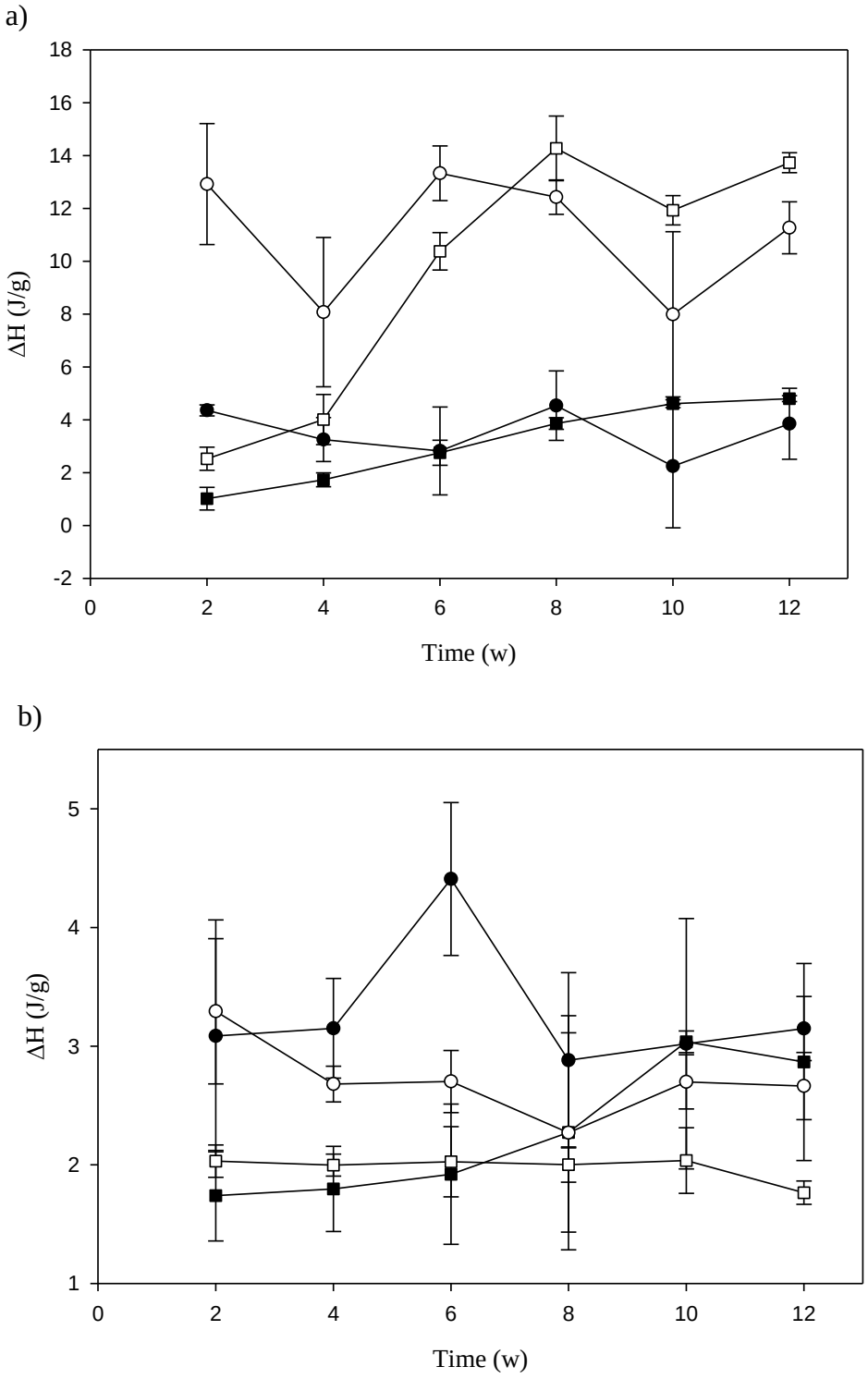

Figure 3-5: Melting enthalpies for a) the soft segment and b) POSS for 1st heat (●) and 2nd heat (○) of PCL_{1k}:POSS and 1st heat (■) and 2nd heat (□) of $(PL_5CL_{95})_{1k}$:POSS.

a)

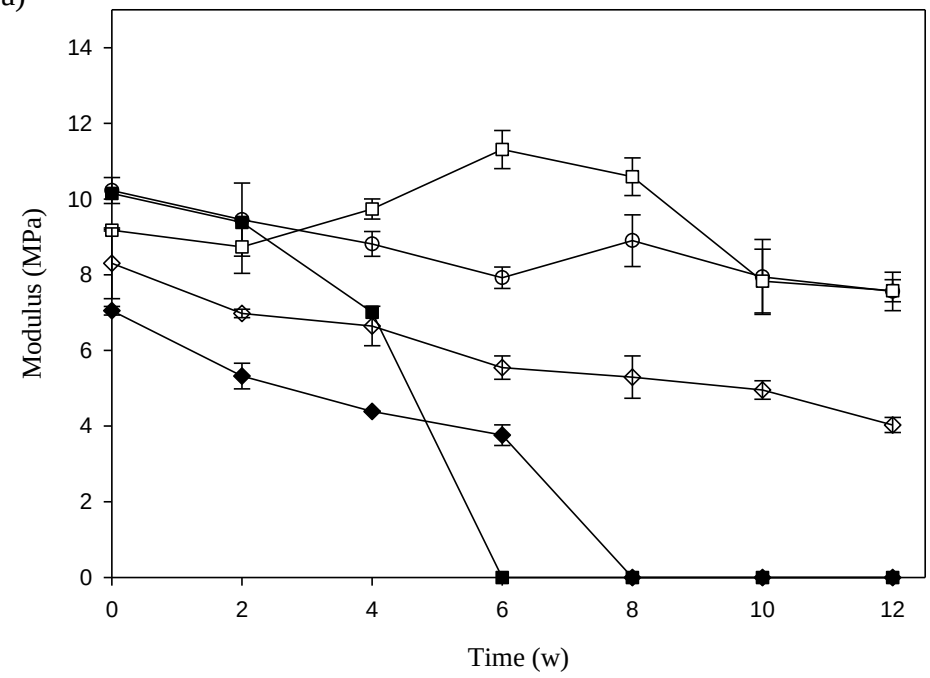
Modulus (MPa)
0
2
4
6
8
10
12
14
0
2
4
6
8
10
12
Time (w)

b)

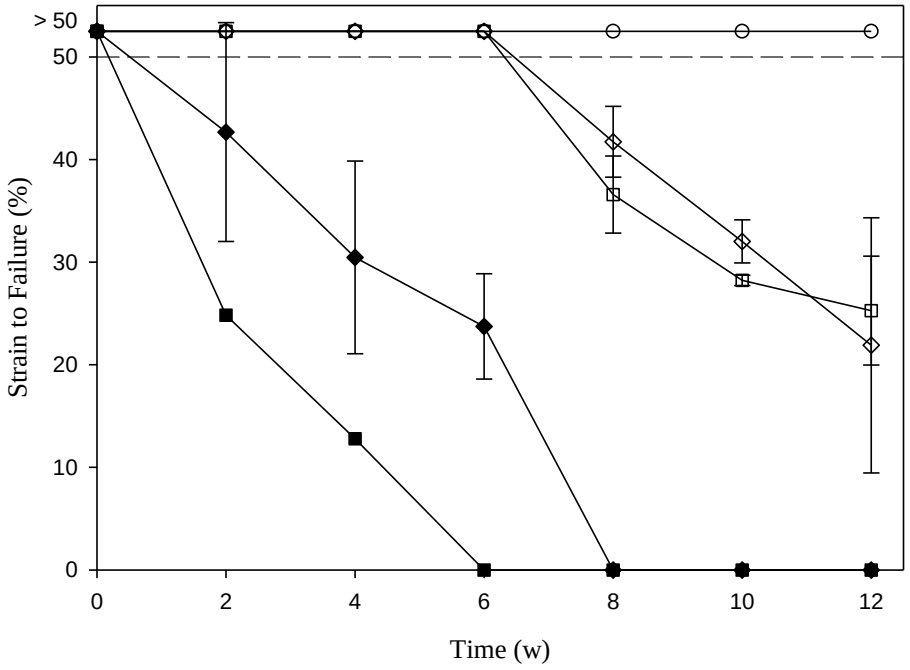
Strain to Failure (%)
> 50
50
40
30
20
10
0
0
2
4
6
8
10
12
Time (w)

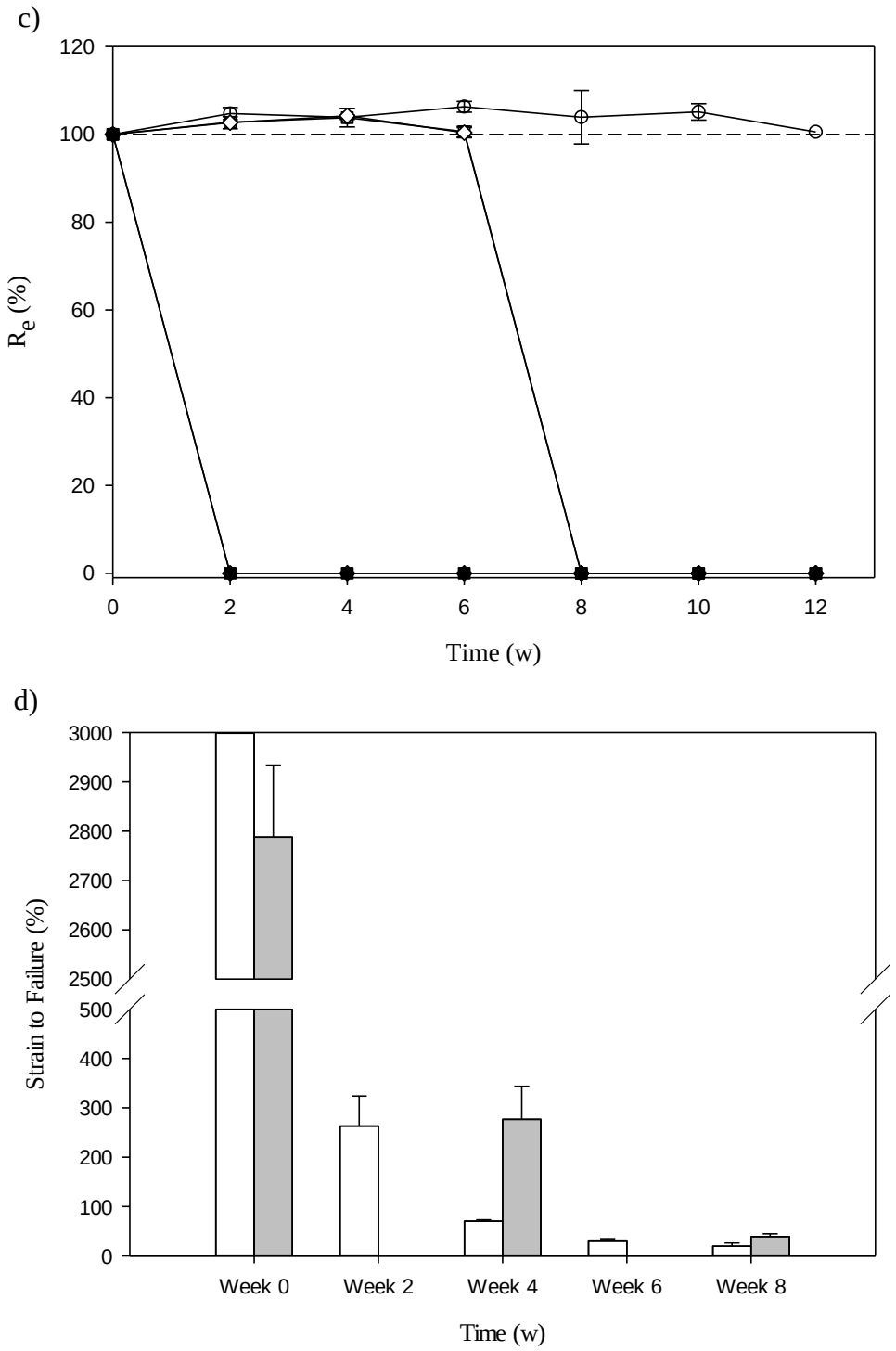

Figure 3-6: a) Modulus, b) strain-to-failure, and c) elasticity, as a percentage of the original, for PCL_{1k}:POSS 70:30 (○), $(PG_5CL_{95})_{1k}$:POSS 70:30 (□), $(PG_{25}CL_{75})_{1k}$:POSS 70:30 (■), $(PL_5CL_{95})_{1k}$:POSS 70:30 (◊), and $(PL_{25}CL_{75})_{1k}$:POSS 70:30 (♦). d) Strain-to-failure for $(PG_5CL_{95})_{1k}$:POSS 70:30 over time for materials tested at dry at room temperature (gray bars) and materials tested in saline at 37 °C (white bars).

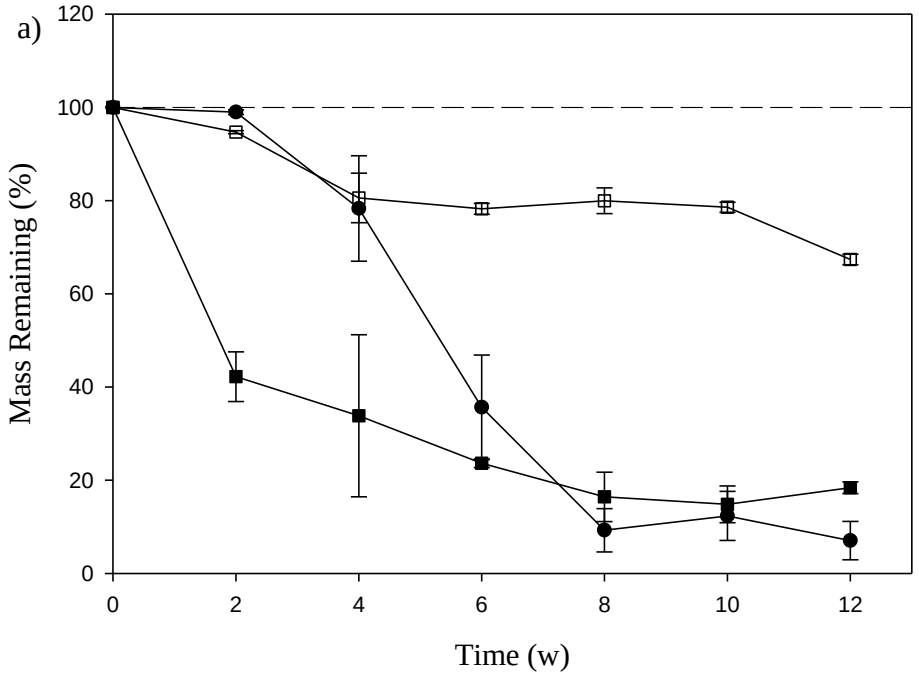
a)
Mass Remaining (%)
Time (w)
0
20
40
60
80
100
120
0
2
4
6
8
10
12

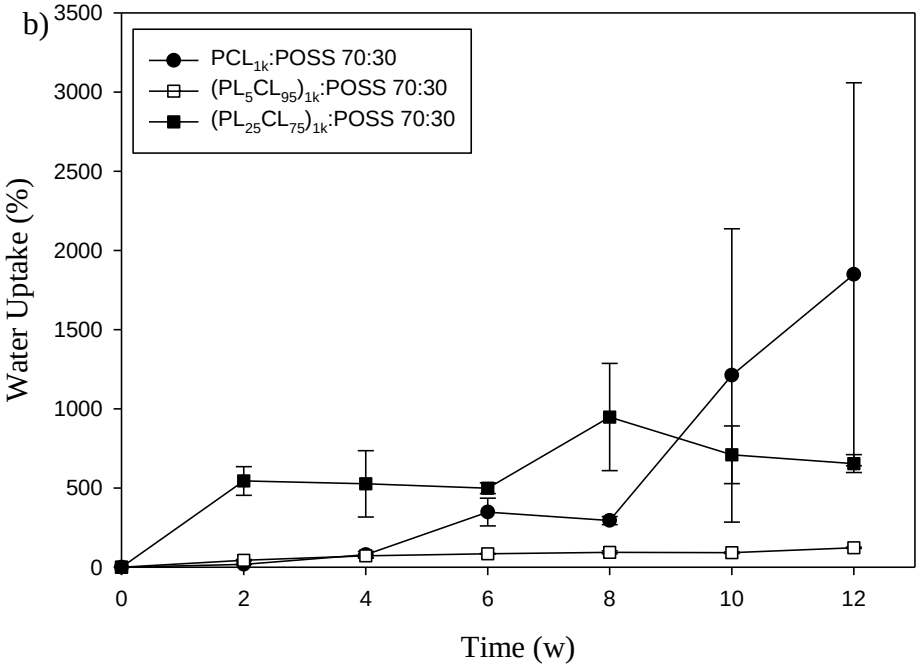
b)
PCL1k:POSS 70:30
(PL5CL95)1k:POSS 70:30
(PL25CL75)1k:POSS 70:30
Water Uptake (%)
Time (w)
0
500
1000
1500
2000
2500
3000
3500
0
2
4
6
8
10
12

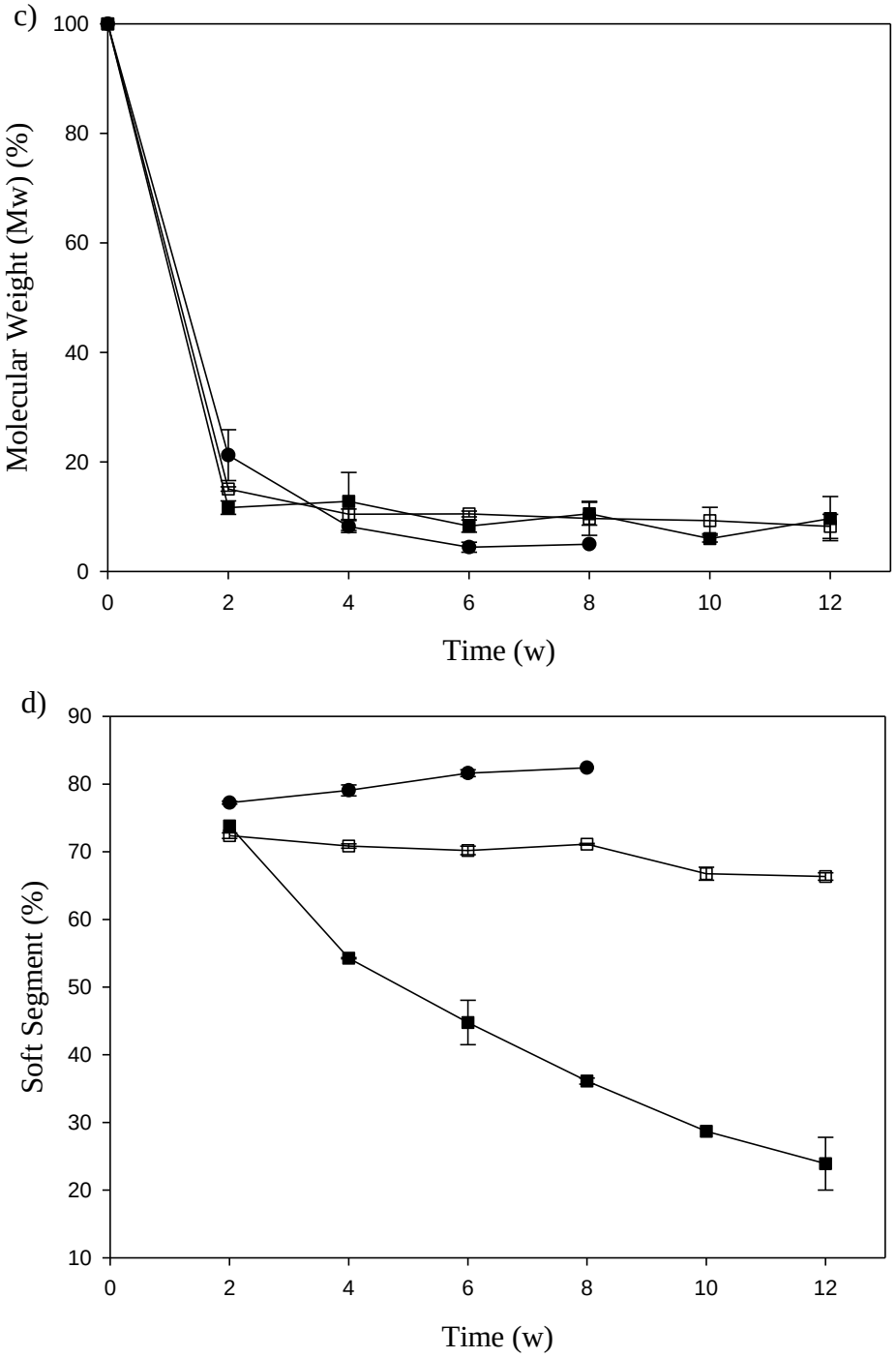

Figure 3-7: a) Mass loss, b) water uptake, c) molecular weight, and d) soft segment weight % for PCL_{1k}:POSS 70:30 (●), $(PL_5CL_{95})_{1k}$:POSS 70:30 (□), and $(PL_{25}CL_{75})_{1k}$:POSS 70:30 (■) for materials degraded at 60 °C.

Table 3-4: Summary of initial film molecular weights (t=0) for the 60 °C degradation study.

Synthesis	M_w[a] (kDa)
PCL_{1k} : POSS 70 : 30	94.6
$(PL_5CL_{95})_{1k}$: POSS 70 : 30	66.1
$(PL_{25}CL_{75})_{1k}$: POSS 70 : 30	77.1

[a]Determined from gel permeation chromatography.

a)

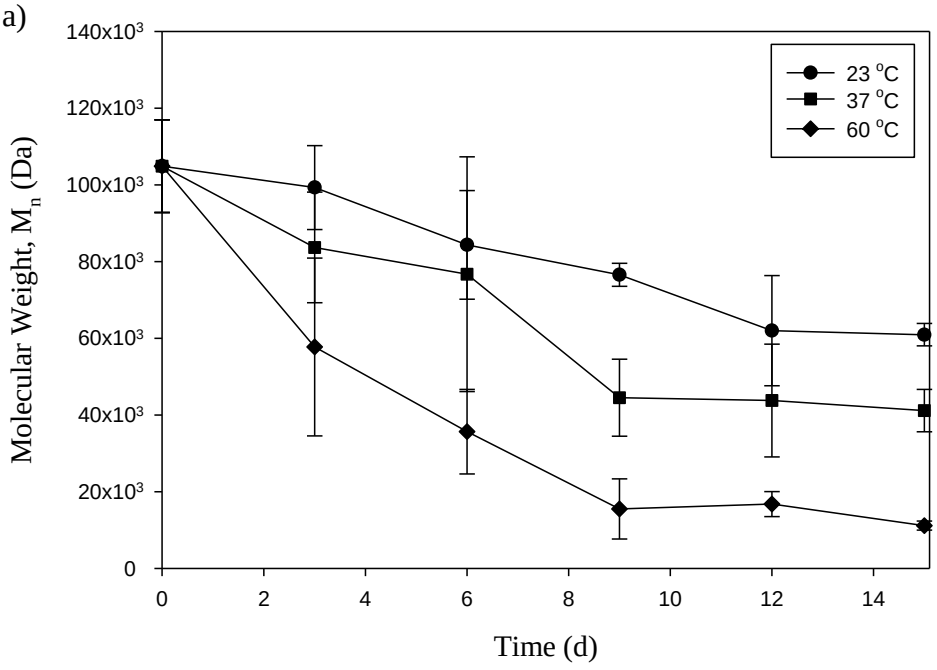
140x10³
120x10³
100x10³
80x10³
60x10³
40x10³
20x10³
0
Molecular Weight, M_n (Da)
0
2
4
6
8
10
12
14
Time (d)
23 °C
37 °C
60 °C

b)

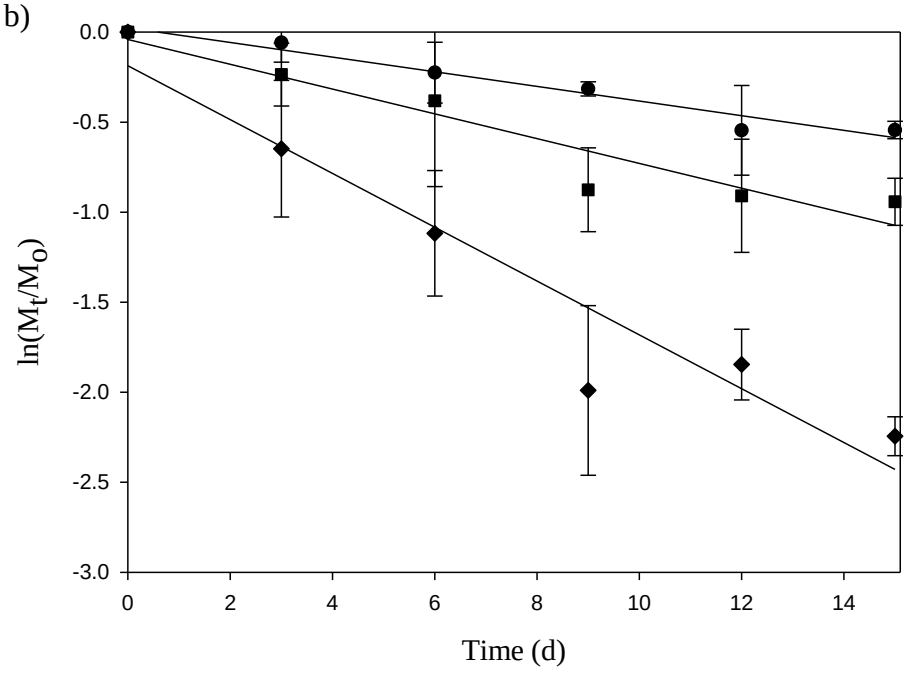
0.0
-0.5
-1.0
-1.5
-2.0
-2.5
-3.0
$\ln(M_t/M_O)$
0
2
4
6
8
10
12
14
Time (d)

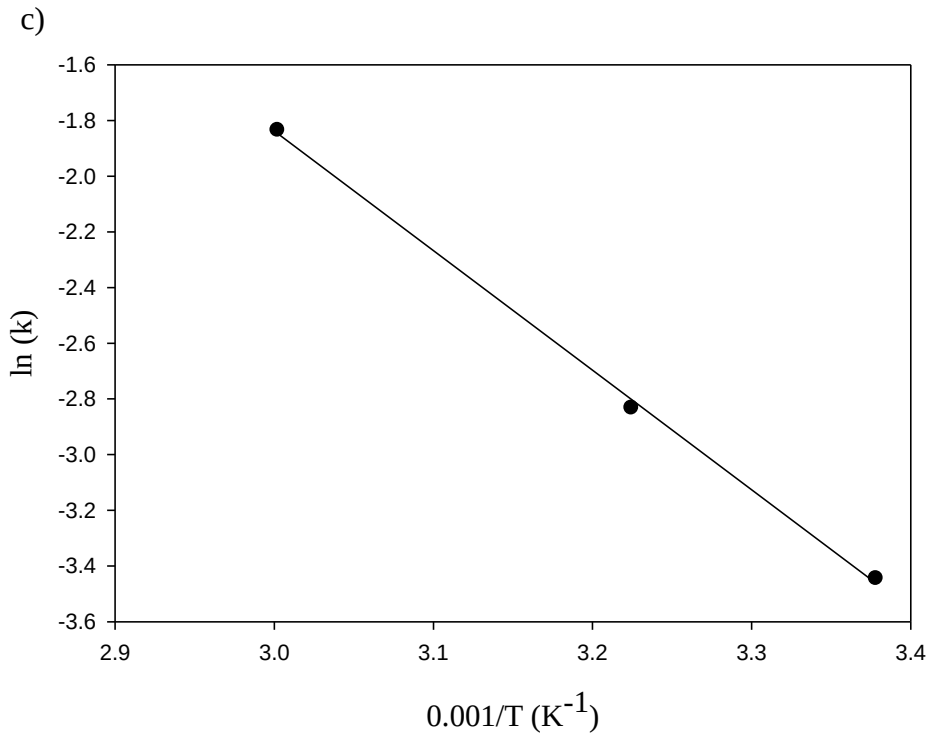

Figure 3-8: a) Molecular weight (M_n) plotted on a linear scale and b) semi-log scale as a ratio with linear fits for PCL_{1k}:POSS 70:30 degraded at 23 ° C (●), 37 °C (■), and 60 °C (♦). c) Linear fit of the rate constants and temperature to determine the activation energy from the Arrhenius equation.

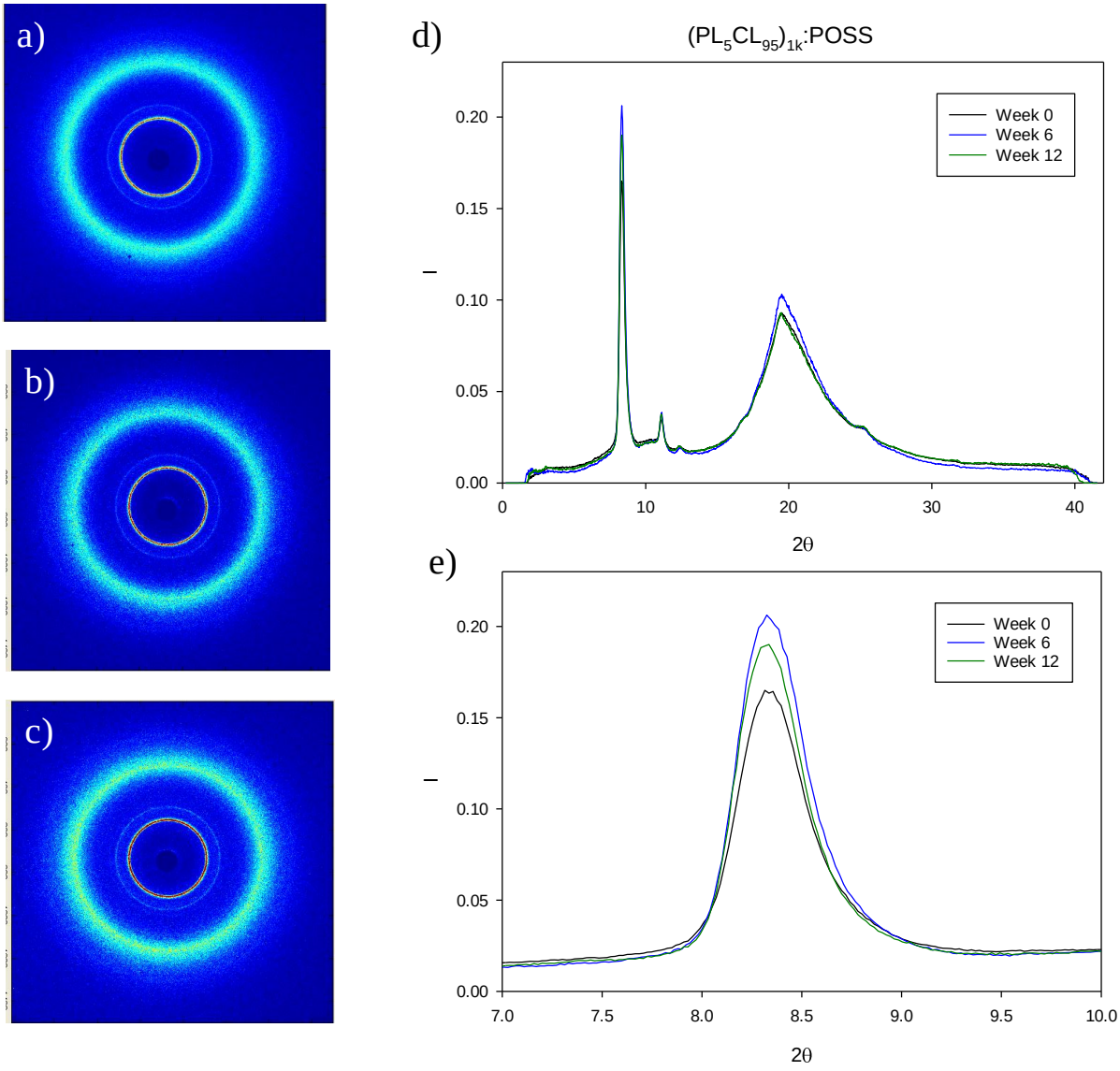

Figure 3-9: Wide-angle x-ray scattering analysis of $(PL_5CL_{95})_{1k}$:POSS. 2-D scattering plots of films degraded for a) 0 w, b) 6 w) and c) 12 w. 1-D plots of intensity at each angle is shown for the d) full range of 2θ and e) a close-up of POSS's crystalline peak.

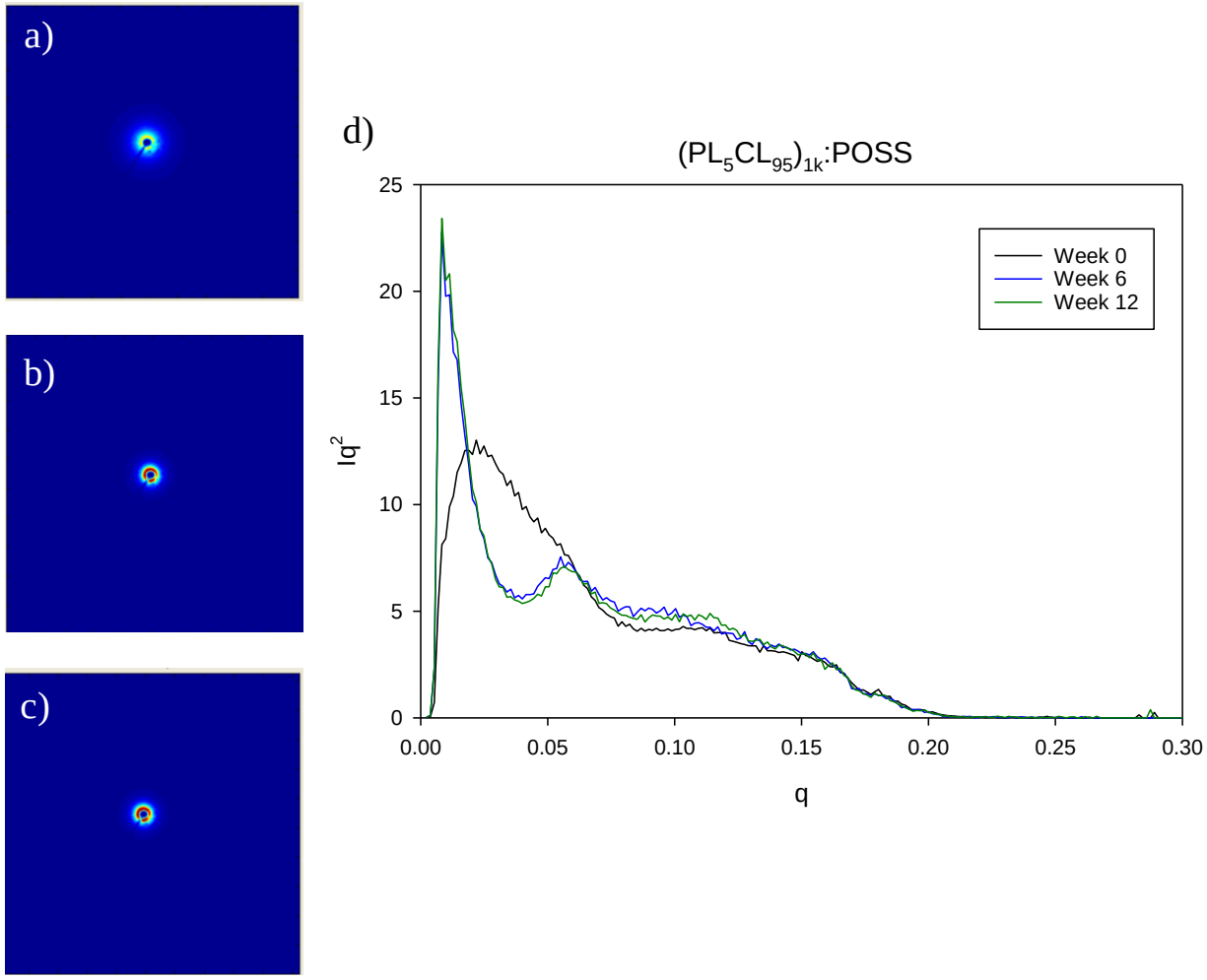

Figure 3-10: Small-angle x-ray scattering analysis of $(PL_5CL_{95})_{1k}$:POSS. 2-D scattering plots of films degraded for a) 0 w, b) 6 w) and c) 12 w. 1-D plots of the d) full range of q.

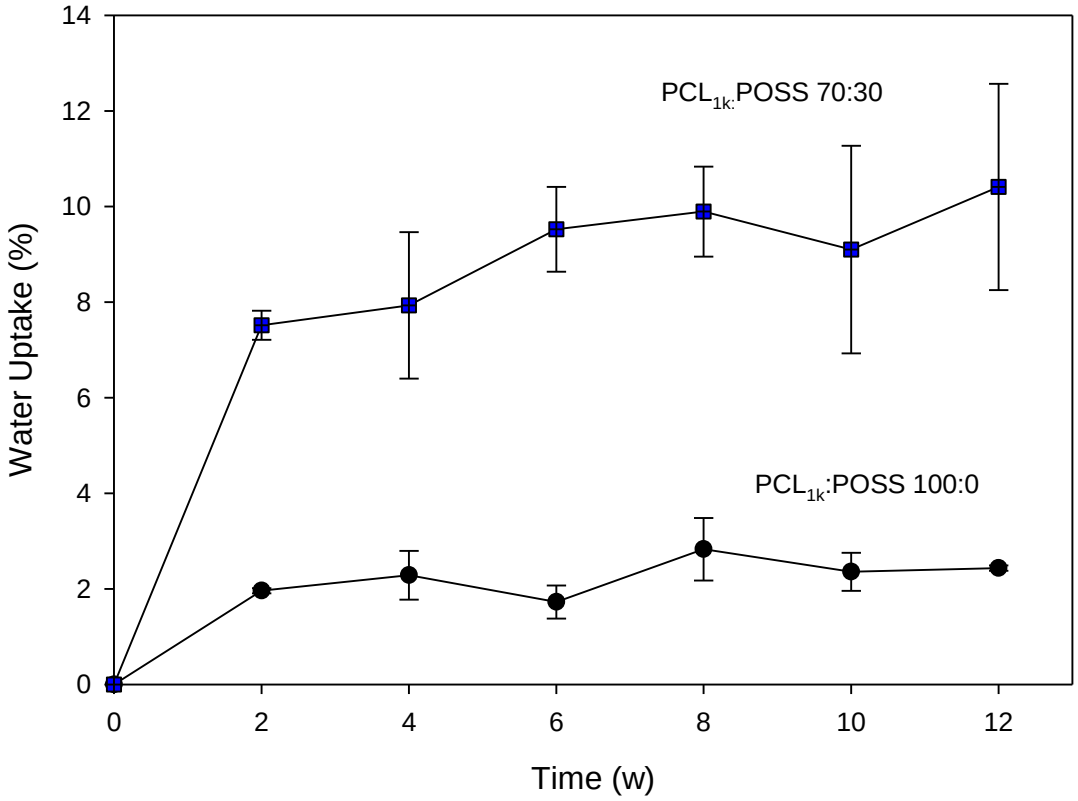

Figure 3-11: Water uptake for PCL_{1k}:POSS 100:0 (●) and PCL_{1k}:POSS 70:30 (■).

Chapter 4: Effect of Catalyst Concentration on PCL_{1k}:POSS Polyurethanes' Physical Properties and Cell Viability

4.1 Synopsis

In order for a material to be considered for use as part of an implantable medical device, it must be tested for biocompatibility. To ensure our biodegradable elastomers were non-toxic as they were designed, a non-contact cytocompatibility was completed with our biodegradable elastomers from Chapter 2 with fibroblast cells. The results showed that all materials were cytotoxic. Therefore, it was hypothesized that the amount of residual organotin catalyst in each polymer was causing the poor cytocompatibility. New PCL_{1k}:POSS polyurethanes were synthesized systematically varying the amount of tin catalyst, utilizing a range of concentrations spanning 1% - 0.01% tin-POMS or 0.1%-0.01% dibutyltin dilaurate (DBTDL). One composition, the polyurethane synthesized with 1% tin-POMS, was re-dissolved and re-precipitated several times to try to wash away the tin. The results showed that decreasing tin concentration positively affected cell viability. 0.01% tin-POMS led to the best cytocompatibility while maintaining high mechanical properties. Materials synthesized with tin-POMS had better cytocompatibility than materials synthesized with DBTDL, and repeated washing did not increase cell viability.

4.2 Introduction

Polyurethanes, or polymers formed by the reaction of isocyanates with hydroxyls or amines, are commonly used as biomaterials as their composition could be easily controlled to dictate a variety of properties.[1] Many polyurethanes intended to be used as biomaterials utilize organotin-based catalysts, such as stannous octoate (tin(II) 2-ethylhexanoate)[2-4] or dibutyltin dilaurate (DBTDL).[5-9] Organotin-based catalysts are used because they are more efficient than other metal-based catalysts (although slightly less efficient than ferric acetyl acetonate),[10] do not

lose catalytic activity over time (like amine catalysts),[11] and facilitate polyurethane reactions much more quickly than un-catalyzed polyurethane reactions.[12] By themselves, tin catalysts have been found to be cytotoxic,[13] but many polymers synthesized with tin-based catalysts have been found to be compatible both *in vitro*[8, 14, 15] and *in vivo*.[8, 16, 17]

Tin-POMS, or tin polyhedral oligomeric metal silsesquioxane, has been developed by Hybrid Plastics to be used as a polyurethane catalyst.[18] Researchers found that tin-POMS has a similar catalytic activity to dibutyltin dilaurate when examining model reactions of 1-butanol and 2-butanol with 4,4'-methylenebis(cyclohexylisocyanate) (H_{12}MDI). Tin-POMS may be preferred over DBTDL or stannous octoate because it is hydrophobic, while the others are hydrophilic, and any water can reduce the catalytic activity of organotin catalysts. It also has higher thermal stability, making the shelf-life longer.

In this work, the cell viability of previously developed biodegradable elastomers, synthesized with Tin-POMS catalyst, were tested using the non-contact CCK-8 cell viability assay. The resulting cell viability was poor, and it was hypothesized that the amount of residual tin-POMS in the synthesized materials caused the poor cell viability. Therefore, a study was conducted that varied the amount of tin-POMS catalyst used in a polyurethane reaction of a biodegradable polymer: PCL_{1k}:POSS. These syntheses were compared with materials synthesized with DBTDL as well as materials re-precipitated in hexanes to try to wash away the tin-POMS. Physical and mechanical properties of all of the synthesized polyurethanes were compared, as well as their cell viabilities.

4.3 Methods

4.3.1 Materials

Poly(ε-caprolactone) diol (M_w ~ 1,250 g/mol) was purchased from Polysciences, Inc. 1,2-PropanediolIsobutyl POSS (AL0130), subsequently referred to as POSS diol, and Tin-POMS catalyst were purchased from Hybrid Plastics. Hexamethylene diisocyanate (HDI) and dibutyltin dilaurate (95%) were purchased from Sigma-Aldrich and used as received. Deuterated chloroform (chloroform-d, 99.8% atom D) and HPLC-grade THF were purchased from Sigma-Aldrich. Toluene, tetrahydrofuran (THF), and *n*-hexanes were purchased from Fisher Scientific. Toluene was dried by refluxing over calcium hydride (Sigma-Aldrich) several times until collection prior to use and stored over 3 Å molecular sieves (Sigma-Aldrich). For cell culture, L929 mouse fibroblasts were acquired from American Type Culture Collection. Cell culture media DMEM-F12 (Invitrogen) was supplemented with 10% Fetal Bovine Serum (Atlanta Biologics) and 1% glutamine-penicillin-streptomycin (Invitrogen). A negative control was made with 1% (g/L) sodium dodecyl sulfate (SDS, Sigma-Aldrich) in the media described above. Finally, the assay used was the CCK-8 assay, or the Cell Counting Kit-8, from Dojindo Molecular Technologies, Inc.

4.3.2 Cell Viability Testing of PCL:POSS, PGCL:POSS, and PLCL:POSS Polyurethanes

The CCK-8 Assay was utilized to test the cytocompatibility of each material. Dr. Eric Finkelstein performed all cell culture activities in this study. The CCK-8 assay is an indirect colorimetric assay based on the cleavage of a yellow tetrazolium salt (2-(2-methoxy-4-nitrophenyl)-3-(4-nitrophenyl)-5-(2,4-disulfophenyl)-2H-tetrazolium, monosodium salt) (WST-8) to an orange water-soluble formazan dye by dehydrogenase activities within the cell. Therefore, this assay measures mitochondrial activity, an analog to cell viability. Material films (discussed in

detail in Chapter 2) were sterilized for 1 hour under UV light on each side and then placed in cell culture medium for 24, 48, or 72 h at 37 °C at a surface area: volume ratio of 3:1 (cm^2:mL). After the given time points, the media of L929 fibroblast cells (at a concentration of 25,000 cells/cm^2 in a 96-well tissue culture polystyrene plate) was replaced with 100 µL of material extract. The cells were incubated at 37 °C in 5% CO_2 and 95% humidified air for 24 hours. Then, 100 µL of cell culture media with 10% (v/v) CCK-8 solution replaced the extract media. The cells were incubated in the CCK-8 solution for 4 h. Absorbance was measured at 450 nm with a plate reader and compared with absorbance of cells growing in cell culture media incubated for the same period (24, 48, or 72 h) with no material (the positive control). All materials were tested in triplicate. A viability of at least 70% of the positive control was considered to be non-toxic, or cytocompatible. The methods of cell viability determination were adapted from ISO Standards ISO 10993-5 and ISO 10993-12.

4.3.3 Polymer Synthesis

Random, multi-block polyurethanes were synthesized from the Poly(caprolactone)$_{1k}$ (PCL_{1k}) diol, POSS diol and hexamethylene diisocyanate, as described in detail in Chapter 2. All syntheses had 70:30 PCL_{1k}:POSS weight percent as a feed ratio. These syntheses were reacted in toluene (10% w/v) for 48 h with varying wt. % of Tin-POMS or DBTDL catalyst at 100 °C under nitrogen, with one HDI addition (corresponding to the difference in PCL molecular weight between 1.25 kDa and 1.2 kDa) added after 25 h. The polyurethanes were precipitated in excess n-hexanes (1:9 toluene: hexane), dried and characterized. PCL_{1k}:POSS synthesized with 1 wt. % tin-POMS was re-dissolved in toluene (10% w/v) and re-precipitated in hexane (1:9 toluene: hexane) and subsequently dried and characterized (designated 2P). This process was repeated, with the resulting material designated 3P.

4.3.4 Proton Nuclear Magnetic Resonance (^{1}H-NMR)

Diols and polyurethanes were dissolved in deuterated chloroform ($CDCl_3$) at a concentration of 10-20 mg/mL. The samples were analyzed in a Bruker Avance III HD 400 MHz spectrometer equipped with a 5 mm outer diameter Prodigy probe. A standard 1D pulse sequence was used with a 30° pulse, relaxation delay time of one second and a temperature of 25 °C.

4.3.5 Gel Permeation Chromatography (GPC)

Molecular weight (M_n and M_w) and polydispersity were determined from gel permeation chromatography (GPC). Samples were dissolved in tetrahydrofuran (THF) at a concentration of 2-5 mg/mL and were passed through a 0.2 µm PTFE filter before injection. Waters Isocratic HPLC System equipped with a temperature controlled differential refractometer (Waters 2414) was used for analysis. Multi-angle laser light scattering was employed (Wyatt miniDAWN) using three angles (45°, 90°, 135°) for in-line absolute molecular weight determination.

4.3.6 Differential Scanning Calorimetry (DSC)

Thermal properties of the polyurethanes were studied by differential scanning calorimetry (DSC) using the TA Q200 instrument. Heat flow was collected while each sample was heated to 200 °C (to remove thermal history), cooled to -70 °C, and heated a second time to 200 °C. The heating rates were 10 °C/min and the cooling rates were 5 °C/min. The second heat was used to determine glass transition temperature (T_g, a step in the curve) and the change in heat capacity or melting transitions (T_m, the peak of the endotherm) and the enthalpy of melting (ΔH_m, area under the curve).

4.3.7 Compression Molding

The PCL_{1k}:POSS polyurethanes were compression molded into films using a Carver 3851-0 press with heating platens. The platens were heated to 130 ºC, slightly above the T_m of POSS.

After the platens thermally equilibrated, the polymer was placed between two Teflon sheets with a 0.45 mm thick Teflon spacer. A compressive stress of 1 metric ton was applied at elevated temperatures and held for 2 minutes. Then the film was cooled to 70 °C, where the polymer was annealed for 30 minutes to promote POSS crystallization before it was cooled to room temperature. The resulting films were flexible and between 0.4 and 0.5 mm in thickness, determined by a digital caliper.

4.3.8 Tensile Testing

A TestResources Model 100P Universal Testing Machine was utilized to determine the tensile properties of the materials. Samples were cut in a dogbone geometry (ASTM Standard D638-03 Type IV, scaled down by a factor of 4) and stretched at a rate of 50 μm/s at room temperature (about 23 °C). Young's modulus and strain-to-failure were determined from engineering stress vs. engineering strain plots.

4.3.9 Cell Viability Testing of the PCL_{1k}:POSS Polyurethanes

The PCL_{1k}:POSS polyurethanes synthesized with the different catalysts or processed with increasing wash cycles were tested with the CCK-8 assay as described above. These materials were incubated in cell culture media for either 24 or 72 h. They were compared to a positive control, media without polymer incubated for the same time period, and a negative control, cells incubated with fresh media and 1% (w/v) SDS. All materials were tested in triplicate. A viability of at least 70% of the positive control was considered to be non-toxic.

4.3.10 Statistical Analysis

T-tests were performed on two means with unequal variances to determine the statistical significance of different sets of data. Two-tailed t-tests with a confidence value of $\alpha = 0.05$ was used for all tests.

4.4 Results

4.4.1 Cell Viability Testing of PCL:POSS, PGCL:POSS, and PLCL:POSS Polyurethanes

Cell viability testing was performed on all 8 polyurethane elastomers from the previous study (Chapter 2) via a non-contact metabolic assay. The results of the cell viability assay of the PCL:POSS, PGCL:POSS, and PLCL:POSS materials are shown in **Figure 4-1**. The 8 materials, despite varying in POSS content and soft segment composition, had cell viability around 40-50% of the positive control for all three incubation time points (24, 48, and 72 h). These cell viabilities were all significantly lower than the positive control and the limit of 70%, above which cells were considered viable. It was hypothesized from this study that too much catalyst was being used for the polyurethane syntheses, as 1 wt. % of tin-POMS was previously used, and the residual catalyst was causing cytotoxicity.

4.4.2 Polymer Synthesis and Molecular Properties

To test this hypothesis, five new PCL_{1k}:POSS polyurethanes were synthesized with tin-POMS, systematically varying the amount of catalyst from 1 wt. % to 0.01 wt. %. Two other polymers were synthesized using dibutyltin dilaurate (DBTDL) as a catalyst, one with 0.1 wt. % and the other with 0.01 wt. % DBTDL. A representative schematic of the PCL_{1k}:POSS syntheses is shown in **Scheme 4-1**. Also, the PCL_{1k}:POSS 70:30 synthesized with 1 wt. % tin-POMS was re-dissolved in toluene and re-precipitated in n-hexanes to try to extract the tin-POMS from the polymer. This was done two consecutive times, with designations 2P and 3P representing the 2nd and 3rd precipitations, respectively. A summary of the polymers with their molecular properties are shown in **Table 4-1**.

From ^{1}H-NMR, incorporation of PCL and POSS into the polyurethane followed previous trends, with POSS having less incorporation than PCL_{1k}. This resulted in 75.7-78.1% PCL content

for the different polymers. Interesting, when the polymer was re-dissolved and re-precipitated, the collected polymer had less POSS content. From GPC, the molecular weights were generally higher for higher catalyst concentrations. For 1 - 0.1 wt. % catalyst, the M_n's of the polymers were greater than 60 kDa and M_w's were greater than 100 kDa, while 0.01 - 0.05 wt. % catalyst resulted in polyurethanes with M_n values < 40 kDa and M_w values < 60 kDa. For both catalysts, 0.1 wt. % catalyst led to the highest molecular weights than the other polymers synthesized with the same catalyst. The polyurethanes had M_w values of 121.9 and 174.6 kDa from tin-POMS and DBTDL, respectively. When re-dissolved and re-precipitated, the molecular weight of the polymer from 1 wt. % tin-POMS dropped from 71.4 kDa as originally synthesized to as low 28.9 kDa for M_n after two precipitations.

4.4.3 Differential Scanning Calorimetry

Differential scanning calorimetry (DSC) was performed for all polymers to determine their thermal properties, as shown in **Figure 4-2** and summarized in **Table 4-2**. All materials showed a glass transition around -51 °C and distinct soft and hard block melting transitions, around 20 °C for PCL_{1k} and around 115 °C for POSS. The polymers synthesized with lower catalyst wt. % (0.01 and 0.05 wt. % Tin-POMS) had a higher PCL melting enthalpy (5.9 J/g) than the melting enthalpy of PCL_{1k}:POSS from 1 wt. % tin-POMS (3.2 J/g). Other than the PCL melting enthalpies, the transitions are similar for all materials.

4.4.4 Tensile Testing

Tensile testing of all PCL_{1k}:POSS materials revealed Young's moduli between 7.88 ± 0.5 and 10.96 ± 1.1 MPa, and strains-to-failure from 1657 ± 120 to 2890 ± 190 %, shown in **Figure 4-3** and is quantified in **Table 4-3**. Decreasing catalyst concentration did not show any consistent trends for the polymers' moduli. The lowest moduli of all ($p < 0.01$) was from the material

produced with 0.1 wt. % tin-POMS catalyst, while the highest was from 0.01% tin-POMS ($p < 0.05$ for all except PCL_{1k}:POSS catalyzed with 0.5 and 0.05 wt. % tin-POMS). Interestingly, there was no statistical difference between the moduli of the re-precipitated materials ($p > 0.05$). As for strain-to-failure, 0.1 wt. % tin-POMS led to the highest strain-to-failure with 2890 ± 190 % ($p < 0.01$) and 0.01% tin-POMS led to the lowest strain-to-failure ($p < 0.05$ for all materials except 1 wt. % tin-POMS and 2P). Again, precipitation had no effect on the strain-to-failure values ($p > 0.05$).

4.4.5 Cell Viability Testing of the PCL_{1k}:POSS Polyurethanes

The synthesized and processed materials were tested with the CCK-8 assay to determine cell viability. The materials were first immersed in L929 cell culture media for 24 or 72 h; the extract was then added to L929 fibroblast cells and the CCK-8 reagent was used to determine cell metabolism and thus cell viability. There was a clear trend of decreasing catalyst concentration and increasing cell viability for 24 h incubation, as shown in **Figure 4-4**. Statistically, only PCL_{1k}:POSS from 0.05% tin-POMS and 0.01 wt. % tin-POMS did not have different cell viabilities as the positive control at 92.4 ± 24.2 % ($p > 0.05$) and 98.3 ± 26.5 % ($p > 0.05$) cell viability, respectively. Conversely, materials from 1 wt. % tin-POMS, 0.1 wt. % DBTDL, and 3P were statistically not different from the negative control, cells treated with 1% SDS, which killed all cells ($p > 0.05$). Although the negative control produced a reading of 20.5 ± 0.5 % cell viability, the numbers were not adjusted for this baseline because some of the cell viability numbers of the experimental groups would have been negative, and there cannot be negative cell viability. The other materials were statistically above the negative control, but below 100% cell viability, with their averages below 70 % cell viability. Interestingly, the tin-POMS materials had a higher cell viability than their respective DBDTL materials. Polyurethane synthesized with 0.1 wt. % tin-

POMS had 25.7 ± 2.7 % cell viability, which was higher than polyurethane from 0.1 wt. % DBTDL at 21.3 ± 0.9 % ($p < 0.01$). Similarly, 0.01% tin-POMS produced a material with greater viability than 0.01% DBTDL ($p < 0.01$), with 98.3 ± 26.5 and 55.7 ± 16.9 % cell viability, respectively.

After 72 h of immersion, the cell viability decreased, as shown in **Figure 4-5**. Only PCL_{1k}:POSS 0.01% tin-POMS was statistically not different from the positive control ($p > 0.05$), but the average was below the 70% cell viability reference and variability was very high. The average of nine samples was 67.2 ± 71.0 %, as some samples had very high cell viability, but some were as low as the negative control. The second and third highest cell viabilities were from PCL_{1k}:POSS 70:30 catalyzed by 0.05% tin-POMS and 0.01% DBTDL with 52.0 ± 23.8 and 42.9 ± 36.0 % cell viabilities, respectively.

4.5 Discussion

The CCK-8 assay is a non-contact colorimetric cell viability assay. Media extracts from the different polymers were added to L929 fibroblast cells and incubated for 24 h. Then, a water-soluble tetrazolium salt, WST-8, was added and reduced by dehydrogenase activities within cells to produce an orange formazan dye, which is also soluble in cell media and is directly proportional to the number of living cells. The experimental groups are normalized to the positive to controls (equal to 100% cell viability) to compare different groups. This method was used first to test the cell viability of the different PCL:POSS, PGCL:POSS, and PLCL:POSS polyurethanes previously synthesized in Chapter 2. The resulting cell viabilities were around 40-50% of the positive control, which were cells in contact with cell media that never came in contact with polyurethane. Because the different materials, regardless of POSS content or soft segment concentration, all had low cell viabilities, it was hypothesized that the tin catalyst, tin-POMS, or tin-polyhedral oligomeric metal silsesquioxane, was the cause of this poor cell viability. This is because only the catalyst and

hexamethylene diisocyanate (HDI) were ubiquitous within each polymer, and HDI has been shown to be a biocompatible polyurethane component.[19, 20] Although many reports have looked at the viability of tin catalysts, this report is the first report to our knowledge that investigates the cytocompatibility of tin-POMS.

We synthesized several polyurethanes with tin-POMS, looking a wide range of catalyst concentrations (0.01 wt. % - 1 wt. %). We also studied two polyurethanes synthesized with another catalyst, dibutyltin dilaurate, as well as the re-precipitated of PCL_{1k}:POSS synthesized with 1 wt. % tin-POMS. All of the polyurethanes had slightly more incorporation of the soft segment, PCL_{1k} diol, than POSS, which is typical of POSS polyurethanes. However, the molecular weight varied. Generally, more catalyst led to materials with higher molecular weight, which is intuitive since all polyurethanes elastomers were synthesized for the same amount of time. 0.1 wt. % catalyst led to polymers with the highest molecular weights, with DBTDL catalyzing a higher molecular weight material than tin-POMS. This difference could be due to the fact that the same weight percent of tin-POMS and DBTDL resulted in more moles of DBTDL, increasing catalytic activity. Interestingly, re-precipitation produced lower molecular weight materials with slightly less POSS content, which could have been the result of preferential re-dissolution of the lower molecular weight, higher PCL content chains. While DSC showed similar transition temperatures for all polymers, with one glass transition and two melting transitions (one for PCL and one for POSS), the melting enthalpies for PCL were higher for lower molecular weight materials. We hypothesize that this could be due to higher crystallization of lower molecular weight polymers because there are fewer POSS molecules to disrupt the PCL crystalline structure, making crystallization easier.

Despite the varying molecular weights and thermal transitions, the mechanical properties as determined by tensile testing followed no trend. All moduli averages were similar, and all

strains-to-failure were above 1650 % strain. This is promising because even the lower molecular weight materials, as created by the lower catalyst concentrations, did not have poor mechanical properties. The difference in molecular weight may affect how the materials degrade, but more work needs to be done to test. One explanation for the varying mechanical properties could be that there were differences in crystallization kinetics during processing, despite efforts to keep the process identical for all materials.

Although molecular weight increased with increasing catalyst, the most obvious trend was increasing cell viability with decreasing catalyst concentration after 24 h of incubation. The high viability with low catalyst concentration and extremely poor cell viability at high catalyst concentrations indicated that our hypothesis was correct: high residual content of tin-POMS was the cause of poor cell viability previously. It is very promising that even though the cytocompatible materials had lower molecular weight, their mechanical properties were still high. DBTDL-catalyzed materials had lower cell viability when compared to the same concentration of tin-POMS materials. Because tin-POMS (1,026.44 g/mol) had a higher formula weight than DBTDL (631.56 g/mol), there were more mole/g DBTDL than tin-POMS in equivalent wt. % reactions. Also, re-precipitation did not improve cell viability to be greater than 70%, but this may be because the starting concentration was too high to affect the viability, as PCL_{1k}:POSS from 0.1% tin-POMS still had very low viability (around 26% of the positive control).

The cell viability was much lower for 72 h extract incubation time than for 24 h. Our hypothesis from this data is that more tin was eluting from the material then after 24 h, resulting in the lower cell viability, although more testing must be done to confirm this. It is possible that the catalyst could be trapped within the polyurethanes, as it has been shown that tin catalysts were retained in PCL diols during ring-opening polymerization and were retained more than other

metallic catalysts, such as zinc.[21] From the 72 h data, it is also hypothesized that these biomaterials could be pre-processed in order to remove the tin from the polyurethane by eluting all the tin with solvent washing or pre-soaking. Despite the variable cell viability *in vitro* after several days, it is possible that the 0.01 wt. % tin-POMS polyurethane could be non-toxic *in vivo*, as previous polyurethanes synthesized with the same wt. % of tin catalyst (100 ppm) were found to be non-toxic *in vivo* when implanted in mice.[16]

4.6 Conclusions

In conclusion, the amount of catalyst used in synthesis affected the cell viability. We found that decreasing the catalyst concentration increased cell viability, with 0.01 wt.% tin-POMS resulting in the material with the best cell viability after incubation for 24 h. Although this material had lower molecular weight than some of the other polyurethanes, it had comparable modulus and high strain-to-failure. The variability of the cell viability of 72 h indicates that pre-processing may need to be done to insure better cell viability, although 0.01 wt. % catalyst has been used *in vivo* in other studies with promising results.

4.7 References

1. Zdrahala, R. J.; Zdrahala, I. J., Biomedical Applications of Polyurethanes: A Review of Past Promises, Present Realities, and a Vibrant Future. *Journal of Biomaterials Applications* **1999,** *14* (1), 67-90.

2. Guan, J.; Sacks, M. S.; Beckman, E. J.; Wagner, W. R., Synthesis, characterization, and cytocompatibility of elastomeric, biodegradable poly(ester-urethane)ureas based on poly(caprolactone) and putrescine. *Journal of Biomedical Materials Research* **2002,** *61* (3), 493-503. DOI: 10.1002/jbm.10204.

3. Martin, D. J.; Poole Warren, L. A.; Gunatillake, P. A.; McCarthy, S. J.; Meijs, G. F.; Schindhelm, K., Polydimethylsiloxane/polyether-mixed macrodiol-based polyurethane elastomers: biostability. *Biomaterials* **2000,** *21* (10), 1021-1029. DOI: http://dx.doi.org/10.1016/S0142-9612(99)00271-9.

4. Skarja, G. A.; Woodhouse, K. A., Synthesis and characterization of degradable polyurethane elastomers containing an amino acid-based chain extender. *Journal of Biomaterials Science, Polymer Edition* **1998,** *9* (3), 271-295. DOI: 10.1163/156856298X00659.

5. Bae, J. S.; Seo, E. J.; Kang, I. K., Synthesis and characterization of heparinized polyurethanes using plasma glow discharge. *Biomaterials* **1999,** *20* (6), 529-537. DOI: 10.1016/S0142-9612(98)00204-X.

6. Woo, G. L. Y.; Mittelman, M. W.; Santerre, J. P., Synthesis and characterization of a novel biodegradable antimicrobial polymer. *Biomaterials* **2000,** *21* (12), 1235-1246. DOI: http://dx.doi.org/10.1016/S0142-9612(00)00003-X.

7. Gorna, K.; Gogolewski, S., In vitro degradation of novel medical biodegradable aliphatic polyurethanes based on ϵ-caprolactone and Pluronics® with various hydrophilicities. *Polymer Degradation and Stability* **2002,** *75* (1), 113-122. DOI: http://dx.doi.org/10.1016/S0141-3910(01)00210-5.

8. Saad, B.; Hirt, T. D.; Welti, M.; Uhlschmid, G. K.; Neuenschwander, P.; Suter, U. W., Development of degradable polyesterurethanes for medical applications: In vitro and in vivo evaluations. *Journal of Biomedical Materials Research* **1997,** *36* (1), 65-74. DOI: 10.1002/(SICI)1097-4636(199707)36:1<65::AID-JBM8>3.0.CO;2-J.

9. Knight, P. T.; Lee, K. M.; Qin, H.; Mather, P. T., Biodegradable Thermoplastic Polyurethanes Incorporating Polyhedral Oligosilsesquioxane. *Biomacromolecules* **2008,** *9* (9), 2458-2467. DOI: 10.1021/bm8004935.

10. Gorna, K.; Polowinski, S.; Gogolewski, S., Synthesis and characterization of biodegradable poly(ϵ-caprolactone urethane)s. I. Effect of the polyol molecular weight, catalyst, and chain extender on the molecular and physical characteristics. *Journal of Polymer Science Part A: Polymer Chemistry* **2002,** *40* (1), 156-170. DOI: 10.1002/pola.10096.

11. Silva, A. L.; Bordado, J. C., Recent Developments in Polyurethane Catalysis: Catalytic Mechanisms Review. *Catalysis Reviews* **2004,** *46* (1), 31-51. DOI: 10.1081/CR-120027049.

12. Heijkants, R. G. J. C.; Calck, R. V. v.; van Tienen, T. G.; de Groot, J. H.; Buma, P.; Pennings, A. J.; Veth, R. P. H.; Schouten, A. J., Uncatalyzed synthesis, thermal and mechanical properties of polyurethanes based on poly(-caprolactone) and 1,4-butane diisocyanate with uniform hard segment. *Biomaterials* **2005,** *26* (20), 4219-4228. DOI: http://dx.doi.org/10.1016/j.biomaterials.2004.11.005.

13. Tanzi, M. C.; Verderio, P.; Lampugnani, M. G.; Resnati, M.; Dejana, E.; Sturani, E., Cytotoxicity of some catalysts commonly used in the synthesis of copolymers for biomedical use. *Journal of Materials Science: Materials in Medicine* **1994,** *5* (6), 393-396. DOI: 10.1007/BF00058971.

14. Guelcher, S. A.; Srinivasan, A.; Dumas, J. E.; Didier, J. E.; McBride, S.; Hollinger, J. O., Synthesis, mechanical properties, biocompatibility, and biodegradation of polyurethane networks

from lysine polyisocyanates. *Biomaterials* **2008,** *29* (12), 1762-1775. DOI: http://dx.doi.org/10.1016/j.biomaterials.2007.12.046.

15. Tseng, L.-F.; Mather, P. T.; Henderson, J. H., Shape-memory-actuated change in scaffold fiber alignment directs stem cell morphology. *Acta Biomaterialia* **2013,** *9* (11), 8790-8801. DOI: http://dx.doi.org/10.1016/j.actbio.2013.06.043.

16. Laschke, M. W.; Strohe, A.; Scheuer, C.; Eglin, D.; Verrier, S.; Alini, M.; Pohlemann, T.; Menger, M. D., In vivo biocompatibility and vascularization of biodegradable porous polyurethane scaffolds for tissue engineering. *Acta Biomaterialia* **2009,** *5* (6), 1991-2001. DOI: http://dx.doi.org/10.1016/j.actbio.2009.02.006.

17. Knight, P. T.; Kirk, J. T.; Anderson, J. M.; Mather, P. T., In vivo kinetic degradation analysis and biocompatibility of aliphatic polyester polyurethanes. *Journal of Biomedical Materials Research Part A* **2010,** *94A* (2), 333-343. DOI: 10.1002/jbm.a.32806.

18. Wang, W.; Wiggins, J. S., Kinetic evaluation of tin-POMS catalyst for urethane reactions. *Journal of Applied Polymer Science* **2008,** *110* (6), 3683-3689. DOI: 10.1002/app.28957.

19. Grad, S.; Kupcsik, L.; Gorna, K.; Gogolewski, S.; Alini, M., The use of biodegradable polyurethane scaffolds for cartilage tissue engineering: potential and limitations. *Biomaterials* **2003,** *24* (28), 5163-5171. DOI: http://dx.doi.org/10.1016/S0142-9612(03)00462-9.

20. Hsu, S.-h.; Tseng, H.-J.; Lin, Y.-C., The biocompatibility and antibacterial properties of waterborne polyurethane-silver nanocomposites. *Biomaterials* **2010,** *31* (26), 6796-6808. DOI: http://dx.doi.org/10.1016/j.biomaterials.2010.05.015.

21. Schappacher, M.; Le Hellaye, M.; Bareille, R.; Durrieu, M.-C.; Guillaume, S. M., Comparative in vitro Cytotoxicity Toward Human Osteoprogenitor Cells of Polycaprolactones Synthesized from Various Metallic Initiators. *Macromolecular Bioscience* **2010,** *10* (1), 60-67. DOI: 10.1002/mabi.200900184.

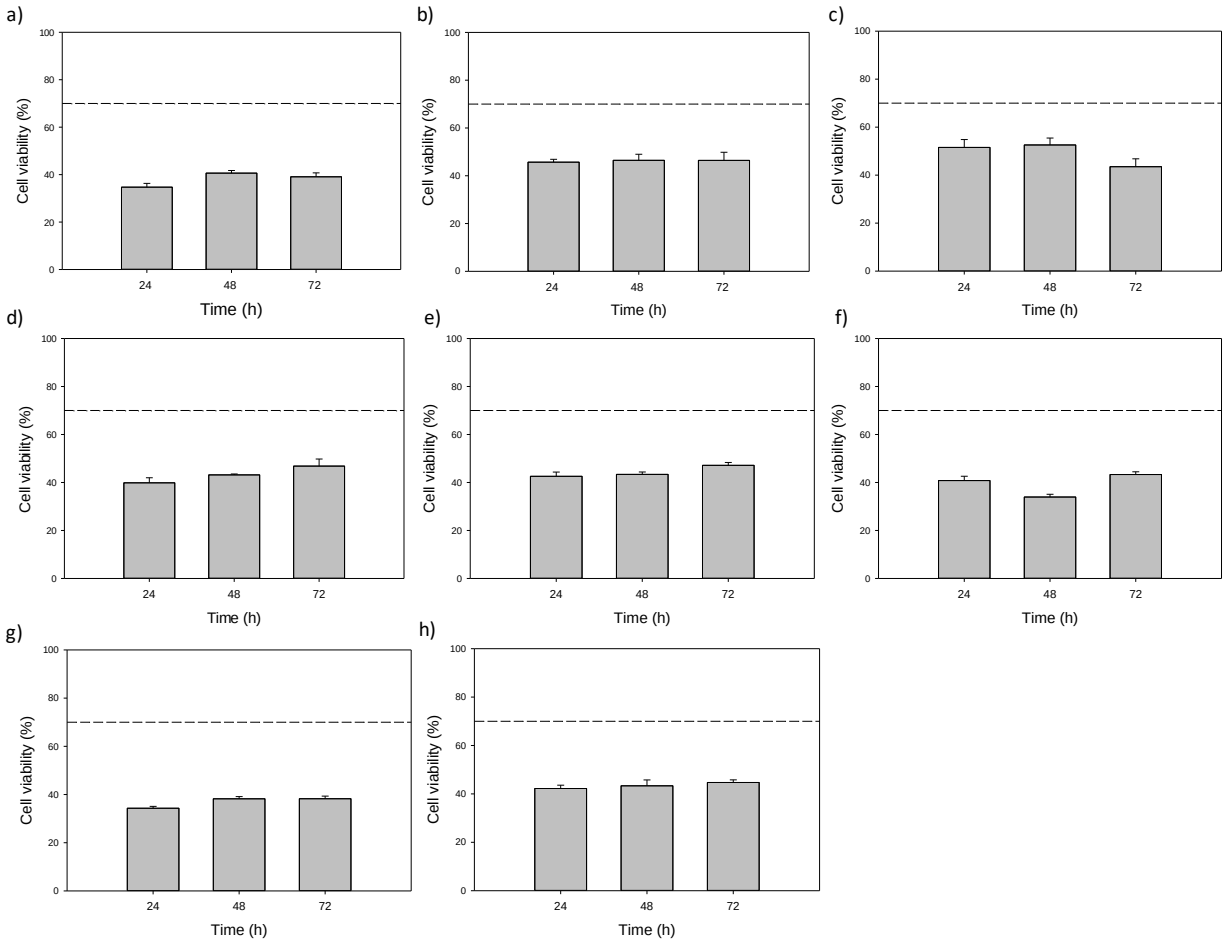

Figure 4-1: Cell viability (%), compared to a positive control (100%), for a) PCL_{1k}:POSS 100:0, b) PCL_{1k}:POSS 90:10, c) PCL_{1k}:POSS 80:20, d) PCL_{1k}:POSS 70:30, e) $(PG_5CL_{95})_{1k}$:POSS 70:30, f) $(PG_{25}CL_{75})_{1k}$:POSS 70:30, g) $(PL_5CL_{95})_{1k}$:POSS 70:30, and h) $(PL_{25}CL_{75})_{1k}$:POSS 70:30. These materials were incubated in media for 24, 48, and 72 h. The reference line is 70% cell viability.

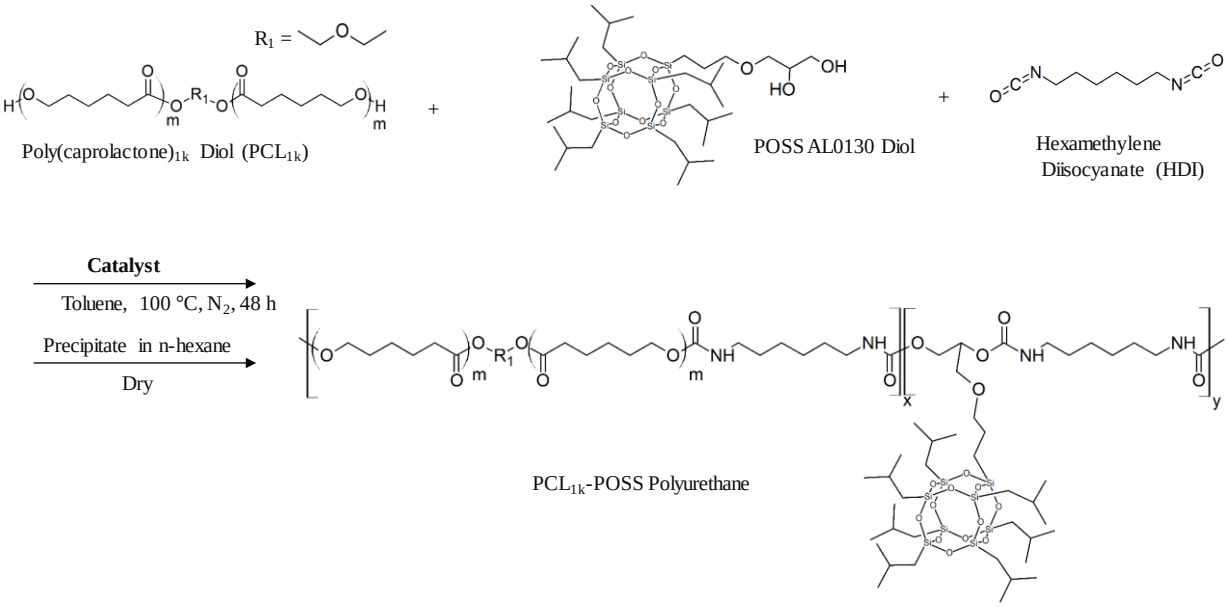

Scheme 4-1: PCL_{1k}:POSS polyurethane synthesis.

Table 4-1: Summary of polyurethanes synthesized with varying catalyst type, concentration and precipitation numbers with their molecular properties.

	Synthesis	Catalyst (Wt. %)	Yield (%)	Input Diol:POSS Ratio (Wt. %)	Actual[a] Diol:POSS Ratio (Wt. %)	Mn[b] (kDa)	Mw[b] (kDa)	PDI[b]
Tin - POMS	PCL:POSS 70:30 - 1	1	83.8	70 : 30	76.6 : 23.4	71.4	102.9	1.44
	PCL:POSS 70:30 - 2	0.5	82.7	70 : 30	76.0 : 24.0	67.5	105.4	1.56
	PCL:POSS 70:30 - 3	0.1	85.7	70 : 30	77.2 : 22.8	61.5	121.9	2.04
	PCL:POSS 70:30 - 4	0.05	84.0	70 : 30	78.1 : 21.9	31.9	62.4	1.95
	PCL:POSS 70:30 – 5	0.01	86.4	70 : 30	76.6 : 23.4	33.3	57.2	1.72
	PCL:POSS 70:30 – 1-2P*	**1**	**-**	**70 : 30**	**77.4 : 22.6**	**35.3**	**55.7**	**1.58**
	PCL:POSS 70:30 – 1-3P*	**1**	**-**	**70 : 30**	**77.6 : 22.4**	**28.9**	**54.6**	**1.89**
DBTDL	PCL:POSS 70:30 - 6	0.1	85.0	70 : 30	75.7 : 24.3	89.7	174.6	1.95
	PCL:POSS 70:30 – 7	0.01	84.2	70 : 30	77.9 : 22.1	28.2	54.6	1.96

[a]Determined from proton nuclear magnetic resonance.
[b]Determined from gel permeation chromatography (n=3).
*P indicates the precipitation number.

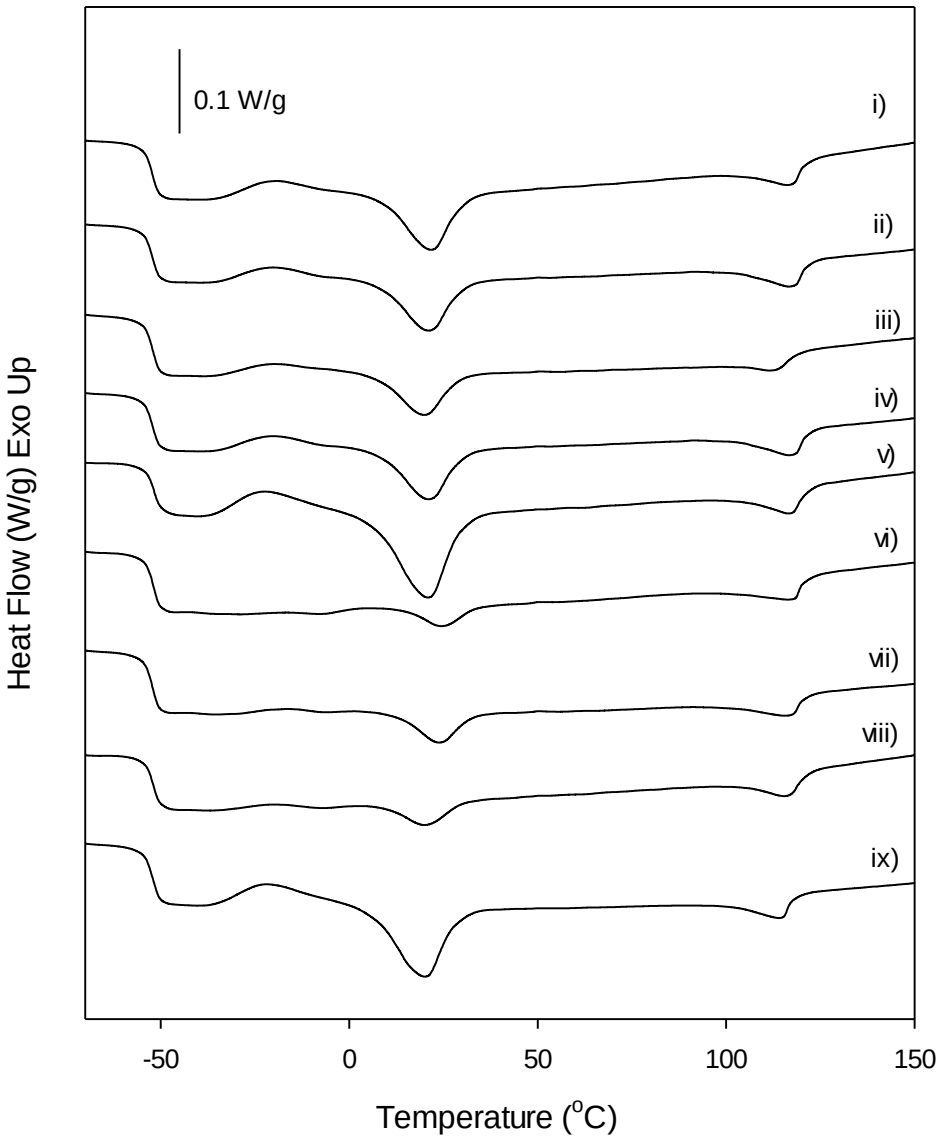

Figure 4-2: Differential scanning calorimetry of PCL_{1k}:POSS 70:30, with second heat shown, synthesized with i) 1 wt. % tin-POMS, ii) 0.5 wt. % tin-POMS, iii) 0.1 wt. % tin-POMS, iv) 0.05 wt. % tin-POMS, v) 0.01 wt. % tin-POMS, vi) 1 wt. % tin-POMS-2P, vii) 1 wt. % tin-POMS-3P, vii) 0.1 wt. % DBTDL, and ix) 0.01 wt. % DBTDL.

Table 4-2: Summary of the thermal properties of the PCL_{1k}:POSS polyurethanes.

	Synthesis	Catalyst (Wt. %)	T_g (°C)	$T_{m,PCL}$ (°C)	ΔH_{PCL} (J/g)	$T_{m,POSS}$ (°C)	ΔH_{POSS} (J/g)
Tin - POMS	PCL:POSS 70:30 - 1	1	-52.1	21.8	3.2	116.9	1.8
	PCL:POSS 70:30 - 2	0.5	-52.1	21.1	3.2	116.9	2.4
	PCL:POSS 70:30 - 3	0.1	-52.2	20.0	2.3	113.0	1.6
	PCL:POSS 70:30 - 4	0.05	-51.9	20.9	5.9	115.5	1.8
	PCL:POSS 70:30 - 5	0.01	-51.9	21.0	5.9	117.0	2.1
	PCL:POSS 70:30 – 1-2P	**1**	-52.2	24.7	2.9	117.6	2.2
	PCL:POSS 70:30 – 1-3P	**1**	-52.2	23.8	2.0	116.7	2.0
DBTDL	PCL:POSS 70:30 – 6	0.1	-51.8	20.3	2.2	116.0	2.6
	PCL:POSS 70:30 – 7	0.01	-51.8	20.0	3.6	114.6	1.7

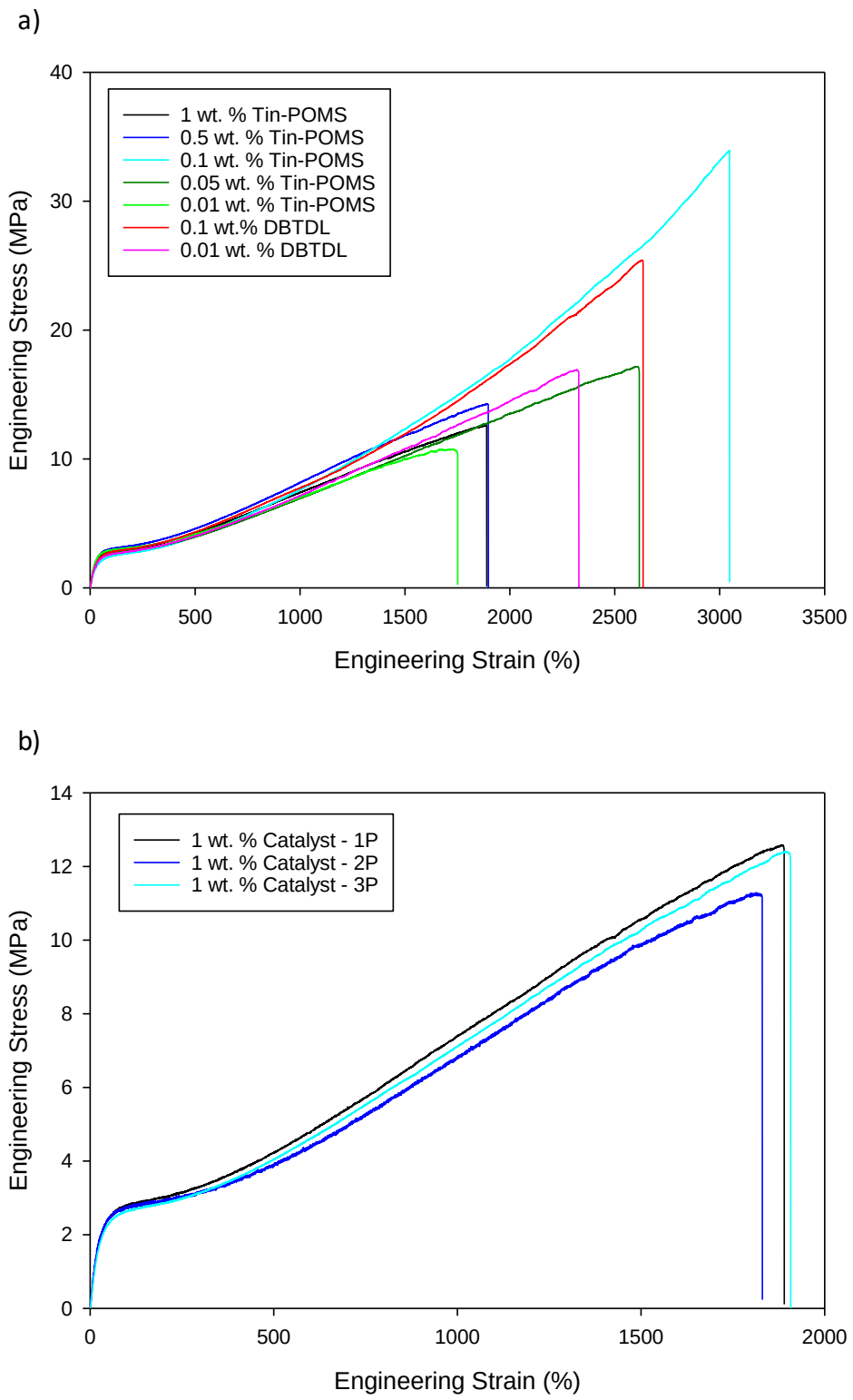

Figure 4-3: Tensile properties of the PCL_{1k}:POSS polyurethanes a) synthesized with different catalysts and b) processed with repeated precipitations.

Table 4-3: Summary of the mechanical properties from tensile testing.

	Synthesis	Catalyst (Wt. %)	Modulus (MPa)	Strain to Failure (%)
Tin - POMS	PCL:POSS 70:30 - 1	1	9.33 ± 0.8	1850 ± 360
	PCL:POSS 70:30 - 2	0.5	10.27 ± 0.5	1880 ± 70
	PCL:POSS 70:30 - 3	0.1	7.88 ± 0.5	2890 ± 190
	PCL:POSS 70:30 - 4	0.05	9.68 ± 0.7	2440 ±120
	PCL:POSS 70:30 - 5	0.01	10.96 ± 1.1	1657 ± 120
	PCL:POSS 70:30 – 1-2P	**1**	9.35 ± 0.3	1750 ± 70
	PCL:POSS 70:30 – 1-3P	**1**	9.18 ± 0.5	1900 ± 140
DBTDL	PCL:POSS 70:30 – 6	0.1	9.29 ± 0.6	2470 ± 180
	PCL:POSS 70:30 – 7	0.01	8.73 ± 0.2	2350 ± 110

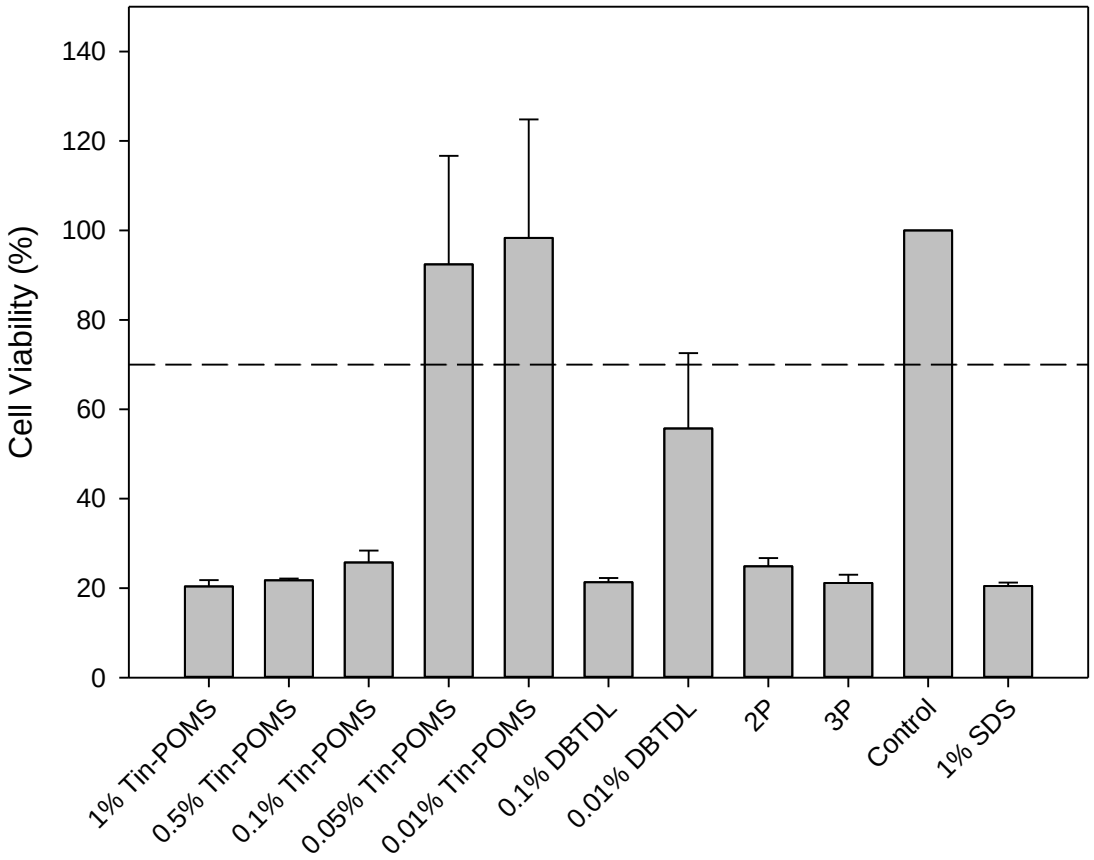

Figure 4-4: Cell viability from the CCK-8 assay of materials from all synthesis and processing conditions after incubation in media for 24 h. All experimental conditions are normalized to the control of 100% cell viability. The reference line is 70% cell viability.

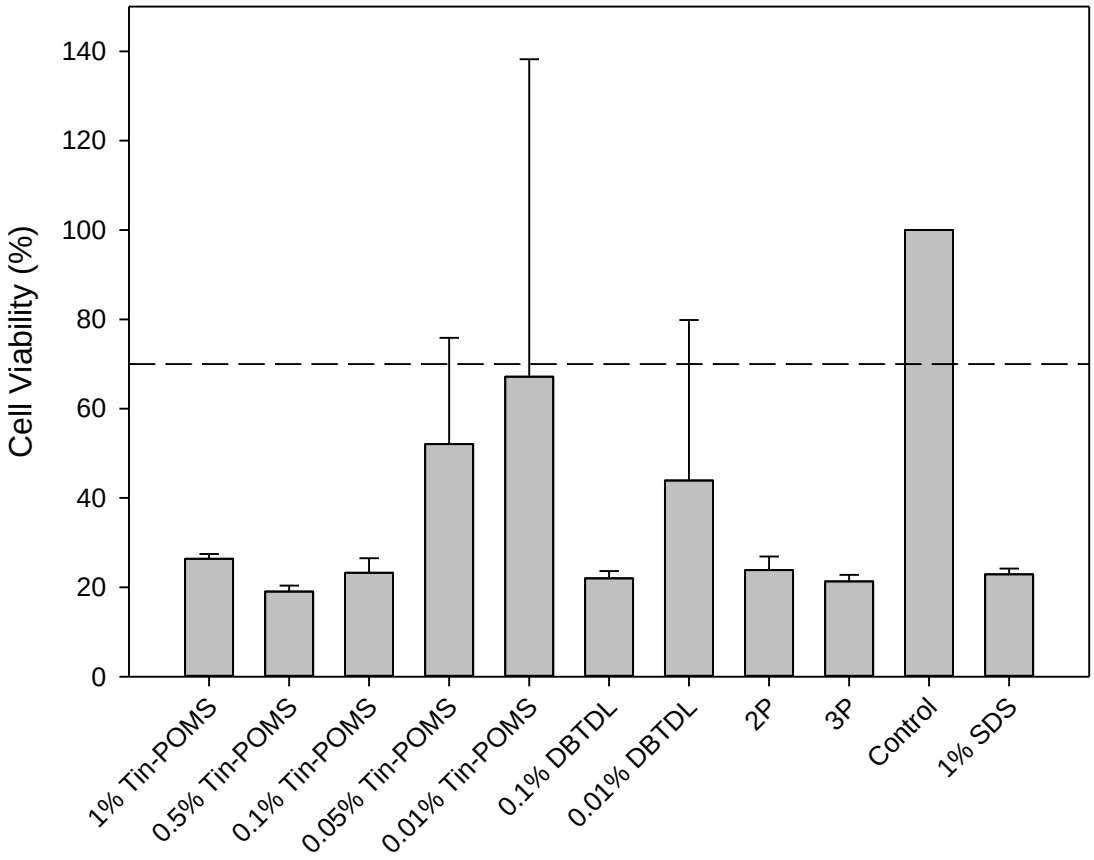

Figure 4-5: Cell viability from the CCK-8 assay of materials from all synthesis and processing conditions after incubation in media for 72 h. All experimental conditions are normalized to the control of 100% cell viability. The reference line is set at 70% cell viability.

Chapter 5: Biodegradable Thermoplastic Shape Memory Elastomeric Composites (SMECs) Via Dual-Electrospinning

5.1 Synopsis

There is a need for biodegradable thermoplastic smart materials for medical devices. Smart technology includes shape memory, or the ability of a material to fix into a temporary shape and return to its original shape upon a stimulus. To achieve the goal of biodegradable thermoplastic smart materials, we have created shape memory elastomeric composites, or SMECs, that utilize two thermoplastic biodegradable materials to de-couple the fixing and recovery mechanisms. The two materials utilized are a semi-crystalline polymer, poly(caprolactone) (PCL), as the fixing agent and our POSS-based biodegradable elastomers (TPE) as the recovery agent. These composites were fabricated by dual-electrospinning TPE and PCL and compacting the resulting blend by melting the PCL, resulting in a matrix of PCL around TPE fibers. The composition of the dual-electrospun SMECs was varied by changing the flow rates of the electrospinning and the composites were tested for thermal and mechanical properties. Increasing PCL loading first decreased the modulus and then increased it; while the opposite trend is true for elasticity. The SMECs had a higher strain-to-failure than the neat elastomer throughout degradation. Contrary to our expectation, fixing 50% or 100% strain into a composition did not affect degradation rate, as the SMECs with fixed strain had similar mass loss, water uptake, morphology, and melting enthalpy as the SMEC with no fixed strain.

5.2 Introduction

There exists a need for thermoplastic biodegradable elastomers in medical devices, which would benefit from smart technology such as shape memory. Shape memory polymers (SMPs) are polymeric materials that can be fixed into a temporary shape and be recovered to their permanent

shape by a stimulus: heat,[1-3] light,[4, 5] solvent,[6, 7] pH,[8, 9] electrical current,[10, 11] or magnetism.[12, 13] A majority of SMPs are recovered by heat, and will be the focus of the work here. There are two requirements of a shape memory polymer: 1) cross-links (covalent or physical) that provide elasticity and recover the SMP to its permanent shape, and 2) a transition segment through which the material can fix into the temporary shape. Utilization of a melting transition temperature (T_m) and physical cross-links would allow for an elastomeric, thermoplastic SMP. Smart elastomeric materials could be utilized for wide array of biomedical applications, including deployable stents,[14] sutures,[1] or tissue engineering scaffolds[15] for soft tissues. Manufacturing of biodegradable biomedical devices could also be improved when the transition temperature is above body temperature; sheets of material could be fabricated and fixed separately into its final shape, making medical devices patient-specific and customizable.

Several non-biodegradable elastomeric SMPs have been fabricated utilizing different chemicals including thermoset liquid crystalline elastomers (LCEs),[16] vulcanized rubber,[17] poly(cyclooctene),[3] poly(ethylene-co-vinyl acetate),[18] acrylates,[19, 20] polyurethanes[21] and thermoplastic LCEs.[22, 23] These materials have optimized chemistry to control the fixing and recovery. Other researchers have created material blends that result in elastomeric SMPs.[24, 25] Previously in our lab, shape memory elastomeric composites (SMECs) were fabricated that exploited different materials for fixing and recovery.[26] This was first done by electrospinning a fixing material, poly(caprolactone) (PCL), and infiltrating it with an thermoset elastomeric matrix, poly(dimethyl siloxane) (PDMS). Fixing and recovery were high in this system, but the PDMS curing took several days. To reduce processing time and increase control over the respective components, thermoplastic SMECs were fabricated by dual-electrospinning PCL and Pellethane®.[27] However, neither of these SMEC systems were fully biodegrdable.

Biodegradable shape memory materials would serve as temporary implantable medical devices that could safely leave the body. Several biodegradable, elastomeric shape memory polymers have been reported on, including thermoset polycitrates,[28, 29] and thermoplastic polyurethanes with poly(caprolactone) and poly(hydroxybutyrate),[30] thermoplastic blends of poly(lactic acid)-co-poly(amide)[31] as well as interpenetrating networks of poly(esterurethane) and poly(ethylene glycol) dimethacrylate.[32] From our lab, biodegradable reconfigurable SMECs have been fabricated by curing poly(anhydride) around an electrospun polyurethane web. These materials could reset their permanent shape, had fixing and recovery, and were fully biodegradable.[33] However, poly(anhydride) degrades quickly (within several days).

In this study, we fabricated biodegradable shape memory elastomeric composites (SMECs) from our synthesized biodegradable elastomers[34] and poly(caprolactone) by dual-electrospinning and compaction. Our goal was to create durable, biodegradable SMECs. Materials with different compositions were characterized for morphology, thermal, mechanical, and shape memory properties. The different compositions were tested for mechanical properties throughout degradation. It was anticipated that increasing the PCL content would decrease the loss of mechanical properties throughout degradation. Next, we fixed different strains into one composition with good fixing and recovery, and examined several properties including mass loss, water uptake, morphology, and thermal properties during degradation and recovery after degradation.

5.3 Methods

5.3.1 Materials

1,4-butanediol (≥ 99%), 1,4-dioxane-2,5-dione (glycolide, ≥ 99%), ε-caprolactone (≥ 97%), and tin(II) 2-ethylhexanoate (stannous octoate, 95%) were all purchased from Sigma-

Aldrich. Glycolide was purified by recrystallization by dissolving in ethyl acetate (Fisher Scientific, Inc.) under reflux at a concentration of 0.2 g/mL. It was placed in a -4 °C freezer overnight, collected and vacuum dried extensively prior to use. ε-Caprolactone was purified by vacuum distillation prior to use. Poly(ε-caprolactone) diol (M_w ~ 1,250 g/mol) was purchased from Polysciences, Inc. 1,2-PropanediolIsobutyl POSS (AL0130), subsequently referred to as POSS diol, and Tin-POMS catalyst were purchased from Hybrid Plastics. Hexamethylene diisocyanate (HDI) was purchased from Sigma-Aldrich and used as received. Toluene, tetrahydrofuran (THF), chloroform, and *n*-hexanes were purchased from Fisher Scientific. Toluene was dried by refluxing over calcium hydride (Sigma-Aldrich) several times until collection prior to use, and stored over 3 Å molecular sieves (Sigma-Aldrich). Deuterated chloroform (chloroform-d, 99.8% atom D), N,N-dimethylformamide (anhydrous, 99.8%, referred to as DMF), phosphate-buffered saline (pH of 7.4), and HPLC-grade THF were purchased from Sigma-Aldrich. Poly(caprolactone) (M_w ~ 80 kDa) (PCL_{80k}) was purchased from Sigma-Aldrich and used as received.

5.3.2 Polyurethane Synthesis

Diol and polyurethane syntheses were described in detail previously (Chapter 2). Briefly, biodegradable diols with a target molecular weight of 1 kDa were synthesized by performing ring-opening polymerization of caprolactone and glycolide in the presence of butane diol and catalyst by heating the reactants to 140 °C and stirring under N_2 for 10 h. When cooled, the diol was dissolved in THF, precipitated, dried, and characterized for molecular weight and composition. The diols synthesized were poly($glycolide_5$-co-$caprolactone_{95}$)$_{1k}$ (PG_5CL_{95})$_{1k}$.

The (PG_5CL_{95})$_{1k}$ diol and purchased PCL_{1k} were used as biodegradable diols in the polyurethane reaction with a target weight ratio of 35:35:30 PCL_{1k}:(PG_5CL_{95})$_{1k}$:POSS or 70:30 (PG_5CL_{95})$_{1k}$:POSS. For each synthesis, the biodegradable diol(s) and POSS diol were dissolved in

distilled in toluene, HDI and tin-POMs were added, and the reaction was heated to 100 °C. HDI was added over time to increase the polyurethane's molecular weight. The resultant polymer was cooled to room temperature and precipitated in n-hexanes, dried and characterized for molecular weight and molecular composition by gel permeation chromatography (GPC) (see Section 2.3.5 for methods) and proton nuclear magnetic resonance (^{1}H-NMR) (Section 2.3.4).

5.3.3 Dual-Electrospinning

The synthesized biodegradable thermoplastic polyurethane elastomer, subsequently referred to as TPE, was dissolved in chloroform and DMF at a concentration of 2.0 g/10 mL 8:2 $CHCL_3$:DMF. PCL_{80k} was also dissolved in 8:2 $CHCL_3$:DMF at a concentration of 2.0 g/10 mL. These solutions were electrospun simultaneously (dual-electrospun) utilizing syringes perpendicular to the rotating/translating drum and 180° from each either. The flow rate for the TPE was 3.0 - 3.3 mL/h, the syringe-to-mandrel distance was 7 cm and the voltage was 16 kV. For PCL_{80k}, the flow rate was 0.6 - 1 mL/h, the syringe tip to mandrel distance was 6 cm and the voltage was 12 kV.

5.3.4 Compression Molding

Dual-electrospun composites (and electrospun PCL-only and TPE-only controls) were dried extensively prior to compression molding. Materials were heated above PCL's melting point (60 °C) (or 130 °C for the TPE control) and compacted under 1 metric ton for 10 minutes (2 minutes for TPE control) before cooling. A 0.45 mm PTFE (Teflon) spacer was used to ensure the thickness of all films.

5.3.5 Scanning Electron Microscopy

A JEOL JSM-5600 scanning electron microscope (SEM) was utilized to visualize the electrospun and dual-electrospun fibers as well as the surface and cross section of the compacted

films. Films and fibers were visualized in secondary electron mode with an accelerating voltage of 7 kV. Samples were sputter-coated with gold for 45 seconds prior to imaging.

5.3.6 Differential Scanning Calorimetry (DSC)

Thermal properties of the materials were studied by differential scanning calorimetry (DSC) using the TA Q200 instrument. Heat flow was collected while each sample was heated to 200 °C (to remove thermal history), cooled to -70 °C, and heated a second time to 200 °C. The heating rate was 10 °C/min and the cooling rate was 5 °C/min. The second heat was used to determine glass transition temperature (T_g, a step in the curve), the change in heat capacity or melting transitions (T_m, the peak of the endotherm) and the enthalpies of melting (ΔH, area under the curve). PCL content in the dual-spun composites was determined by:

$$PCL\ (\%) = \frac{\Delta H_{SMEC}}{\Delta H_{PCL}} * 100 \quad \textbf{(5-1)}$$

Where ΔH_{SMEC} is melting enthalpy for the PCL curve within the SMEC, while ΔH_{PCL} is the melting enthalpy for the PCL-only control.

5.3.7 Dynamic Mechanical Analysis

A TA Instruments Q800 dynamic mechanical analyzer (DMA) was utilized to determine the temperature-dependent viscoelastic properties of the polyurethanes. Samples in a dogbone geometry were loaded at room temperature, cooled to -20 °C and heated to 140 °C at a rate of 3 °C/minute. In order to maintain tension, applied load was kept at 108% of dynamic load. All runs were performed with a frequency of 1 Hz and 15 μm (<0.1%) amplitude.

5.3.8 Tensile Testing

TestResources Model 100P Universal Testing Machine was utilized to determine the tensile properties of the materials. Samples were cut in a dogbone geometry (ASTM Standard D638-03 Type IV, scaled down by a factor of 4) and stretched at a rate of 50 μm/s dry at room

temperature (about 23 °C) or hydrated in 0.9% (9 g/1L) NaCl solution at 37 °C. Young's modulus and strain-to-failure were determined from engineering stress vs. engineering strain plots.

5.3.9 Elasticity Testing

Elasticity, here termed R_E, was determined using the "squeeze/pull off" test of a TA AR-G2 Rheometer with custom tensile clamps. Dogbone-shaped samples were stretched 50 µm/s to 50% strain and then returned to the starting position at the same rate. Elasticity was determined from the following equation:

$$R_E\,(\%) = \frac{\varepsilon_f - \varepsilon_r}{\varepsilon_f - \varepsilon_i} * 100 \qquad \textbf{(5-2)}$$

Where ε_i is a small initial strain (where stress equals zero), ε_f is the strain that the polymer is stretched to, and ε_r is the strain recovered (where stress equals zero upon unloading).

5.3.10 Shape Memory Testing

Using the TA Q800 DMA in controlled force mode, dogbones of the SMECs were stretched to 20% strain at 60 °C at a rate of 0.02 N/min and cooled to 20 °C at 3 °C /min to fix the strain. Force was unloaded 0.05 N/min at 20 °C. The SMEC was then heated to 80 °C at a rate of 3 °C/min for recovery. The SMEC was cooled to 60 °C and the cycle was repeated 3 times. Fixing (R_f) and recovery (R_r) ratios were determined by:

$$R_f(\%) = \frac{\varepsilon_f - \varepsilon_i}{\varepsilon_d - \varepsilon_i} * 100 \textbf{ (5-3)}$$

$$R_r(\%) = \frac{\varepsilon_f - \varepsilon_r}{\varepsilon_f - \varepsilon_i} * 100 \textbf{ (5-4)}$$

Where ε_i is the strain at the beginning of each cycle (initial stain before stretching), ε_d is the strain the material is deformed to after cooling (stain of deformation), ε_f is the strain left after unloading (the fixed strain), and ε_r is the strain after heating (strain of recovery).

5.3.11 X-Ray Diffraction (XRD)

Wide-angle x-ray scattering (WAXS) and small-angle x-ray (SAXS) experiments were conducted to ascertain the molecular and nano-scale ordering and orientation of the various polymeric samples. For this purpose, a Rigaku S-MAX3000 pinhole camera system was utilized, with a MicroMax-002 generator operating with Cu Kα emission (λ = 1.5406), voltage of 45 kV and current of 0.88 mA. Wide-angle scattering patterns were collected at a sample-detector distance of 122.7 mm (resulting in scattering angles $3° < 2\theta < 40°$) using Fujifilm image plates (CR HR-V) with a FujiFilm FLA7000 reader. Small-angle scattering patterns were collected using an area detector at a sample-detector distance of 1550 mm. Data were recorded in the range of $0.0054 < q < 0.16$ Å^{-1}, where $q=(4\pi/\lambda)\sin\theta$, where 2θ is the scattering angle. Samples were exposed to radiation for 30 minutes to achieve adequate x-ray counts for analysis, which was performed using SAXSgui software v2.03.04.

5.3.12 Degradation Study I

Compression-molded dogbones of different SMEC compositions were degraded in PBS rotating at 60 RPM at 37 °C for two degradations studies. First, a degradation study was performed to examine how mechanical properties (modulus and strain-to-failure) changed over the course of 4 w. Samples were stretched at a rate of 50 μ/s at 37 °C in 0.9% NaCl solution.

5.3.13 Degradation Study II

For the second degradation study, one SMEC composition (27% PCL with $(PG_5CL_{95})_{1k}$:POSS 70:30 as the TPE), was degraded at different fixed strains over the course of two months. To fix a strain, dogbones were first heated to 70 °C for five minutes and then cooled to -20 °C for 10 minutes to remove thermal history. Then, samples were heated to 60 °C for five minutes and then stretched to 0% (no strain), 50% or 100% strain with a custom manual stretching

apparatus. The samples were then cooled under tension (if strained) to -20 °C for 15 minutes. Then, to ensure uniform thickness throughout the sample, the dogbone tabs were cut off. Samples were weighed for initial mass and placed in PBS. At predetermined time points, samples were removed, weighed for wet mass, dried extensively and weighed for dry mass. Mass remaining and water uptake were determined from the equations below:

$$\text{mass remaining (\%)} = \left(\frac{m_d}{m_i}\right) * 100 \textbf{ (5-5)}$$

$$\text{water uptake (\%)} = \left(\frac{m_{wet} - m_d}{m_d}\right) * 100 \textbf{ (5-6)}$$

with m_i being the initial weight of the sample, m_{wet} being the mass of the wet sample, and m_d the mass of the dry sample. Degraded samples were studied with differential scanning calorimetry (DSC), scanning electron microscopy (SEM) and x-ray diffraction (WAXS and SAXS) to determine the changing crystallinity, surface topography, and microstructure with degradation. After two months (8 w) of degradation, materials fixed at 50% and 100% strain were heated to 70 °C to recover the fixed strain after degradation.

5.3.14 Statistical Analysis

T-tests were performed on two means with unequal variances to determine the statistical significance of different sets of data. Two-tailed t-tests with a confidence value of $\alpha = 0.05$ was used for all tests.

5.4 Results

5.4.1 Polyurethane Synthesis I

The polyurethane (TPE) synthesized for the first part of the SMEC study was PCL_{1k}:$(PG_5CL_{95})_{1k}$:POSS 35:35:30. The synthesis schematic is shown in **Scheme 5-1**, and the molecular and thermal properties of the polyurethane is shown in **Table 5-1**. This material utilized $(PG_5CL_{95})_{1k}$ diol, which had a molecular weight 1.84 kDa (M_w) and an actual molar ratio of

4.3:95.7 glycolide:caprolactone. The molecular weight of the TPE was high: M_n equal to 104.6 kDa and M_w equal to 140.9 kDa. The actual weight ratio of the polyurethane components was close to the target value at 38.1:37.0:24.9 PCL_{1k}:$(PG_5CL_{95})_{1k}$:POSS. There were two melting transitions in this material, 20.4 °C for the soft segment and 118.1 °C for POSS. The melting enthalpies for these transitions were low: 5.2 and 2.0 J/g, respectively.

5.4.2 Dual-Electrospinning, Compression Molding, and Scanning Electron Microscopy

The polyurethane was dual-electrospun with linear polycaprolactone (M_w = 80 kDa), as shown in **Scheme 5-2a**. The dual-electrospun webs were compacted into films by compacting above PCL's melting transition, as shown schematically in **Scheme 5-2b**. There were four materials of interest: the TPE, two Shape Memory Elastomeric Composites (or SMECs), one with an input ratio of 15% PCL (85% TPE) and 25% PCL (75% TPE), and only PCL. Going forward, the materials are named TPE, 15% PCL SMEC, 25% PCL SMEC and PCL, respectively. The resulting electrospun webs are shown in **Figure 5-1, (i)-(iv)**. The polyurethane (TPE) fibers were small, about 0.78 ± 0.4 µm in diameter (average of 50 fibers). The PCL fibers were larger, about 2.2 ± 0.5 µm in diameter. The composite fibers, nominally 15% PCL and 25% PCL, showed fiber diameters that have a mixture of the larger and smaller fibers, though predominately the smaller fibers, as the TPE dominated the web. In the second row of **Figure 5-1, (v)-(viii)**, the resulting compacted films (shown as the dogbone cutouts) increased in opacity as with increasing PCL (left to right). The surface of the films, shown by scanning electron microscopy images (**Figure 5-1, (ix)-(xii)**) revealed smooth surfaces for all films with no porosity. The cross sections of these compacted film were shown in **Figure 5-1, (xiii) – (xvi)**. The TPE and PCL cross sections were smooth and had no fiber morphology, while the 15% and 25% PCL SMECS revealed small fibers in a solid matrix.

5.4.3 Differential Scanning Calorimetry (DSC)

Differential scanning calorimetry was performed to determine the thermal transitions of the individual and composite materials. The second heat (exotherm up) of each thermogram is shown in **Figure 5-2** and the transitions are quantified in **Table 5-2**. As mentioned above, there were two melting transitions for the TPE, one for the soft segment at 20.4 °C, and one for the hard segment (POSS) at 118.1 °C. For PCL, there was one melting transition at 55.7 °C. As the amount of PCL in the materials increased, the melting enthalpy of the PCL increased, while the melting enthalpies of the soft segment and POSS decreased. Using **Equation 5-1**, the amount of PCL in the composites was determined by comparing the melting enthalpy of PCL in the composite to the melting enthalpy of only PCL. The actual PCL percentages in the composites are 7% and 33% for the 15% PCL and 25% PCL SMECs, respectively.

5.4.4 Dynamic Mechanical Analysis

Dynamic mechanical analysis was performed to determine the mechanical properties across a wide temperature range for each material. The results are shown in **Figure 5-3** and quantified in **Table 5-3**. PCL had one melting transition around 60 °C and yields at that temperature. In the temperature range tested, the TPE had two melting transitions, one for the soft segment around -10 °C which led to a rubbery plateau until the POSS melted at 110 °C. The SMECs showed a combination of these transitions, with a PCL melting and a POSS melting. 25% PCL SMEC had a higher modulus than 15% PCL SMEC before the PCL melting transition and a lower storage modulus after the transition. These results of the storage moduli at 25 °C and 37 °C were quantified. PCL had the highest storage modulus at 25 °C with 181.3 MPa, which was higher than 25% PCL SMEC at 31.2 MPa. The TPE had the next highest storage modulus with 10.6 MPa at room temperature. 15% PCL SMEC had the lowest storage modulus (8.3 MPa at 25 °C). At body temperature, PCL had the highest storage modulus of 140.0 MPa. The same trends were

followed for body temperature as room temperature, and the materials decreased in modulus from PCL in the following order: 25% PCL SMEC (24.2 MPa), TPE (10.1 MPa), and 15% SMEC (6.7 MPa).

5.4.5 Tensile Testing

Tensile testing was performed to determine Young's modulus and strain-to-failure for each material, as shown in **Figure 5-4** and quantified in **Table 5-4**. First, the TPE was tested to determine the difference between dry mechanical properties at room temperature and wet mechanical properties at body temperature. The modulus and strain-to-failure of the TPE were lower for the hydrated mechanical properties than the dry mechanical properties ($p < 0.05$ and $p < 0.01$ for modulus and strain-to-failure, respectively). The dry Young's modulus for the TPE was 9.3 ± 0.6 MPa while the hydrated, heated Young's modulus was 8.2 ± 0.8 MPa, while the strain-to-failure dropped from 1970 ± 270 % dry to 670 ± 133 % hydrated.

The amount of PCL in the composites affected the mechanical properties when tested hydrated at body temperature. PCL's Young's modulus (71.7 ± 6.5 MPa) was higher than the TPE's modulus ($p < 0.01$). 25% PCL SMEC also had a higher Young's modulus than the TPE at 11.2 ± 1.9 MPa ($p < 0.05$), but was much lower than PCL's ($p < 0.01$). Interestingly, 15% PCL SMEC had the lowest modulus of all materials with a Young's modulus of 5.3 ± 0.5 MPa ($p < 0.1$). PCL's strain-to-failure was the highest of all materials at 2690 ± 160 % ($p < 0.01$) while the TPE had the lowest strain-to-failure (670 ± 133 %, $p < 0.01$). 15% PCL SMEC and 25% PCL SMEC had higher strains-to-failure than the TPE with 1380 ± 190 % ($p < 0.01$) and 1500 ± 53 % ($p < 0.01$), respectively, although statistically the SMEC strains-to-failure are not different ($p > 0.05$).

5.4.6 Elasticity Testing

The composites were also tested for elastic recovery of strain at room temperature by stretching the materials to 50% strain and determining the strain recovered upon unloading, as shown in **Figure 5-5a**. Elastic recovery (R_E) was quantified using **Equation 5-2** in **Figure 5-5b** and was found to increase with each cycle for all materials. Pure PCL had the lowest elastic recovery (R_E) with less than 50% strain recovery for the first cycle. Pure TPE had the second highest recovery with 72%. The composites had higher elastic recovery, greater than 80% recovery for the first cycle and 87% recovery during cycles 2 and 3, which is higher than the TPE which had 84 and 82% recovery for cycles 2 and 3, respectively.

5.4.7 Shape Memory Testing

Shape memory properties, fixing and recovery, were determined using the dynamic mechanical analyzer, as shown in **Figure 5-6**. Fixing and recovery ratios, R_f and R_r, were determined using **Equations 5-3** and **5-4**, respectively, and quantified in **Table 5-5**. Fixing was better for 25% PCL SMEC than 15% PCL SMEC. Both 15% PCL SMEC and 25% PCL SMEC had greater than 90% recovery for cycles 2 and 3. The first cycle's recovery for 15% PCL SMEC is lower, which could be attributed to a training cycle that is common in shape memory tests.

5.4.8 Degradation Study I

The materials were degraded at 37 °C and tested to determine their modulus and strain-to-failure over time. The evolution of the moduli and strains-to-failure are shown in **Figure 5-7** and **Table 5-6**. PCL's Young's modulus increased over the course of 4 weeks from 71 ± 6.5 to 113.7 ± 4.0 MPa ($p < 0.01$) at 2 w and to 116.1 ± 4.1 MPa at 4 w ($p < 0.01$ from 0 w, $p > 0.05$ from 2 w). Alternatively, TPE's Young's modulus decreased from 8.2 ± 0.8 to 6.3 ± 0.3 MPa ($p < 0.05$). 15% PCL SMEC and 25% PCL SMEC's moduli changed over the course of 4 w, but not

significantly. When comparing the different materials at the same time point, PCL had the highest modulus ($p < 0.01$ for samples) during 2 w and 4 w. 15% PCL SMEC had the lowest modulus throughout degradation ($p < 0.05$ for all materials) at 2 w and 4 w. 25% SMEC had a significantly higher modulus than TPE at 4 w ($p < 0.0.1$).

Strain-to-failure dropped for the TPE (670 ± 133 %) to 75 ± 19 % after 2 w ($p < 0.01$) and to 40 ± 3 % after 4 w ($p < 0.01$). The composites' strains-to-failure also decreased over time. 15% PCL SMEC's strain-to-failure decreased from 1380 ± 190 % to 550 ± 324 % ($p < 0.01$), to 140 ± 7 ($p < 0.05$). 25% PCL strain-to-failure also decreased from 1500 ± 53 % to 471 ± 76% ($p < 0.01$) after 2 w and to 112 ± 16% after 4 w ($p <0.01$). Conversely, the strain-to-failure of PCL did not change significantly during the 4 w degradation study. When comparing across samples during the same time point, PCL had the highest strain while the TPE had the lowest strain-to-failure for all time points ($p < 0.1$ for PCL, $p < 0.05$ for TPE). The SMECs had higher strain-to-failure than the TPE ($p < 0.05$ at 2 w, $p < 0.01$ at 4 w). Interestingly, the strain-to-failure was not statistically different between the SMECs during 2 w, but was during 4 w ($p < 0.01$).

5.4.9 Polyurethane Synthesis II and Degradation Study II

5.4.9.1 Polyurethane Synthesis

Another TPE, $(PG_5CL_{95})_{1k}$:POSS 70:30 was synthesized and incorporated into a SMEC to test how a fixed strain affected the SMEC's degradation profile. This TPE synthesis was illustrated in **Scheme 5-3**. The molecular and thermal properties of this TPE are shown in **Table 5-7**. This polyurethane had 2.1 mol % glycolide in the soft segment, and had a PGCL:POSS ratio of 73.1:26.9. The TPE had a T_g at -48.8 °C, and two melting transitions for the soft segment and POSS, with low melting enthalpies (< 3.5 J/g) for each.

5.4.9.2 SMEC Processing, Fixing, and Thicknesses

The materials were dual-electrospun and compacted like before, and the resulting SMEC had 27% PCL, which was determined from DSC (results not shown). As indicated in **Scheme 5-4,** materials were fixed to 0%, 50%, or 100% strain by heating to 60 °C, stretching to the specified strain (or not), and cooling for 15 minutes under load. **Figure 5-8** shows the initial fixed strain for each time point before degradation, as well as the sample thickness for each time point before degradation. The actual fixed strains in the 50% strained samples, as displayed in **Figure 5-8a**, were higher than the target ($p < 0.05$ for all time points). The averages for fixed 100% strain in the SMEC were higher than 100%, but were not statistically different than the target. The thicknesses of the 0% strained samples were higher than the other samples ($p < 0.05$). Averages for 0% strained (i.e. unstrained) samples were 0.34 – 0.35 mm, while thicknesses of the 50% strained samples were between 0.27 – 0.29 mm and 100% strained samples were 0.25 – 0.26 mm. 0% and 50% strained samples showed statistical difference between their thicknesses only at 4 w ($p < 0.05$), due to the variability among samples at other time points.

5.4.9.3 Mass Remaining, Water Uptake, and Fixed Strain Throughout Degradation

The mass remaining and water uptake of the degradation study are shown in **Figure 5-9**. Materials fixed at different strains showed similar mass loss and water uptake ($p > 0.05$). After 8 w, all materials had around 98% mass remaining. Water uptake increased over time, and at 8 w there was about 12% water uptake for the SMEC fixed at all strains ($p < 0.05$ compared to 0 w). **Figure 5-10** displays how the fixed strain changed over time. The materials did not recover and slightly lengthened with degradation. This change in length was not significant for 2 w ($p < 0.05$ compared to 0 w).

5.4.9.4 Surface Morphology Throughout Degradation

Scanning electron microscopy was performed on the surface and cross section of films throughout degradation. The surface of the films showed little change in morphology during the first month of degradation, as shown in the micrographs in **Figure 5-11**. However, by 8 w, the surface of the films for each fixed strain showed an increased roughness. The cross sections, displayed in **Figure 5-12** showed a rough morphology during weeks 0 and 4 for all strains, which was also seen in the cross sections of the previous SMECs before degradation. However, by 8 w, voids started to form for all strains.

5.4.9.5 Crystallinity and Alignment Throughout Degradation

Differential scanning calorimetry and X-ray diffraction were performed to determine how crystallinity and molecular alignment changed with degradation. PCL's melting enthalpy changed with degradation, as displayed in **Figure 5-13**. At 0 w, the materials showed similar enthalpy of melting for PCL, around 20 J/g. This increased throughout degradation, and by 8 w, the PCL melting enthalpy for all fixed strains was 32 J/g. Statistically, PCL's melting enthalpy did not change for all time points across the different strains ($p > 0.05$).

WAXS and SAXS were performed to determine molecular alignment. In **Figure 5-14**, the stretch direction is left to right. WAXS profiles of the SMEC not strained (0%, Week 0) revealed an inner crystalline ring which was correlated to POSS and an outer ring and halo that corresponded to the crystalline and amorphous regions of PCL. 50% strain and 100% strain showed an increase in alignment, as shown by the concentration of intensity along the meridian of the PCL ring and the equator of the POSS ring. An increase in intensity along these axes indicated an increase in alignment. In the SAXS patterns, the halo corresponded to long-range order of PCL. The concentration along the equator shows long-range alignment of PCL in the 50% and 100%

strained samples. The alignment was maintained throughout degradation for 8 w. The intensity of the alignment does not decrease with degradation.

5.4.9.6 Recovery After Degradation

Finally, recovery of these materials was attempted after 8 w of degradation by heating to 70 °C for several hours. The strain over time is displayed along with WAXS and SAXS images before and after heating in **Figure 5-15**. There was a slight decrease in strain in the first hour; however, there was no significant recovery for either the 100% strained or 50% strained samples. When looking at the WAXS and SAXS patterns before and after heating, there was alignment evident in the WAXS of PCL and POSS, as well as long-range PCL alignment in the SAXS patterns for both strains. However, after heating, the alignment was lost in the PCL in both WAXS and SAXS. In contrast, the POSS alignment remained in both the 50% and 100% fixed samples after heating.

5.5 Discussion

Biodegradable thermoplastic elastomers were synthesized and combined (by dual-electrospinning and compaction) with PCL, a biodegradable semi-crystalline material, to develop a fully-biodegradable shape memory elastomeric composite (SMEC). Two thermoplastic materials were used in this approach to ensure the composition could be easily controlled. The polyurethane (TPE) was designed to have a sub-ambient melting point to allow for chain mobility and POSS as the hard segment to provide physical cross-links through POSS crystallization. The polyurethane requires a high enough molecular weight to be electrospun into fibers, as electrospun low molecular weight materials formed beads. PCL is a commonly electrospun material with a single melting transition temperature (~ 55 °C). These materials, TPE and PCL, were chosen for the composite to separate the fixing and recovery. The TPE served as the recovery material; the

elasticity provided by the soft segment and cross-links from the POSS would serve as the physical cross-links required. The PCL served as the fixing material, with PCL's melting temperature serving as the transition temperature.

The biodegradable TPE and PCL were dual-electrospun to separate the two polymers on a sub-micron scale. This was preferable to blending or casting to ensure good mixing and therefore good shape memory properties, as shown previously in our group by Robertson et al.[27] The specific compositions (15% PCL and 25% PCL) were chosen as these compositions, when made with non-degradable Pellethane®, had both high shape fixing and recovery. Compacting the materials by heating above PCL's melting point created a matrix of PCL around TPE fibers, as was evident in the SEM micrographs. PCL fibers were larger than the TPE fibers when electrospun, and when compacted, the cross sections of the SMECs showed only small diameter fibers present. The surfaces of the films were smooth because they conformed to the smooth Teflon molds. The increase in opacity of the bulk films with increasing PCL content was due to the increased PCL crystallinity.

Differential scanning calorimetry showed that the SMECs had the thermal transitions of both the TPE and linear PCL. The TPE has a POSS melting transition around 110 °C, which is considered low from a polymer processing standpoint, and a soft segment melting point around room temperature. PCL has a melting point between the two with a much larger melting enthalpy. The SMECs show all three of those melting transitions. From the PCL melting enthalpy of the SMECs, we calculated the amount of PCL in each composite. The actual amounts of the PCL in the SMECs are 7% and 33% which are close to the target values of 15% and 25%, respectively. The difference could be attributed to the spraying of fibers not on the collector, which has been seen by other members of the group.

The mechanical properties of the four materials, as determined by DMA, tensile and elasticity testing showed interesting properties. The properties did not follow linear trends with increasing PCL content. PCL had the highest storage modulus, Young's modulus and lowest elasticity. Conversely, 15% PCL SMEC had the lowest storage modulus, Young's modulus, and highest elasticity. Interestingly, although 25% PCL SMEC had higher moduli than the TPE, it also had higher elastic recovery for three cycles.

In the TPE, POSS crystals provided the cross-links that allowed the strained material to recover. Because the soft segment was melted at room temperature, the materials were elastomeric. PCL's crystallization was much higher, and the elasticity of the semi-crystalline material was much lower. However, when these materials were combined, the relatively low amount of PCL improved elasticity. Increasing the amount of PCL from 0% to 7% and to 33% (to 15 and to 25% nominally) increased the number of cross-links via crystallites, allowing the SMEC to recover more strain than the neat TPE. However, because of the increased crystallization of PCL, there was less elastic recovery in the 25% PCL SMEC than the 15% PCL SMEC.

The TPE, when tested by wet, heated mechanical testing, had lower mechanical properties than when tested dry at room temperature. Hydration and heat could have disrupted crystallinity of the soft segment and POSS, resulting in a lower modulus. The saline solution that wetted and infiltrated the material was not load bearing, which could have influenced the lower strains-to-failure.

Shape memory properties of the SMECs were also tested. These compositions showed good fixing and recovery, with increasing PCL content contributing to increased fixing. PCL did not have shape memory in this temperature range because it yielded at its melting transition, and TPE did not have shape memory in this temperature range because there was no thermal transition

to pass through to allow fixing. Because there is a trade-off between fixing and recovery with the different material concentrations, it is hypothesized that increasing the PCL content to increase the amount of fixing to 100% would decrease the elastomer in the matrix and reduce the recovery. This was evident in the SMEC work by Robertson et al.

As these materials are biodegradable, a study was conducted to look at the evolution of mechanical properties throughout degradation in PBS at body temperature (37 °C). Materials were degraded for 4 w and mechanical testing was performed in saline solution at 37 °C every 2 w. PCL's modulus increased over time as PCL annealed at 37 °C during degradation. As the time scale of degradation is several years for PCL,[35] the strain-to-failure does not significantly change over the course of 4 weeks. TPE's modulus and strain-to-failure decreased over time as chain scission occurred, as seen previously in Chapter 3. The decrease in the TPE's modulus over time could be the result of the decreasing number of cross-links between the chains during hydrolysis. The SMECs' moduli do not change significantly over time, although their averages decrease and then increase slightly. This could be caused by the breakdown of the biodegradable elastomer (TPE) and the simultaneous crystallization of PCL. The SMECs mechanical properties are closer to the TPE than PCL as the TPE constitutes most of the material. The strain-to-failure was higher for PCL than the other materials, and lowest for TPE. The SMECs had higher strain-to-failure than the TPE as they had PCL to re-enforce the TPE. The SMECs could be utilized as an elastomeric material that requires a higher strain-to-failure than just TPE.

A second elastomer was synthesized, dual-electrospun and compacted with PCL to result in a 27% PCL SMEC. The PCL content was close to the 33% PCL target, which was chosen because it had good fixing and recovery in the previous study. This material was stretched and fixed at different strains to determine how a fixed strain in the material affected degradation.

Stretching was done manually, as the strain limits are lower than 100% on mechanical testing instruments such as the dynamic mechanical analyzer. Due to the different cooling kinetics between the shape memory cycle and manual fixing, there was elongation upon crystallization of the PCL which was not seen in the shape memory cycle. This elongation upon crystallization caused the fixed strain to be higher than the expected values of 50 and 100%. We also tracked the thickness of each sample, as hydrolysis of materials can be dependent on thickness and therefore the rate of water diffusion.

Despite differences in thickness and fixed strains, the degradation rates of these materials were similar based on mass loss, surface morphology, and PCL enthalpy of melting. As the TPE hydrolyzed and water broke ester bonds of the soft segment, the chains shortened which allowed more water to fill voids. When the chains were below the entanglement length, they diffused out of the material. By 8 w, only about 2% of the mass diffused away. We also know from the above degradation study that the strain-to-failure of the SMEC was much lower as a result of chain scission. The scanning electron micrographs showed some voids forming at both the surface and cross section of SMECs at 8 w, indicating that mass loss has occurred. Strain as high as 100% did not affect degradation rate, although it has been shown that strain decreases oxidative degradation in poly(ester urethanes) due to soft segment orientation.[36]

The fixed strains were maintained throughout degradation and was not recovered. Also, the molecular alignment was maintained throughout degradation. Alignment of PCL is seen in both WAXS (alignment along the meridian) and SAXS (along the equator, in the stretch direction). POSS has alignment along the equator in WAXS, which is typical for stretched POSS-containing-materials. Because the degradation temperature was below recovery temperature, the material does not recover over time.

Because chain scission had occurred and the elastomer had lost its mechanical properties, it could not recover after degradation for 8 w. When heated to the recovery temperature (70 °C), there was some thermal expansion and shrinking, but no recovery. When looking at the WAXS and SAXS patterns for 50% and 100% strained samples, PCL alignment was lost after re-melting, but POSS keeps its alignment as the samples could not recover. This indicated that when the PCL melted and rearranged, there was not enough TPE to reverse the POSS alignment.

We imagine these composites could be utilized as implantable medical devices. The composition could be tuned based on the biodegradable elastomer chemistry as well as the PCL content. Our current system allows materials to be fabricated as a sheet and fixed into the desired shape. If we desired a deployable device (a material that could be fixed externally and recovered at body temperature) we could replace the PCL with a thermoplastic PCL polyurethane that has a transition temperature around 37 °C, which include the materials introduced in Chapter 6.

5.6 Conclusion

In conclusion, biodegradable thermoplastic shape memory elastomeric composites (SMECs) have been fabricated that have tunable mechanical properties based on their composition, which could be controlled by adjusting the flow rates during dual-electrospinning. These materials have good shape memory properties. They degrade over time by hydrolysis, as shown by the decrease in mechanical properties over time. Fixed strains up to 100% had no effect on the degradation rate, and the material remained fixed throughout degradation.

5.7 References

1. Lendlein, A.; Langer, R., Biodegradable, Elastic Shape-Memory Polymers for Potential Biomedical Applications. *Science* **2002,** *296* (5573), 1673.

2. Tobushi, H., Thermomechanical properties in a thin film of shape memory polymer of polyurethane series. *Smart materials and structures 5* (4), 483-491. DOI: 10.1088/0964-1726/5/4/012.

3. Liu, C., Chemically Cross-Linked Polycyclooctene: Synthesis, Characterization, and Shape Memory Behavior. *Macromolecules 35* (27), 9868-9874. DOI: 10.1021/ma021141j.

4. Lendlein, A.; Jiang, H.; Jünger, O.; Langer, R., Light-induced shape-memory polymers. *Nature* **2005,** *434* (7035), 879-882. DOI: 10.1038/nature03496.

5. Lee, K. M., Light-activated shape memory of glassy, azobenzene liquid crystalline polymer networks. *Soft matter* **2011,** *7* (9), 4318. DOI: 10.1039/c1sm00004g.

6. Huang, W. M., Water-driven programmable polyurethane shape memory polymer: Demonstration and mechanism. *Applied physics letters* **2005,** *86* (11), 114105. DOI: 10.1063/1.1880448.

7. Hu, Z., Synthesis and application of modulated polymer gels. *Science (New York, N.Y.)* **1995,** *269* (5223), 525-527.

8. Han, X.-J., pH-Induced Shape-Memory Polymers. *Macromolecular rapid communications. 33* (12), 1055-1060. DOI: 10.1002/marc.201200153.

9. Hu, Y., A Shape-Memory DNA-Based Hydrogel Exhibiting Two Internal Memories. *Angewandte Chemie (International ed.) 55* (13), 4210-4214. DOI: 10.1002/anie.201511201.

10. Luo, X., Conductive shape memory nanocomposites for high speed electrical actuation. *Soft matter* **2010,** *6* (10), 2146-2149. DOI: 10.1039/c001295e.

11. Cho, J. W., Electroactive Shape-Memory Polyurethane Composites Incorporating Carbon Nanotubes. *Macromolecular rapid communications. 26* (5), 412-416. DOI: 10.1002/marc.200400492.

12. Mohr, R.; Kratz, K.; Weigel, T.; Lucka-Gabor, M.; Moneke, M.; Lendlein, A., Initiation of shape-memory effect by inductive heating of magnetic nanoparticles in thermoplastic polymers. *Proceedings of the National Academy of Sciences of the United States of America* **2006,** *103* (10), 3540-3545.

13. Schmidt, A. M., Electromagnetic Activation of Shape Memory Polymer Networks Containing Magnetic Nanoparticles. *Macromolecular Rapid Communications* **2006,** *27* (14), 1168-1172. DOI: 10.1002/marc.200600225.

14. Wache, H. M., Development of a polymer stent with shape memory effect as a drug delivery system. *Journal of materials science. Materials in medicine* **2003,** *14* (2), 109-112. DOI: 10.1023/A:1022007510352.

15. Bencherif, S. A.; Sands, R. W.; Bhatta, D.; Arany, P.; Verbeke, C. S.; Edwards, D. A.; Mooney, D. J., Injectable preformed scaffolds with shape-memory properties. *Proceedings of the National Academy of Sciences* **2012,** *109* (48), 19590-19595.

16. Rousseau, I. A., Shape Memory Effect Exhibited by Smectic-C Liquid Crystalline Elastomers. *Journal of the American Chemical Society 125* (50), 15300-15301. DOI: 10.1021/ja039001s.

17. Heuwers, B., Shape-Memory Natural Rubber: An Exceptional Material for Strain and Energy Storage. *Macromolecular chemistry and physics 214* (8), 912-923. DOI: 10.1002/macp.201200649.

18. Li, J., Semi-crystalline two-way shape memory elastomer. *Polymer (Guilford) 52* (23), 5320-5325. DOI: 10.1016/j.polymer.2011.09.030.

19. Li, J., Dynamic Mechanical Behavior of Photo-Cross-linked Shape-Memory Elastomers. *Macromolecules 44* (13), 5336-5343. DOI: 10.1021/ma2004019.

20. Fuhrer, R., Crosslinking Metal Nanoparticles into the Polymer Backbone of Hydrogels Enables Preparation of Soft, Magnetic Field-Driven Actuators with Muscle-Like Flexibility. *Small (Weinheim an der Bergstrasse, Germany) 5* (3), 383-388. DOI: 10.1002/smll.200801091.

21. Wilson, T. S., Shape memory polymers based on uniform aliphatic urethane networks. *Journal of applied polymer science 106* (1), 540-551. DOI: 10.1002/app.26593.

22. Jeong, H., Synthesis and properties of thermotropic liquid crystalline polyurethane elastomers. *Polymer (Guilford)* **2000,** *41* (5), 1849-1855. DOI: 10.1016/S0032-3861(99)00334-1.

23. Ahir, S. V., Self-Assembled Shape-Memory Fibers of Triblock Liquid-Crystal Polymers. *Advanced functional materials 16* (4), 556-560. DOI: 10.1002/adfm.200500692.

24. Zhang, H., A novel type of shape memory polymer blend and the shape memory mechanism. *Polymer (Guilford) 50* (6), 1596-1601. DOI: 10.1016/j.polymer.2009.01.011.

25. Weiss, R. A., New Design of Shape Memory Polymers: Mixtures of an Elastomeric Ionomer and Low Molar Mass Fatty Acids and Their Salts. *Macromolecules 41* (9), 2978-2980. DOI: 10.1021/ma8001774.

26. Luo, X., Preparation and Characterization of Shape Memory Elastomeric Composites. *Macromolecules 42* (19), 7251-7253. DOI: 10.1021/ma9015888.

27. Robertson, J. M.; Birjandi Nejad, H.; Mather, P. T., Dual-Spun Shape Memory Elastomeric Composites. *ACS Macro Letters* **2015,** *4* (4), 436-440. DOI: 10.1021/acsmacrolett.5b00106.

28. Serrano, M. C., Novel Biodegradable Shape-Memory Elastomers with Drug-Releasing Capabilities. *Advanced materials (Weinheim) 23* (19), 2211-2215. DOI: 10.1002/adma.201004566.

29. Espinha, A.; Concepción Serrano, M.; Blanco, Á.; López, C. In *Shape-memory effect for self-healing and biodegradable photonic systems*, 2014; pp 91270B-91270B-13.

30. Hsu, S.-h., Synthesis and characterization of waterborne polyurethane containing poly(3-hydroxybutyrate) as new biodegradable elastomers. *Journal of materials chemistry. B, Materials for biology and medicine* **2015,** *3* (47), 9089-9097. DOI: 10.1039/C5TB01773D.

31. Zhang, W., Surprising shape-memory effect of polylactide resulted from toughening by polyamide elastomer. *Polymer (Guilford) 50* (5), 1311-1315. DOI: 10.1016/j.polymer.2009.01.032.

32. Zhang, S.; Feng, Y.; Zhang, L.; Sun, J.; Xu, X.; Xu, Y., Novel interpenetrating networks with shape-memory properties. *Journal of Polymer Science Part A: Polymer Chemistry* **2007,** *45* (5), 768-775. DOI: 10.1002/pola.21832.

33. Lawton, M. I.; Tillman, K. R.; Mohammed, H. S.; Kuang, W.; Shipp, D. A.; Mather, P. T., Anhydride-Based Reconfigurable Shape Memory Elastomers. *ACS Macro Letters* **2016,** *5* (2), 203-207. DOI: 10.1021/acsmacrolett.5b00854.

34. McMullin, E.; Rebar, H. T.; Mather, P. T., Biodegradable Thermoplastic Elastomers Incorporating POSS: Synthesis, Microstructure, and Mechanical Properties. *Macromolecules* **2016,** *49* (10), 3769-3779. DOI: 10.1021/acs.macromol.6b00470.

35. Nair, L. S.; Laurencin, C. T., Biodegradable polymers as biomaterials. *Progress in Polymer Science* **2007,** *32* (8-9), 762-798. DOI: 10.1016/j.progpolymsci.2007.05.017.

36. Schubert, M. A.; Wiggins, M. J.; Anderson, J. M.; Hiltner, A., The effect of strain state on the biostability of a poly(etherurethane urea) elastomer. *Journal of biomedical materials research* **1997,** *35* (3), 319-329.

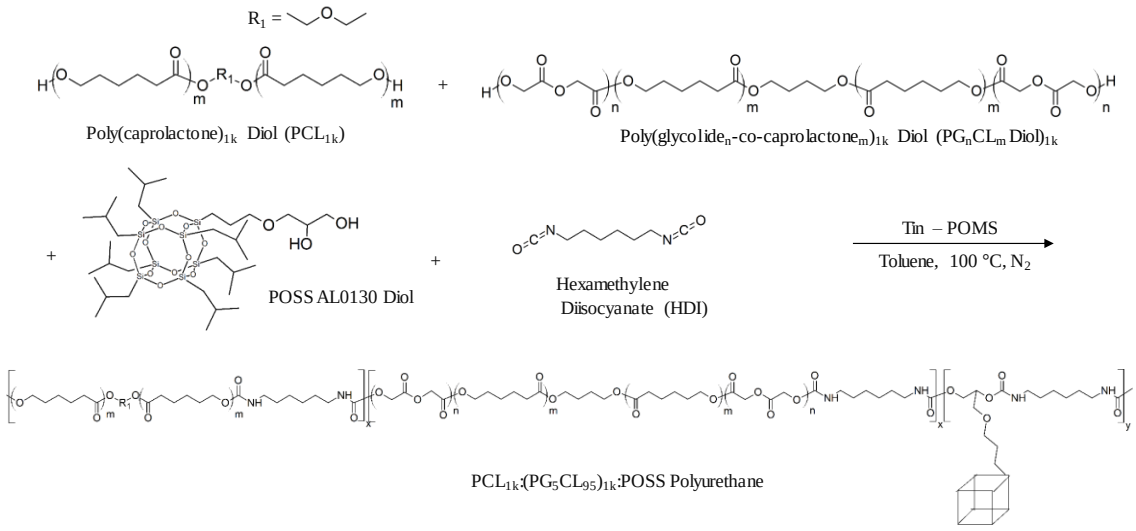

Scheme 5-1: Polyurethane synthesis of PCL_{1k}:$(PG_5CL_{95})_{1k}$:POSS polyurethane.

Table 5-1: Molecular and thermal properties of PCL_{1k}:$(PG_5CL_{95})_{1k}$:POSS.

Synthesis	Actual[a] G:C (Molar)	Input PCL:PGCL:POSS Ratio (Wt. %)	Actual[a] PCL:PGCL: POSS Ratio (Wt. %)	M_n[b] (kDa)	M_w[b] (kDa)	PDI[b]	T_g[c] (°C)	$T_{m,Soft}$[c] (°C)	ΔH_{Soft}[c] (J/g)	$T_{m,POSS}$[c] (°C)	ΔH_{POSS}[c] (J/g)
PCL_{1k}:PG_5CL_{95}:POSS	4.3 : 95.7	35 : 35 : 30	38.1 : 37.0 : 24.9	104.6	140.9	1.36	-51.5	20.4	5.2	118.1	2.0

[a]Determined from proton nuclear magnetic resonance.
[b]Determined from gel permeation chromatography.
[c]Determined from differential scanning calorimetry.

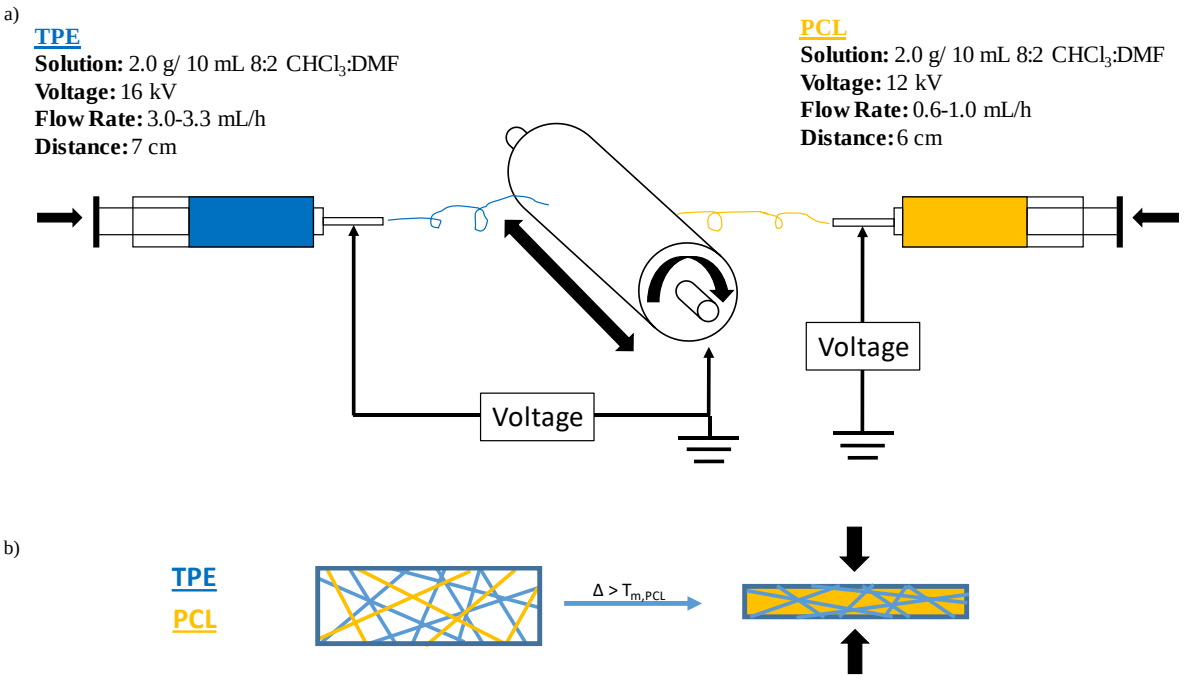

Scheme 5-2: Schematic of SMEC processing. a) Dual-electrospinning set-up. b) Compaction of dual-electrospun films.

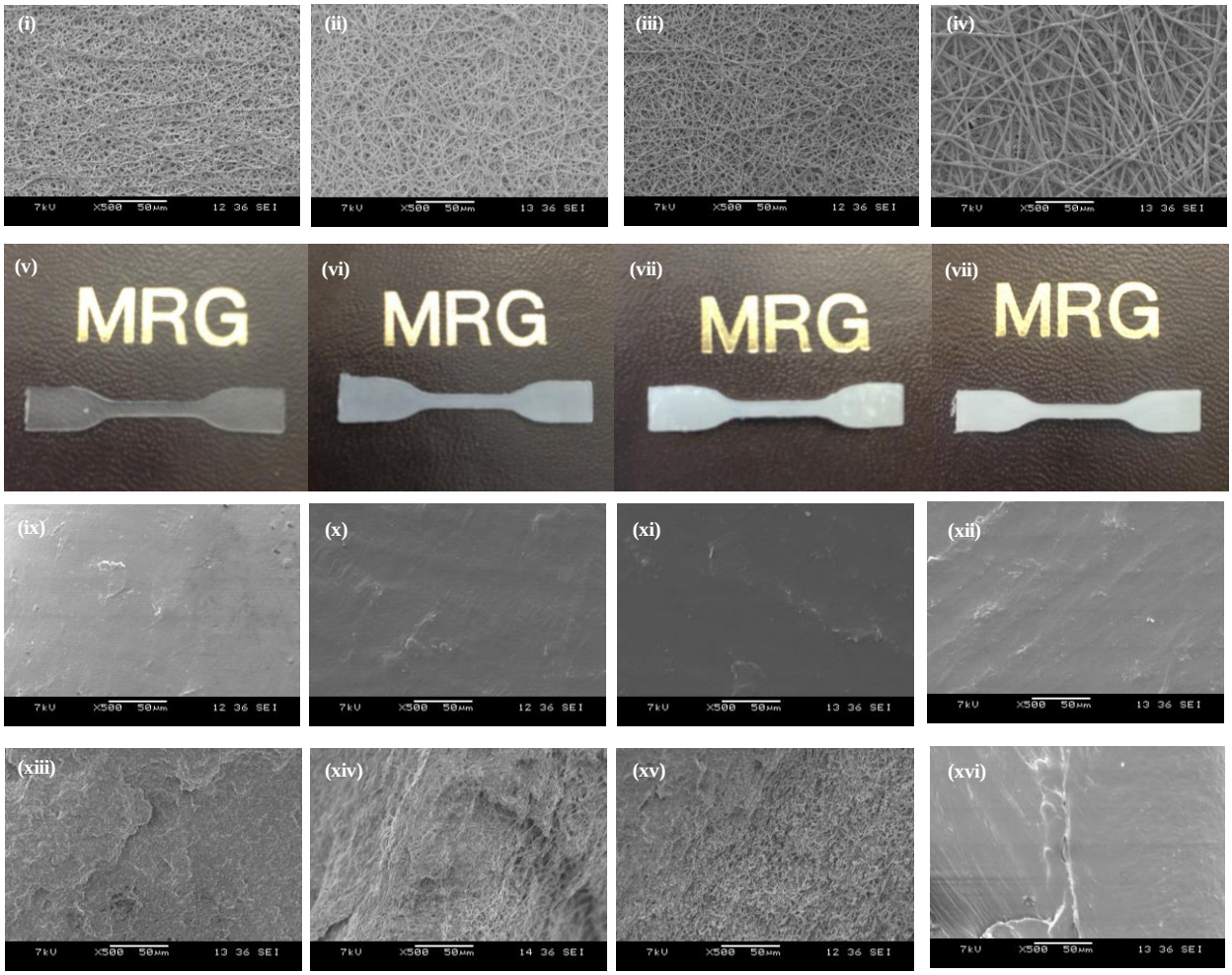

Figure 5-1: Scanning electron micrographs and photographs of the different electrospun materials and dual-electrospun composites. Scanning electron micrographs of the electrospun or dual-electrospun webs for (i) TPE, (ii) 15% PCL SMEC, (iii) 25% PCL SMEC, and (iv) PCL. In the second row, images of the compacted films are shown for (v) TPE, (vi) 15% PCL SMEC, (vii) 25% PCL SMEC, and (viii) PCL. The third row of images shows the surfaces of the compacted films: (ix) TPE, (x) 15% PCL SMEC, (xi) 25% PCL SMEC, and (xii) PCL. The bottom row shows the cross section of these materials: (xiii) TPE, (xiv) 15% PCL SMEC, (xv) 25% PCL SMEC, and (xvi) PCL.

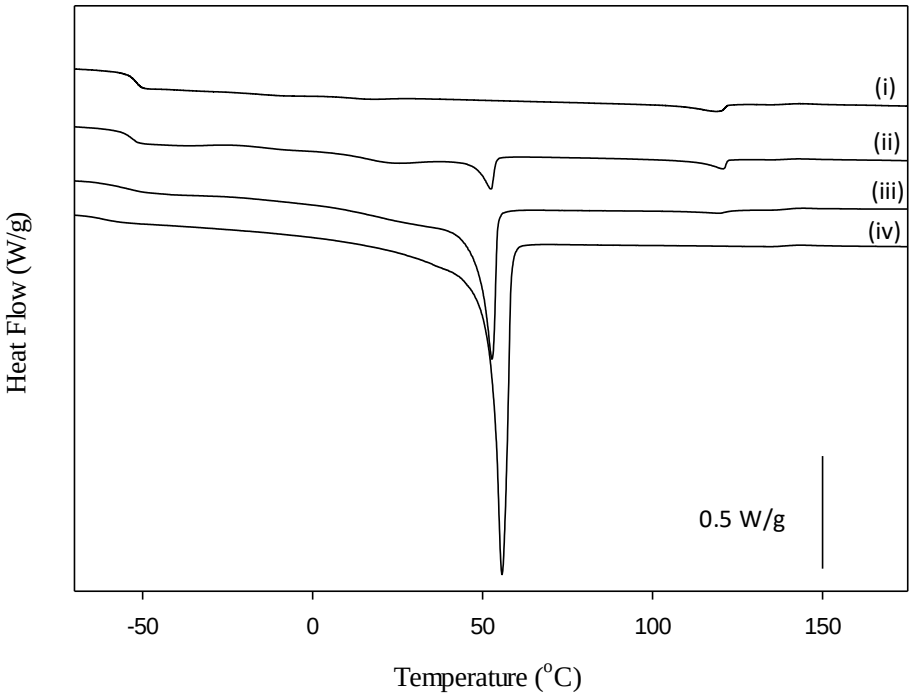

Figure 5-2: Differential scanning calorimetry, with the second heat shown (exotherm up) of (i) TPE, (ii) 15% PCL SMEC, (iii) 25% PCL SMEC, and (iv) PCL.

Table 5-2: Summary of the thermal transitions of each compacted material from the DSC thermograms.

Sample	$T_{m,Soft}$ (°C)	ΔH_{Soft} (J/g)	$T_{m,PCL}$ (°C)	ΔH_{PCL} (J/g)	PCL (%)	$T_{m,POSS}$ (°C)	ΔH_{POSS} (J/g)
TPE	20.4	5.2	-	-	0	118.1	2.0
15% PCL SMEC	22.5	1.7	52.4	3.9	7	120.8	1.6
25% PCL SMEC	-	-	52.7	18.9	33	119.6	1.0
PCL	-	-	55.7	56.8	100	-	-

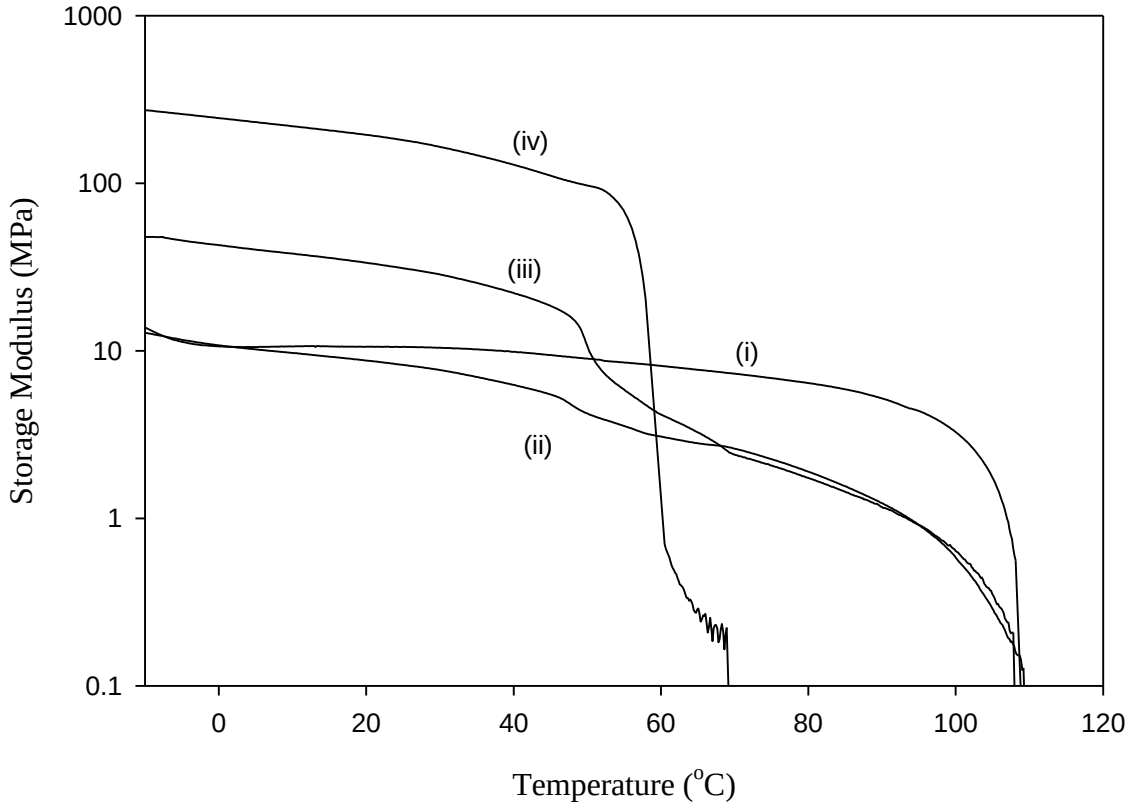

Figure 5-3: Dynamic mechanical analysis of (i) TPE, (ii) 15% PCL SMEC, (iii) 25% PCL SMEC, and (iv) PCL.

Table 5-3: Summary of the storage moduli and tanδ values at 25 °C and 37 ° C of the four materials.

Material	E'_{25} (MPa)	E'_{37} (MPa)	Tanδ at 25 °C	Tanδ at 37 °C
TPE	10.6	10.1	0.092	0.092
15% PCL SMEC	8.3	6.7	0.084	0.107
25% PCL SMEC	31.2	24.2	0.080	0.096
PCL	181.3	140.0	0.033	0.035

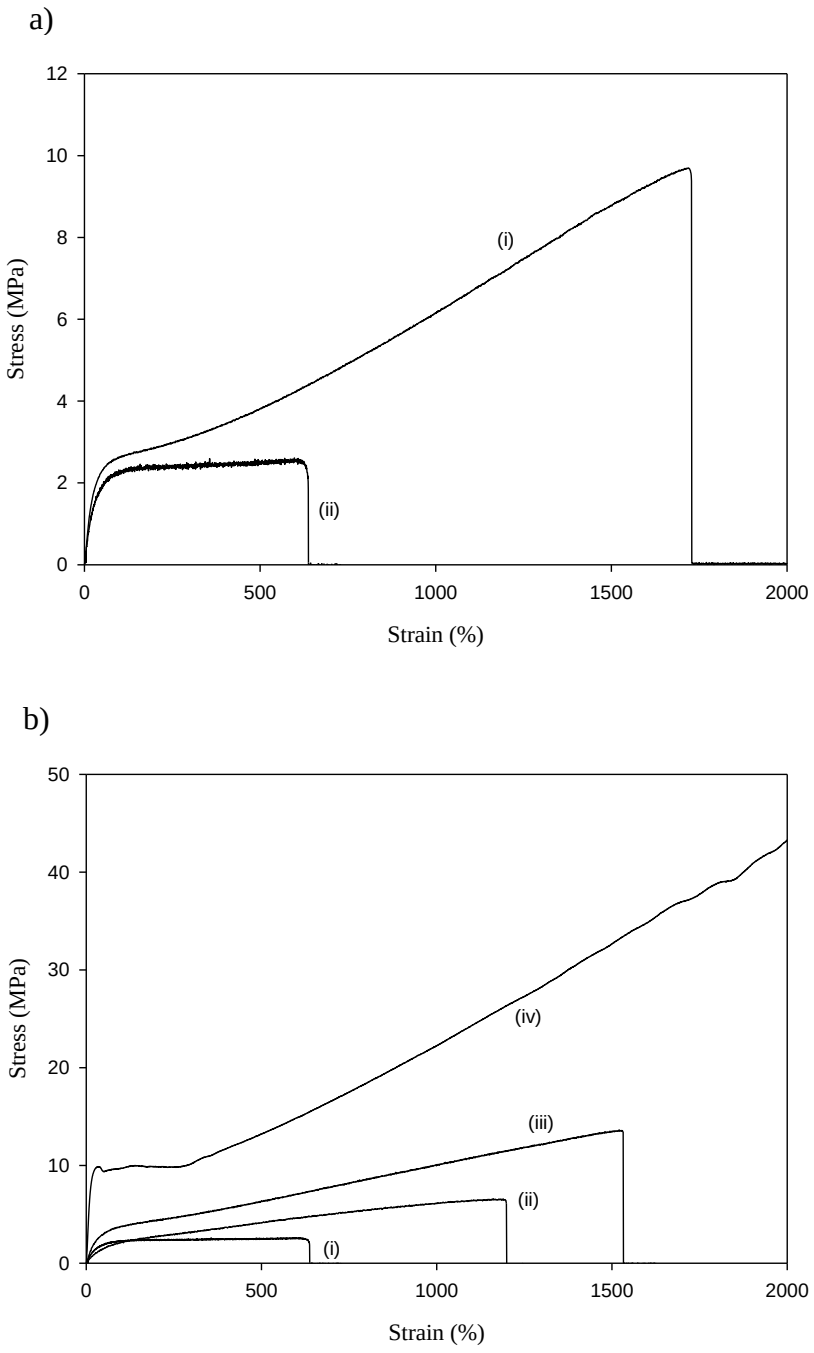

Figure 5-4: a) Tensile testing of TPE: (i) dry at room temperature and (ii) hydrated at 37 °C. b) Tensile testing hydrated (in saline solution) at 37 °C of (i) TPE, (ii) 15% PCL SMEC, (iii) 25% PCL SMEC, and (iv) PCL. Representative stress-strain curves are shown.

Table 5-4: Summary of the mechanical properties from tensile tests (n=5).

Sample	Modulus (MPa)	Strain to Failure (%)
TPE[a]	9.3 ± 0.6	1970 ± 270
TPE[b]	8.2 ± 0.8	670 ± 133
15% SMEC[b]	5.3 ± 0.5	1380 ± 190
25% SMEC[b]	11.2 ± 1.9	1500 ± 53
PCL[b]	71.7 ± 6.5	2690 ± 160

[a]Tensile testing performed dry at room temperature (22 °C).
[b]Tensile testing performed in saline solution at body temperature (37 °C).

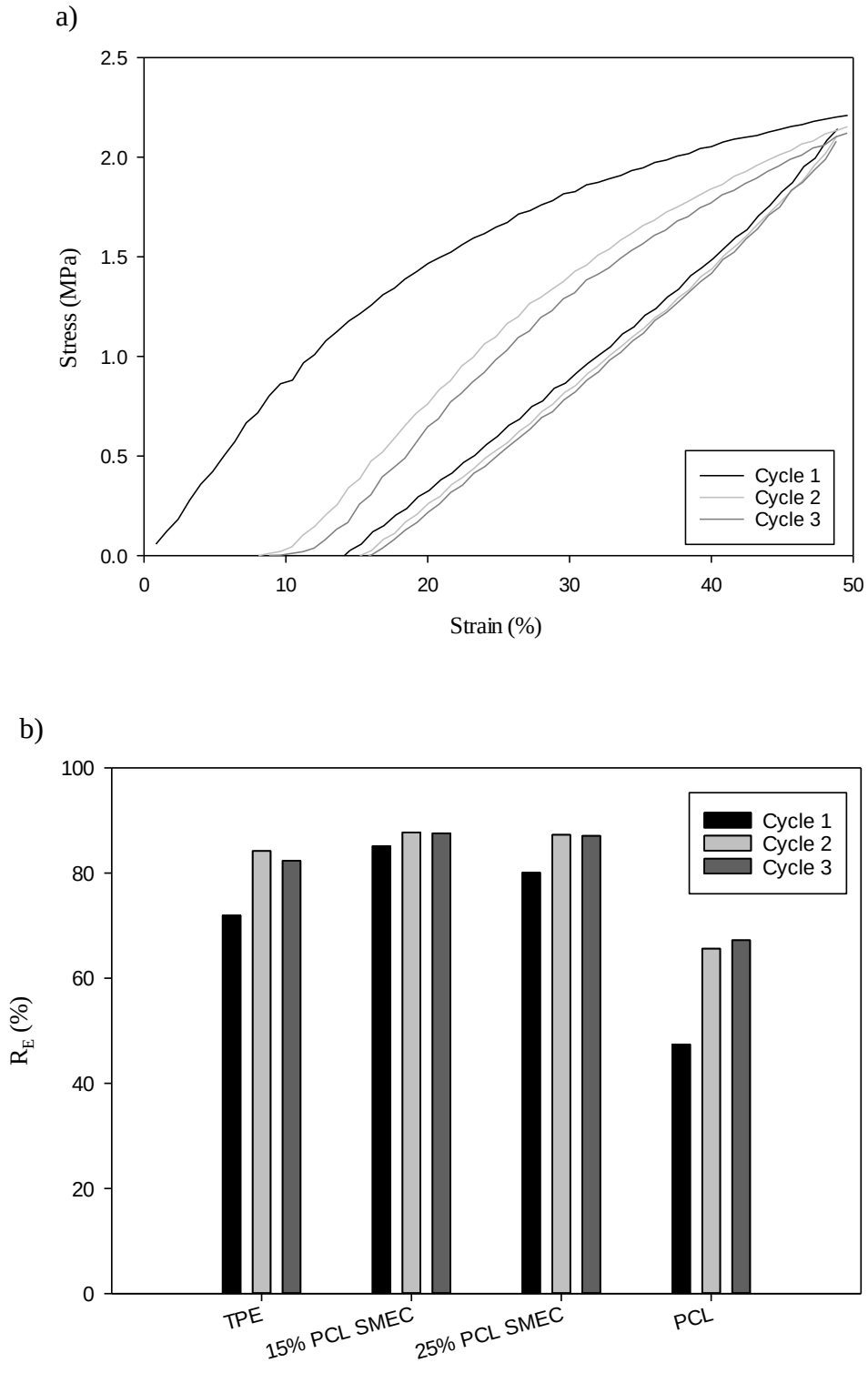

Figure 5-5: Elasticity testing of all materials. a) An example curve of a material (here TPE) stretched to 50% strain and recovered for 3 cycles. b) Strain recovery (R_E) for each material.

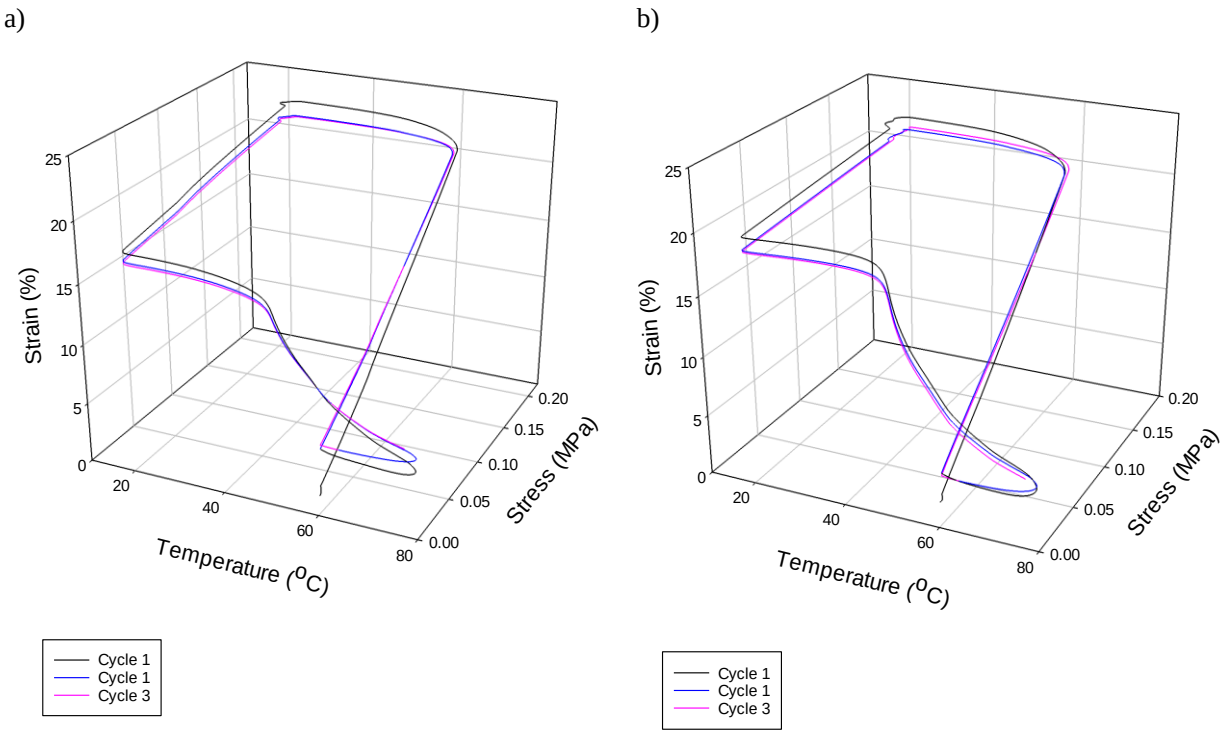

Figure 5-6: Shape memory testing for 3 cycles of the composite materials: a) 15% PCL SMEC and b) 25% PCL SMEC.

Table 5-5: Summary of the fixing and recovery ratios for 15% PCL SMEC and 25% PCL SMEC.

	15% PCL SMEC		25% PCL SMEC	
Cycle	R_f (%)	R_r(%)	R_f (%)	R_r(%)
1	81	84	92	92
2	77	99	91	101
3	77	90	90	92

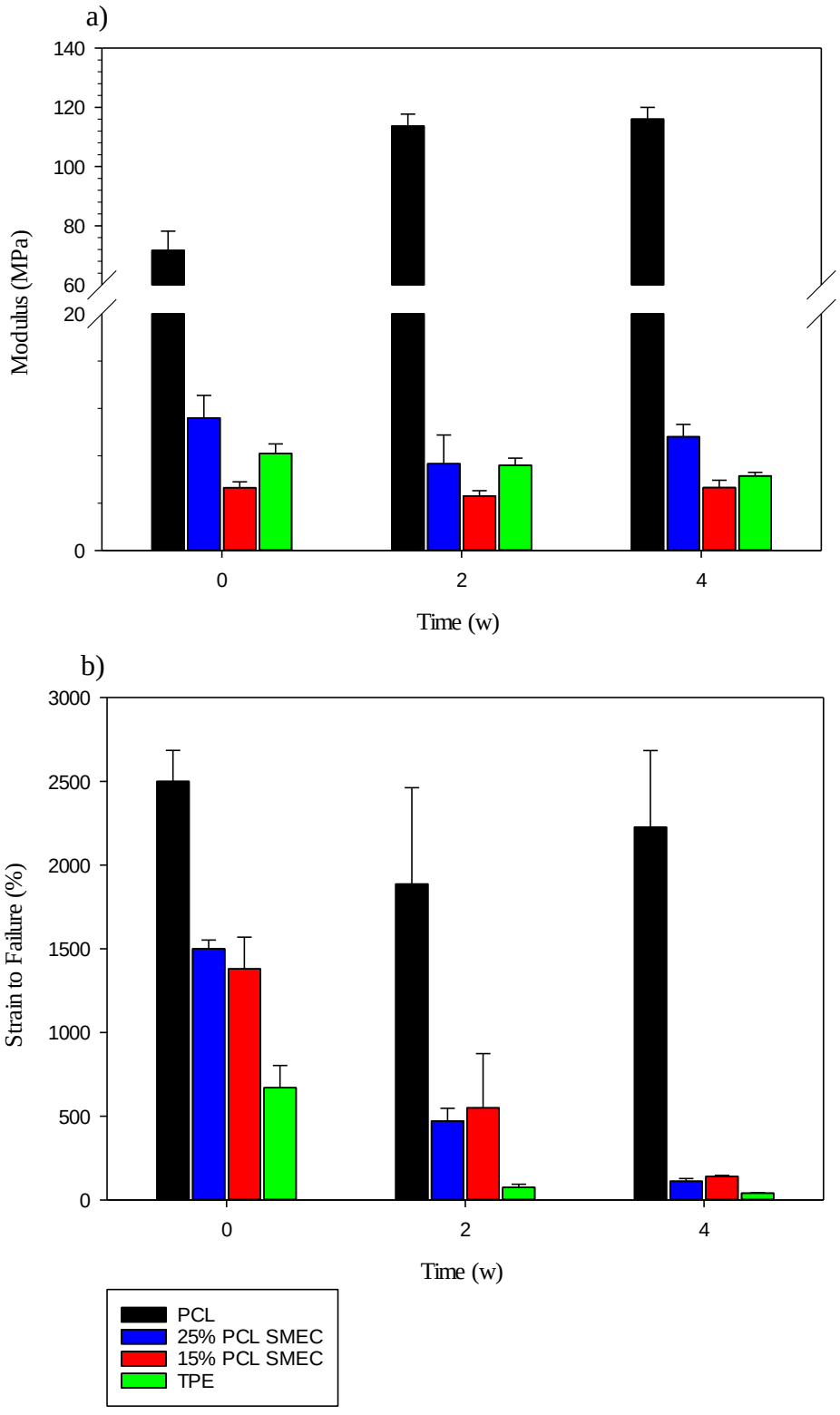

Figure 5-7: Mechanical properties of materials throughout degradation: a) Young's modulus (MPa) and b) strain-to-failure (%) (n=5).

Table 5-6: Summary of the mechanical properties during degradation.

Sample	Modulus (MPa)			Strain to Failure (%)		
	Week 0	Week 2	Week 4	Week 0	Week 2	Week 4
PCL	71.7 ± 6.5	113.7 ± 4.0	116.1 ± 4.1	2500 ± 185	1887 ± 575	2226 ± 458
25% PCL SMEC	11.2 ± 1.9	7.3 ± 2.4	9.6 ± 1.1	1500 ± 53	471 ± 76	112 ± 16
15% PCL SMEC	5.3 ± 0.5	4.6 ± 0.5	5.3 ± 0.6	1380 ± 190	550 ± 324	140 ± 7
TPE	8.2 ± 0.8	7.2 ± 0.6	6.3 ± 0.3	670 ± 133	75 ± 19	40 ± 3

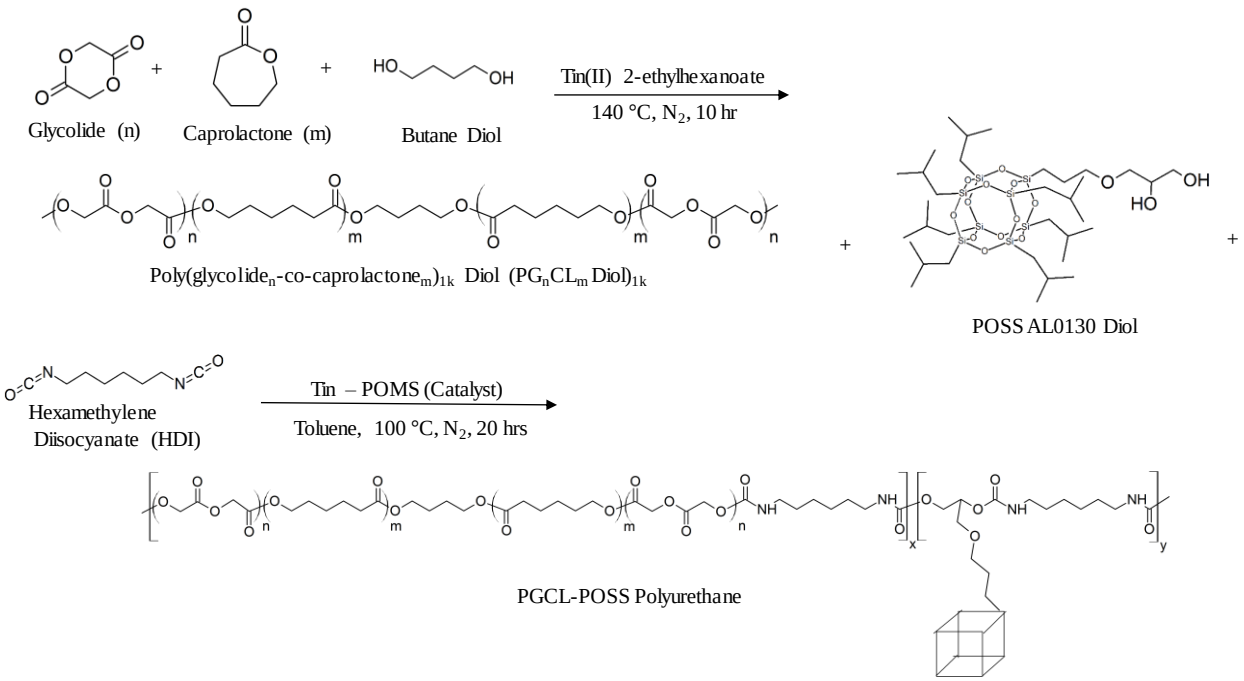

Scheme 5-3: Diol and polyurethane synthesis of $(PG_5CL_{95})_{1k}$:POSS.

Table 5-7: Molecular and thermal properties of $(PG_5CL_{95})_{1k}$:POSS.

Synthesis	Actual[a] G:C (Molar)	Input PGCL:POSS Ratio (Wt. %)	Actual[a] PGCL: POSS Ratio (Wt. %)	M_n[b] (kDa)	M_w[b] (kDa)	PDI[b]	T_g[c] (°C)	$T_{m,Soft}$[c] (°C)	ΔH_{PGCL}[c] (J/g)	$T_{m,POSS}$[c] (°C)	ΔH_{POSS}[c] (J/g)
PG_5CL_{95}:POSS	2.1 : 97.9	70 : 30	73.1 : 26.9	78.1	99.5	1.27	-48.8	24.8	3.3	122.7	2.4

[a]Determined from proton nuclear magnetic resonance.
[b]Determined from gel permeation chromatography.
[c]Determined from differential scanning calorimetry.

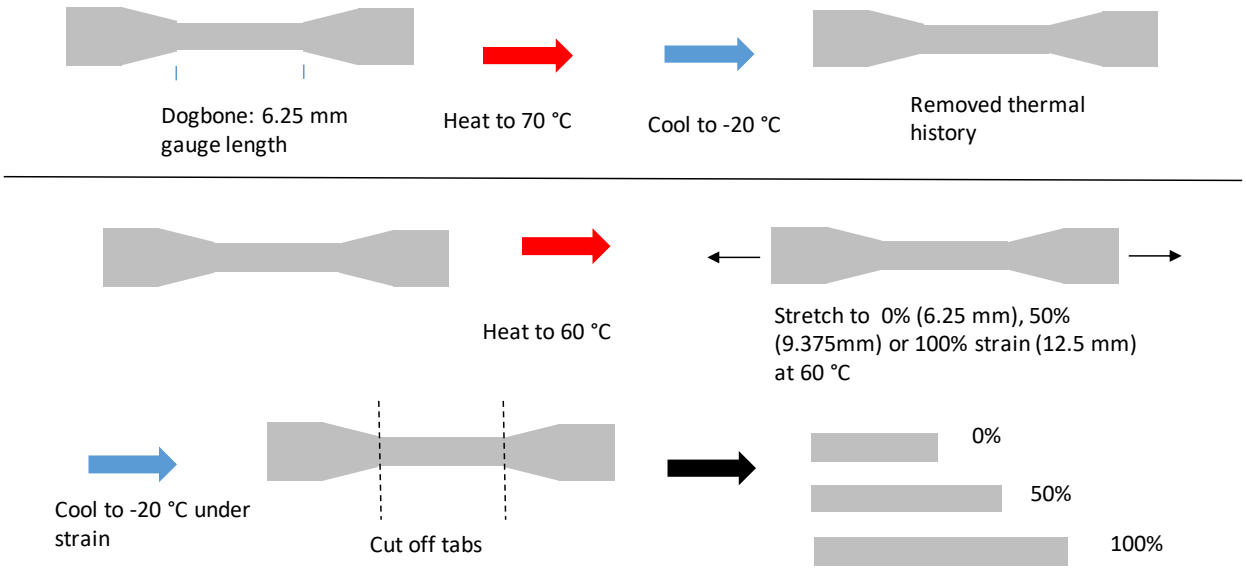

Scheme 5-4: Schematic of fixing samples for a degradation study: a) removal of thermal history and b) fixing samples to 0%, 50% and 100% strain.

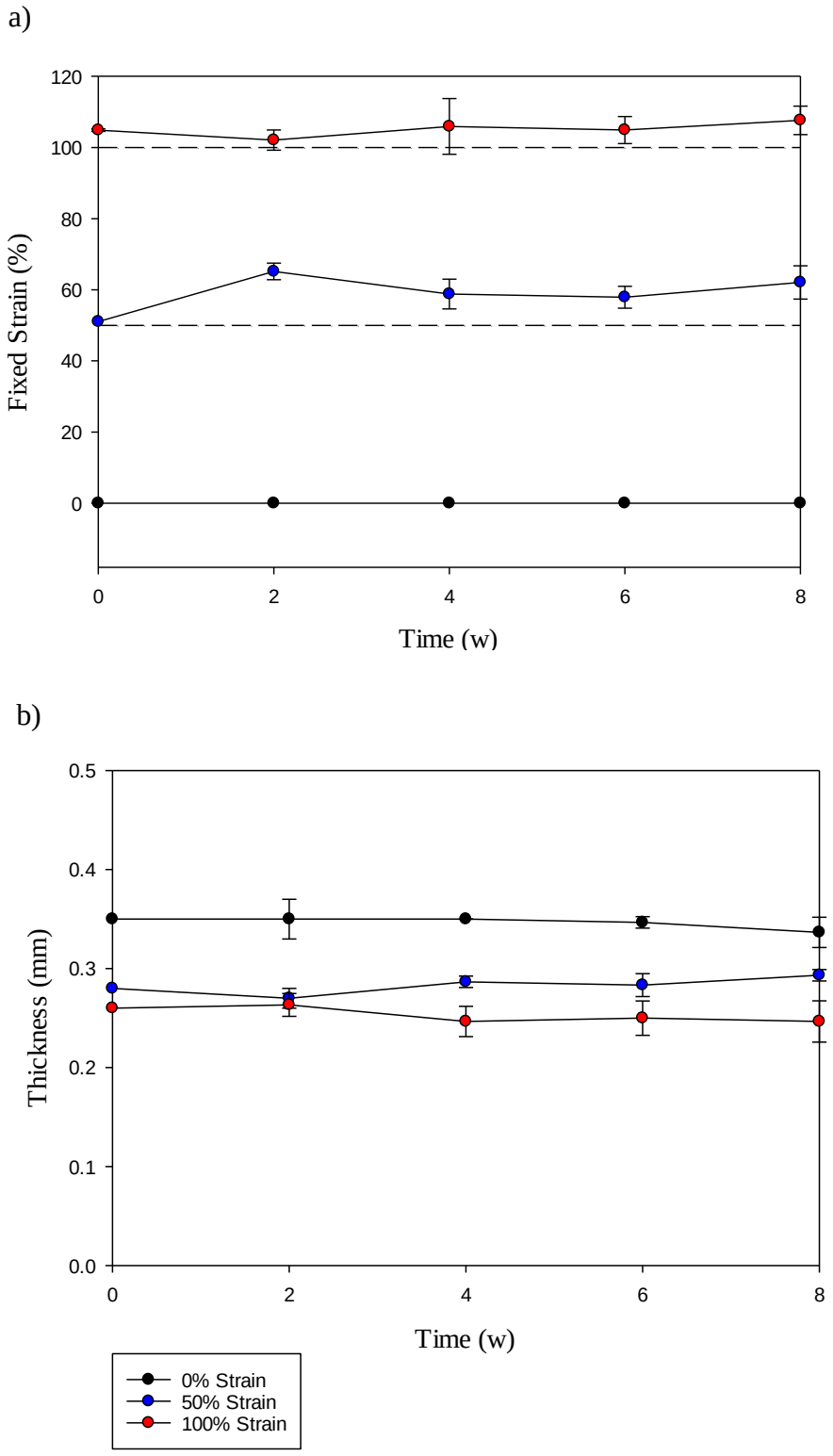

Figure 5-8: Samples before degradation: a) actual fixed strain with reference lines indicating the target fixed strain and (b) thickness (n=3).

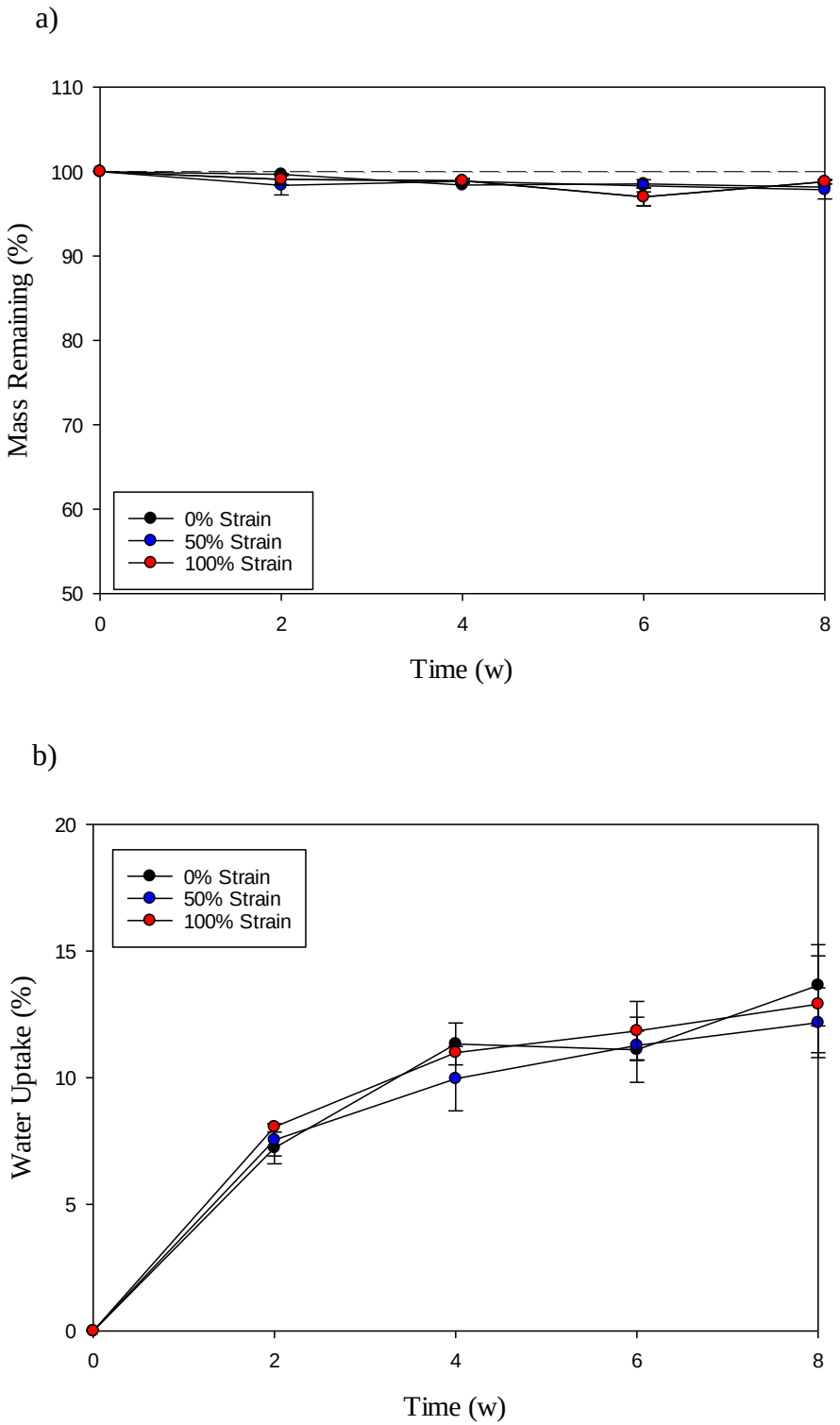

Figure 5-9: Properties of fixed SMECs throughout degradation: a) mass loss and b) water uptake (n=3).

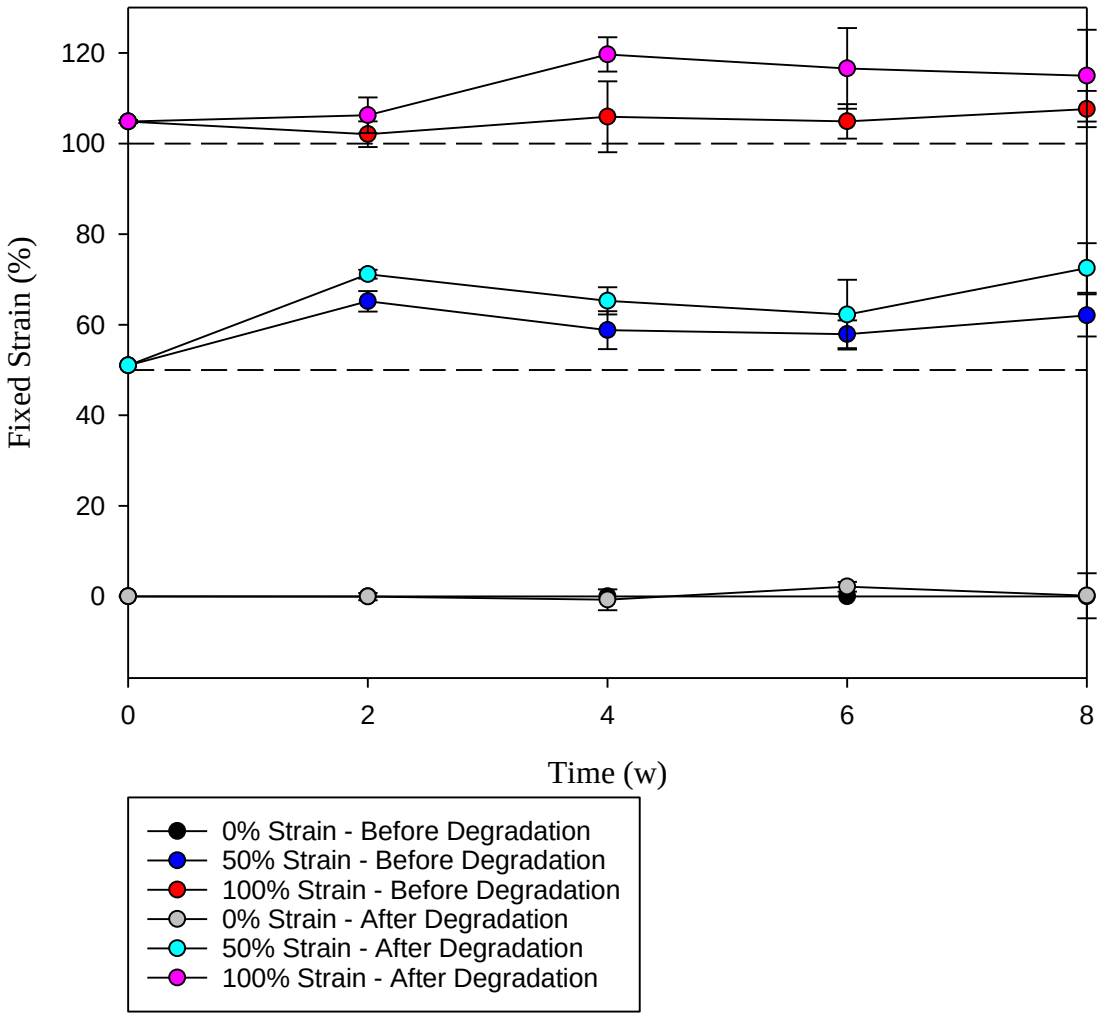

Figure 5-10: Fixed strain before and after degradation (n=3).

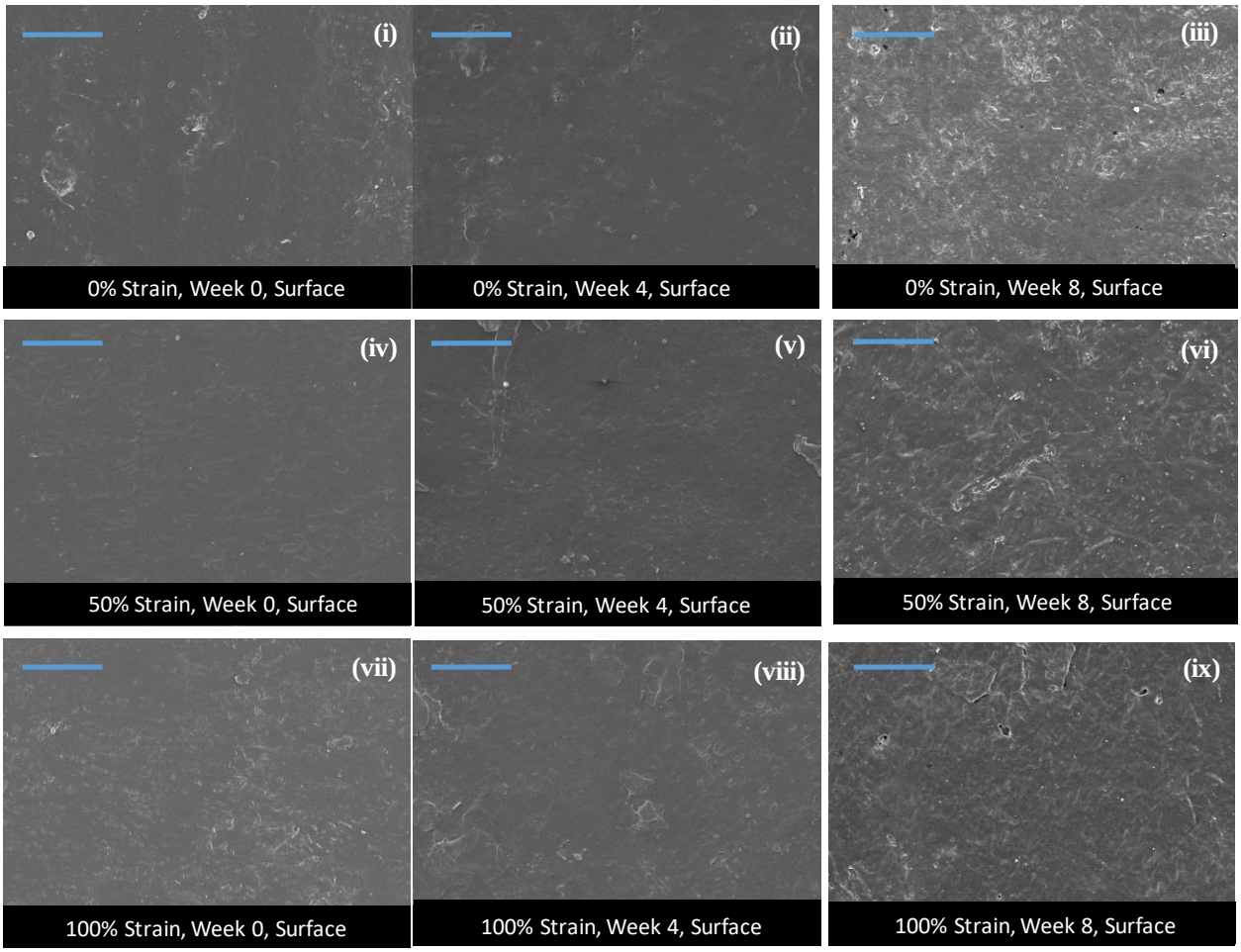

Figure 5-11: Scanning electron micrographs for the SMECs degraded at different fixed strains. Surface images of a SMEC with 0% strain at (i) 0 w, (ii) 4 w, (iii) and 8 w; 50% strain at (iv) 0 w, (v) 4 w, and (vi) 8 w; and 100% strain at (vii) 0 w, (viii) 4 w, and (ix) 8 w. Scale bar represents 50 μm.

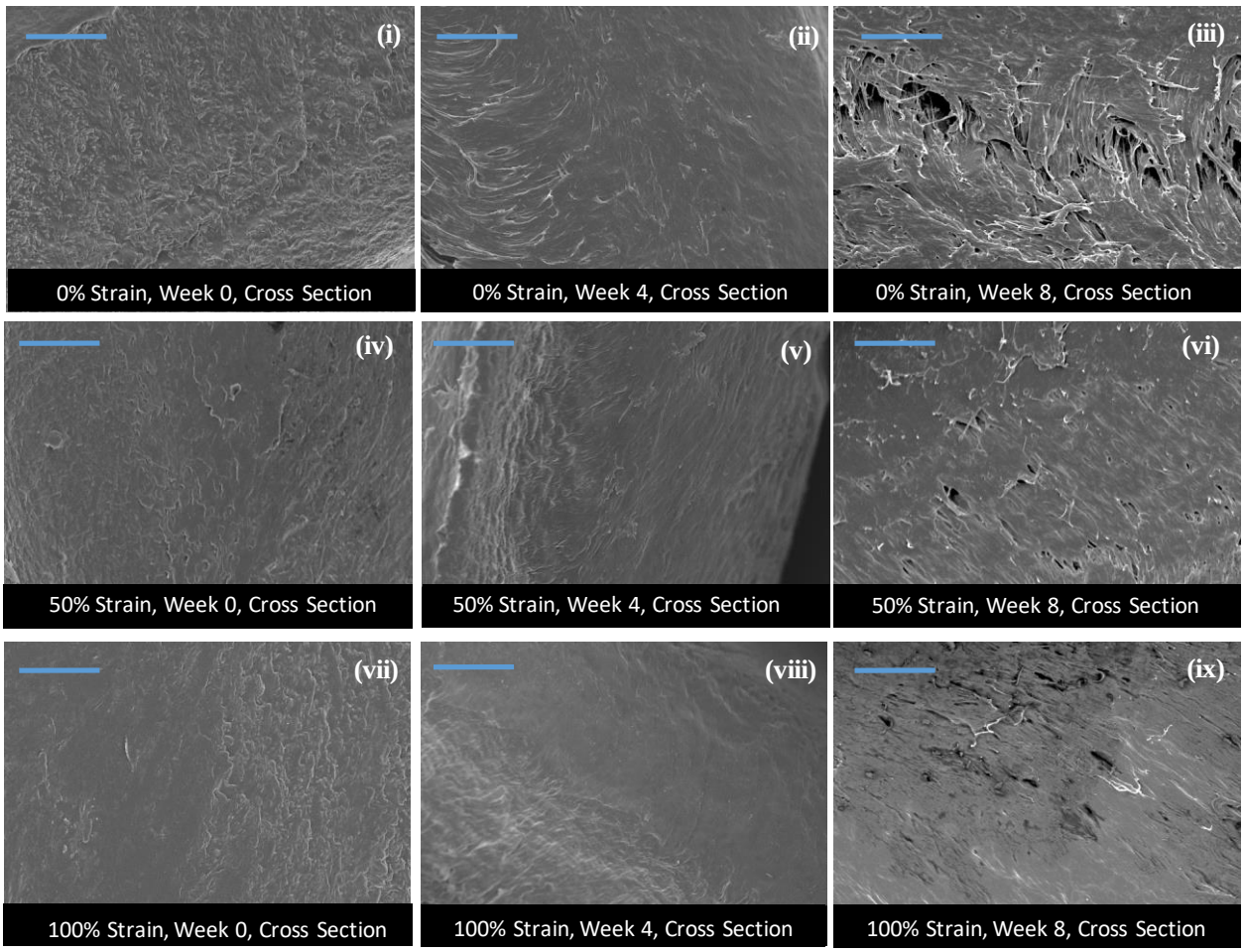

Figure 5-12: Scanning electron micrographs for the SMECs degraded at different fixed strains. Cross sectional images of a SMEC with 0% strain at (i) 0 w, (ii) 4 w, and (iii) 8 w; 50% strain at (iv) 0 w, (v) 4 w, and (vi) 8 w; and 100% strain at (vii) 0 w, (viii) 4 w, and (ix) 8 w. Scale bar represents 50 µm.

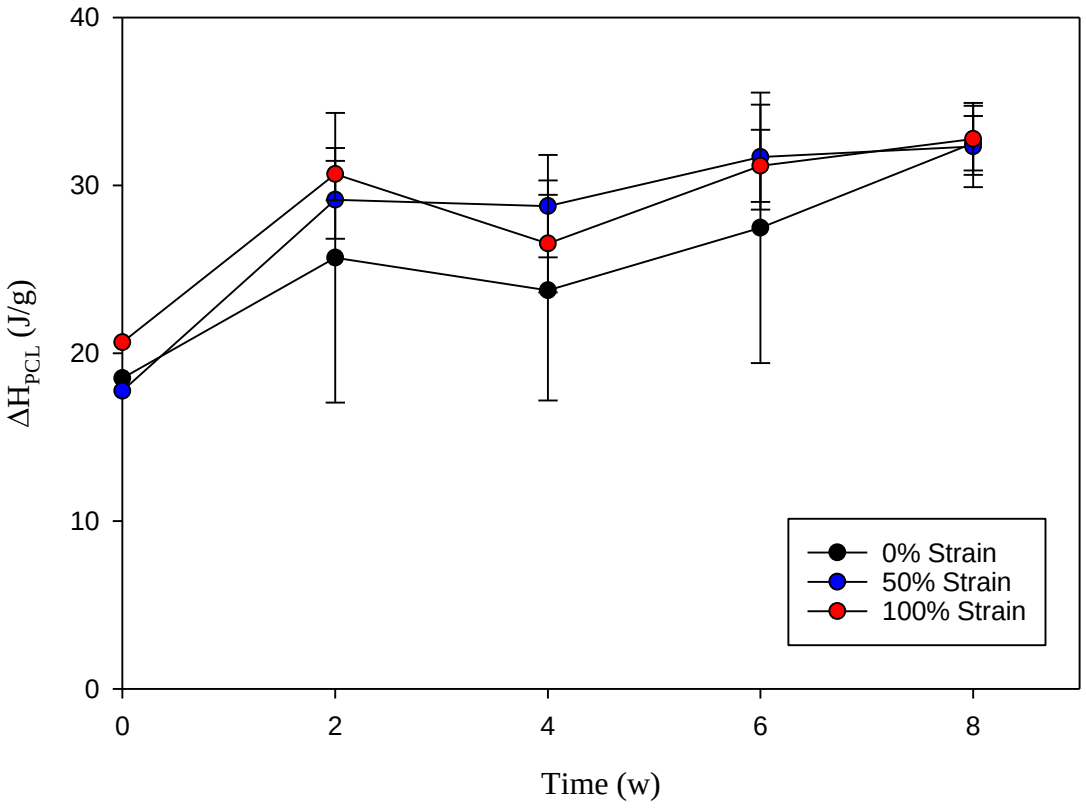

Figure 5-13: The enthalpy of melting of the PCL (ΔH_{PCL}) portion of the SMECS fixed at 0% strain, 50% strain, and 100% strain (n = 3), determined from differential scanning calorimetry throughout degradation.

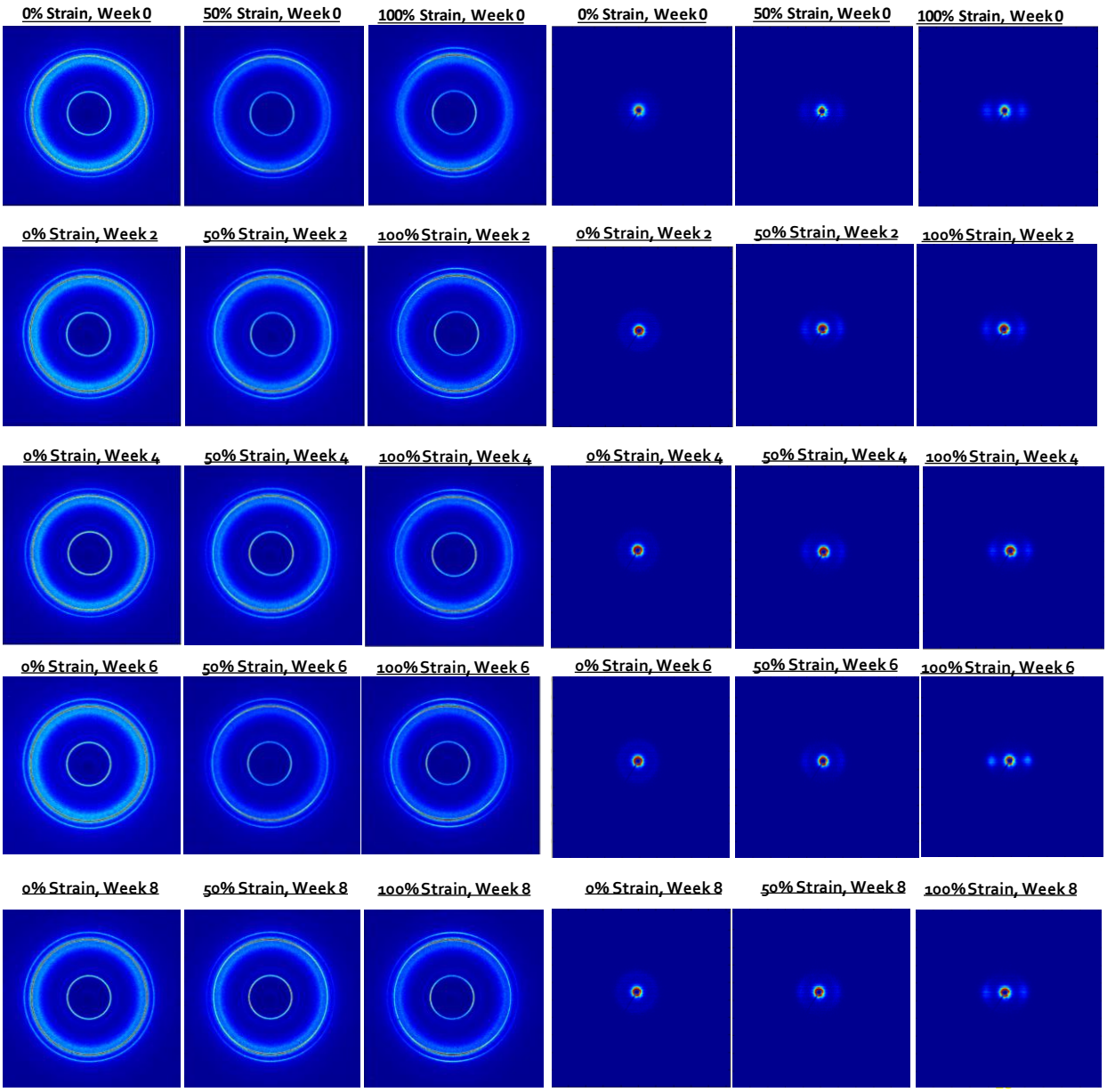

Figure 5-14: X-ray diffraction of the SMEC with different fixed strains through degradation with WAXS 2-D images on the left and SAXS 2-D images on the right. The direction of stretch is ↔.

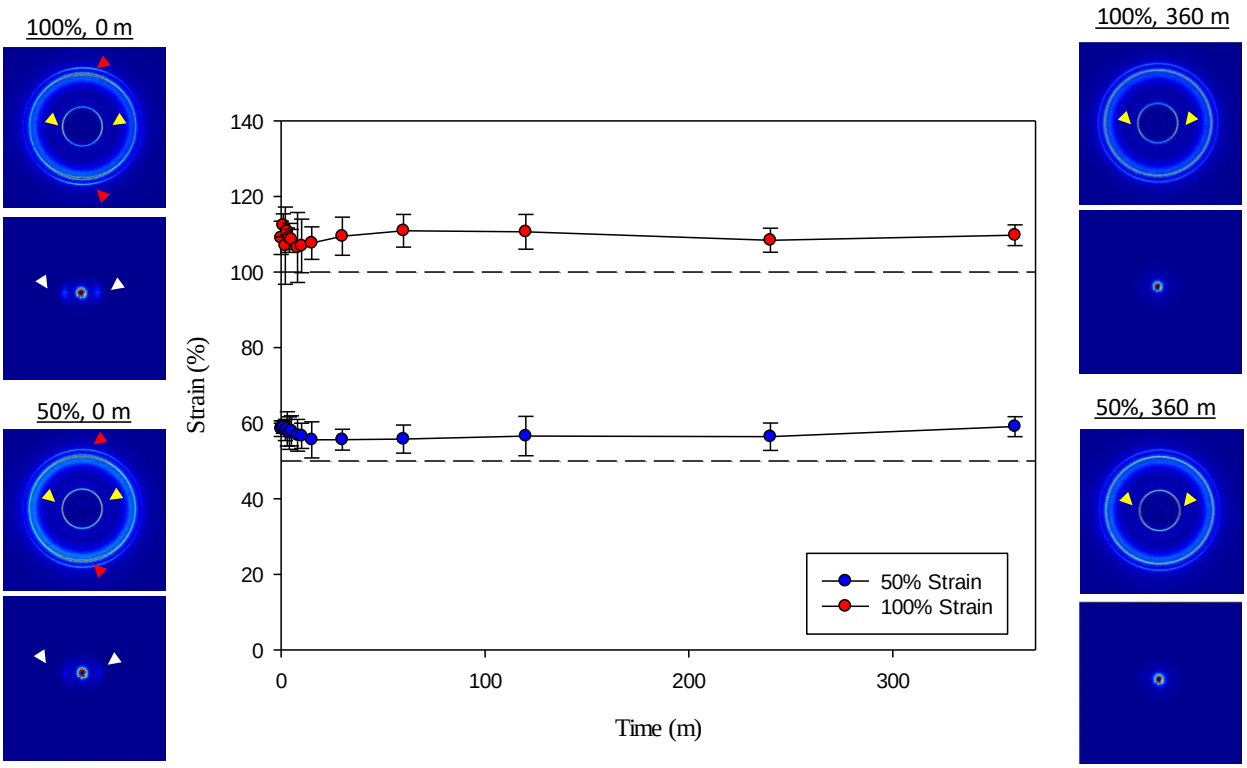

Figure 5-15: Recovery profile of the SMECs with fixed strain by heating at 70 °C for several hours after they were degraded for 8 w. WAXS and SAXS profiles of before and after recovery for each. Stretch direction is ↔. Alignment of PCL in WAXS is indicated by the red arrows, alignment of POSS in WAXS is indicated by the yellow arrows, and alignment of PCL in SAXS is indicated by the white arrows.

Chapter 6: Biodegradable Polyurethanes with Alternative Hard Blocks to POSS- PCL_{1k}:PCL Polyurethanes

6.1 Synopsis

Previously, we have developed thermoplastic polyurethane elastomers with short chain polycaprolactone (PCL) in the soft segment and POSS diol in the hard segment.[1] These PCL:POSS elastomers, while having desirable properties, may be too expensive to mass produce due to the high cost of POSS. This chapter looks at a simpler and cost-effective alternative by utilizing two distinct poly(caprolactone) diols as both the soft segment and the hard segment of the polyurethane. Several polyurethanes were synthesized and studied with different hard blocks sizes and different weight ratios of soft to hard blocks. Increasing the wt. % of the hard block caused an increase in melting transition, crystallinity and modulus but decreased elasticity, while increasing the size of the hard block decreased elasticity at room temperature. One sample featuring a longer length hard block had extremely high molecular weight and therefore had a rubbery plateau at temperatures above its melting transition in dynamic mechanical analysis. This indicated that there was a large degree of entanglements for that sample. This material also had high elastic recovery at body temperature and attractive shape memory properties. From this study, PCL:PCL polyurethanes could be an alternative to the PCL:POSS polyurethanes and cost less to produce.

6.2 Introduction

Biodegradable, thermoplastic polyurethane elastomers were previously introduced containing caprolactone-based soft segments and POSS (and hexamethylene diisocyanate) as a hard segment.[1] While POSS has a desirable low melting transition,[2, 3] provides physical cross-links[4] and provides degradation resistance,[5] POSS is expensive. Therefore, multi-block polyurethanes with different hard segments could be developed that would be lower-cost. Some

diols that have been considered to replace POSS diol include poly(l-lactide) diol, 1,8-octanediol and poly(caprolactone) diol. These were selected because they contain two hydroxyl groups, can crystallize above body temperature, and cost less than POSS diol. The different structures of these potential hard blocks are displayed in **Figure 6-1**, and a summary of their properties (including cost at a research level) are summarized in **Table 6-1**.

One hard block alternative, poly(l-lactide), is a semi-crystalline polyester that has a glass transition around 60-65 °C and a melting temperature around 175 °C. It is a biodegradable material that degrades by hydrolysis between six months and 5 years and has been approved by the FDA for medical devices.[6] Poly(l-lactide) was determined to be about $2.35/g for the raw materials, which is much lower than the $6.24/g for POSS diol (AL0130). 1,8-octanediol, another hard block alternative, is a fatty acid diol that is water soluble and non-toxic.[7] It has a melting temperature around 57-61 °C and is available from Sigma-Aldrich for as low as $1.02/g.

Our third hard-block alternative, poly(caprolactone) (PCL) diol could be used as the hard segment of the polyurethane with the caprolactone-based soft segments. The glass transition temperature of PCL is about -50 °C and the melting transition of PCL increases with increasing molecular weight until it reaches an asymptotic plateau value of about 60 °C.[6] Poly(caprolactone) degrades by hydrolysis over the course of several years and is degradable by enzymes. The mixing of the two chemically similar blocks in a multi-block polyurethane could result in an intermediate melting temperature, but ideally, the hard block would crystallize and the soft segment would be amorphous, resulting in a phase-separated hard block and soft block. Poly(caprolactone) is the most cost-effective hard block material, with either a purchased diol or synthesized diol costing about $0.30/g – $0.37/g.

In this work, polyurethanes with distinct PCL's serving as both the soft segment and part of the hard segment with hexamethylene diisocyanate were synthesized. Two PCL hard segment molecular weights, 3 kDa and 12 kDa, were selected for comparison along with two soft segment to hard segment ratio, 70:30 and 90:10 wt. %. Three polyurethanes were synthesized and tested for thermal, morphological and mechanical properties and compared with a linear polycaprolactone with a molecular weight of 80 kDa. We anticipated that the synthesized polyurethanes would have lower melting points, enthalpies of melting, and moduli than linear PCL_{80k}. Also, increasing the molecular weight and wt. % of the hard segment would result in higher thermal and mechanical properties when compared to the polyurethanes with lower molecular weight or wt. % of the hard segment.

6.3 Methods

6.3.1 Materials

1,4-butanediol (≥ 99%), ε-caprolactone (≥ 97%), and tin 2-ethylhexanoate (stannous octoate, 95%) were all purchased from Sigma-Aldrich. ε-Caprolactone was purified by vacuum distillation prior to use. Poly(ε-caprolactone)$_{1k}$ diol (M_w ~ 1,250 g/mol) was purchased from Polysciences, Inc. Poly(ε-caprolactone)$_{3k}$ diol (Mw~ 3,000 g/mol) was purchased from Scientific Polymer Products, Inc. Tin-POMS (the polyurethane catalyst) was purchased from Hybrid Plastics. Hexamethylene diisocyanate (HDI) was purchased from Sigma-Aldrich and used as received. Toluene, tetrahydrofuran (THF), and *n*-hexanes were purchased from Fisher Scientific. Toluene was dried by refluxing over calcium hydride (Sigma-Aldrich) several times until collection, and stored over 3 Å molecular sieves (Sigma-Aldrich) prior to use. HPLC-grade THF was purchased from Sigma-Aldrich. Poly(caprolactone) (M_w ~ 80 kDa) (PCL_{80k}) was purchased from Sigma-Aldrich.

6.3.2 Diol Synthesis

Poly(caprolactone)$_{12k}$ (PCL_{12k}) diol was synthesized by ring-opening polymerization of ε-caprolactone in the presence of butane diol with a target molecular weight (M_n) of 12,000 g/mol (12 kDa), as shown in **Scheme 6-1**. First, a 250 mL Schlenk flask with a magnetic stir bar was extensively vacuumed and purged with nitrogen gas several times. Next, 33.0 g (0.289 moles, 32.1 mL) of ε-caprolactone, 0.25 g (0.0027 moles, 0.25 mL) of butane diol, and 5 drops of tin 2-ethylhexanoate were added via syringe to the air-free flask. The flask was then heated to 140 °C (over the course of a half hour) and reacted for 10 h under nitrogen gas. At the end of the reaction period, the flask was cooled to room temperature, and the product was a hard, white solid. The polymer was dissolved in 40 mL of THF and precipitated in excess cold n-hexanes (~400 mL). The diol was collected, dried and characterized for molecular composition and thermal properties prior to polyurethane synthesis.

6.3.3 Polyurethane Synthesis

Polyurethanes were designed to have crystalline PCL hard blocks and amorphous soft segments of repeating units of PCL_{1k} and hexamethylene diisocyanate (HDI). Therefore, a synthesized or purchased PCL hard block diol was reacted with PCL_{1k} diol and HDI with a target weight ratio of 90:10 or 70:30 soft block PCL:hard block PCL. The synthesis schematic is shown in **Scheme 6-2.** The three synthesized polyurethanes were PCL_{1k}:PCL_{3k} 90:10, PCL_{1k}:PCL_{3k} 70:30, and PCL_{1k}:PCL_{12k} 90:10, with the nomenclature indicating the soft segment length: hard segment length and the weight ratio of the two. As a representative example, the synthesis of PCL_{1k}:PCL_{3k} 70:30 will be described. The poly(caprolactone)s, 7 g (5.6 mmol) of PCL_{1k} diol and 3 g (1 mmol) of PCL_{3k} diol, were first dissolved in distilled toluene (100 mL) under N_2 gas; a slight excess of HDI (1.12 g, which is equal to 1.065 mL or 6.65 mmol) and tin-POMS (1 wt. %) were

then added and the reaction was heated to 100 °C. The polyurethane reacted under N_2 for several hours. HDI was added in small increments over time to increase the molecular weight. The polyurethane was cooled and precipitated in n-hexanes, dried and characterized, as described below.

6.3.4 Gel Permeation Chromatography (GPC)

Molecular weight (M_n and M_w) and polydispersity index (M_w/M_n) were determined using gel permeation chromatography (GPC). Samples were dissolved in tetrahydrofuran (THF) at a concentration of 2-5 mg/mL and were passed through a 0.2 μm PTFE filter before injection. A Waters Isocratic HPLC System equipped with a temperature controlled differential refractometer (Waters 2414) was used along with a multi-angle laser light scattering system (Wyatt miniDAWN) using three angles (45°, 90°, 135°) for in-line absolute molecular weight determination.

6.3.5 Differential Scanning Calorimetry (DSC)

Thermal properties of the materials were studied by differential scanning calorimetry (DSC) using the TA Q200 instrument. Heat flow rate was collected while each sample was heated to 200 °C (to remove thermal history), cooled to -70 °C, and heated a second time to 200 °C. The heating rates were 10 °C/min and the cooling rates were 5 °C/min. The second heat was used to determine glass transition temperature (T_g, a step in the curve), the change in heat capacity or melting transitions (T_m, the peak of the endotherm) and the enthalpy of melting (ΔH, area under the curve).

6.3.6 Compression Molding

The PCL:PCL polyurethanes and PCL_{80k} were compression molded into films using a Carver 3851-0 press with heating platens. The platens were heated to 70 °C, above the melting point of PCL. After the platens equilibrated, polymer was placed between two Teflon sheets with

a 0.45 mm thick Teflon spacer. A compressive force of 1 metric ton was applied at elevated temperatures and held for 10 minutes. The resulting films varied in physical properties; they were flexible or rigid and between 0.4 and 0.5 mm in thickness, determined by a digital caliper. The 90:10 films were translucent but PCL_{1k}:PCL_{3k} 70:30 and PCL_{80k} were white.

6.3.7 Wide-Angle X-Ray Scattering (WAXS)

Wide-angle x-ray scattering (WAXS) experiments were conducted to ascertain the molecular and nano-scale ordering and orientation of the various polymeric samples. For this purpose, a Rigaku S-MAX3000 pinhole camera system was utilized, with a MicroMax-002 generator operating with Cu Kα emission ($\lambda = 1.5406$), voltage of 45 kV and current of 0.88 mA. Wide-angle scattering patterns were collected at a sample-detector distance of 122.7 mm (resulting in scattering angles $3° < 2\theta < 40°$) using Fujifilm image plates (CR HR-V) with a FujiFilm FLA7000 reader. Samples were exposed to radiation to achieve adequate x-ray counts for analysis, which was performed using SAXSgui software v2.03.04.

6.3.8 Dynamic Mechanical Analysis

A TA Instruments Q800 dynamic mechanical analyzer (DMA) was utilized to determine the temperature-dependent viscoelastic properties of the polyurethanes. Samples in a dogbone geometry were loaded at room temperature, cooled to -25 °C and heated to 140 °C at a rate of 3 °C/minute. In order to maintain tension, applied load was kept at 108% of dynamic load. All runs were performed with a frequency of 1 Hz and 15 μm (<0.1%) amplitude.

6.3.9 Elasticity Testing

Elasticity, here termed R_E, was determined using the "squeeze/pull off" test of a TA AR-G2 Rheometer with custom tensile clamps at both room temperature and 37 °C. Dogbone samples

were stretched 50 µm/s to a 50% strain and then returned to the starting position at the same rate. Elasticity was determined from the following equation:

$$R_E\ (\%) = \frac{\varepsilon_f - \varepsilon_r}{\varepsilon_f - \varepsilon_i} * 100 \qquad \textbf{(6-1)}$$

Where ε_i is a small initial strain (where stress equals zero), ε_f is the strain that the polymer is stretched to, and ε_r is the strain recovered (where stress equals zero upon unloading).

6.3.10 Shape Memory Testing

Using the TA Q800 DMA in controlled force mode, a dogbone of PCL_{1k}:PCL_{12k} 90:10 was tested for shape memory properties at 60 °C. It was stretched to 20% strain at a rate of 0.02 N/min and cooled to 10 °C at 3 °C /min to fix the strain. Force was unloaded 0.05 N/min at 20 °C. The elastomer was then heated to 80 °C at a rate of 3 °C/min for recovery. PCL_{1k}:PCL_{12k} 90:10 was cooled to 60 °C and the cycle was repeated 3 times. Fixing (R_f) and recover (R_r) ratios were determined by:

$$R_f(\%) = \frac{\varepsilon_f - \varepsilon_i}{\varepsilon_d - \varepsilon_i} * 100 \textbf{ (6-2)}$$

$$R_r(\%) = \frac{\varepsilon_f - \varepsilon_r}{\varepsilon_f - \varepsilon_i} * 100 \textbf{ (6-3)}$$

Where ε_i is the strain at the beginning of each cycle (initial stain before stretching), ε_d is the strain the material is deformed to after cooling (strain of deformation), ε_f is the strain after unloading (the fixed strain), and ε_r is the strain after heating (strain of recovery).

6.3.11 Statistical Analysis

T-tests were performed on two means with unequal variances to determine the statistical significance of different sets of data. Two-tailed t-tests with a confidence value of $\alpha = 0.05$ was used for all tests.

6.4 Results

6.4.1 Diol and Polymer Synthesis and Molecular Properties

Polyurethanes were synthesized with poly(caprolactone) as the soft and hard segments. The two hard segments utilized were a commercially available poly(caprolactone)$_{3k}$ diol and a synthesized poly(caprolactone)$_{12k}$ diol. The diol synthesis scheme is presented in **Scheme 6-1**. As shown in **Table 6-2**, the resulting molecular weight was close to the target, with M_n = 12.2 kDa, M_w = 14.1 kDa, and the PDI = 1.15. Several polyurethanes were synthesized for comparison, two with PCL_{3k} diol and one with the synthesized PCL_{12k} diol mentioned above as the hard block. The polymers synthesized were PCL_{1k}:PCL_{3k} 90:10, PCL_{1k}:PCL_{3k} 70:30 and PCL_{1k}:PCL_{12k} 90:10. The subscripts indicate the diol length and numbers indicate the weight ratio of the respective components. The synthesis scheme is below in **Scheme 6-2**, and a summary of the polyurethanes' molecular weights are presented in **Table 6-3**. These materials have high molecular weight, with M_w > 100 kDa for all. PCl_{1k}:PCL_{12k} 90:10 had a particularly high molecular weight with M_w = 588.0 kDa.

6.4.2 Differential Scanning Calorimetry

Differential scanning calorimetry determines thermal properties such as glass transition and melting transition temperatures. The thermal properties of the three diols, three polyurethanes, and PCL_{80k}, are shown in **Figure 6-2** (with exotherm up) and summarized in **Table 6-4**. The diols increased in melting temperature with increasing length, from 39.3 °C for PCL_{1k} diol, to 55.0 °C for PCL_{12k}. Alternatively, the glass transition temperature dropped from 1.3 °C for PCL_{1k} to -60 °C for PCL_{3k} and PCL_{12k} diol. The synthesized polyurethane elastomers all had similar glass transitions around -51 °C. However, the melting temperature varied based on composition. The two materials that had 90:10 composition had lower melting transitions, 33.1 °C and 33.5 °C for

the PCL_{3k} and PCL_{12k} hard blocks, respectively. PCL_{1k}:PCL_{3k} 70:30 had a slightly higher melting temperature at 38.5 °C. The melting enthalpies of these polyurethanes were around 30 J/g, although PCL_{1k}:PCL_{3k} 70:30 had the highest at 33.9 J/g. These were compared to PCL_{80k}, which had the highest melting point and enthalpy of melting with 56.5 °C and 52.7 J/g, respectively. The glass transition temperature of this polymer was -60.4 °C.

6.4.3 Wide-Angle X-Ray Scattering

The microstructure of the polyurethanes and PCL_{80k} determined from wide-angle x-ray scattering is shown in **Figure 6-3** as a one-dimensional curve and **Figure 6-4** as two-dimensional plots. The 1-D scans show that crystallinity increased with increasing amounts of hard segment, as the peaks at 2θ = 21.4° (d-spacing (d) = 4.15Å) and 23.6 (d = 3.77Å) corresponding to PCL crystallinity increased and sharpened for PCL_{1k}:PCL_{3k} 70:30 and even more for PCL_{80k}. In the 2-D scans, this corresponded to the sharp lines. The two 90:10 materials are mostly amorphous, as shown by the broad curve between 2θ = 15° - 25° in the 1-D plots and the wide halos in the 2-D plots, in contrast with the results from DSC.

6.4.4 Dynamic Mechanical Analysis

Storage moduli were determined from dynamic mechanical analysis (DMA) shown in **Figure 6-5** and **Table 6-5.** PCL_{1k}:PCL_{3k} 90:10 had the lowest storage moduli, with a modulus of 36.3 MPa at 25 °C and a storage modulus of 5.1 MPa at 37 °C. Above this polyurethane's melting point, it yielded at about 42 °C. By comparison, $PCL_{1k}PCL_{3k}$ 70:30 had higher moduli at 25 and 37 °C, 80.1 MPa and 33.4 MPa, respectively. However, this material yielded at the same temperature as $PCL_{1k}PCL_{3k}$ 90:10 at 42 °C. PCL_{80k} showed similar mechanical properties as the previously discussed polyurethanes, although all values were higher in magnitude. PCL_{80k} had a storage modulus of 181.4 MPa at 25 °C and 140.6 at 37 °C. It yielded at two temperatures during

its melting transition, at 59.4 °C and at 69.4 °C. PCL_{1k}:PCL_{12k} 90:10 showed a unique mechanical profile in that beyond its melting transition it displayed a rubbery plateau extending to greater than 100 °C. This polymer had moduli of 51.7 MPa and 2.2 MPa at 25 °C and 37 °C, respectively.

6.4.5 Elasticity Testing

Examples curves of elastic recovery of the different elastomers and the quantification of elastic recovery (R_E) are shown in **Figure 6-6**. Specifically, PCL_{1k}:PCL_{3k} 90:10 tested at room temperature is displayed in **Figure 6-6a**, PCL_{1k}:PCL_{3k} 70:30 tested at room temperature in **Figure 6-6b**, PCL_{1k}:PCL_{12k} 90:10 tested at room temperature in **Figure 6-6c**, and PCL_{1k}:PCL_{12k} 90:10 tested at 37 °C is displayed in **Figure 6-6d**. The two PCL_{1k}:PCL_{3k} materials could not be tested at 37 °C as these materials flowed at that temperature and did not generate a force when stretched; instead, they broke. Also, to note, the scale for stress for PCL_{1k}:PCL_{3k} 70:30 is four times higher than the other stresses. Generally, while all elastomers had greater than 70% elasticity after three cycles at room temperature, elasticity was lower for materials with higher molecular weight or wt. % hard blocks.

The values of the elastic recovery are displayed in **Figure 6-6e**. PCL_{1k}:PCL_{3k} 90:10 had the highest elastic recovery with greater than 80% recovery for the three consecutive cycles. For the first cycle, this was significantly higher than PCL_{1k}:PCL_{3k} 70:30, which had a recovery of 61.6 ± 2.5 % ($p < 0.01$), and PCL_{1k}:PCL_{12k} 90:10, which had an elastic recovery of 56.7 ± 6.8 % ($p < 0.01$) at room temperature. The elastic recovery values for the other cycles were similar to each other, but PCL_{1k}:PCL_{3k} 90:10 was significantly higher than PCL_{1k}:PCL_{12k} 90:10 for all three cycles. When PCL_{1k}:PCL_{12k} 90:10 was heated to body temperature, the elasticity was higher than the elasticity at room temperature, but only for the first cycle ($p < 0.05$). For PCL_{1k}:PCL_{3k} 90:10 at room temperature and PCL_{1k}:PCL_{12k} 90:10 at 37 °C, the elasticity did not increase with

consecutive cycle ($p > 0.05$). However, PCL_{1k}:PCL_{12k} 90:10's elasticity tested at room temperature increased between each cycle ($p < 0.05$), while PCL_{1k}:PCL_{3k} 70:30's elasticity only increased between the first and second cycle ($p < 0.01$). From Chapter 5, we know that PCL's elasticity at room temperature is less than 50% for the first cycle.

6.4.6 Shape Memory Testing

Finally, shape memory testing was performed on PCL_{1k}:PCL_{12k} 90:10 using the dynamic mechanical analyzer because it showed a rubbery plateau after the melting transition during DMA, indicating it could have shape memory properties. The three-dimensional plot of the shape memory cycle is shown in **Figure 6-7** and the quantification of fixing and recovery ratios are shown in **Table 6-6**. As indicated by the curve and table, both fixing and recovery were high with fixing ratios (R_f) of 98%, 97%, and 97% and recovery ratios of 107%, 100%, and 87% for cycles 1, 2, and 3, respectively.

6.5 Discussion

Polyurethanes' multi-block nature allows for control over the chemical composition of the soft and hard blocks as well as the ratio between the hard block and soft block. In this work, we focused on soft segments and hard segments of the same composition, poly(caprolactone), as this would be a lower-cost material than PCL_{1k}:POSS, as shown in **Table 6-1**. We synthesized three polyurethanes with either PCL_{3k} or PCL_{12k} diol and either 90:10 or 70:30 soft to hard block ratio. All of these materials had high molecular weights, which would promote desirable mechanical properties.

The new polyurethane elastomers prepared showed a single melting transition by differential scanning calorimetry, indicating either a mixing of the soft and hard segments of the polyurethane or an amorphous nature in the soft segment. The goal was to have phase separated

materials with hard and soft segments; we hypothesize this could be more evident by processing,[8, 9] or by incorporating a comonomer into the soft segment to reduce its crystallinity.[10, 11] The polyurethane with the highest melting transition was PCL_{1k}:PCL_{3k} 70:30, despite PCL_{12k} diol having a higher melting transition temperature than PCL_{3k} diol. The 20% higher PCL_{1k} content in PCL_{1k}:PCL_{12k} 90:10 elastomer resulted in a lower melting transition temperature than the 70:30 material. The larger block (12 kDa) only led to a slightly higher melting transition than the smaller hard block (3 kDa) of the same weight percentages. When compared to PCL_{80k}, all polyurethanes had a lower melting transition, indicating that the hexamethylene diisocyanate between PCL chains disrupted the poly(caprolactone) crystallization, resulting in a lower melting transition.

X-Ray diffraction analysis showed different trends than the differential scanning calorimetry scans, which may be due to the processing of the films used for x-ray analysis. The compression molded films may not have been fully crystallized, as compared to the 2nd heat DSC scans in which the elastomers' thermal history was removed. $Poly(caprolactone)_{80k}$ had the highest crystallinity, with crystallites with d-spacing of 4.15 Å and 3.77 Å, corresponding to Miller indices of 110 and 200 from an orthorhombic unit cell, as shown previously.[12, 13] PCL_{1k}:PCL_{3k} 70:30 had lower crystallinity, with less defined peaks of the same crystallite structure. The other materials were more amorphous, as indicated by the broad halo in both the 1-D and 2-D WAXS patterns.

Dynamic mechanical analysis was performed to determine the effect of block size and block ratio on the thermo-mechanical properties of the polyurethanes. Increasing the hard block length or hard block content increased the modulus at room temperature. These polyurethanes had lower mechanical properties than PCL_{80k} below the PCL melt temperature due to their lower crystallinity. $PCL_{1k}PCL_{12k}$ 90:10 had a rubbery plateau after the melting transition, which could

be attributed to entanglements due to the extremely high molecular weight, which was seen previously in poly(caprolactone):poly(ethylene glycol) high molecular weight polyurethanes.[14]

The elasticity of all polyurethanes synthesized with PCL_{3k} diol was high at room temperature. The cross-links needed for elasticity were provided by physical interactions (POSS crystallites). For PCL_{1k}:PCL_{12k}, the elasticity was high at room temperature and even at body temperature. While the other materials yielded at body temperature during elasticity testing, PCL_{1k}:PCL_{12k} 90:10's entanglements allowed for high elastic recovery at 37 °C. The material's elasticity was actually higher at body temperature, which we attribute to the melting of crystals that could have impeded recovery at room temperature. If the other materials had higher molecular weight, we hypothesize they could behave like PCL_{1k}:PCL_{12k} 90:10 at body temperature after the melting transition.

The shape memory capabilities of PCL_{1k}:PCL_{12k} 90:10 polyurethane were high, with almost perfect fixing and recovery as determined from the 3D plot. Shape memory materials require two things: cross-links and a switching transition, which come from the entanglements and the melting transition, respectively.[15, 16] Having good shape memory would allow for a smart, biodegradable and elastomeric medical device.

6.6 Conclusions

In conclusion, PCL:PCL polyurethanes have been synthesized with high molecular weight and elasticity and the prospect of being more cost-effective than the PCL:POSS polyurethanes. In particular, PCL_{1k}:$POSS_{12k}$ 90:10 had good elasticity both at room temperature and body temperature due to the high molecular weight and high entanglements. This material also had good shape memory capabilities, which would allow for a smart, biodegradable elastomer.

6.7 References

1. McMullin, E.; Rebar, H. T.; Mather, P. T., Biodegradable Thermoplastic Elastomers Incorporating POSS: Synthesis, Microstructure, and Mechanical Properties. *Macromolecules* **2016,** *49* (10), 3769-3779. DOI: 10.1021/acs.macromol.6b00470.

2. Li, G.; Wang, L.; Ni, H.; Pittman, C. U., Polyhedral Oligomeric Silsesquioxane (POSS) Polymers and Copolymers: A Review. *Journal of Inorganic and Organometallic Polymers 11* (3), 123-154. DOI: 10.1023/A:1015287910502.

3. Tanaka, K., Advanced functional materials based on polyhedral oligomeric silsesquioxane (POSS). *Journal of materials chemistry* **2012,** *22* (5), 1733-1746. DOI: 10.1039/C1JM14231C.

4. Knight, P. T.; Lee, K. M.; Qin, H.; Mather, P. T., Biodegradable Thermoplastic Polyurethanes Incorporating Polyhedral Oligosilsesquioxane. *Biomacromolecules* **2008,** *9* (9), 2458-2467. DOI: 10.1021/bm8004935.

5. Kannan, R. Y.; Salacinski, H. J.; Odlyha, M.; Butler, P. E.; Seifalian, A. M., The degradative resistance of polyhedral oligomeric silsesquioxane nanocore integrated polyurethanes: An in vitro study. *Biomaterials* **2006,** *27* (9), 1971-1979. DOI: http://dx.doi.org/10.1016/j.biomaterials.2005.10.006.

6. Nair, L. S.; Laurencin, C. T., Biodegradable polymers as biomaterials. *Progress in Polymer Science* **2007,** *32* (8-9), 762-798. DOI: 10.1016/j.progpolymsci.2007.05.017.

7. Yang, J., Novel Citric Acid-Based Biodegradable Elastomers for Tissue Engineering. *Advanced materials (Weinheim) 16* (6), 511-516. DOI: 10.1002/adma.200306264.

8. Koberstein, J. T.; Russell, T. P., Simultaneous SAXS-DSC study of multiple endothermic behavior in polyether-based polyurethane block copolymers. *Macromolecules* **1986,** *19* (3), 714-720. DOI: 10.1021/ma00157a039.

9. Koberstein, J. T.; Galambos, A. F., Multiple melting in segmented polyurethane block copolymers. *Macromolecules* **1992,** *25* (21), 5618-5624. DOI: 10.1021/ma00047a010.

10. Pack, J. W.; Kim, S. H.; Cho, I. W.; Park, S. Y.; Kim, Y. H., Microstructure analysis and thermal property of copolymers made of glycolide and epsilon-caprolactone by stannous octoate. *Journal of Polymer Science Part a-Polymer Chemistry* **2002,** *40* (4), 544-554. DOI: 10.1002/pola.10123.

11. Cai, Q.; Bei, J. Z.; Wang, S. G., Synthesis and properties of ABA-type triblock copolymers of poly(glycolide-co-caprolactone) (A) and poly(ethylene glycol) (B). *Polymer* **2002,** *43* (13), 3585-3591. DOI: 10.1016/s0032-3861(02)00197-0.

12. Alvarado-Tenorio, B.; Romo-Uribe, A.; Mather, P. T., Microstructure and Phase Behavior of POSS/PCL Shape Memory Nanocomposites. *Macromolecules* **2011,** *44* (14), 5682-5692. DOI: 10.1021/ma2005662.

13. Ceccorulli, G.; Scandola, M.; Kumar, A.; Kalra, B.; Gross, R. A., Cocrystallization of Random Copolymers of ω-Pentadecalactone and ε-Caprolactone Synthesized by Lipase Catalysis. *Biomacromolecules* **2005,** *6* (2), 902-907. DOI: 10.1021/bm0493279.

14. Gu, X.; Mather, P. T., Entanglement-based shape memory polyurethanes: Synthesis and characterization. *Polymer* **2012,** *53* (25), 5924-5934. DOI: http://dx.doi.org/10.1016/j.polymer.2012.09.056.

15. Lendlein, A.; Kelch, S., Shape-Memory Polymers. *Angewandte Chemie International Edition* **2002,** *41* (12), 2034-2057. DOI: 10.1002/1521-3773(20020617)41:12<2034::AID-ANIE2034>3.0.CO;2-M.

16. Mather, P. T.; Luo, X.; Rousseau, I. A., Shape Memory Polymer Research. *Annual Review of Materials Research* **2009,** *39* (1), 445-471. DOI: 10.1146/annurev-matsci-082908-145419.

Polyhedral Oligomeric Silsesquioxane (POSS Diol)

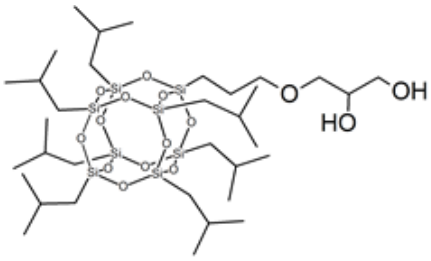

1,8-Octanediol

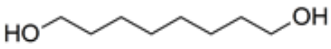

Poly(l-lactide) Diol (PLLA Diol)

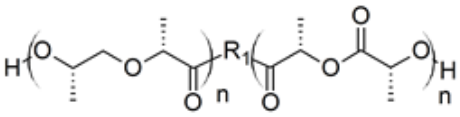

Poly(caprolactone) Diol (PCL Diol)

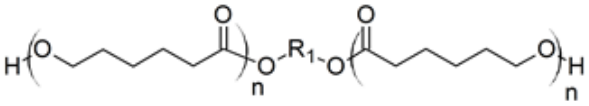

Figure 6-1: Molecules that could be used with hexamethylene diisocyanate as the hard block in our polyurethanes.

Table 6-1: Summary of the properties of the hard block alternatives (not including the isocyanate).

Hard Block	Formula Weight (g/mol)	T_g (°C)	T_m (°C)	Degradation (y)	Price ($/g)
POSS Diol	949.64	-	120	-	6.24[a]
1,8-Octanediol	146.23	-	57-61	-	1.02[b]
Poly(L-Lactide) Diol	3k – 12k	60-65	175	0.5-5	2.33 – 2.36[c]
Poly(Caprolactone) Diol	3k – 12k	-50	40-55	2-3	0.30[c] – 0.37[d]

[a]Price from Hybrid Plastics.
[b]Price from Sigma-Aldrich.
[c]Price calculated from price of raw materials – does not include cost of labor.
[d]Price from Scientific Polymer Products.

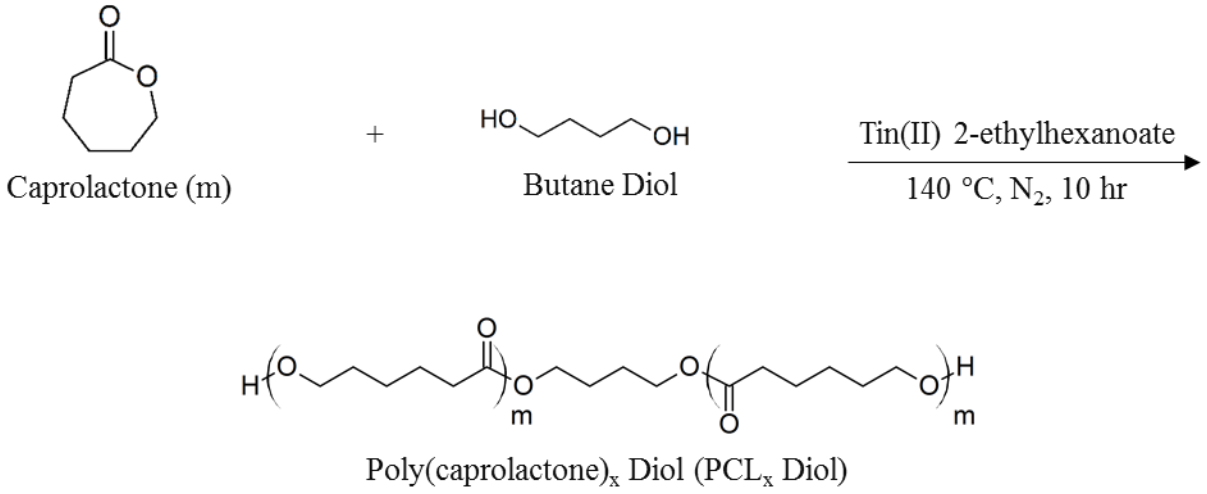

Scheme 6-1: Schematic of poly(caprolactone) diol synthesis.

Table 6-2: Characteristics of the diol synthesized.

Synthesis	**M_n[a] (kDa)**	**M_w[a] (kDa)**	**PDI[a]**
PCL_{12k}	12.2	14.1	1.15

[a]Determined from gel permeation chromatography.

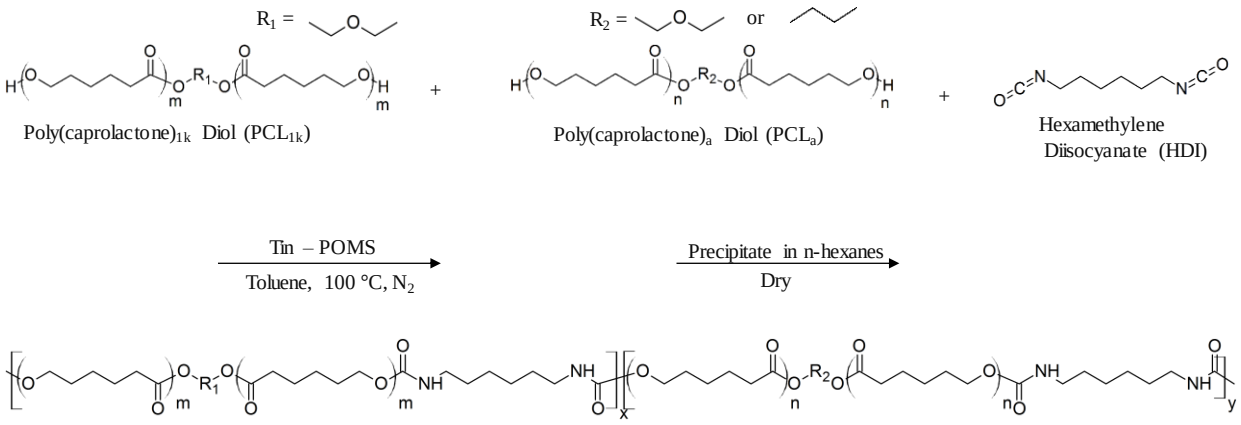

Scheme 6-2: Schematic of polyurethane synthesis with poly(caprolactone) as the soft block and hard block.

Table 6-3: Synthesized polyurethanes and their molecular weights.

Polymer	Input PCL_{soft}:PCL_{hard} (wt. %)	Input PCL_{soft}:PCL_{hard} (mol. %)	M_n[a] (kDa)	M_w[a] (kDa)	PDI[a]
PCL_{1k}:PCL_{3k} 70:30	70 : 30	5.6 : 1	64.1	100.7	1.57
PCL_{1k}:PCL_{3k} 90:10	90 : 10	21.6 : 1	208.5	368.5	1.77
PCL_{1k}:PCL_{12k} 90:10	90 : 10	86.4 : 1	352.5	588.0	1.67

[a]Determined from gel permeation chromatography.

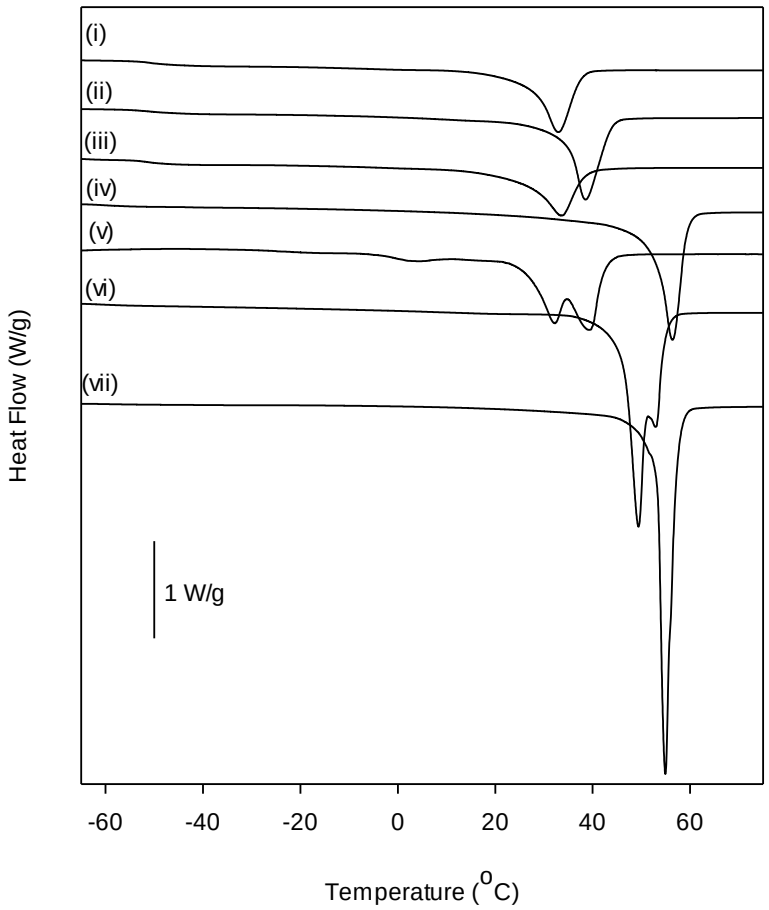

Figure 6-2: Differential scanning calorimetry of (i) PCL_{1k}:PCL_{3k} 90:10, (ii) PCL_{1k}:PCL_{3k} 70:30, (iii) PCL_{1k}:PCL_{12k} 90:10, (iv) PCL_{80k}, (v) PCL_{1k} diol, (vi) PCL_{3k} diol, and (vii) PCL_{12k} diol.

Table 6-4: Summary of the thermal properties from DSC.

Polymer	T_g (°C)	T_m (°C)	ΔH_m (J/g)
PCL_{1k}:PCL_{3k} 70:30	-51.4	38.5	33.9
PCL_{1k}:PCL_{3k} 90:10	-50.7	33.1	31.4
PCL_{1k}:PCL_{12k} 90:10	-51.6	33.5	29.4
PCL_{80k}	-60.4	56.5	52.7
PCL_{1k} Diol	1.3	39.3	49.4
PCL_{3k} Diol	-61.4	49.4	73.2
PCL_{12k} Diol	-60.1	55.0	71.4

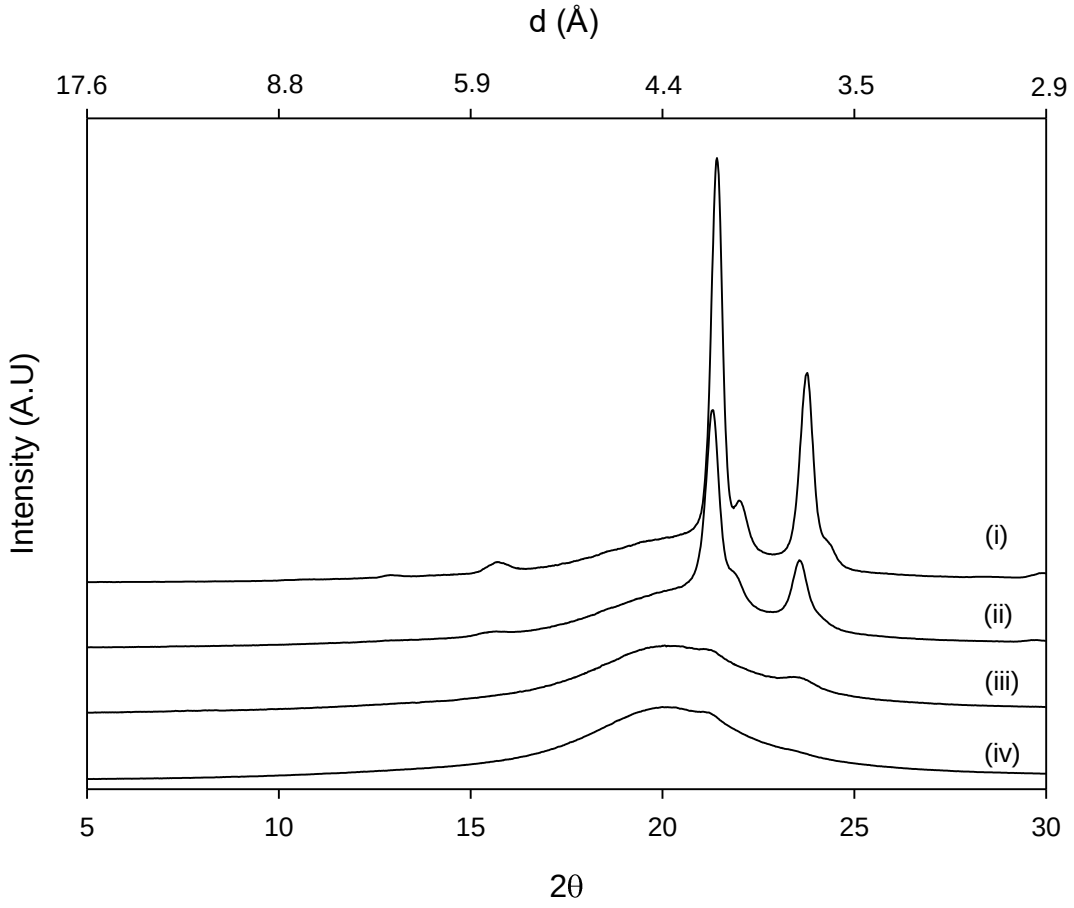

Figure 6-3: Wide-angle x-ray 1-D plots of (i) PCL_{80k}, (ii) PCL_{1k}:PCL_{3k} 70:30, (iii) PCL_{1k}:PCL_{3k} 90:10, and (iv) PCL_{1k}:PCL_{12k} 90:10.

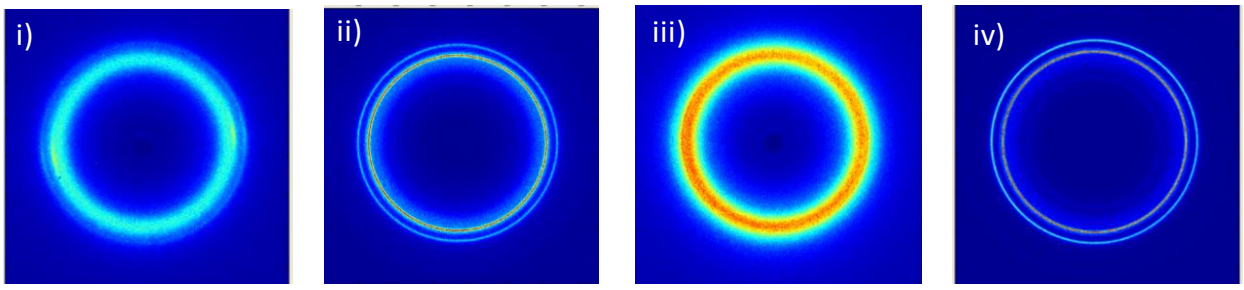

Figure 6-4: Wide-angle x-ray 2-D pictograms of (i) PCL_{1k}:PCL_{3k} 90:10, (ii) PCL_{1k}:PCL_{3k} 70:30, (iii) PCL_{1k}:PCL_{12k} 90:10, and (iv) PCL_{80k}.

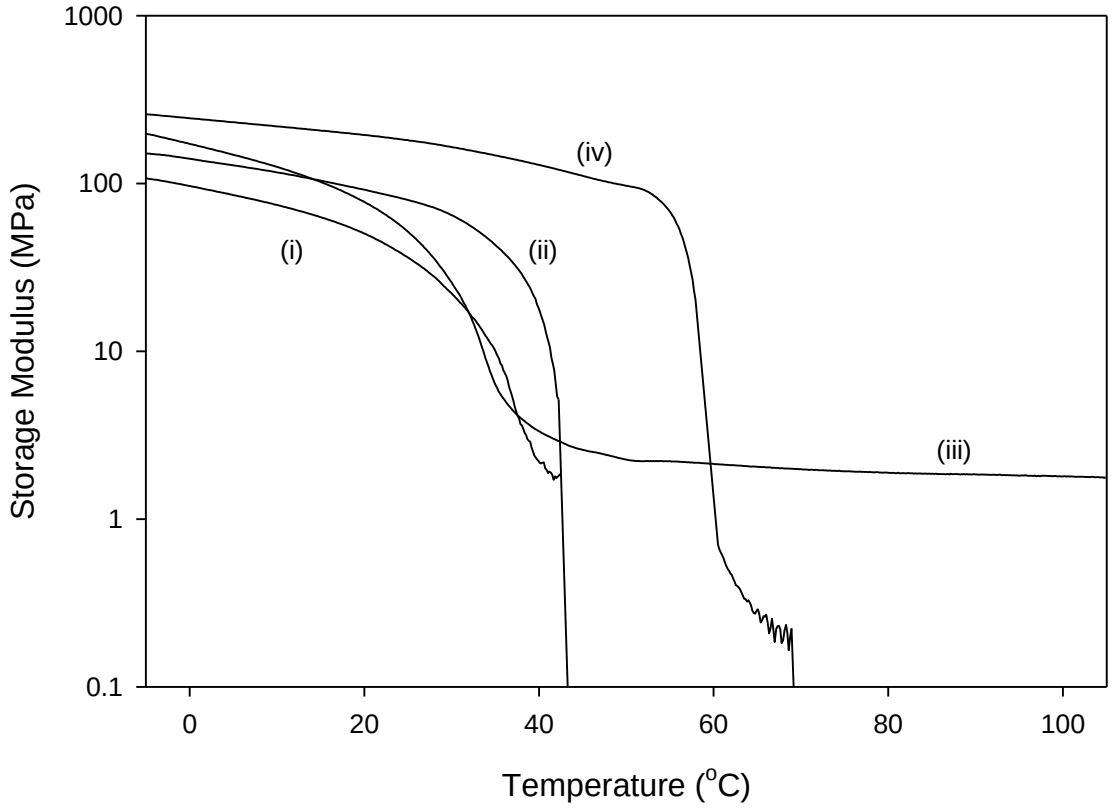

Figure 6-5: Dynamic mechanical analysis of (i) PCL_{1k}:PCL_{3k} 90:10, (ii) PCL_{1k}:PCL_{3k} 70:30, (iii) PCL_{1k}:PCL_{12k} 90:10 and (iv) PCL_{80k}.

Table 6-5: Summary of the storage moduli and tanδ values from DMA.

Polymer	E'_{25} (MPa)	E'_{37} (MPa)	Tanδ at 25 °C	Tanδ at 37 °C
PCL_{1k}:PCL_{3k} 90:10	36.3	5.1	0.043	0.114
PCL_{1k}:PCL_{3k} 70:30	80.1	33.4	0.043	0.069
PCL_{1k}:PCL_{12k} 90:10	51.7	2.2	0.043	0.229
PCL_{80k}	181.3	140.0	0.033	0.035

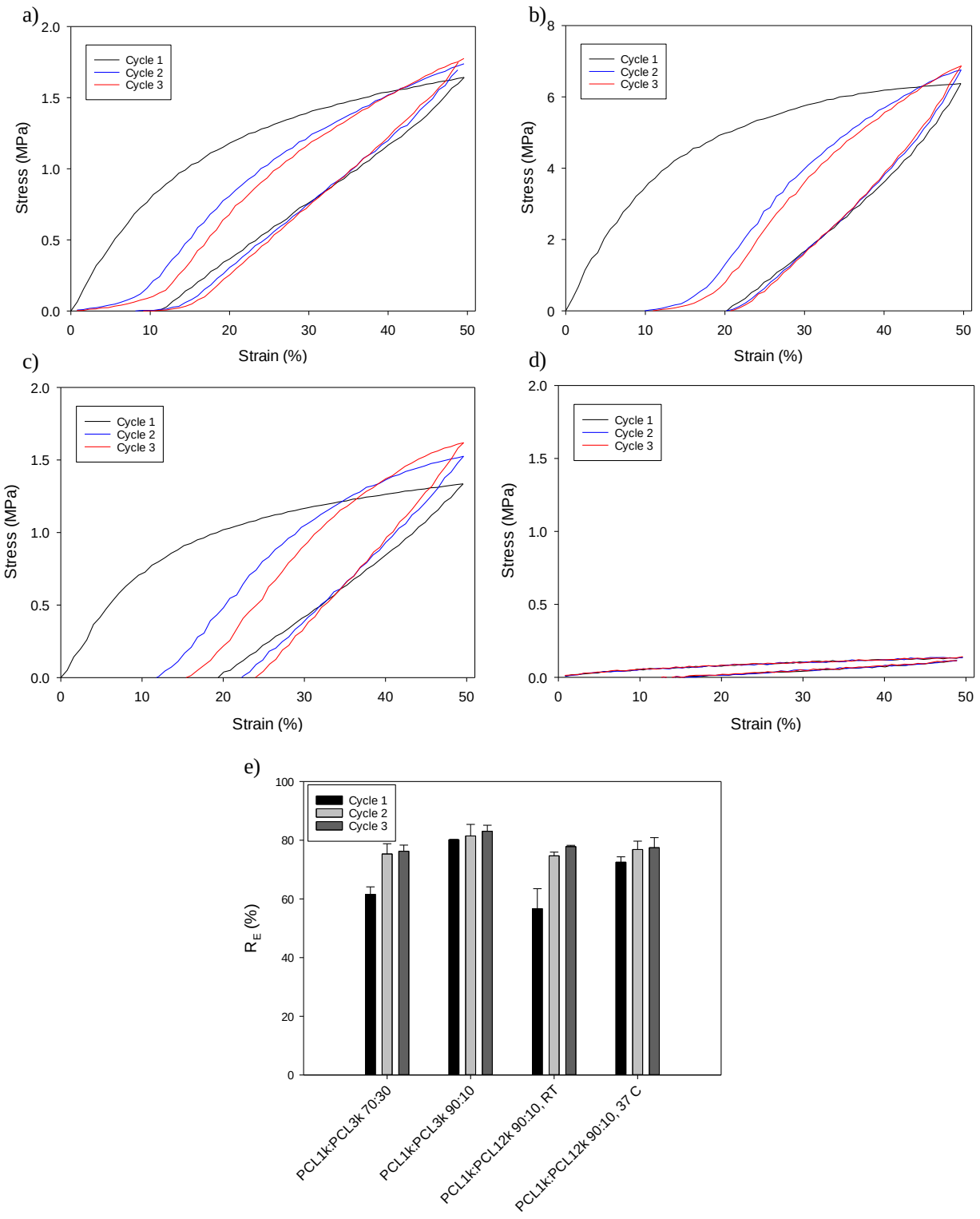

Figure 6-6: Elasticity testing of a) PCL_{1k}:PCL_{3k} 90:10, b) PCL_{1k}:PCL_{3k} 70:30, and c) PCL_{1k}:PCL_{12k} 90:10 at room temperature; and d) PCL_{1k}:PCL_{12k} 90:10 at 37 °C. e) Quantification of elastic recovery.

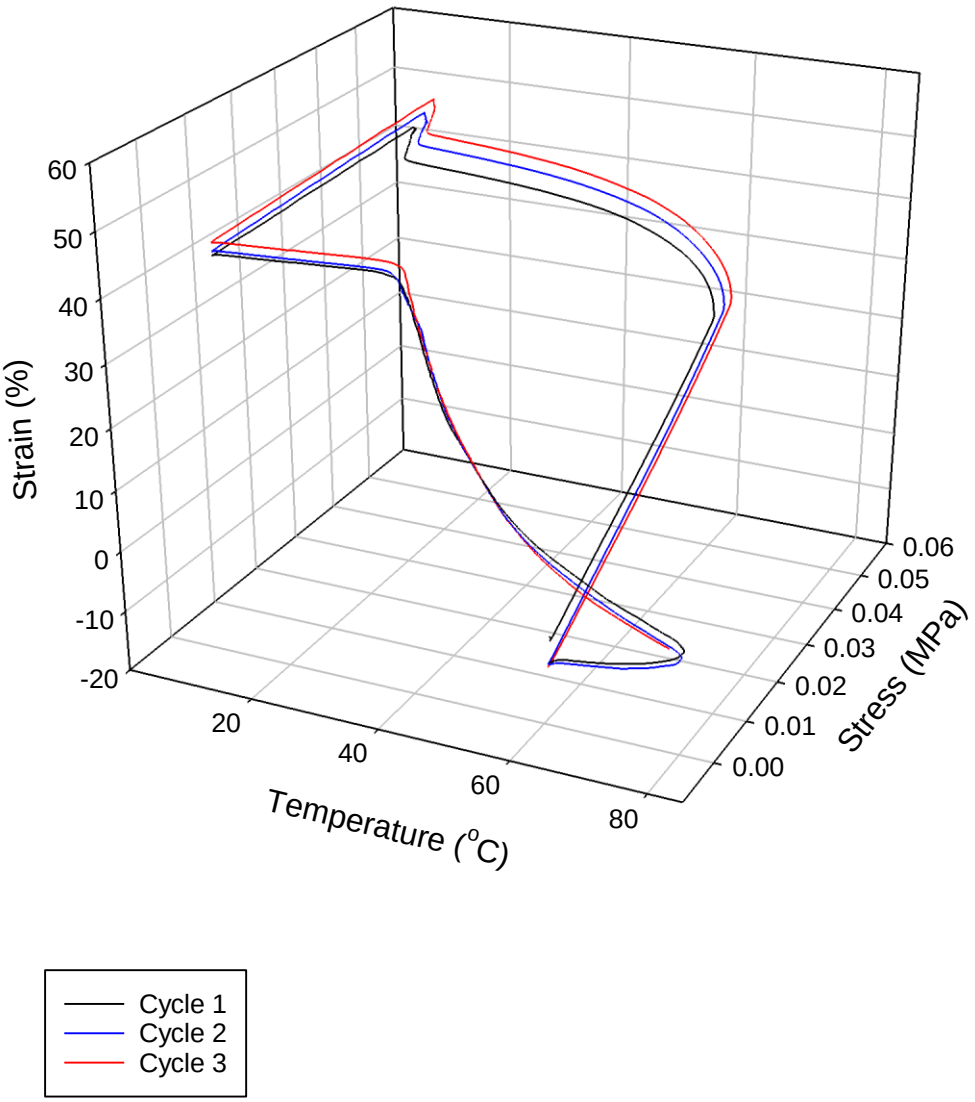

Figure 6-7: Shape memory test of PCL_{1k}:PCL_{12k} 90:10 polyurethane with three cycles.

Table 6-6: Fixing and recovery values of PCL_{1k}:PCL_{12k} 90:10 for three cycles.

Cycle	R_f (%)	R_r(%)
1	98	107
2	97	100
3	97	87

Chapter 7: Conclusions and Future Work

7.1 Overall Conclusions

This dissertation focused on the development of thermoplastic biodegradable elastomers and thermoplastic biodegradable smart materials that had controllable properties. These elastomers and smart materials were developed to be utilized as or incorporated into implantable medical devices. Generally, two polyurethane systems were researched with different hard segments: POSS and poly(caprolactone) diols (both with hexamethylene diisocyanate). First, for the POSS polyurethanes, controlling the composition of the soft segment as well as the soft segment to hard segment ratio allowed for a range of thermal and mechanical properties. The effect of the soft segment composition on degradation was also studied, focusing on the physical, thermal, and mechanical properties throughout degradation. Increasing soft segment content increased the rate of degradation. Cell viability testing was performed on these materials, and the results led to studying the effect of catalyst concentration and type on cell viability. Decreasing catalyst concentration increased cell viability. The POSS-based elastomers were also processed into shape memory elastomeric composites, and the properties of these were extensively studied. The properties could be controlled by the electrospinning parameters and the composition affected degradation. However, fixed strain had no effect on degradation. Finally, several polymers were investigated with PCL as the hard segment to be a lower-cost alternative to the PCL_{1k}:POSS materials. These materials had high molecular weights and controllable mechanical properties.

7.2 Biodegradable Thermoplastic Elastomers Incorporating POSS: Synthesis, Microstructure and Mechanical Properties

7.2.1 Conclusions

Novel, thermoplastic biodegradable elastomers were developed utilizing a biodegradable soft segment and POSS diol as the hard segment. These materials had controllable thermal and mechanical properties based on the POSS content and composition of the soft segment. Increasing POSS content increased the mechanical properties and increased the temperature range of the rubbery plateau after soft segment melting in DMA. Comonomer in the soft segment decreased the thermal transition of the soft segment and lowered the mechanical properties. All elastomers had high elasticity (>70% elastic recovery) which was increased by pre-straining the material. These materials have the potential for use as soft and elastic implantable biodegradable materials.

7.2.2 Future Directions

Material properties could be further studied to look at the mechanical properties such as modulus, strain-to-failure, and elasticity at physiological conditions. Also, different processing techniques, such as extrusion, casting, electrospinning, etc. could be employed to determine how processing affects the thermal, mechanical and microstructural properties of these elastomers. Studies determining shelf-life could be performed to understand the stability of these materials at dried and ambient conditions. More work could be done to fully understand the effect of pre-straining on mechanical properties, looking specifically at the time-dependence of the pre-stretch on elasticity and extensive x-ray analysis. Finally, different compositions of materials, such as 50:50 PCL:POSS or $(PG_{50}CL_{50})_{1k}$ could be investigated for harder or faster-degrading applications.

7.3 Degradation Behavior of Novel Biodegradable, Thermoplastic Elastomers Incorporating POSS

7.3.1 Conclusions

The biodegradable elastomers introduced in Chapter 2 were degraded in PBS at both 37 °C and 60 °C. At 37 °C, increasing the comonomer content caused an increase in degradation rate. Water uptake and mass loss increased over time with increasing comonomer content as mechanical properties decreased. Also, these materials' molecular properties were studied, showing that the soft segment preferentially degraded by hydrolysis. When degraded at 60 °C, the materials with or without comonomer showed different degradation profiles. Polyurethanes with d,l-lactide in the soft segment degraded similarly to how they degraded at 37 °C (but to a higher magnitude), while PCL_{1k}:POSS was stable for a couple of weeks and then degraded rapidly.

7.3.2 Future Directions

Hydrolytic degradation in neutral buffer was studied for the thermoplastic elastomers with different soft segments. Because PCL degrades enzymatically, a future study of enzymatic degradation could be considered. Also, degradation in simulated or natural biological fluids, such as esophageal fluid, blood, or urine could be studied *in vitro* to determine site-specific degradation profiles. *In vivo* implantation and degradation studies would also need to be performed to further study the degradation mechanism of these biomaterials.

7.4 Effect of Catalyst Concentration on PCL_{1k}:POSS Polyurethanes' Physical Properties and Cell Viability

7.4.1 Conclusions

The amount of organotin catalyst affected cell viability and was the cause of poor cell viability from materials introduced in Chapter 2. Decreasing the catalyst concentration used in polyurethane synthesis increased cell viability, with PCL_{1k}:POSS from 0.01 wt.% tin-POMS

having the best cell viability after incubation for 24 h. Although this material had lower molecular weight than some of the other polyurethanes, it had comparable modulus and high strain-to-failure. The variability of the cell viability at 72 h indicates that pre-processing may need to be done to ensure better cell viability, although polyurethanes utilizing 0.01 wt. % organotin catalyst have been used *in vivo* in other studies with promising tissue compatibility.

7.4.2 Future Directions

For future studies, it is possible to take alternative approaches to synthesizing polyurethanes. One alternative is to use no catalyst, which will remove all tin from the reaction but increase the duration of synthesis to several days.[1] This could make commercialization of these materials more difficult, but there would be no possible threat of tin toxicity. Another approach could be the utilization of ionic species in the backbone of the polyurethane to self-catalyze the polyurethane reaction, as researchers did with cationic amine and anionic alginate species.[2] Their molecular weights were high (M_w > 40 kDa), but the interactions of the ionic species could have adverse effects within the body's environment, as ion release may result in a variety of cell responses.[3] Finally, organic catalysts could be used in place of organometallic catalysts. Recently, research with polyurethane syntheses using organic acids,[4, 5] bases,[5] or guanine catalysts[6] has increased. Many of the catalysts showed similar activity as dibutyltin dilaurate, although our system would have to be adapted, as many of the catalysts require different reaction conditions.

7.5 Biodegradable Thermoplastic Shape Memory Elastomeric Composites (SMECs) Via Dual-Electrospinning

7.5.1 Conclusions

Thermoplastic biodegradable shape memory elastomeric composites (SMECs) were created by dual-electrospinning a biodegradable elastomer (TPE) with poly(caprolactone) to create a fully-biodegradable smart composite. Varying the flow rates of dual-electrospinning controlled

the composition, which resulted in controllable thermal, mechanical and shape-memory properties. These materials' mechanical properties decreased with degradation by hydrolysis. It was found that fixing a strain (up to 100%) in the SMEC did not affect its degradation rate. However, the fixed strain was not recoverable after degradation as the recovery material (TPE) degraded. This phenomenon could be exploited for a fixed biomedical device.

7.5.2 Future Directions

The force profile of the SMEC recovery could be studied to determine how much work could be performed by the SMEC. This information could determine the application the SMECs are used for. For example, a shape memory deployable stent would need to exert a force on the surrounding tissue to prevent occlusion. Also, a different transition temperature for the SMEC recovery could be investigated for a material that is triggered by physiological conditions. If the SMEC was fabricated from the PCL:POSS and PCL:PCL polyurethane, the material could be fixed and recovered around body temperature, which could be investigated for a deployable shape memory elastomeric composite.

7.6 Biodegradable Polyurethanes with Alternative Hard Blocks to POSS: PCL:PCL Polyurethanes

7.6.1 Conclusions

Poly(caprolactone) was used to replace POSS as a lower-cost hard block alternative. Several polyurethanes were synthesized that had high molecular weight and high elasticity. One composition had a high degree of entanglements, which led to a rubbery plateau after its melting transition and therefore shape memory properties.

7.6.2 Future Directions

The materials synthesized were characterized for thermal and mechanical properties. However, a degradation study and a cell viability study need to be performed to understand how

these materials degrade *in vitro* and interact with cells. New materials could be synthesized with comonomer in the soft segment in order to increase the amorphous nature of the soft segment. Also, the other possible hard segments, such as poly(l-lactide) diol and octane diol, could be investigated.

7.7 Other Future Directions

The elastomers, with either PCL or POSS as the hard segment, could be investigated as a drug delivery system. Some initial work was done in collaboration with Melodie I. Lawton and Hannah T. Rebar to investigate these materials as a drug-eluting system with a model hydrophobic drug, Rhodamine B (RhB). This florescent material was embedded in $(PL_5CL_{95})_{1k}$:POSS, either by electrospinning the polymer with a solution of RhB or by soaking the material in a solution of RhB and D.I. water, as shown in **Scheme 7-1**. These RhB-loaded polymers were then placed in D.I. water, and the RhB elution was studied over time to determine the drug release. Drug release was measured by a plate reader with the DI water replaced after every reading to provide a sink condition.

Initial drug release results, displayed in **Figure 7-1**, showed that soaking the materials, the "sponge method," allowed for more drug uptake than electrospinning with their current parameters. The polyurethane also allowed for more drug uptake than $poly(caprolactone)_{80k}$. Interestingly, the polyurethane film exhibits a more controlled drug release than the polyurethane fibers and PCL fibers, as indicated by the slower release of RhB. More work needs to be done to quantify the uptake of the drug during both electrospinning and the absorption method. Drug release needs to be compared when the uptake has been standardized. Also, we can work to further control the drug release.

Another study we could pursue is to use these materials as tissue engineering scaffolds for replacing soft tissues. Several soft tissues have Young's moduli similar to our materials, such as lung and kidney tissue, which is averaged at 10 MPa, and skin tissue, which is around 30 MPa.[7] Culturing cells on our materials would provide the cells a similarly stiff mechanical environment to their natural state. Because these materials are biodegradable, the scaffold will degrade overtime and leave a completely natural tissue.

7.8 References

1. Heijkants, R. G. J. C.; Calck, R. V. v.; van Tienen, T. G.; de Groot, J. H.; Buma, P.; Pennings, A. J.; Veth, R. P. H.; Schouten, A. J., Uncatalyzed synthesis, thermal and mechanical properties of polyurethanes based on poly(-caprolactone) and 1,4-butane diisocyanate with uniform hard segment. *Biomaterials* **2005,** *26* (20), 4219-4228. DOI: http://dx.doi.org/10.1016/j.biomaterials.2004.11.005.

2. Daemi, H.; Rajabi-Zeleti, S.; Sardon, H.; Barikani, M.; Khademhosseini, A.; Baharvand, H., A robust super-tough biodegradable elastomer engineered by supramolecular ionic interactions. *Biomaterials* **2016,** *84*, 54-63. DOI: http://dx.doi.org/10.1016/j.biomaterials.2016.01.025.

3. Hoppe, A.; Güldal, N. S.; Boccaccini, A. R., A review of the biological response to ionic dissolution products from bioactive glasses and glass-ceramics. *Biomaterials* **2011,** *32* (11), 2757-2774. DOI: http://dx.doi.org/10.1016/j.biomaterials.2011.01.004.

4. Sardon, H.; Engler, A. C.; Chan, J. M. W.; García, J. M.; Coady, D. J.; Pascual, A.; Mecerreyes, D.; Jones, G. O.; Rice, J. E.; Horn, H. W.; Hedrick, J. L., Organic Acid-Catalyzed Polyurethane Formation via a Dual-Activated Mechanism: Unexpected Preference of N-Activation over O-Activation of Isocyanates. *Journal of the American Chemical Society* **2013,** *135* (43), 16235-16241. DOI: 10.1021/ja408641g.

5. Sardon, H.; Pascual, A.; Mecerreyes, D.; Taton, D.; Cramail, H.; Hedrick, J. L., Synthesis of Polyurethanes Using Organocatalysis: A Perspective. *Macromolecules* **2015,** *48* (10), 3153-3165. DOI: 10.1021/acs.macromol.5b00384.

6. Alsarraf, J.; Ammar, Y. A.; Robert, F.; Cloutet, E.; Cramail, H.; Landais, Y., Cyclic Guanidines as Efficient Organocatalysts for the Synthesis of Polyurethanes. *Macromolecules* **2012,** *45* (5), 2249-2256. DOI: 10.1021/ma2026258.

7. McKee, C. T.; Last, J. A.; Russell, P.; Murphy, C. J., Indentation versus tensile measurements of young's modulus for soft biological tissues. *Tissue Engineering, Part B: Reviews* **2011,** *17*, 155+.

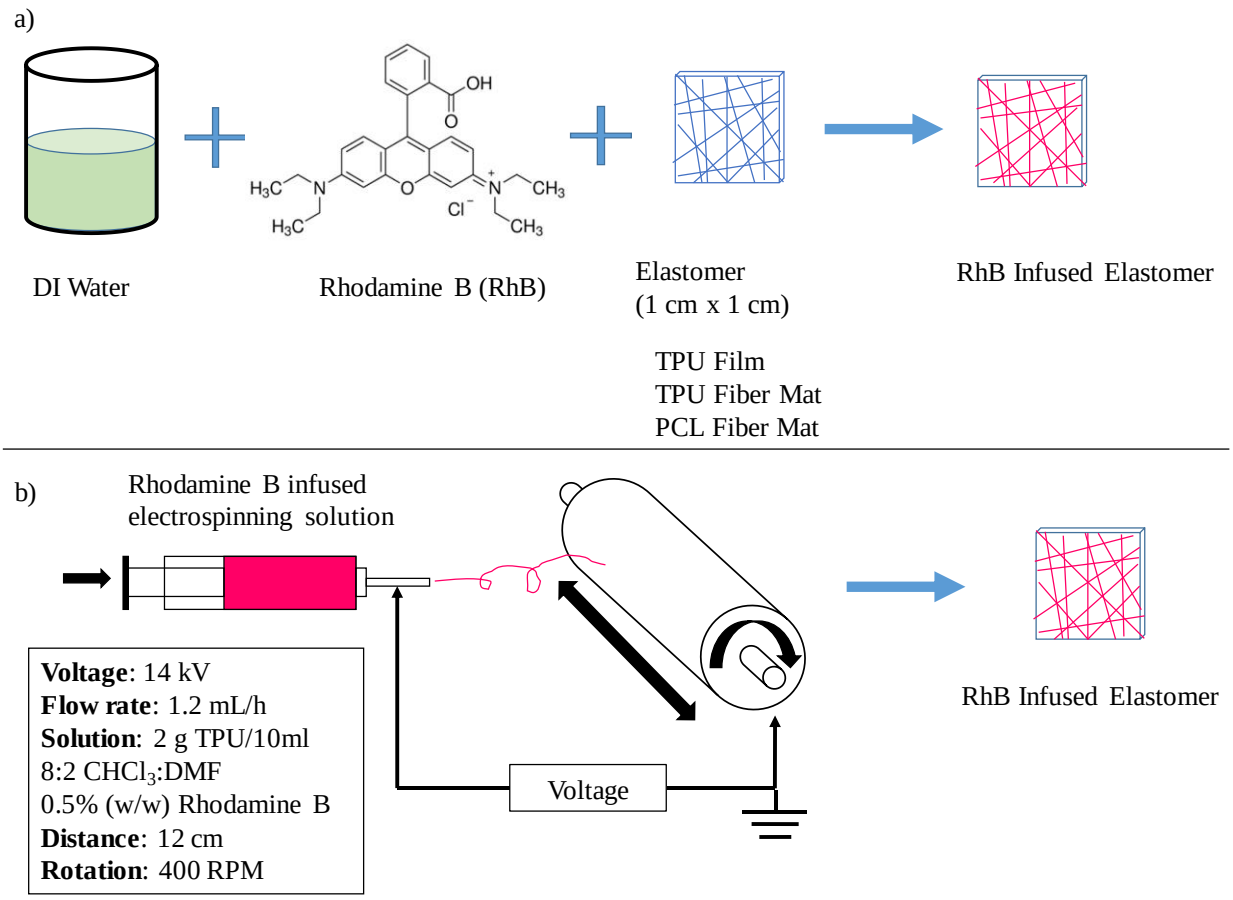

Scheme 7-1: Process of imbibing the biodegradable elastomers and PCL with Rhodamine B (RhB): a) "The Sponge Method" is when a material is soaked in a solution of RhB. b) Electrospinning a polymer/RhB solution. Both result in RhB-infused elastomers.

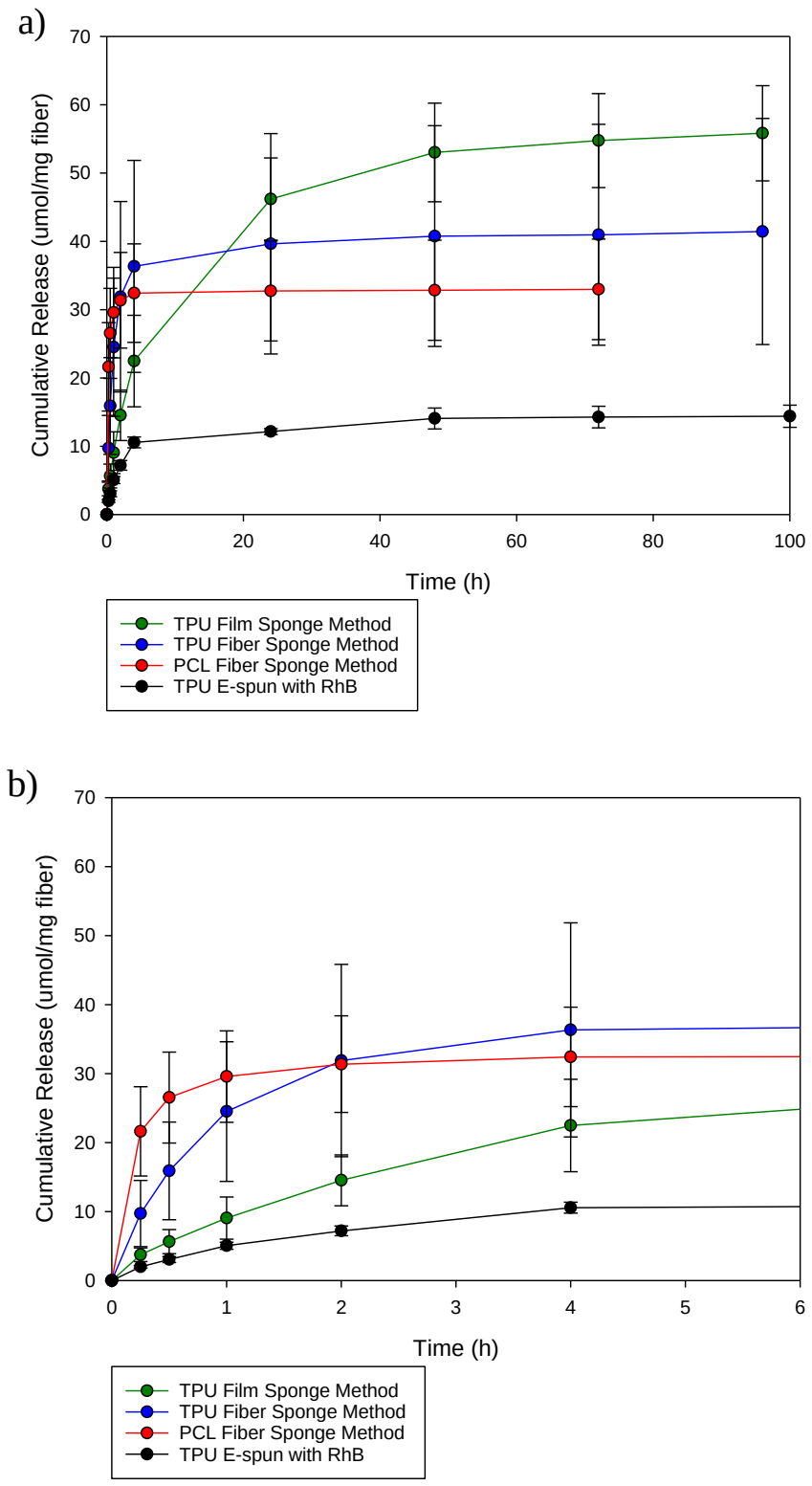

Figure 7-1: Cumulative drug release of the four tested materials over a) 100 h and b) 6 h.

Appendix: Development of a Biodegradable, Shape Memory Polymer with Controlled Physical Properties

A.1 Introduction

There is a need for biodegradable, smart materials for a variety of applications, including a self-deploying stent. Previously in our group, thermoplastic biodegradable, shape memory polyurethanes were developed with a glassy soft segment and POSS as the hard segment.[1] These materials had a storage modulus over 1 GPa at room and body temperature and showed good fixing and recovery with an adequate concentration of POSS. However, a softer shape memory material may be beneficial in order to better match surrounding tissues. The goal of this research is to develop a soft, semi-crystalline shape-memory polymeric stent that can be fixed in a smaller state and deployed in a body with a heated balloon. Some requirements for this stent include good mechanical stability (remain stable for up to 3-4 months), a transition temperature between 40 and 55 °C, and complete degradation within one year.

To achieve the goals specified above, polymers were designed with a specific architecture. Poly(ethylene glycol):poly(caprolactone) (PEG:PCL) diols were synthesized by ring opening polymerization of caprolactone in the presence of a short poly(ethylene glycol) (PEG) chains. The diols were designed to be 6 kDa or 12 kDa to maximize crystallinity of the PCL. They were also designed to be synthesized with different PEG initiators (600 Da, 1 kDa, and 2kDa) to control wettability. Poly(ethylene glycol) is a semi-crystalline material with a melting transition around 45 °C (which can change with molecular weight) that was incorporated into the soft segment because it easily absorbs water.[2] The PEG:PCL diols were then reacted with polyhedral oligomeric silsesquioxane (POSS) diol and a diisocyanate to form a polyurethane. To achieve shape memory, the POSS molecules are the physical cross-linker that hold the permanent shape, while the

PEG:PCL diols are the transition segment. We anticipate that changing the chemistry in the soft segment would control the thermal, mechanical and wettability properties as well as its degradation rate.

A.2 Methods

Polymer Synthesis: First, PEG:PCL diols were synthesized by ring opening polymerization of caprolactone in the presence of poly(ethylene glycol), the initiator, in a similar scheme to previous diol syntheses. Target molecular weights were 6 kDa and 12 kDa. These materials were synthesized by adding all of the reactants in an air-free flask and heating to 140 °C, as shown in **Scheme A-1**. Once the diols were collected and characterized for molecular weight, they were reacted with hexamethylene diisocyanate (HDI) and POSS diol (AL0104) at a molar ratio of 1:4 (PEG:PCL):POSS. This ratio was chosen so there would be enough POSS to provide shape memory properties as determined from the previous study. Five syntheses were performed, three with PEG:PCL diols of 12 kDa in molecular weight (PEG with 2 kDa, 1 kDa, and 600 Da) and two PEG:PCL diols of 6 kDa molecular weight (PEG of 2 kDa and 1 kDa).

Molecular Characterization: Proton nuclear magnetic resonance and gel permeation chromatography were performed to determine the polyurethanes' molecular properties. See 2.3.4 and 2.3.5 for exact methods.

Thermal Characterization: Differential Scanning Calorimetry was performed on the five polyurethanes to determine their thermal transitions. See 2.3.6 for exact methods.

Contact Angle Measurements: Wetting behavior was important for these polyurethanes. To determine the wettability as a function of PEG of POSS content, static contact angle measurements were studied using a Rame-Hart 240-F1 standard goniometer. A droplet of Millipore water was placed on a compression molded film of each polyurethane. For compression molding methods,

please refer to 2.3.7. For contact angle measurements, 100 scans were averaged for each image (n=3).

Mechanical Characterization: To understand the mechanical properties of the different polyurethanes, dynamic mechanical analysis (DMA) and shape memory test were performed on compression molded films of each material. For exact DMA methods, see 2.3.11. For shape memory, polymers were heated to 60 °C for 10 minutes, clamped around a glass rod and placed in the -4 °C freezer for 10 minutes to fix a strain. To recover, the materials were heated to 60 °C for 30 minutes.

A.3 Results

The polymer scheme is presented in **Scheme A-1**. The five polymers synthesized were tested for molecular properties, which are displayed in **Table A-1**. The molecular weights for these materials were moderate, with M_w values ranging from 26.4 to 60.5 kDa. The polydispersity indexes (PDIs) of these materials were narrow, ranging from 1.1-1.4. ^{1}H-NMR was used to determine the actual PEG and POSS content in each polymer. For PEG, content decreased with decreasing length of the PEG. POSS content varied between 18 and 29 wt. % of the polymer. These characteristics affected the wetting and mechanical properties, as described below.

Differential scanning calorimetry was performed on all materials to determine the thermal properties. As shown in **Figure A-1** and quantified in **Table A-2**, there were three thermal transitions in each polymer, a glass transition and two melting transitions. The lower melting transition corresponded to the PEG:PCL diols and the higher melting transitions corresponded to POSS diol. The enthalpy of melting for the 12 kDa soft segments increased with decreasing size of the polyethylene glycol, which could be due to the better crystallization of PCL. The 6 kDa soft segments showed the opposite trend, which could be due to the high amount of PEG_{2k} in

$(PEG_{2k}:PCL)_{6k}$:POSS. There were clear POSS melting transitions in all polyurethanes with enthalpies of melting between 1.1 and 1.8 J/g.

Contact angle measurements were taken to determine the polyurethanes' wettability. As shown in **Figure A-2**, $(PEG_{2k}:PCL)_{12k}$:POSS had the lowest content angle. It has a high PEG content, which is hydrophilic, conflicting with the hydrophobic PCL and POSS components. Decreasing the PEG size increased the contact angle as the material became more hydrophobic. Interestingly, for the 6 kDa soft segments, the contact angle decreased with decreasing PEG length. This could be because $(PEG_{2k}PCL)_{6k}$:POSS had a high POSS content, and the hydrophobicity of the POSS caused an increased contact angle despite the high PEG content.

Dynamic mechanical analysis was performed to examine the mechanical properties of these materials, displayed in **Figure A-3**. These materials had storage moduli around 100 MPa at room and body temperature, which is about an order of magnitude lower than the glassy polyurethanes previously published in our group. Also, the size of the soft segment affected the melting transition material, as the smaller soft segments melted at a lower temperature than the soft segment.

Finally, shape memory testing was performed on each material, shown in **Figure A-4**. Materials with the larger soft segment (12 kDa) had better fixing, indicated by the tighter coil (mimicking the size of the glass rod it was fixed around). Alternatively, the materials with the 6 kDa soft segments had poor fixing, which is indicated by the larger radius. This difference in fixing could be due to the crystallization of the materials, shown in the cooling curve from DSC in **Figure A-5** and quantified in **Table A-3**. The material with a 12 kDa soft segment had a larger enthalpy of crystallization and a higher crystallization temperature, allowing it to have better fixing. Interestingly, all materials recovered most of their fixed curvature, but the materials with better

fixing show a slight indent after recovery, indicating that the recovery was not 100%. Quantification of these materials needs to be completed.

A.4 Conclusions and Future Work

In conclusion, biodegradable shape memory polyurethanes with controllable properties were synthesized. The size of the soft segment, length of PEG within the soft segment, and amount of POSS content all played a role in thermal, mechanical, and wettability properties. These materials had good fixing and recovery properties, and meet our lower modulus requirements. For future work, an extensive degradation study needs to be performed on these materials to determine how the soft segment composition affects degradation. Also, shape memory studies need to be quantified and studied for more detail. Finally, cell viability and other *in vitro* studies need to be done in order to make sure these materials will not be cytotoxic.

A.5 References

1. Knight, P. T.; Lee, K. M.; Qin, H.; Mather, P. T., Biodegradable Thermoplastic Polyurethanes Incorporating Polyhedral Oligosilsesquioxane. *Biomacromolecules* 2008, *9* (9), 2458-2467. DOI: 10.1021/bm8004935.

2. Gu, X.; Wu, J.; Mather, P. T., Polyhedral Oligomeric Silsesquioxane (POSS) Suppresses Enzymatic Degradation of PCL-Based Polyurethanes. *Biomacromolecules* 2011, *12* (8), 3066-3077. DOI: 10.1021/bm2006938.

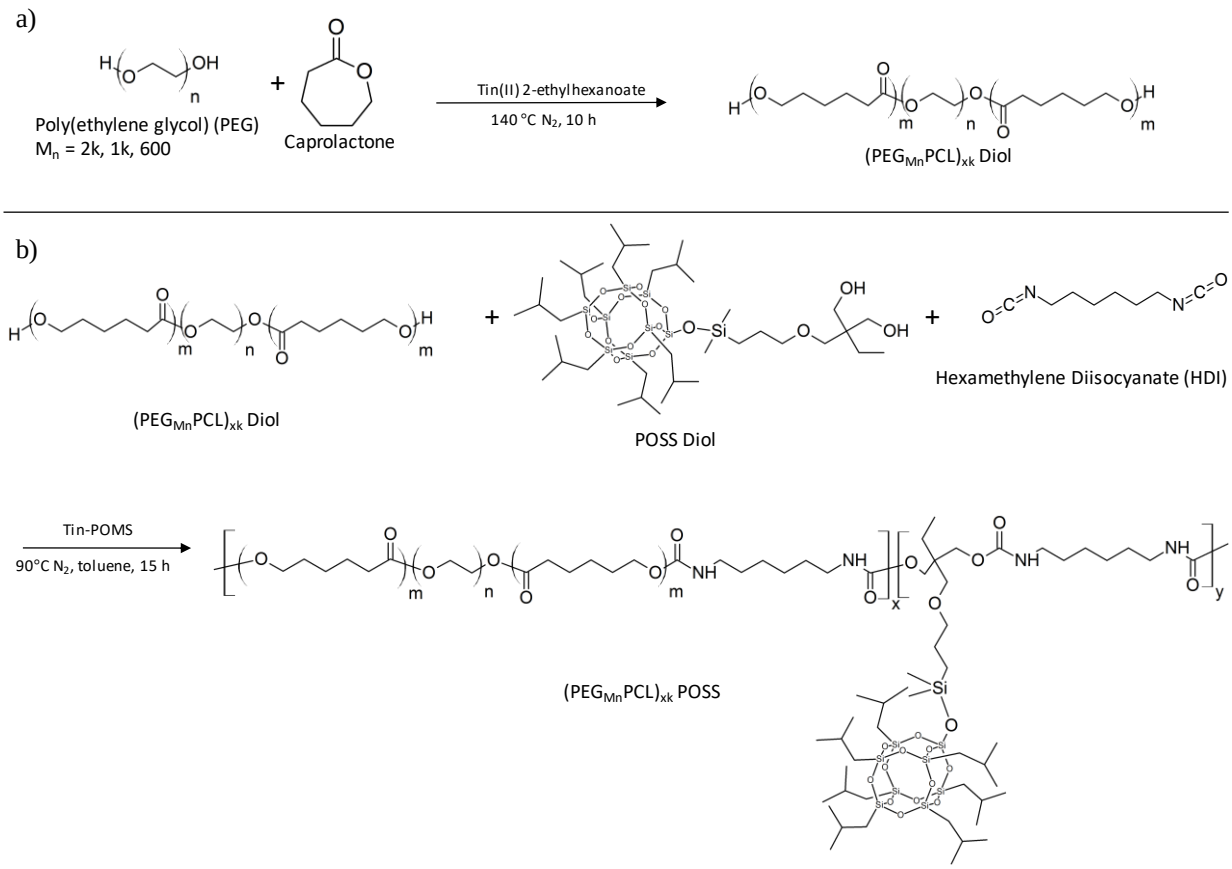

Scheme A-1: Schematics of a) diol synthesis and b) polyurethane synthesis.

Table A-1: Summary of (PEG:PCL):POSS syntheses and their molecular properties.

Synthesis	Diol M_n (kDa)	Diol PDI	Polyurethane M_n (kDa)	Polyurethane M_w (kDa)	Polyurethane PDI	Actual PEG Content (Wt. %)	Actual POSS Content (Wt. %)
$(PEG_{2k}:PCL)_{12k}$:POSS	14.6	1.2	28.4	36.9	1.3	9.9	27.7
$(PEG_{1k}:PCL)_{12k}$:POSS	12.6	1.1	20.3	26.4	1.3	8.3	27.4
$(PEG_{600}:PCL)_{12k}$:POSS	16.7	1.2	42.6	59.7	1.4	3.2	20.5
$(PEG_{2k}:PCL)_{6k}$:POSS	7.0	1.1	55.0	60.5	1.1	20.0	29.5
$(PEG_{1k}:PCL)_{6k}$:POSS	9.3	1.1	26.6	37.2	1.4	8.7	18.6

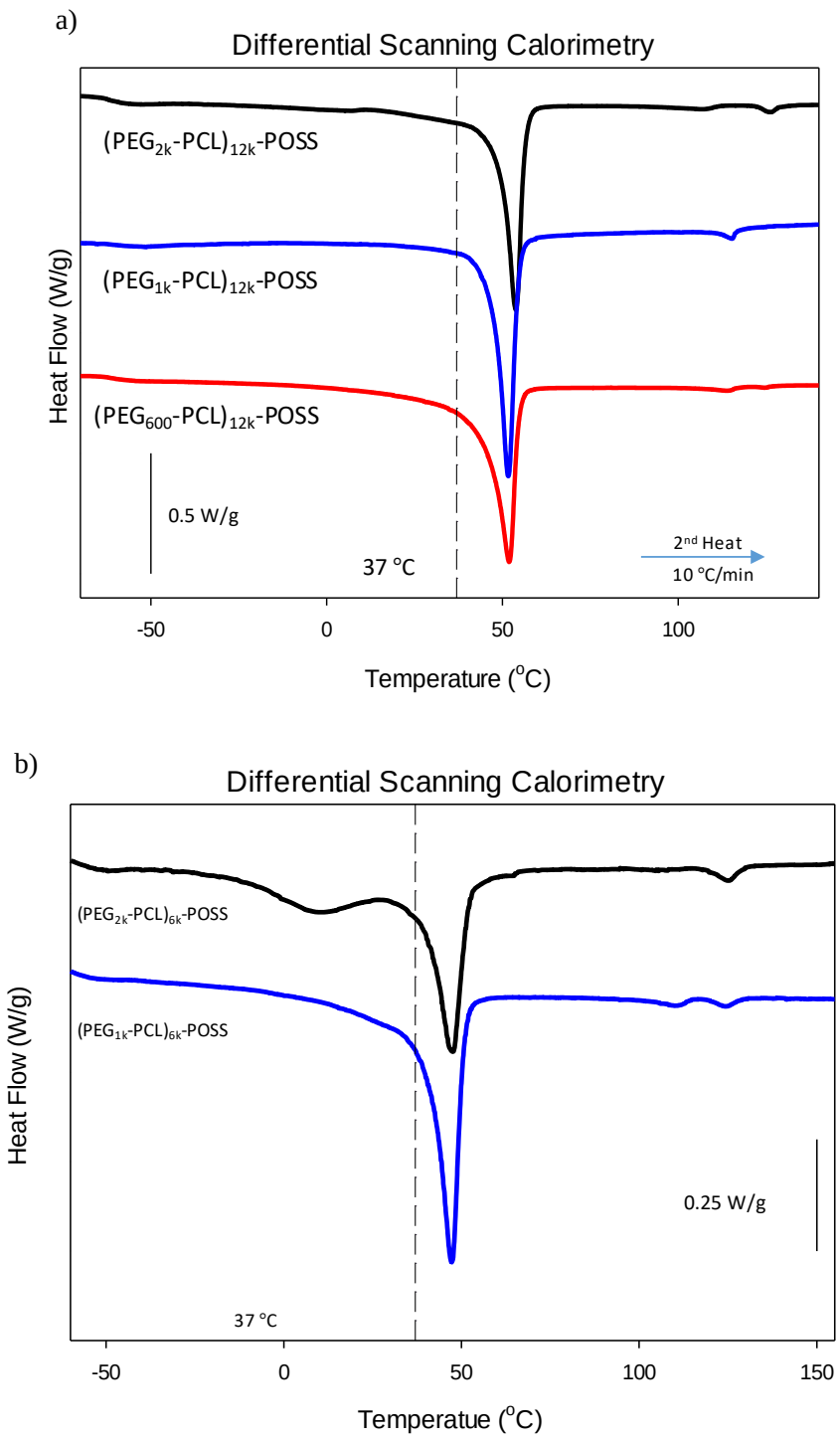

Figure A-1: Differential scanning calorimetry of a) soft segments with a molecular weight of 12 kDa and b) soft segment with a molecular weight of 6 kDa.

Table A-2: Summary of the thermal properties.

Synthesis	T_g (°C)	$T_{m,PCL}$ (°C)	ΔH_{PCL} (J/g)	$T_{m,POSS}$ (°C)	ΔH_{POSS} (J/g)
$(PEG_{2k}:PCL)_{12k}$:POSS	-61.0	53.8	36.9	126.4	1.8
$(PEG_{1k}:PCL)_{12k}$:POSS	-60.1	51.5	43.8	113.3	1.3
$(PEG_{600}:PCL)_{12k}$:POSS	-53.0	51.9	44.9	114.0	1.1
$(PEG_{2k}:PCL)_{6k}$:POSS	-59.0	8.7/47.5	41.8	118.4	1.2
$(PEG_{1k}:PCL)_{6k}$:POSS	-57.6	47.28	37.4	124.4	1.3

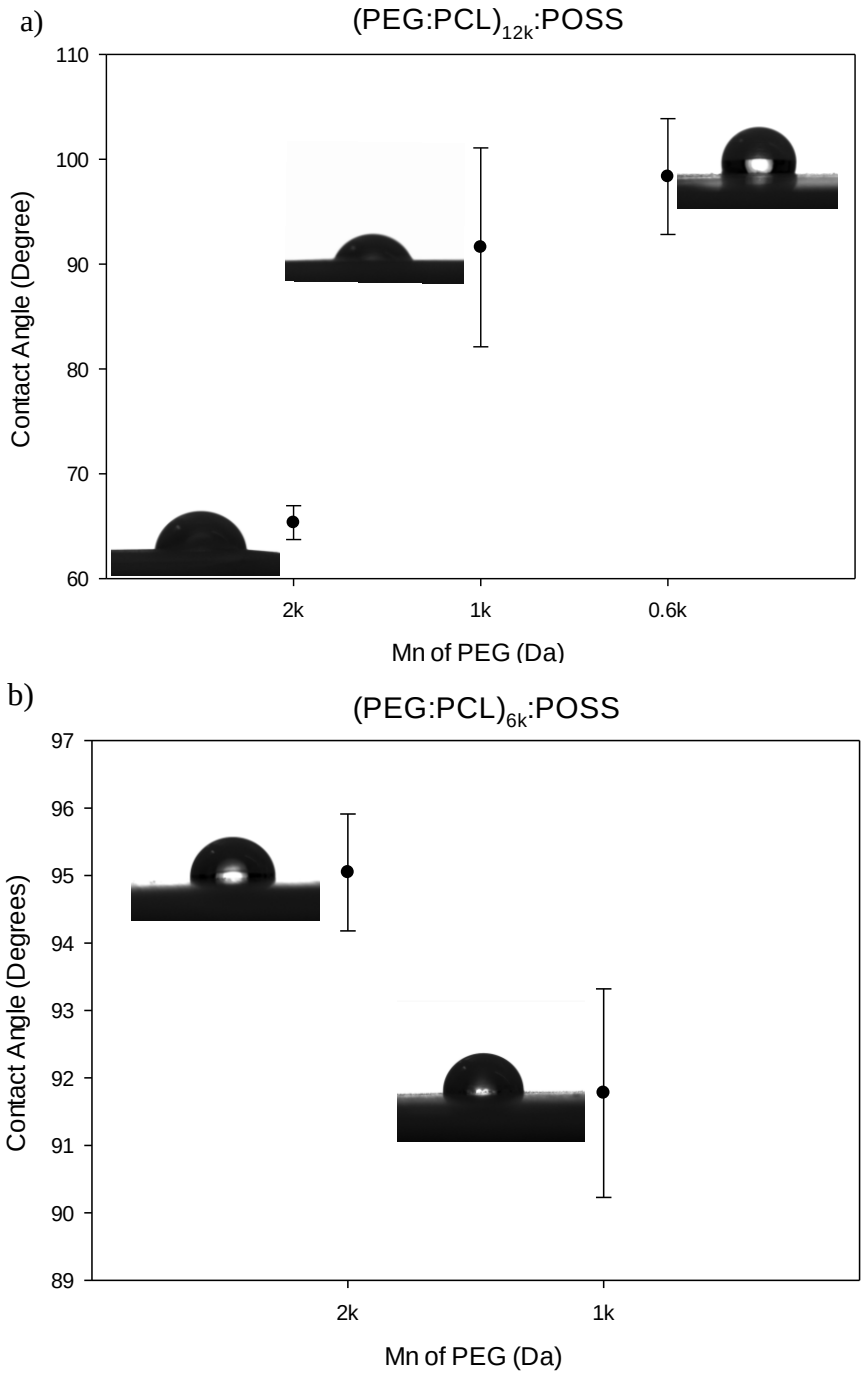

Figure A-2: Contact angle measurements of polyurethanes with a) soft segments with a molecular weight of 12 kDa and b) soft segment with a molecular weight of 6 kDa.

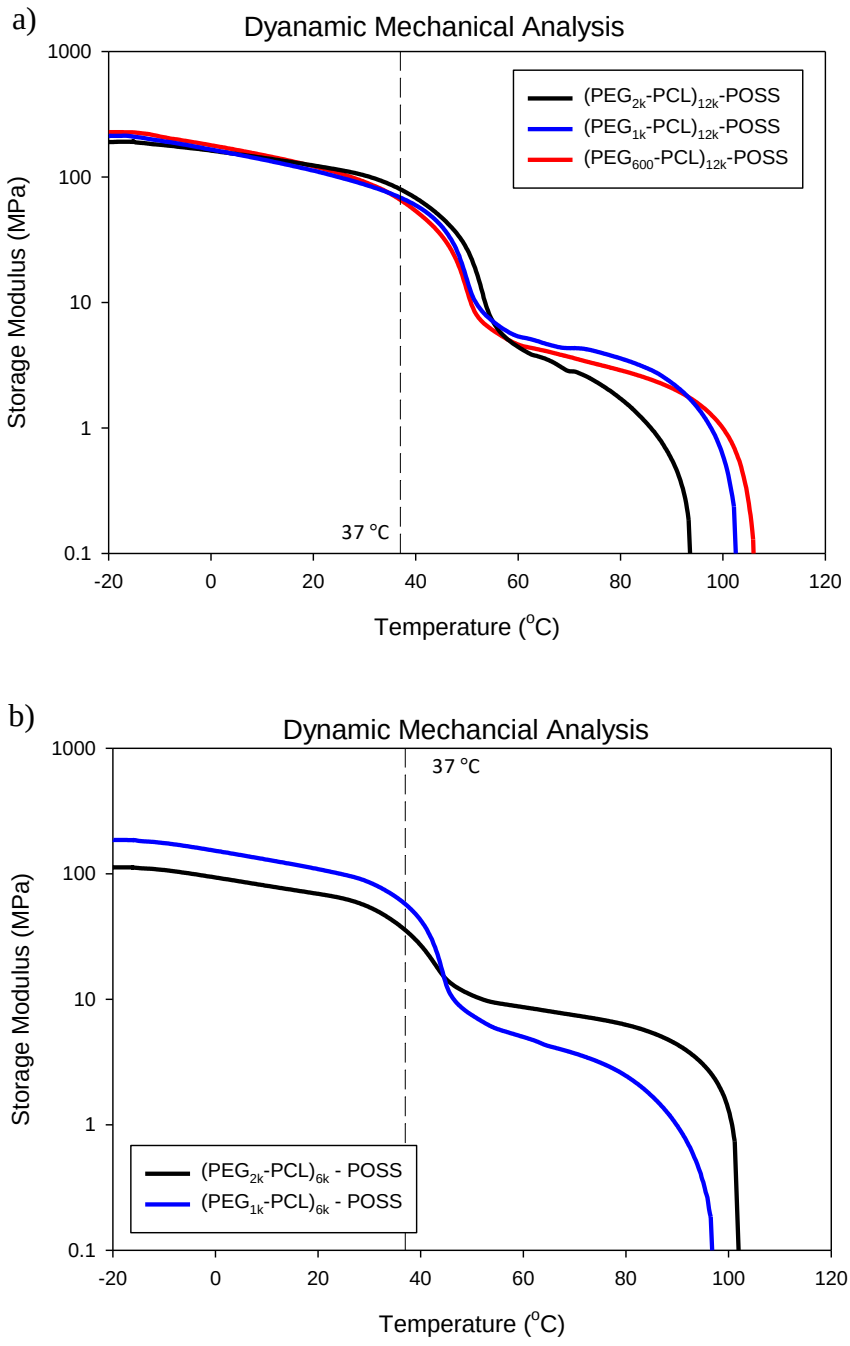

Figure A-3: Dynamic mechanical analysis of the polyurethanes with a) soft segments with a molecular weight of 12 kDa and b) soft segment with a molecular weight of 6 kDa.

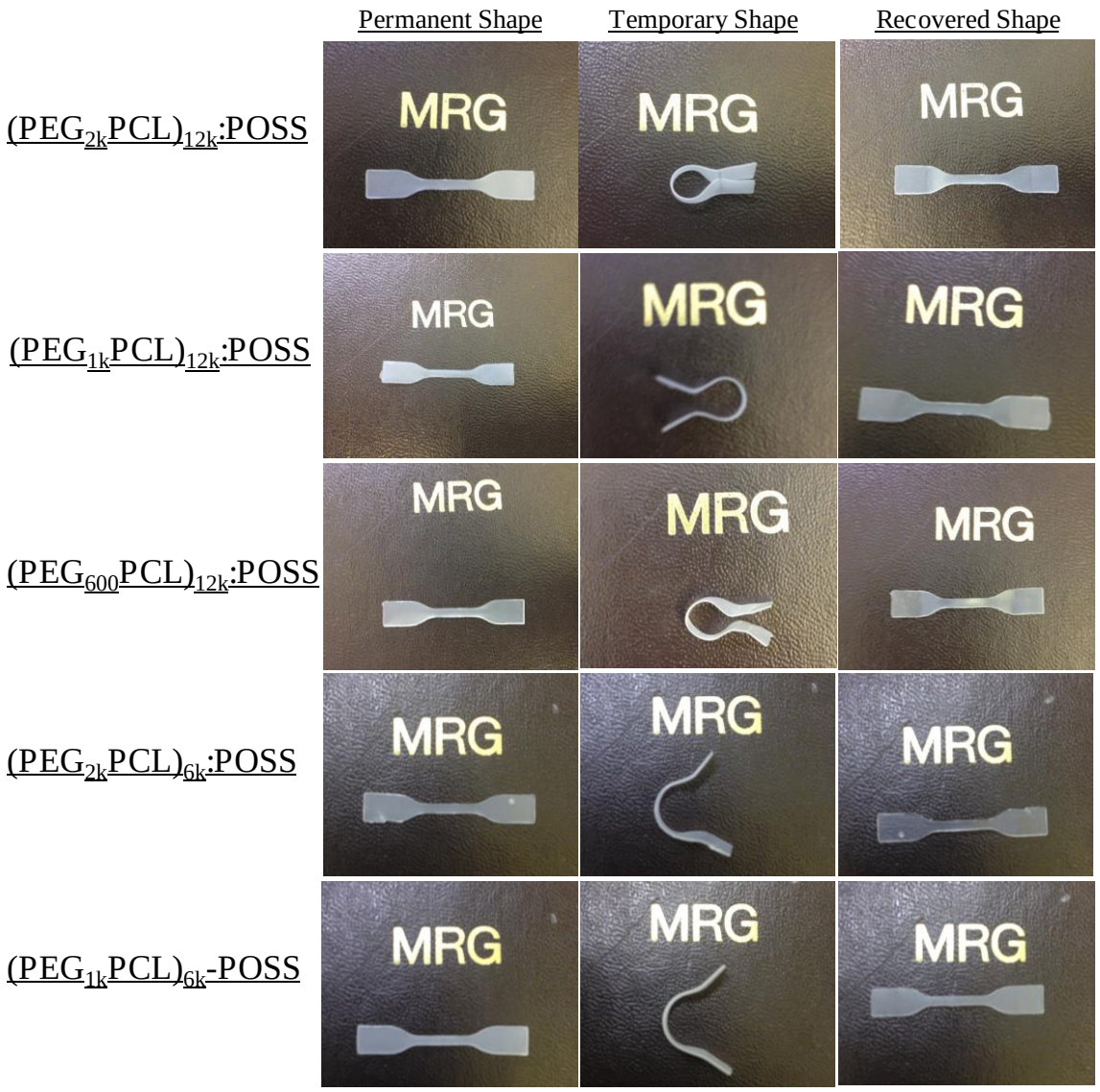

Figure A-4: Shape memory testing of each polyurethane with images of the dogbone initially, after fixing, and after recovery.

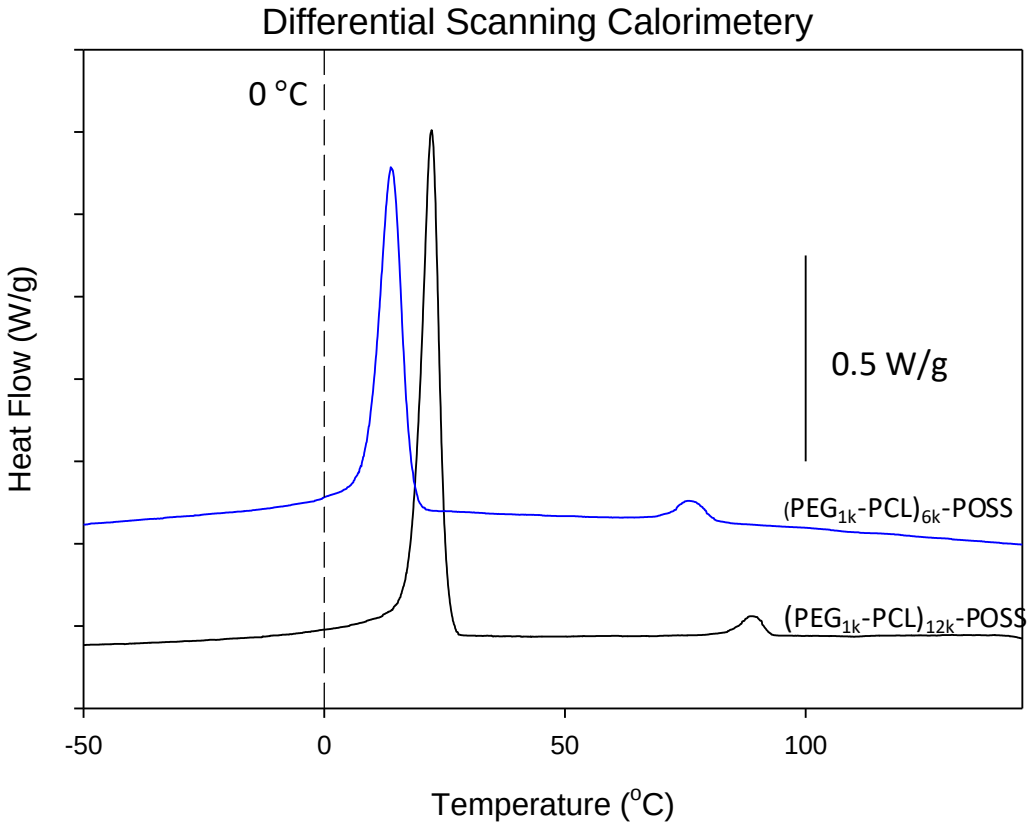

Figure A-5: Differential scanning calorimetry of two polyurethanes, with first cooling shown (exotherm up).

Table A-3: Summary of the thermal characteristics of the soft segment upon cooling.

Synthesis	T_c (°C)	ΔH_c (°C)
$(PEG_{1k}PCL)_{12k}$:POSS	22.3	38.6
$(PEG_{1k}PCL)_{6k}$:POSS	13.8	34.8

VITA

NAME OF AUTHOR**:** Erin McMullin

PLACE OF BIRTH**:** New Brunswick, New Jersey, USA

DATE OF BIRTH**:** July 28, 1989

EDUCATION:

B.S. in Engineering Science (Biomedical), The College of New Jersey (2011)

Ph.D. in Bioengineering, Syracuse University (2011 to Dec. 2016)

SELECTED PUBLICATIONS, PRESENTATIONS AND PATENTS:

Erin McMullin, Hannah T. Rebar, and Patrick T. Mather. "Biodegradable Thermoplastic Elastomers Incorporating POSS: Synthesis, Microstructure, and Mechanical Properties." *Macromolecules* 49 3769–3779 (2016).

Mather, Patrick T.; McMullin, Erin; Frie, Euphemia. 2016. "Thermoplastic elastomers utilizing amorphous and crystalline blocks of the same composition." Disclosed to Syracuse University June 24, 2016.

Erin McMullin, Phillip A. Falcone, Jaimee M. Robertson, and Patrick T. Mather. "Thermoplastic biodegradable shape memory elastomeric composites by dual-electrospinning." *Oral Presentation. 10th World Biomaterials Congress*. Montreal, Canada. May 18, 2016.

Erin McMullin, Hannah T. Rebar, and Patrick T. Mather. "Biodegradable, thermoplastic elastomers utilizing POSS as a hard segment." *Oral Presentation. 250th American Chemical Society National Meeting and Exposition. Boston, MA.* August 16 – 20, 2015.

Erin McMullin and Patrick T. Mather. "Development of a Biodegradable, Shape Memory Polymer with Controlled Physical Properties." *Oral Presentation. 2014 MRS Fall Meeting and Exhibit. Boston, MA.* November 30 – December 5, 2014.

Erin McMullin, Hannah T. Rebar, Patrick T. Mather. "Development of Bioabsorbable, Thermoplastic Elastomers." *Poster Presentation. Stevenson Lectures Series. Syracuse University. Syracuse, NY.* October 17, 2014

Award: Best Commercial Potential

Erin McMullin, Kazuki Ishida, Emily J. Mesing, Patrick T. Mather. "A Water-Triggered Shape Memory Polymer for Industrial Applications." *Poster Presentation. Stevenson Lectures Series. Syracuse University. Syracuse, NY.* November 26, 2012